

Aus dem
Institut für Physiologie I
des Universitätsklinikums Bonn
Direktor: Prof. Dr. med. (I) Bernd K. Fleischmann

**Pluripotent stem cells as a model system for the
investigation of cardiovascular development and disease**

Habilitationsschrift
zur Erlangung der *venia legendi*
der Hohen Medizinischen Fakultät
der Rheinischen Friedrich-Wilhelms-Universität Bonn
für das Lehrgebiet
„Physiologie“

Vorgelegt von
PhD, Daniela Malan
aus Pinerolo (Turin, Italien)
Wissenschaftliche Mitarbeiterin
an der Rheinischen Friedrich-Wilhelms-Universität Bonn
Bonn 2025

Meiner Familie und
Davide
in Dankbarkeit
gewidmet

Die folgenden aufgelisteten sechs Originalarbeiten liegen der kumulativen Habilitationsschrift zu Grunde, welche die wesentlichen Ergebnisse der Publikationen zusammengefasst und diskutiert.

- I. Cokić M, Brüggmann T, Sasse P * and Malan D*. Optogenetic stimulation of Gi signaling enables instantaneous modulation of cardiomyocyte pacemaking. *Frontiers in Physiology* DOI: 10.3389/fphys.2021.768495 Nov. 2021 (IF:4.5)
- II. Zhang M*, Malan D*, Stallmeyer B, Müller J, Fleischmann BK, Schulze-Bahr E, Sasse P, Greber B. Human iPS cell model of type 3 long QT syndrome recapitulates drug-based phenotype correction. *Basic Res Cardiol*. 2016 Mar;111(2):14. doi: 10.1007/s00395-016-0530-0 (IF:6.03)
- III. Friedrichs S*, Malan D*, Voss Y, Sasse P. Scalable Electrophysiological Investigation of iPS Cell-Derived Cardiomyocytes Obtained by a Lentiviral Purification Strategy *J. Clin. Med*. 2015, 4(1), 102-123; doi:10.3390/jcm4010102 (IF:1.10)
- IV. Malan D, Elischer A, Hesse M, Wickström SA, Fleischmann BK, Bloch W. Deletion of integrin-linked kinase in endothelial cells results in defective RTK signalling caused by caveolin one mislocalization. *Development*. 2013 Mar;140(5):987-95. DOI: 10.1242/dev.091298. PubMed PMID: 23404105 (IF:6.5).
- V. Malan D*, Friedrichs S*, Fleischmann BK, Sasse P. Cardiomyocytes obtained from induced pluripotent stem cells with long-QT syndrome 3 recapitulate typical disease-specific features in vitro. *Circ Res*. 2011 Sep 30;109(8):841-7. DOI: 10.1161/CIRCRESAHA.111.243139. Epub 2011 Jul 28. PubMed PMID: 21799153 (IF:9.48).
- VI. Malan D, Reppel M, Dobrowolski R, Roell W, Smyth N, Hescheler J, Paulsson M, Bloch W, Fleischmann BK. Lack of laminin gamma1 in embryonic stem cell-derived cardiomyocytes causes inhomogeneous electrical spreading despite intact differentiation and function. *Stem Cells*. 2009 Jan;27(1):88-99. doi: 10.1634/stemcells.2008-0335. PubMed PMID: 18927478 (IF:7.7).

*geteilte Autorenschaft

Datum des Habilitationskolloquiums: 30.01.2025

Table of contents:

1	Abbreviation	7
2	Introduction	8
2.1	Generation of murine and human embryonic stem (ES) cells	10
2.2	Generation of induced pluripotent stem (iPS) cells	13
2.3	Stem cell differentiation into cardiovascular cells: endothelial cells (ECs).....	19
2.4	In vitro differentiation of pluripotent stem cells into cardiomyocytes.....	22
2.5	Pluripotent stem cells as model to investigate early aspects of cardiovascular development and disease mechanisms.	26
2.5.1	Role of Extracellular Matrix in cardiovascular diseases	27
2.5.2	Pluripotent cells as model for Long QT Syndromes	30
2.6	Summary of Key Challenges Addressed in the Papers	34
3	Results	35
3.1	Role of extracellular matrix proteins in cardiovascular development using the ES system:	35
3.1.1	Deletion of integrin-linked kinase in endothelial cells results in defective RTK signaling caused by caveolin 1 mislocation. Development. 2013 Mar;140(5):987-95. DOI: 10.1242/dev.091298. PubMed PMID: 23404105 (IF:6.5).....	36
3.1.2	Lack of Laminin γ 1 in embryonic stem cell-derived cardiomyocytes causes inhomogeneous electrical spreading despite intact differentiation and function. Stem Cells. 2009 Jan;27(1):88-99. doi: 10.1634/stemcells.2008-0335. PubMed PMID: 18927478 (IF:7.7).	55
3.2	Cardiomyocytes differentiated from iPS cells as a model for studying monogenic heart disease:	72

3.2.1	Cardiomyocytes obtained from induced pluripotent stem cells with Long-QT syndrome 3 recapitulate typical disease-specific features in vitro. Circ Res. 2011 Sep 30;109(8):841-7. DOI: 10.1161/CIRCRESAHA.111.243139. Epub 2011 Jul 28. PubMed PMID: 21799153 (IF:9.48).....	72
3.2.2	Scalable electrophysiological investigation of iPS cell-derived cardiomyocytes obtained by a lentiviral purification strategy. J. Clin. Med. 2015, 4(1), 102-123; doi:10.3390/jcm4010102 (IF:1.10).....	89
3.2.3	Human iPS cell model of type 3 long QT syndrome recapitulates drug-based phenotype correction. Basic Res Cardiol. 2016 Mar;111(2):14. doi: 10.1007/s00395-016-0530-0 (IF:6.03).....	115
3.3	Future perspective using optogenetic tools within stem cell derived cardiomyocytes:	129
3.3.1	Optogenetic Stimulation of Gi Signaling Enables Instantaneous Modulation of Cardiomyocyte Pacemaking. Frontiers in Physiology DOI: 10.3389/fphys.2021.768495 Nov. 2021 (IF:4.5)	129
4	Discussion.....	142
4.1	Role of ECM in development and in the functional integrity of cardiovascular cells	142
4.2	Modeling cardiovascular disease with iPS cells.....	148
	Challenges in personalized medicine: non-clonal iPS and automated iPS cell generation	151
	Challenges in disease modeling: Genetic variability and choice of controls.....	153
	Challenges in disease modeling: Maturation and purification of differentiated cells	155
	Comparison of readout systems for disease modeling and screening	160
4.3	Future perspectives: organoids	163

4.4	Future perspectives: Drug screening for GPCRs using optogenetics	165
5	Summary.....	169
6	Overlapping uses of current research activities declaration	172
7	Bibliography	173
8	Acknowledgments	195
9	Curriculum Vitae.....	196
10	Statements	200

1 Abbreviations

AP: Action Potential

APD: Action Potential duration

Ca^{2+}_i : Intracellular Calcium

EAD: early after depolarization

EB: embryoid body

EC: endothelial cell

ECM: extracellular matrix

ES cell: embryonic stem cell

FPD: field potential duration

GPCR: G protein-coupled receptors

iPS cell: induced pluripotent stem cell

INa^+ : Sodium Current

ICa^{2+} : Calcium Current

LWO: long wavelength-sensitive cone opsin

LQTS: long-QT syndrome

MEF: mouse embryonic fibroblasts

RTK: receptor tyrosine kinase

2 Introduction

Embryonic stem (ES) cells and induced pluripotent stem (iPS) cells have become attractive models for studying development and disease mechanisms in vitro.

An extraordinary characteristic of these cells is pluripotency. Pluripotent cells have no predetermined program; they are in an undifferentiated ground state and can be differentiated in any somatic cell type and into germ cells of the body, with the exception of extraembryonic tissues required for the development of the placenta. Pluripotent cells have the remarkable ability to self-renew and undergo clonal expansion, ensuring a continuous supply of cells in response to physiological demands or for tissue repair, maintenance and regeneration. In addition, they can develop and acquire specific functions through cell differentiation (Wray et al., 2010). This property can circumvent the known issues with cells of the cardiovascular system that are difficult to differentiate and maintain in culture.

Cardiovascular diseases are the leading cause of death worldwide, and the WHO states in their report in 2019 that 17.9 million people died from cardiovascular disease, representing 32% of all global deaths. These numbers are increasing further in western countries because of the higher incidence of these diseases in an aging population. The impact of cardiovascular diseases extends beyond mortality rates. They also significantly burden healthcare systems and economies due to the costs associated with diagnosis, treatment, and long-term management.

My research deals with cardiovascular development and biological characterization of main components of the cardiovascular system, such as endothelial and cardiac muscle cells.

This work aims to show how the unique property of pluripotency could help basic medical research in the cardiovascular field. ES and iPS cells enabled me to explore early steps of cardiovascular development, that occur in the embryo and that are challenging to investigate due to limited accessibility making it difficult to observe and study these processes directly in vivo. One aim of the selected papers summarized in the following chapters is to provide insight

into the role of extracellular matrix (ECM) in cardiovascular development. Given that traditional knock-out mouse models lacking fundamental proteins building the ECM are lethal at the embryonic stage, I have used instead pluripotent cells to mimic cardiovascular development and differentiation. I have studied the role of laminin $\gamma 1$ for cardiac muscle because its deletion in skeletal muscle causes pathologies, such as congenital muscle dystrophy. I therefore wanted to elucidate the cellular and functional effects of disrupted basement membrane formation on cardiomyocytes, including ECM abnormalities and impaired electrical signal propagation (Malan et al., 2009). Other ECM proteins like ILK also have a role as central mediators of cell-ECM interactions with cytoskeletal components, thus for instance, in keratinocytes impairing caveolae formation. Therefore, I explored whether the deletion of ILK in endothelial cells (ECs) will result in defective signaling caused by mislocalization of caveolin 1, potentially affecting EC apoptosis, proliferation, migration, and vascular development (Malan et al., 2013)

In addition, pluripotent stem cells can be generated with gene defects or from patients with specific cardiovascular diseases, creating disease-specific cell lines. Pluripotent cells, such as human iPS and ES cells, are used in clinical trials to replace diseased cells, like in Parkinson's disease. Additionally, these cells are explored for replacing cardiac muscle cells lost after myocardial infarction or stroke, aiding in understanding disease mechanisms and testing potential interventions, including drug effects on cardiovascular function, reducing reliance on animal models or clinical trials for initial testing (Gyöngyösi et al., 2016, Stoddard-bennett and Reijo Pera 2019, Attar et al., 2021).

Next, through the differentiation of iPS cell-derived cardiomyocytes, carrying a human mutation linked to long-QT syndrome 3 (LQTS3), I could replicate disease-specific features, showcasing their potential for investigating disease mechanisms. The focus then shifted to developing a scalable purification method for these cardiomyocytes and exploring drug interventions to correct abnormal phenotypes, demonstrating the applicability of iPS cell-derived models for drug screening and personalized medicine approaches.

In addition, the new research is focus to broaden insights by applying a new optogenetic tool to ES cell-derived cardiomyocytes. This involved utilizing optogenetic techniques, coupled with the expression of long wavelength-sensitive cone opsin (LWO), to achieve instantaneous modulation of pacemaking activity through activating the Gi signaling pathway. The combination of optogenetics with ES cell technology aimed to provide deeper insights into the temporal dynamics and functional consequences of Gi pathway activation in early cardiomyocytes, contributing to a comprehensive understanding of cardiac physiology and potential therapeutic interventions.

2.1 Generation of murine and human embryonic stem (ES) cells

Our understanding and biological insight into pluripotent stem cells are based on decades of basic science work in mouse ES cells. Mouse ES cells were first derived in 1981 from the inner cell mass of the blastocyst stage embryo of the mouse at 3.5 days post coitum (Evans and Kaufman, 1981). They possess the remarkable potential to give rise to specialized cell lineages of all three embryonic germ layers: ectoderm, mesoderm, endoderm, and germ cells (Morrison et al., 1997, Silva et al., 2008, Wray et al., 2010). ES cells are pluripotent but not totipotent because they can neither generate an entire embryo nor extraembryonic tissue (see Fig. 1).

The great impact of ES cell technology for science and medicine was recognized in 2007 with the Nobel Prize to three scientists, Martin J Evans, Oliver Smithies, and Mario Capecchi, for their discoveries on generating and also on using ES cells to create genetically modified mice. Capecchi and Smithies were the first to use homologous recombination to alter genes in mammalian cells to correct disease-causing mutations in bone marrow stem cells, using them to treat certain inherited blood diseases. Evans managed to cultivate embryonic stem cells from mice and then had the vision to use genetically modified ES cells, creating KO mice. The gold standard method for mice generation is the tetraploid complementation, which it is performed using blastocysts with twice the normal number of chromosomes (tetraploid), putative ES cells are then injected forming whole, non-chimeric, fertile mice. Since 1989, when homologous recombination in ES cells used to generate gene-targeted mice was first reported,

nearly 50,000 targeted genetic allele modifications have been created, and knock-out mice have been generated by homologous recombination in ES cells. This method, has been instrumental in advancing our understanding of specific signaling pathways, protein alterations, and the molecular components' roles in disease, differentiation, and cellular/tissue development (Capecchi, 2005). This significant progress has substantially enhanced our comprehension of processes underlying disease mechanisms and related phenomena.

The cultivation of Mouse ES cells lays a crucial role in maintaining pluripotency. When cultured in media with serum and supplements, ES cells are kept on feeder layers of mouse embryonic fibroblasts (MEF). It was observed that MEF produces the leukemia inhibitory factor, a soluble glycoprotein of the interleukin (IL)-6 family, which activates transcription of STAT3 signaling and thereby maintaining pluripotency. Consequently, the removal of MEF or inactivation of STAT3 promotes differentiation of pluripotent ES cells. Therefore, undifferentiated ES cells are cultivated in medium supplemented with LIF to activate STAT3. The bone morphogenetic protein BMP, a molecule also known to trigger so-called “inhibitory-of-differentiation” target genes, is often added to maintain pluripotency during the expansion culture procedure. Cultivation on feeder layers of fibroblasts is not always necessary, as it has been shown that LIF alone is sufficient to maintain pluripotency in serum culture conditions (Wobus and Boheler, 2005). Fascinating studies by Smith and his working group (Ying et al., 2008, Silva et al., 2008) showed that a real stem cells' ground state, like in the inner cell mass of the blastocyst, is not dependent on the presence of external cytokine stimuli that leads to STAT3 activation, since it was possible to create stem cells from blastocysts of mice lacking STAT3. The study shows that ES cells in their ground state are self-sufficient, thus capable of self-renewal independent of external signals. Nevertheless, in normal culture conditions, mouse ES cells require STAT3 activation to maintain the ground state characteristics (Wang et al., 2017).

In 1998, James Thomson and coworkers (Thomson et al., 1998) derived the first human embryonic stem cell line from human blastocysts. The isolation techniques and culture of mouse ES cells were fundamental for generating and maintaining human ES cells. Human ES

cells express the markers Oct3/4, Nanog, and telomerase, and they have the capability of teratoma formation showing the development of all three primary germ layers if transplanted in immunodeficient mice, thus sharing pluripotency features with mouse ES cells. However, they also have distinct characteristics, such as specific proteoglycans as cellular markers like TRA-1-60 and TRA-1-80 and different subtypes of stage-specific antigens like SSEA-3 and -4, absent in mouse ES cells. A significant difference with mouse ES cells is that LIF cannot maintain human ES cell pluripotency and prevent differentiation. Some human ES lines created at the beginning were even missing its receptor (Richards et al., 2004, Wobus, 2005). Thus, human ES cells resemble mouse ES cells in pluripotency despite a high variability of stemness markers. The property of self-renewal in human ES is maintained through cultivation on MEF, human feeder cells, or conditioned media or factors as in mTESR, and E8 media. Serum and substrate of plating like Matrigel, a complex mixture of ECM proteins isolated from Engelbreth-Holm-Swarm tumor, further helps to preserve pluripotency. Using animal-derived products poses the risk of cross-species contamination with non-human antigens like sialic acid Neu5Gc, against which many humans have circulating antibodies, thus activating the complement system (Kubikova et al., 2009). Like serum, feeder cells and other animal-derived products can significantly compromise the clinical application of human stem cells and are best avoided wherever possible.

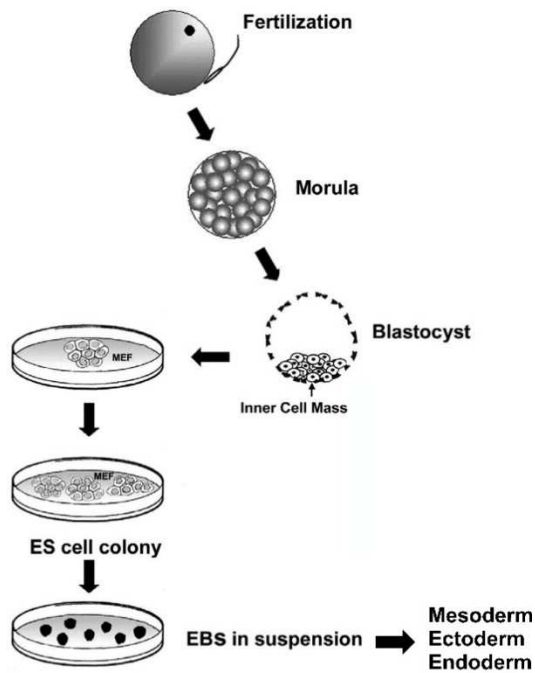


Figure 1 Generation of ES cells. A fertilized egg develops into the blastocyst stage. Isolated cells from the inner cell mass are cultured in this pluripotent state on mouse fibroblasts, forming colonies and differentiated in Embryoid bodies (EBs) giving rise to different cell lineages (modified from Gepstein L, *Circulation Research*. Volume: 91, Issue: 10, Pages: 866-876).

2.2 Generation of induced pluripotent stem (iPS) cells

In 2006 a landmark report by Shinya Yamanaka revolutionized biomedicine and opened up a new era in stem cell biology. It was long thought that cell diversity is unidirectional, namely that primitive cells could differentiate into specialized cells, but the reverse was not plausible. The contrary was proven by the other Nobel prize laureate, John Gurdon, in 1962 with the first reprogramming demonstration of somatic cells to the pluripotent state. The generation of tadpoles was achieved by reprogramming by transplanting nuclei of intestinal epithelial somatic cells of tadpoles into enucleated unfertilized frog egg cells (Gurdon, 1962). Moreover, the fusion of somatic cells with ES cells to generate cells expressing pluripotency genes showed that ES cells possess factors that can reprogram somatic cells (Tada et al., 2001). Based on this observation, Shinya Yamanaka and Kazutoshi Takahashi conducted conclusive reprogramming experiments using retrovirus-mediated gene transduction to deliver reprogramming factors into somatic cells to turn on the expression of pluripotency genes. They

discovered four “Yamanaka factors” which are the sex-determining region Y box-containing gene 2 (Sox2), Oct3/4, tumor suppressor Krüppel-like factor 4 (Klf4), and proto-oncogene c-Myc (Takahashi and Yamanaka, 2006). Yamanaka remarkably created a new type of pluripotent cell termed iPS cells from fully differentiated somatic cells (Takahashi and Yamanaka, 2006). The fundamental importance of this discovery is further underscored by the fact that the Nobel Prize for Physiology and Medicine was already awarded six years later.

The morphology, proliferation, and differentiation potential of the generated mouse iPS cells were comparable to mouse ES cells and characterized by the expression of bonafide pluripotency markers Oct3/4, Nanog, and SSEA1. Upon differentiation, these iPS cells can, akin ES cells, generate all the different somatic cell types and germ cells, thus fulfilling the criteria of pluripotency. For instance, they can differentiate into specific cardiovascular cell types, like endothelial cells and cardiomyocytes (see Fig. 2). Since the beginning of their discovery, it was clear that iPS cells have the potential to serve as a valuable alternative to ES cells in various research and therapeutic applications.

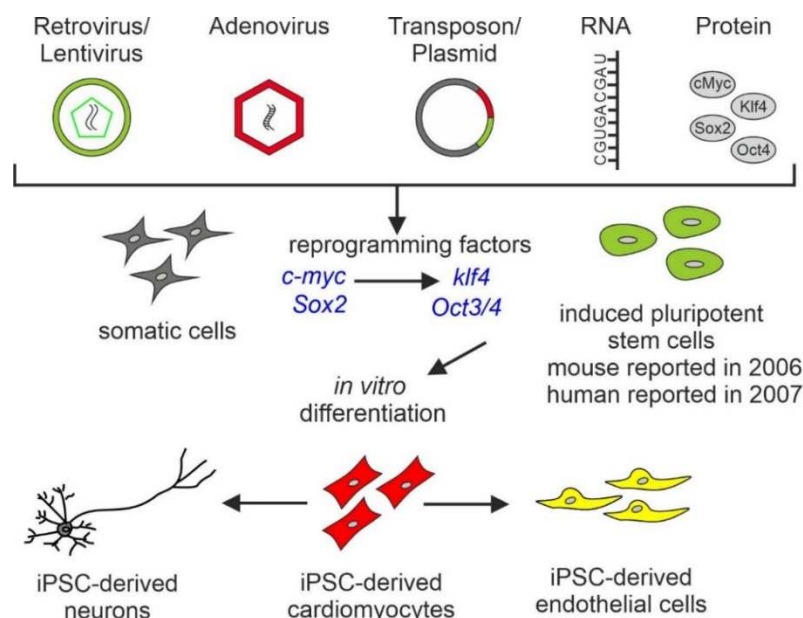


Figure 2 Principle of iPS cell generation: iPS cells can be generated from somatic cells by overexpression of the four factors Oct4, Sox2, Klf4, and c-Myc with integrating (retro- and lentiviruses) and non-integrating (adeno- and Sendai viruses) viral vectors, the use of transposons and polycistronic plasmids, in vitro-derived mRNA molecules or proteins. Both mouse and human iPS were generated with this method, and through in vitro differentiation, different cell types were obtained (modified from Friedrichs et al., 2012).

After the generation of mouse iPS cells, human iPS cells were created just one year later (Yu et al., 2007, Takahashi et al., 2007, Park et al., 2008). This discovery was another important breakthrough in stem cell research because for the first time, it was possible to generate pluripotent stem cell lines that can be patient-specific and serve as disease modeling. Human iPS cells also enable to investigate early developmental steps in humans. In addition, it was also proposed that an unlimited amount of syngeneic human tissue or cells could be generated which could be interesting for therapeutic cell replacement approaches.

Before iPS cell discovery, the prospect of human ES cell research raised in Germany major ethical and legal discussions, particularly concerning the protection of human embryos. In Germany the Embryonenschutzgesetz § 8 ESchG “Act on the Protection of Embryos” governs the use of human ES cells. According to this law an embryo is the already fertilized, viable egg cell and any totipotent cell removed from it. In line with this definition, German law prohibits the use of human embryos for the purpose of generating ES cell lines. This means that the use of surplus embryos from in vitro fertilization procedures to create ES cell lines is also forbidden. However, an important exception exists within the Embryonenschutzgesetz, as the use of human ES cells that were generated abroad prior to a certain date for research purposes is allowed in Germany, provided that these cell lines were obtained from sources that adhered to the ethical standards and regulations of the country where they were derived.

Considering the ethical and legal issues surrounding human ES cell research in Germany, the advent of induced pluripotent stem (iPS) cells brought forth crucial distinctions, the primary one being the source of origin of the cells. The generation of iPS cells through the introduction of reprogramming factors into somatic cells offers a distinct advantage, notably by circumventing ethical concerns. Human iPS cells like all pluripotent cells are able to differentiate into cells of all three germ layers, and mirroring the developmental potential of human ES cells. They can self-renew maintaining their undifferentiated state allowing for the production of large quantities of stem cells.

It has been demonstrated that human ES cells have their own unique genetic identity, whereas human iPS cells retain the genetic identity of the human somatic cells from which they were derived. For instance, iPS cells generated from pancreatic islet β cells maintained an open chromatin structure at key beta cell genes, with a unique DNA methylation signature differing from ES cells and iPS cells derived from other cell types. Thus, a certain persistence of donor cells' gene expression remained (Stadtfeld and Hochedlinger 2010, Bar-Nur et al., 2011).

Even if generating iPS cells is technically simple, multiple transgene integration is required to ensure efficient and successful reprogramming. Each reprogramming factor integrates into the genome at different genomic loci, and the number of integration events can vary between cells. The presence of integrated reprogramming factors in the genome of iPS cells allows for stable and heritable expression of pluripotency-related genes, enabling the cells to maintain their pluripotent state. However, it is important to note that the integration of reprogramming factors using viral vectors carries some limitations and potential risks, such as the possibility of insertional mutagenesis and unpredictable genetic dysfunction potentially affecting their safety and suitability for therapeutic application (Okita et al., 2007, Takahashi et al., 2007).

When iPS cells are fully reprogrammed and pluripotent undergo silencing of the reprogramming factors (Ghaedi and Niklason, 2019). Nevertheless, in human iPS, some residual expression of exogenous factors is still detected in iPS cell lines when reprogrammed by retroviral transduction. This could cause the induction of improper transcriptional changes at the end of reprogramming (Papp and Plath, 2011). After Yamanaka discovery, many studies were conducted to narrow down the use of the four factors, eliminating the oncogenic factor c-Myc, because offspring of chimeric mice showed tumor formation in 20% of all cases (Okita et al., 2007). Indeed, c-Myc-free iPS cells showed a reduced tumor risk formation. However, a difference was noted in the efficiency of pluripotent cell generation, as it was ten times less efficient (0.002%) when iPS cells were generated with only three factors (Oct3/4, Sox2, and Klf4) compared to four (Nakagawa et al., 2008, Wernig et al., 2008). Researchers are continually exploring alternative reprogramming methods to mitigate these limitations and

concerns and improve the efficiency and safety of iPS cell generation (see Fig 2). Nowadays the most common delivery methods mRNA and Sendai virus-based offer non-integrating approaches for introducing reprogramming factors into somatic cells. mRNA-based reprogramming allows for transient expression of the reprogramming factors. Once the proteins are synthesized, they perform their function, but the mRNA is rapidly degraded and eliminated from the cells. Additionally, mRNA-based reprogramming enables precise control over the levels and timing of reprogramming factor expression. By adjusting the concentration and duration of mRNA delivery, researchers can optimize the reprogramming process and increase its efficiency. The Sendai virus is a negative single stranded RNA virus which has been modified to serve as a vector for the reprogramming factors. The virus does not integrate into the host genome. Instead, it delivers the reprogramming factors as RNA molecules, which are eventually degraded and eliminated from the cells. This transient expression reduces the risk of genomic integration and avoids long-term expression of the reprogramming factors, which could interfere with cell behavior or introduce genetic abnormalities. As far as reprogramming efficiency is concerned, mRNA is particularly efficient (2.1%), followed by Sendai virus (0.1%). Considering the success rates (percentage of samples for which at least three iPS colonies have been generated), Sendai viruses are by far better (94%) compared with the mRNA method, in which the success rate was significantly lower (27%). Another clear advantage of the Sendai virus method vs. the mRNA is the less amount of work, as there is no requirement for chemical measures to inactivate the innate immune system and for daily transfections due to the very short half-life of mRNA (Schlaeger et al., 2015). However, most methods so far have been proven to be highly time-consuming and of low efficiency in generating pluripotent ground-state cells (Hou et al., 2013, Prasad et al., 2016).

An alternative approach to speed up the time of generation of specific cell lineages is direct reprogramming. This technology consists in transiently expressing the Yamanaka factors in somatic cells such as fibroblasts with different growth factors or signaling pathway modulators, bringing the cells toward an epigenetically unstable intermediate multipotency stage, thus

avoiding pluripotency, before re-directing it towards the target cell lineage. This kind of reprogramming could use the “non-complete” pluripotent status of the iPS cells and their epigenetic memory to favor the differentiation of cells towards a specific lineage which is challenging to obtain from iPS cell-based in vitro differentiation approaches. Overall, the idea behind direct reprogramming challenges traditional concepts of cell fate and offers a more direct and efficient approach to generate specific cell lineages. One of the potential advantages of direct reprogramming is the bypassing of the pluripotent stage, which can save time and potentially accelerate the process of generating functional cells for various applications and the reduced risk of teratoma formation associated with the pluripotency of iPS cells. However recent reports show that high methylated regions due to inefficient silencing of the somatic cell genes could enhance tumorigenicity (Prasad et al., 2016, Erharter et al., 2019).

Moreover, direct reprogramming could retain epigenetic hallmarks of the cell of origin, for example, ageing hallmarks, making the cells obtained through direct reprogramming more suitable for modelling ageing-related disease (Carter et al., 2020; Wang et al., 2021). Most direct reprogramming protocols work out well to generate so-called induced neural stem cells (called neurospheres) with further differentiation into more mature phenotypes like neurons, astrocytes and oligodendrocytes (Wang et al., 2013, Kim et al., 2011). However, direct reprogramming of cells into cardiomyocytes, specifically using human cardiac fibroblasts, has been found to be less efficient compared to reprogramming of other cell types (Yamanaka, 2020). The underlying reasons for the lower efficiency of direct cardiac reprogramming in human fibroblasts are not yet fully understood. Human cardiac fibroblasts may possess inherent differences in their gene expression profiles, epigenetic modifications, and cellular properties compared to mouse fibroblasts. These differences can affect the reprogramming process and limit the efficiency of cardiomyocyte conversion. Furthermore, the genetic and molecular networks that govern cardiomyocyte development and maturation might be more complex and stringent in human cells compared to mice and functional maturation is challenging and remains a major hurdle in direct cardiac reprogramming. In addition, the

precise combination and dosage of reprogramming factors, as well as the duration of their expression, are critical for successful reprogramming in particular of mesodermal origin. Finding the optimal combination and balance of factors for human cardiac fibroblasts is still an ongoing research endeavor.

2.3 Stem cell differentiation into cardiovascular cells: endothelial cells (ECs)

The differentiation of stem cells into cardiovascular cells holds great promise for regenerative medicine and the treatment of cardiovascular diseases. In order to better target pluripotent cells towards a specific differentiated cell type, it is crucial to understand the principal steps of lineage segregation during embryonic development. The process begins at the blastocyst stage, where trophoblast cells constitute the outer layer of the blastocyst and give rise to extraembryonic tissues. Meanwhile, the inner cell mass differentiates into the epiblast and primitive endoderm. During gastrulation, the epiblast cells give rise to the three germ layers: endoderm, mesoderm, and ectoderm, as well as primordial germ cells. Organogenesis will follow, and each germ layer will develop into different tissues. The neural plate and tube will form from the ectoderm, while the mesoderm differentiates in lateral and somatic plate mesoderm. The first develops into the splanchnic mesoderm comprising the heart and blood islands, the latter segments in somites forming muscle, skeleton, and dermis. The blood islands contain stem cells called hemangioblasts which can give rise to angioblast or hematopoietic cells, differentiating subsequently in the endothelial or hematopoietic lineage.

When working with ES or iPS cells, many protocols refer to the formation of embryoid bodies, which mimic the early stages of embryonic development. After embryoid body formation, signaling pathways are activated to guide the cells towards the development of one of the three germ layers. Subsequently, the cells are pushed further along the desired differentiation pathway. In the context of cardiovascular cells, once the pluripotent cells have been directed towards the mesodermal lineage, specific protocols can be used to further differentiate them into various subtypes of cardiovascular cells. These protocols involve the modulation of

signaling pathways and the provision of appropriate growth factors and culture conditions to mimic the developmental cues that drive cardiovascular lineage specification. Understanding the principles of developmental biology and the stepwise processes involved in differentiation is crucial for guiding pluripotent cells towards specific cell lineages, including those relevant to cardiovascular development.

The dogma of biology, which stated that ECs could originate only from angioblast during embryo development, was overturned in 1997 when endothelial progenitor cells (EPC) were described. Asahara and coworkers first isolated hematopoietic progenitor cells from human blood, which could be differentiated in ECs (Asahara et al., 1997). The expression of CD34 membrane protein characterized these cells. Subsequent studies confirmed the existence of EPCs, these were predominantly localized in bone marrow or at an early stage in the peripheral circulation, which were positive for CD133, CD34, and vascular endothelial growth factor receptor 2 (VEGFR2) surface markers (Peichev et al., 2000, Quirici et al., 2001, Wahl et al., 2007). Nevertheless, EPC biology is still not clearly understood, and there is a lack of a unified definition of EPCs with objective specific markers since many are also expressed in other cell types, and phenotypical characterization of EPCs remains controversial.

Over the years, many different protocols have been applied to induce the differentiation of murine and human ES cells into ECs. As mentioned before the most common approach is the embryoid body (EB) technique which is a very helpful model for studying the developmental steps of vascular generation and angiogenesis. EB formation through the hanging drop method is followed by culture in suspension on day three of differentiation and plating on day five in DMEM media with Fetal Calf Serum (FCS) (Wobus and Boheler, 2005). FCS brings some concerns due to the presence of unknown factors which could have immunogenic potential and brings the risk of pathogen transmission. Additionally, it has been reported that patients who have received cell transplantations with MSCs expanded in FCS exhibit antibodies against bovine antigens (Antoninus et al., 2015). Recently, alternative approaches using standardized human platelet derivatives showed reproducible and beneficial results for growth and expression

of functional ECs in vitro meeting safety requirements for in vivo use (Peters et al., 2022). Sequential application of growth factors such as VEGF alone or in a cocktail with bFGF, IL-6, EPO, Activin A, or bone morphogenetic protein 4 enhanced the endothelial expression markers (Festag et al., 2007). Human iPS cell differentiation protocols into EC are mainly based on the enhancement of mesodermal formation by canonical Wnt signaling pathway activation with CHIR99021 and BMP4, Activin A, VEGF, followed by vascular specification with VEGF and TGF- β inhibitor (Orlova et al., 2014, Lian et al., 2014). In addition to the sequential application of growth factors, cytokines, and small molecules, the overexpression of specific transcription factors can be utilized to drive stem cells towards the EC lineage, such as ETV2 (also known as ER71). Overexpression of ETV2 in pluripotent stem cells or other cell types like human amniotic fluid-derived cells can induce their conversion into ECs (Kim et al., 2023).

Isolation of single ECs from ES or iPS cells is mainly done by fluorescence activated cell sorting (FACS) and immunomagnetic cell sorting (MACS) using endothelial markers such as CD31, VE-Cadherin or VEGFR2 (see Figure 3). Cell cultures of isolated ECs are often difficult, the cells recover poorly from the isolation procedure, and because they are not immortalized cells, they cannot be maintained and expanded except for a few passages. Immortalized lines like HUVEC are preferable for experiments that require more stable and mature cells. HUVECs are known to express more markers such as eNOS, E-selectin, VE-Cadherin and VEGFR2 than EPCs or ECs derived from pluripotent cells, however iPS cell-derived ECs offer the advantages of patient-specificity, disease modeling, genetic manipulation, and developmental studies.

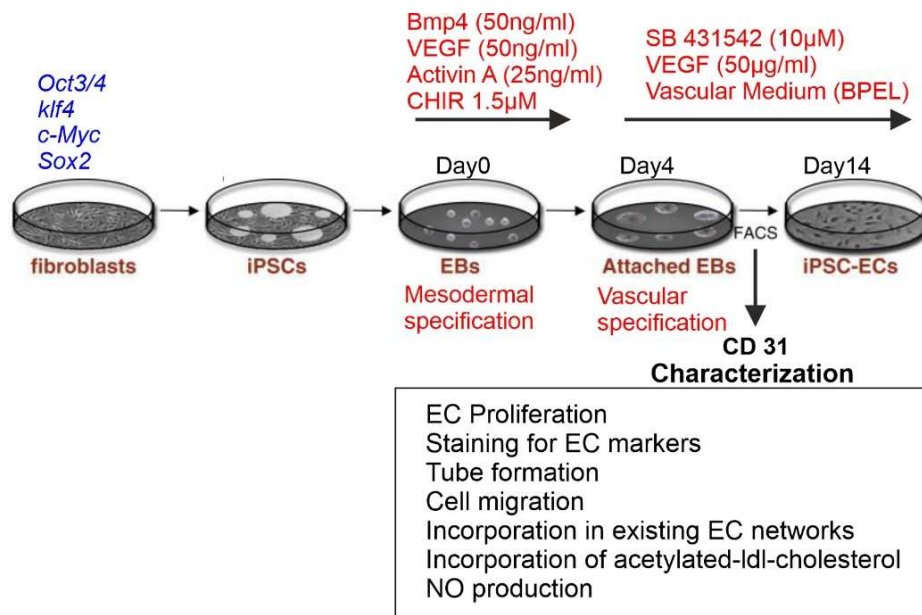


Figure 3 Differentiation of iPS cells into ECs. iPSCs are generated by overexpressing Oct4, Sox2, Klf 4, and c-Myc. Endothelial differentiation is initiated by culturing human iPS cells for 14 days in differentiation media supplemented with bone morphogenetic protein 4 (BMP4) and vascular endothelial growth factor (VEGF). The presence of activin A enhances between days 0 and 3 mesodermal specification. Cells are then FACS using an antibody directed against CD31. The vascular specification is initiated by applying VEGF and the transforming growth factor- β (TGF- β) pathway small-molecule inhibitor SB431542. Characterization of EC function is achieved by analysis of proliferation, the ability to generate capillary-like structures (in matrigel), and the ability to incorporate them in a pre-existing EC network. Other functional tests include the capability of the iPS cell-derived-ECs to incorporate acetylated-LDL cholesterol and to produce nitric oxide. (Modified from Orlova et al., 2014; Volz et al., 2012).

2.4 In vitro differentiation of pluripotent stem cells into cardiomyocytes

Just like the differentiation of ECs, cardiomyocyte differentiation also relies on mesodermal induction as a key mechanism. During embryonic development, the heart is among the first organs to form, mesoderm cells migrate and position themselves between the ectoderm and endoderm within the primitive streak. It is through signals from the adjacent cells, particularly the endoderm, that mesodermal induction is promoted. Factors involved in cardiac specification expressed in the endoderm include members of the transforming growth factor β superfamily, Wingless/INT (Wnt) proteins, and fibroblast growth factors (FGFs).

Mouse ES cell-derived cardiomyocytes were first obtained after removing self-renewal components like leukemia inhibitory factor (LIF) or feeder cells through the aggregation of 400-800 cells into the embryoid bodies (EB) in media with a high content (20%) of fetal calf serum

(FCS). A variation of this protocol consists of spontaneous aggregation in 3D clumps with the dilution of cells in medium with 20% FCS placed on a shaker by so-called mass culture. With this approach higher numbers of cells are obtained. Cardiomyocytes can differentiate spontaneously in this medium, and cardiomyocyte differentiation is stimulated by adding either DMSO, retinoic acid (Wobus et al., 1997), or small molecules like Dynorphin (Ventura et al., 2003). Differentiation in EBs was also performed using mouse iPS cells and human ES with similar medium conditions (Kehat et al., 2001).

The EB-based in vitro differentiation technique as described above proved inefficient for the in vitro differentiation of human iPS cells. One of the first differentiation protocols from human iPS cells to cardiomyocytes involved the mechanical passaging of cellular clumps followed by a co-culture with mouse endoderm-like cells END2. END2 plays an important inductive role in differentiating cardiogenic precursor cells in the adjacent mesoderm in developing embryos. This method has therapeutic limits due to the presence of animal cells and the low yield and purity of tissues (Mummery et al., 2003).

At the beginning of the last decade, the most promising differentiation protocol for cardiomyocytes took advantage of the Wnt signaling modulation. First, the activation of the canonical Wnt signaling enhances β -catenin activation and dissociation, having a positive effect on mesoderm commitment. The activation of the Wnt/ β -catenin signaling is achieved by inhibition of Glycogen Synthase-Kinase 3, Gsk-3 β , by applying CHIR99201 in the medium. The first mesodermal markers, such as Brachyury and Eomesodermin, activate the cardiac mesoderm transcription factor 1, Mesp1. Mesp1 is critical, since it induces Dickkopf Wnt signaling pathway inhibitor 1, which drives cardiac lineage specification. Wnt signaling usually has a biphasic effect; after an initial mesoderm enhancement at early stages, it represses heart development. The repressing Wnt signaling effect on heart development at later stages can be blocked by small molecule inhibitors of Wnt ligand production such as IWP (blocks Wnt protein secretion and activity) and Wnt antagonists such as C59 (Lian et al., 2012, 2013; Ueno et al., 2007; Zhao et al., 2019). Lian and colleagues (Lian et al., 2012) established a

breakthrough protocol which is precisely based on this biphasic action of Wnt. They sequentially activated the canonical Wnt signaling by Gsk-3 β inhibitor treatment and later inhibited Wnt pathways for cardiac specification by small molecules like IWR and XAV939 (Lian et al., 2012). Moreover, they observed that the B27 supplement without insulin is essential to expand the cardiac population (see Figure 4). Later protocols from this group proposed that the addition of putrescine, progesterone, and sodium selenite instead of albumin because of animal derivation, combined with the reduction of the CHIR and IWP-2 concentrations enhances cardiac differentiation (Lian et al., 2015). In contrast recent protocols recommend the addition of albumin in order to achieve a more robust cardiomyocyte differentiation (Lin and Zou, 2020). Together with the group of Greber (Zhang et al., 2015), we also worked on this topic and explored essential cardiac differentiation requirements to obtain bulk expansion, which could be helpful for drug screening and also cell transplantation approaches. This approach is also based on the modulation of the Wnt signaling pathway with CHIR99201 as activator, and IWP2 or C59 as inhibitors best applied at days 2-3. In addition, efforts were made to minimize the presence of expensive additives such as B27 by replacing them with other serum-free media (Knock-out DMEM) (see Figure 4) providing a high yield of 50 and 75% cells (Zhang et al., 2015). A significant improvement for the generation of large numbers of cells is achieved by a low seeding of differentiated cardiomyocytes. In this case, contact inhibition is removed, and the application of CHIR99201 acts as a mitogen, giving massive cardiomyocyte production with up to 241-fold increase from day 12 to day 42, through induction of proliferation (Buikema et al., 2020).

The development of the differentiation media went from the use of complex sera and feeder layers to chemically defined (RPMI/B27) or serum-free media with small molecules which do not require genetic modification of human iPS cells and have been shown to be effective at modulating the Wnt/ β -catenin pathways (Santoro et al., 2021). The focus for the next generation of cardiomyocyte differentiation protocols will be to identify conditions that are as simple to use and as defined as possible (see also Figure 4 summary).

After cardiac induction, specification, and proliferation, enrichment of cardiomyocytes with a high purity degree is essential to prevent tumor formation in case of cell therapy purposes or to prevent false results by contamination of other cell types in case of drug screenings.

Having said this, a problem of cardiomyocyte in vitro differentiation is that a relatively low yield and mixed cell populations containing different cardiac and other cell types are obtained (Kehat et al., 2001). Therefore, the need for solid enrichment approaches, primarily based on antibiotic selection strategies, was investigated. One of the first attempts was made on murine ES pluripotent cells with the generation of genetically modified ES cells carrying a fusion gene comprised of a cardiac-specific promoter like α MHC and an antibiotic resistance gene like neomycin or puromycin (Klug et al., 1996, Friedrichs et al., 2015). When differentiated into cardiomyocytes, they can be selected by their antibiotic resistance and be purified for a 99% cardiac population. A more elegant approach for purification is possible in human iPS cells. This is due to their ability to metabolize lactate via oxidative phosphorylation. In fact, it has been shown by transcriptome and fluxome analysis that cardiomyocytes can use lactate in TCA metabolism and survive under glucose-depleted and lactate-abundant conditions using lactate as an alternative energy source. Importantly, other cell types cannot do this (Tohyama et al., 2013). When cardiomyocytes differentiated from pluripotent cells are in a glucose-free and lactate medium, it was found that they were the only ones to survive, giving a 95% enrichment in cardiomyocytes compared to around 15% when using simple in vitro differentiation protocols (Tohyama et al., 2013, Kadari et al., 2015).

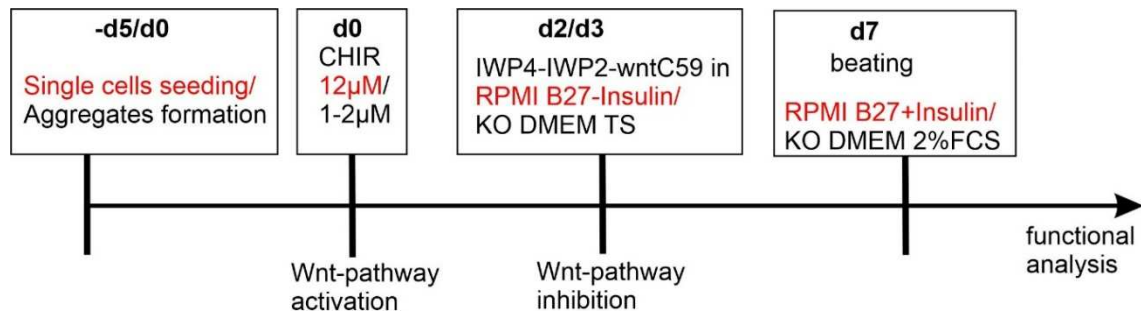


Figure 4. Cardiac differentiation scheme summary using a 2D (single cell) (Lian 2012, red) or 3D (aggregate) (Zhang et al., 2015, black culture). At day 0 (d0), the activation of the Wnt signaling pathway with CHIR99021 is induced. Different media and concentrations of CHIR are used depending on the protocol. Lian (Lian et al., 2012, red) uses RPMI B27 - Insulin. Zhang (Zhang et al., 2015) uses KO DMEM with Insulin Transferrin Selenium. The medium was changed on day 1 or 2, and on day 2 or 3 (d2/3), depending on protocols, small molecules like IWP2, IWP4, or Wnt C59 were added to inhibit the Wnt pathway. After that, cells were maintained in either RPMI/B27 or KO DMEM 2% FCS from day 7 on, where beating cells appeared. Modified from (Lian et al., 2012).

2.5 Pluripotent stem cells as model to investigate early aspects of cardiovascular development and disease mechanisms.

Pluripotent stem cells, including iPS cells and ES cells, offer a valuable platform for studying early aspects of cardiovascular development and unraveling the mechanisms underlying cardiovascular diseases. In my studies summarized in the next chapters I explored whether pluripotent stem cell models offer a valuable tool to study the impact of specific genetic alterations on cardiovascular development and disease. I achieved this by analyzing the electrophysiological properties and signaling pathways in ES cell-derived cardiomyocytes and EC using different knock-out models of extracellular matrix protein evidencing that deletion of integrin-linked kinase in ECs leads to defective receptor tyrosine kinase (RTK) signaling, providing insights into the role of integrin signaling in cardiovascular development (Malan et al., 2013). Furthermore, lack of laminin $\gamma 1$ in mouse ES cell-derived cardiomyocytes results in inhomogeneous spreading of the electrical excitation wave despite intact differentiation and signaling transduction highlighting the importance of extracellular matrix components in cardiac electrical propagation (Malan et al., 2009).

2.5.1 Role of Extracellular Matrix in cardiovascular diseases

Many disease processes in the cardiovascular field are linked to complex multicellular interactions between signaling pathways and ECM proteins as well as cytoskeletal proteins. The fundamental impact of the research on ECM was finally honored by the recognition of the Albert Lasker Award for Basic Medical Research in 2022 for the analysis of multicellular communication by integrin receptors, mediating cell and ECM interactions in physiology and disease. The ECM is a meshwork of proteins surrounding most cells and organs of multicellular organisms forming basement membranes. The main protein components of ECM and basement membrane are proteoglycans (perlecan, aggrecan), collagens, and glycoproteins (fibronectins, laminins, tenascins, elastin, and thrombospondin). There are several ECM-affiliated proteins that comprehend secreted factors such as TGF β and cytokines or ECM regulators such as kinases like integrin-linked kinase (ILK). These proteins constitute the functional units of the ECM (Naba et al., 2016).

Laminins are essential structural molecules in the basement membranes, which are thin layers of ECM surrounding cells. Laminin is a multi-domain, heterotrimer glycoprotein made of 1 α , 1 β , and 1 γ chains. The C-terminus of the laminin α chain binds to cell surface receptors, such as integrins, α -dystroglycan, and sulfated glycolipids. In parallel, intermolecular binding between the adjacent laminins' N-terminus forms a distinct network. Collagen IV self-assembly builds a second network creating a specific mesh by molecular bridges with nidogen, elastins, and perlecan, giving tensile strength and structure to the basement membrane (Glentis et al., 2014, Hohenester and Yurchenco, 2013).

Most ECM macromolecules of the basement membranes can establish highly functional interactions with the cells of tissue through cell surface receptors such as integrins. Integrins are heterotrimeric glycoproteins of two subunits α and β , and are the major receptors for cell adhesion to ECM proteins. Each subunit crosses the membrane once, with most of the glycoprotein residing in the extracellular space and two short cytoplasmic domains. At present, more than ten different β and more than twenty different α subunits have been described. While

β can join numerous α subunits, the latter generally associate only with one type of β subunit. All these complex associations lead to the formation of about 30 different integrin variants. The $\beta 1$ family of integrins, which we investigated more in detail, constitutes the primary collagen and laminin receptors, and through inside-out signaling, integrins play pivotal roles in various cellular processes, including cell growth, division, and survival. By relaying signals from within the cell to the ECM, integrins influence key events such as angiogenesis and repair mechanisms, cell adhesion processes fundamental for tumor progression, but also in terminal maturation and differentiation, intracellular signaling pathways integrity, leukocyte trafficking, and platelets aggregation (Alday-Parejo et al., 2019; Bloch et al., 2001; Kim et al., 2011b).

The cytoplasmic region of $\beta 1$ and $\beta 3$ integrin also interacts with ILK. Despite being classified as a serine/threonine protein kinase, ILK lacks key residues necessary for its catalytic activity. As a result, ILK is often referred to as a pseudokinase. ILK is another component of the ECM molecule complex which can regulate integrin-mediated signaling transduction. ILK consists of three structurally distinct regions. At the NH₂ terminus, four ANK repeats are found. At the COOH-terminal of the ANK domain is a pleckstrin-like motif. The C-terminus domain shows significant homology with other catalytic domains of protein kinases. It binds Paxillin, Parvin, and Pinch, through which ILK connects to the actin in the cytoskeleton, thus building a direct connection between the extracellular environment and the cytoskeleton organization. ILK is localized in the clustering of cytoplasmic regions called focal adhesions mediating the interaction with integrins and downstream signaling pathways like Akt/PKB or Gsk-3. Thus, ILK plays a role in suppressing apoptosis and promoting cell survival (see Figure 5 as a summary of the complex interaction of ECM and cytoskeleton in the cells).

It has been shown that many congenital and age-related cardiac diseases can arise from disturbances of structural ECM proteins or their integrin receptors. It is known that ECM changes significantly after birth, coinciding with the decreased regenerative capacity of tissues. ECM deposition increase is a hallmark of dilated cardiomyopathy, hypertrophy, and heart failure. The structural changes and deposition of the matrix in the fibrotic heart cause slow

conduction areas, triggering life-threatening arrhythmias. The impact of fibrosis in arrhythmogenesis is governed by the extent to which electrical connections between myocytes are disrupted. Cardiac arrhythmias are mainly due to reentry and ectopy. In reentry, one or more waves propagate continuously through the tissue, either in a regular and organized manner (e.g., atrial flutter) or in a more chaotically and irregularly (e.g., ventricular fibrillation). In ectopy, a depolarizing current occurs during diastole in sites with abnormal cardiomyocytes not coupled to healthy cardiomyocytes generating proarrhythmic action potentials.

The role of ECM in signaling pathways regulation and modulation of development through the connections with integrins and the ILK-cytoskeleton axis was further substantiated by the fact that ILK-deficient mice die after implantation due to defects in F-actin distribution blocking the epiblast reorganization (Sakai et al., 2003). Mice with mutations in the paxillin-binding site showed vasculogenesis and growth deficiencies and died at early embryonic developmental stages (Moik et al., 2013). Interestingly, $\beta 1$ integrin deletion in ES cells resulted in defective vascular development with reduced endothelial differentiation because of impact of integrins on vascular signaling pathways such as eNOS or AKT (Malan et al., 2010; Morello et al., 2009). Moreover, in cardiomyocytes, muscarinic signaling is altered due to defective G-protein coupling, in case that $\beta 1$ integrin is lacking during development, as integrin deficiency causes an atypical G_i protein clustering, impairing the function of G_i -associated signaling microdomains and a disruption of the cytoskeletal integrity (Bloch et al., 2001, Malan et al., 2010). In addition, human mutations in the ILK gene also showed endothelial defects, namely dilated vessels, hemorrhages, and heart failure due to disruption of ECs leading to insufficient oxygen supply and cardiomyocyte defects (Wang et al., 2006, Knöll et al., 2007). Similar cardiovascular defects were found in laminin $\alpha 4$ knock-out mice (Knöll et al., 2007). Indeed, the interactions between laminin $\alpha 4$, integrin, and ILK play a fundamental role in maintaining cardiac cell shape and morphology. Several mutations in ILK linked to missense variants (p.H33N, p.H77Y) causing ILK-pinch disruptions have been reported in family members suffering from dilated cardiomyopathy or arrhythmogenic cardiomyopathy. Thus, ILK has

become a relevant gene for genetic diagnosis and counseling patients with hereditary cardiomyopathy (Brodehl et al., 2019).

The role of ECM proteins in many biological processes and for disease motivated me to investigate their pathophysiological relevance in the cardiovascular system. Pluripotent stem cells cultivated in 3D structures, such as EBs or organoids, are highly advantageous for investigating and analyzing ECM defects in vitro. Unlike traditional 2D cell cultures, 3D models provide a more realistic environment in which cells can interact with their surrounding ECM components in a spatially and temporally relevant manner. I could investigate the consequences of laminin $\gamma 1$ disruption, evaluate its arrhythmogenic potential, and elucidate how ILK deficiency affects critical vascular signaling pathways and endothelial development.

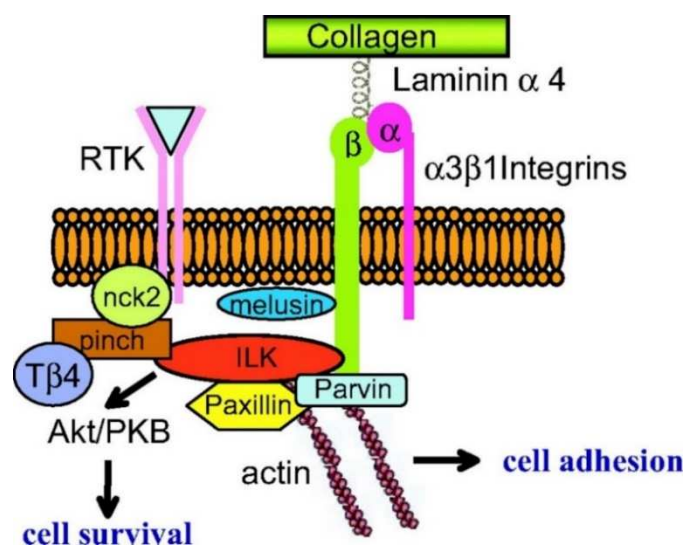


Figure 5: ECM interaction with cytoskeleton: Laminin $\alpha 4$ binds collagen and integrin molecules connected with ILK. ILK links the cytoskeleton via parvin/paxillin, and the activation of laminin-integrin-ILK pathways modulates AKT kinase activity through receptor tyrosine kinase (RTK). Bidirectional signal integration plays a crucial role in cell responses like survival adhesion, migration, and differentiation. From (Knöll et al., 2007).

2.5.2 Pluripotent cells as model for Long QT Syndromes

Human pluripotent cells offer a distinct advantage over animal cells or tissues for disease modeling, primarily due to the fundamental disparities in physiology, metabolism, and immune system. Such variations can potentially influence the severity of disease symptoms and hinder the identification of effective therapeutic compounds. Notably, mice are inadequate models when studying cardiac ion channel diseases and repolarization-related disorders due to their

strongly different action potential characteristics because of differing expression of K⁺ channels and ion channels related to repolarization. Cardiomyocytes derived from the iPS cells obtained from a patient should express the same cardiac channels. Such a property was advantageous in studying monogenetic diseases like long QT syndromes (LQTS), as described later. LQTS are monogenetic cardiac life-threatening pathologies classified into 17 subtypes based on the mutations associated with 15 autosomal dominant genes, known as LQT1-15. Each subtype is associated with mutations in genes coding for ion channels, such as KCNQ1, KCNH2, SCN5A, ANK2, KCNE1, KCNE2, KCNJ2, CACNA1C, CAV3, SCN4B, AKAP9, SNTA1, KCNJ5, CALM1, and 2, respectively (Wallace et al., 2019).

Differentiated cells from patients with monogenetic diseases have the advantage of having clear readouts reflecting the target cells' pathophysiology. For instance, in LQTS, APs shape, and electrophysiological properties have a clear phenotype. First, iPS cells helped me to prove the possibility of creating a cellular model of a specific disease and to investigate the disease-specific arrhythmia phenotype (Friedrichs et al., 2015; Malan et al., 2011). Second, the findings contribute to understanding the disease onset and provide insights into potential therapeutic strategies for LQT diseases (Malan et al., 2016).

The most common LQTS types are LQTS1 and 2 (40–55% and 35–35% of all LQTS patients, respectively), caused by loss of function mutations in the repolarizing K⁺ channels. LQTS1 shows a reduction of the slow delayed rectifier Ks channel, with mutations in the KCNQ1 gene (Shalaby et al., 1997, Gouas et al., 2004, Park et al., 2005, Hedley et al., 2009), whereas LQTS2 results in the reduction of the rapidly activating delayed rectifier Kr channel, due to the mutation in the KCNH2 gene (Hedley et al., 2009, Zhou et al., 1998). These mutations cause trafficking or gating properties alterations or the formation of non-functional channels, therefore are known as loss-of-function mutations. Most LQTS1 patients experience cardiac events during exercise, whereas patients with LQTS2 experience it during emotional events or auditory stimuli.

Gain-of-function mutations can also cause LQTS in depolarizing channels. The most common form (2–8% of LQTS cases) is LQTS3, due to the gain of function mutations in the *Scn5a* gene encoding the alpha-subunit of cardiac voltage-activated Na⁺ channels (Hedley et al., 2009). Due to these mutations, Na⁺ and late Na⁺ currents are increased, and faster recovery from inactivation and reactivation of the Na⁺ current during the late phase of the AP was observed (Makielski, 2016). These biophysical changes in the channel properties favor a prolonged APD that is frequency-dependent and stronger at low heart rates. For this reason, lethal arrhythmias occur in LQTS3 patients preferentially at rest and during sleep (Schwartz et al., 2001). Other less abundant LQTS are caused by mutations of β -subunits of K⁺ channels, the cardiac Ca²⁺ channel, or even cytoskeletal and structural proteins (LQTS4-13) (Hedley et al., 2009).

Studies on LQTS2 showed that differentiated iPS cell-derived cardiomyocytes depict the typical phenotype of LQTS with AP duration increase and EADs upon β -adrenoceptor stimulation. Notably, there was a difference between the cells derived from family members with the same mutations. In the study that investigated the *KCNH2* G1681A (p.Ala561Thr) mutation (Matsa et al., 2011), the mother did not show any EADs in accordance with the clinical data which define the mother as an asymptomatic carrier who presents a prolonged QTc in ECG but does not require therapeutic intervention. In contrast, the daughter needed drug therapy to prevent arrhythmogenic events. From these data, it becomes obvious that significant variations in the phenotype occur in family members, possibly due to additional polymorphisms. In the LQTS2 with a different mutation, the *KCNH2* p.Ala614Val mutation (Itzhaki et al., 2011), iPS cell-derived cardiomyocytes were fundamental to evidence differences in the induction of the arrhythmic events. In the p.Ala614Val mutation, isoprenaline was not an inducer of AP duration shortening and EADs, probably due to different mutation locations in the ion channels. These data evidenced different phenotypes in LQTS2 according to the mutations and, consequently, a possible different therapeutic approach. The study of the group of Matsa demonstrated the importance of the LQTS2 iPS-derived cardiomyocytes as a disease model since β blockers in these cardiomyocytes and patient indeed stabilize the

electrophysiological properties of cardiomyocytes, with less EADs. Moreover, K⁺ channel activators such as nicorandil and PD118057 rescued prolonged action potential. Notably, the study showed how combined treatment with PD118057 and β blockers could be deleterious, leading to excessive shortening of AP duration and enhancing EAD events. Overall, these studies also demonstrated that by using patient-derived cells we can explore the real physiological condition of the patients and that the genetic background can influence the entity of the illness. Considering Matsa's experiments, it was intriguing for us to obtain a cellular model for LQTS3 that would allow the analysis of the phenotype and drugs to indicate the appropriate therapy. The peculiarity of LQTS3 is that it manifests mainly during phases of cardiac bradycardia, but the drug therapy at the time of our studies was still with β -blockers, which logically does not seem appropriate because they act on frequency inhibition. LQTS3 syndrome sparked our interest because, at the time, no one had used iPS cells for modeling that disease, but despite of the fact that cardiac events are less frequent when compared with LQTS1 and LQTS2, LQTS3 are more lethal with a 20% chance of death in these families. To test whether iPS cell-derived cardiomyocytes showed the typical features of the Na⁺ channel gain of function mutation and to generate the disease model, we used and reprogrammed, as a proof of principle, fibroblasts from heterozygous mice carrying the human KPQ deletion in the cardiac Scn5a Na⁺ channel. These mice with the KPQ mutation were reported to show APD prolongation with signs of EADs and development of spontaneous polymorphic ventricular arrhythmias in vivo. At that time, my working hypothesis was to investigate whether iPS cell-derived cardiomyocytes could successfully replicate the disease-specific features of LQTS3 in vitro. At that moment, it remained uncertain whether the phenotype of LQTS3, characterized by complex arrhythmias occurring at low frequencies, could be accurately phenocopied after reprogramming and in vitro differentiation in cardiomyocytes due to their immaturity.

2.6 Summary of Key Challenges Addressed in the Papers

The following results chapter will summarize the published papers on the importance of ES/iPS cells as a model to study the development and differentiation mechanisms of cardiovascular system. I investigated the significance of ECM proteins in development of cardiomyocytes and EC and their connection to disease. To explore the impact of ECM defects, I utilized the EB in vitro differentiation approach. These 3D models proved advantageous over traditional 2D cultures as they more closely mimic the natural environment, allowing for meaningful interactions between cells and their surrounding ECM components. Through this approach, I also investigated how the absence of ILK influences crucial vascular signaling pathways and the development of ECs. Additionally, I studied the effects of disrupting laminin $\gamma 1$ in developing cardiovascular cells and assessed its potential to cause arrhythmias. Subsequently, iPS cells were discovered and at the beginning, my working hypothesis was to investigate whether iPS cell-derived cardiomyocytes could serve as an in vitro model that recapitulate the specific disease phenotype. The study aimed to assess key disease-related features such as APD and EADs, thus establishing an in vitro model that captures these disease-specific characteristics.

In addition, I illustrated how to implement the use of pluripotent cells for screening and therapeutic purposes using an antibiotic resistance-based purification method to obtain a pure population of cardiomyocytes. Moreover, in that study we indicated the possibility to generate non-clonal lines, as a quick method of iPS lines generation. We also tested iPS-derived cardiomyocytes from patients with different mutations in the *Scn5a* gene, verifying that the disease phenotype in cardiomyocytes remains intact in other LQTS3 models. Patient-derived cardiomyocytes were further used to test specific drugs which may help to find adequate or alternative therapies for the patients. Thus, I could show that stem cell-derived cardiovascular cells can recapitulate disease phenotypes in vitro which allows the exhaustive investigation of the disease's molecular mechanisms and the use of pharmacological screening.

3 Results

3.1 Role of extracellular matrix proteins in cardiovascular development using the ES system:

Malfunctions of the proteins of the ECM are responsible for various diseases in the cardiovascular field. For instance, in atherosclerosis, but also in cases of vessel aneurysm, there is a progressive accumulation of disrupted elastins, collagen and lipids that weaken the vessel walls (Iozzo and Gubbiotti, 2018). An interesting molecule belonging to the ECM component is ILK whose deletion causes the disaggregation of the endothelium of vessels (Serrano et al., 2013, Noguchi et al., 2013). Interestingly, the ILK direct interaction partner, $\beta 1$ integrin, show involvement in vascular development, as its deletion causes less development of ECs and vessel network formation. Also, other ECM proteins, such as laminin $\alpha 4$, can alter the structural integrity of cardiac and ECs. Mutations of ILK and laminin $\alpha 4$ create structural defects in cells, which are the basis of dilated or arrhythmogenic cardiomyopathies (Friedrich et al., 2004, Sasaki et al., 2004, Wang et al., 2006, White et al., 2006, Knöll et al., 2007). At the time, when I decided to study the role of ECM in cardiovascular development, the available ILK or laminins knock-out mouse models were mostly general and therefore lethal during embryonic development. The group of Sakai showed that mice lacking the expression of ILK die at perinatal stage because the proper polarization of epiblast cells failed during early embryonic development. Additionally, the study showed that ILK deficiency resulted in the abnormal accumulation of actin filaments in cells, which disrupted their normal functions (Sakai et al., 2003). The Cre-loxP system was then employed to selectively delete ILK in ECs. This was achieved by crossing the ILK-floxed mice with transgenic mice expressing Cre recombinase under the control of an endothelial-specific promoter, such as Tie2-Cre. As a result of this genetic manipulation, ILK expression could be specifically abolished in ECs, but also in these mice embryonic lethality due to placental insufficiency was found (Friedrich et al., 2004). The laminin $\alpha 4$ knock-out mouse survives embryonic development, but about 20% died

at perinatal stage and those surviving had increased mortality due to sudden death (Wang et al., 2006). Many laminins knock-out models, such as for laminin β 1 and γ 1 displayed embryonic or perinatal lethality due to improper basement membrane formation during embryonic development (Smyth et al., 1999, Miner et al., 2004).

Hence, mouse models did not allow dissection of the pathomechanisms exerted by these ECM components on tissues and cells at postnatal stages, as most of these genetic models died prematurely. Therefore, I took advantage of an ES cell line, in which either ILK or laminin γ 1 was knocked out to dissect mechanisms of cardiovascular pathophysiology. Moreover, with the pluripotent ES system, it was possible to get insights into cell interactions and developmental mechanisms when a specific ECM component like ILK or laminin is deleted.

3.1.1 Deletion of integrin-linked kinase in endothelial cells results in defective RTK signaling caused by caveolin 1 mislocation. Development. 2013 Mar;140(5):987-95. DOI: 10.1242/dev.091298. PubMed PMID: 23404105 (IF:6.5).

Aim of the study

This work explores the role of ILK in EC development and function using ILK knock-out (-/-) mouse embryonic stem cells. In mice, a conditional knock-out strategy with the Tie2-Cre-loxP system was employed to selectively delete ILK in ECs. Deletion of ILK in ECs resulted in vascular disruption and impairment (Friedrich et al., 2004). Because the mice die at an early embryonic stage, it was impossible to get mechanistic insights into the molecular interactions that lead to the observed delayed vascular development. Hence, we took advantage of ES cells deficient for ILK (-/-) to study the potential relevance of ILK for EC biology. Our study revealed a strongly reduced formation of vessel-like structures in ILK (-/-) EBs because of defective EC signaling. My working hypothesis based on the known role of ILK in regulating caveolae enrichment into the plasma membrane in keratinocytes. Additionally, given the known modulation of EC signaling by molecules like RAS, nitric oxide, G-proteins, and growth factors (e.g., VEGF) localized within caveolae, it suggests a potential role for ILK in governing signaling regulation through control of caveolae.

Methods and Results

Several studies showed that caveolin-1, a protein component of caveolae, interacts with ILK and regulates cell adhesion and migration in the skin. We therefore hypothesized that ILK modulates the crosstalk between growth factors and their receptors, integrins and signaling microdomains built by caveolae and connected with cytoskeleton components.

ILK deletion caused a substantial alteration of the morphological characteristics of endothelial structures in EB development with a higher proportion of single ECs, with fewer clusters and vessel-like networks in ILK (-/-) than in wild-type EBs. In the absence of ILK, EC properties, including proliferation, apoptosis, and migration, were strongly altered. Specifically, ILK deficiency led to increased levels of EC proliferation and apoptosis, as well as impaired migration during late stages of development. To confirm that these severe EC phenotypic changes were directly caused by ILK deficiency we performed rescue experiments by ILK re-expression in the knock-out ES cell line (see Fig 1, page 989, (Malan et al., 2013)). The ILK dependency of the phenotype was highlighted by a partial rescue in the differentiation of vessel-like structures.

To study the molecular mechanisms underlying the defective EC development, we investigated the expression and distribution pattern of VEGFR2, the main receptor for VEGF involved in vasculo-angiogenesis. ECs were MACS-sorted (M-ECs) with CD31 (PECAM1), a specific endothelial marker, after in vitro differentiation of ILK (-/-) ES cells and wild-type ES cells. VEGFR2 is a Tyrosine kinase receptor (RTK) which triggers the recruitment and activation of phospholipase C gamma (PLC γ), an enzyme that cleaves a membrane-bound phospholipid, phosphatidylinositol 4,5-bisphosphate (PIP2), to generate inositol 1,4,5-trisphosphate (IP3) and diacylglycerol (DAG). IP3 then diffuses to the endoplasmic reticulum (ER), where it binds to IP3 receptors (IP3Rs) and induces the release of stored calcium ions (Ca²⁺) into the cytosol. This results in an increase of cytosolic calcium, which acts as a second messenger to regulate various cellular processes, including metabolism, gene expression and cell proliferation. The M-ECs showed similar VEGFR2 expression in both knock-out and wild-type M-ECs, as

indicated by immunofluorescence and western blot analysis. The phosphorylation of the receptor, which indicates its functionality, was also preserved. To check the downstream signaling pathway in wild-type and ILK (-/-) M-ECs, cytosolic calcium (Ca^{2+}_i) imaging was performed. The VEGF agonist induced an increase of (Ca^{2+}_i) in wild-type cells, whereas ILK (-/-) M-ECs lacked a clear response. The lack of (Ca^{2+}_i) response was also seen by applying other tyrosine kinase agonists such as EGF. In contrast, Bradykinin, a Gq protein coupled agonist, and the direct activation of its downstream signaling target PLC γ were still effective and increased (Ca^{2+}_i). These results proved that ILK deficiency causes defective tyrosine kinase signaling, whereas G-protein coupled receptors and signaling remain unaltered. (See Fig 2 and 3, page 990).

In ECs caveolae are essential and well expressed because they cluster specific signaling molecules, thus allowing the activation of VEGF/PLC γ /PtdIns(4,5)P₂ (PIP₂) downstream signaling pathways. The dependency of signaling clusters on functional tyrosine kinase receptor signaling was corroborated by analyzing lipid rafts disruption by beta-cyclodextrin incubation. Again, VEGF stimulation on cells with damaged lipid rafts lacked the increase of (Ca^{2+}_i). In contrast, the activation of Gq-coupled receptors showed the typical increase of Intracellular Ca^{2+} and intact function. These experiments indicated that the microdomain for Gq signaling remained intact despite caveolae disruption. However, the exact clustering of RTK at the plasma membrane was essential for activating their intracellular signaling pathways (see Fig 4, page 991).

Caveolin 1 is the main constituent of caveolae and was implicated in the ILK phenotype in keratinocytes. Therefore, a caveolin 1-egfp construct was created to study caveolae formation and turnover in ILK (-/-) ECs (see Fig 4, page 991). Fluorescence microscopy analysis of M-ECs transfected with the caveolin 1-egfp fusion protein confirmed differences in the membrane localization and therefore clustering alteration between wild-type and ILK (-/-) cells. The caveolin 1-egfp protein was preferentially close to the plasma membrane in wild-type and randomly distributed to the center near the nucleus in ILK (-/-) cells. The kinetics of clustering

and membrane association was further investigated using Live fluorescence imaging, which showed disruption of the trafficking of caveolin 1-egfp proteins. Most caveolin 1-egfp fusion proteins in ILK (-/-) were stationary, mainly in the region near the nucleus, and only a few were able to reach the plasma membrane (Fig 5, page 992). The average velocities of the caveolin 1-egfp protein were slower in the absence of ILK than in wild-type cells. Thus, striking defects in caveolin 1 dynamics and positioning are due to the lack of ILK structural-functional regulation.

Because of the importance of ILK in regulating caveolin trafficking to the plasma membrane and its role in connecting the cytoskeleton with the extracellular environment, we next investigated whether the defects in caveolin 1 positioning were linked to cytoskeleton dysregulation. The ILK (-/-) M-ECs showed a different distribution of microtubules, especially regarding their interaction with cortical actin, as they were distributed in dense packs positioned in the center and much less in the periphery of the cells. The tips of microtubules did contact the cortical actin network, and actin per se accumulated in the peripheral areas of the cells. The exposition to latrunculin, a potential agent to disrupt lipid rafts and caveolae, corroborated these findings in wild-type cells. Latrunculin disrupts F-actin, and fewer stress fibers were observed after its application. Furthermore, caveolin 1 molecules redistributed to the center of the cells, and the actin network accumulated in the periphery of the cells. This specific pattern recapitulated the ILK (-/-) M-ECs phenotype (Fig 6, page 993).

Thus, the data reveal that the organization of both microtubules and actin networks is disrupted in ILK (-/-) ECs and that the microtubules do not interact with the cortical actin. Moreover, the data indicate cortical actin- and ILK-dependent subcellular distribution of caveolin 1.

Conclusion

We discovered a critical role of ILK in EC biology, particularly in vessel formation and maturation during vasculogenesis. The absence of ILK led to a significant impairment in EC phenotype, characterized by a failure to mature and continue the process of vasculogenesis. Our findings demonstrated that ILK directly influences specific cellular signaling pathways, as

evidenced by the lack of an intracellular Ca^{2+} increase upon activation of VEGFR2 or other RTKs. This is mediated through ILK's regulation of caveolin 1 movement and positioning, which in turn impacts the spatial arrangement of caveolae, signaling microdomains, and downstream signaling components. Additionally, the functional signaling microdomains also strictly depend on correct actin interactions with the microtubules. In summary, ILK plays a pivotal role in tyrosine kinase receptor-dependent signaling, exerting a significant influence on EC development and function by modulating caveolae placement and maintaining the integrity of actin and tubulin subcellular structures.

Development 140, 987-995 (2013) doi:10.1242/dev.091298
 © 2013. Published by The Company of Biologists Ltd

Deletion of integrin linked kinase in endothelial cells results in defective RTK signaling caused by caveolin 1 mislocalization

Daniela Malan¹, Andrea Elischer², Michael Hesse¹, Sara A. Wickström^{3,4}, Bernd K. Fleischmann^{1,*} and Wilhelm Bloch^{2,*}

SUMMARY

Integrin linked kinase (ILK) connects the ILK-Pinch-Parvin complex with integrin adhesion sites. Because of the functional relevance of integrin-linked signaling for endothelial cell (EC) biology, we have explored this pathway in *Ilk*^{-/-} embryonic stem (ES) cells differentiated into ECs and vessel-like structures. We have focused in particular on the mechanistic relevance of ILK-Pinch-Parvin complex-related signaling for EC development and tube formation. Our analysis revealed that the formation of vessel-like structures was strongly reduced in *Ilk*^{-/-} ES cells and that this phenotype could be rescued by re-expression of ILK in ES cells. ECs were MACS sorted from wild-type (WT) and *Ilk*^{-/-} ES cells and functional analysis using intracellular calcium imaging as the read-out yielded a complete lack of vascular endothelial growth factor- and epidermal growth factor-dependent responses. The possibility of a caveolin 1-related defect was investigated by transfecting WT and *Ilk*^{-/-} ECs with a caveolin 1-EGFP fusion protein. Time-lapse microscopy showed that the prominent phenotype is due to altered dynamics of caveolin 1 and to a lack of positioning of caveolin 1 in the vicinity of the plasma membrane and that it is rescued by re-expressing ILK in the *Ilk*^{-/-} ES cells. We also found that the defect is caused by the perturbed organization of microtubules and cortical actin filaments. Thus, ILK is required as a scaffold to allow actin-microtubule interactions and correct positioning of caveolin 1 close to the plasma membrane. This is crucial for signaling compartmentalization in ECs and explains the key role of ILK for EC development and function.

KEY WORDS: Integrin linked kinase (ILK), Endothelial cells, Tyrosine kinase signaling, Mouse

INTRODUCTION

Integrin linked kinase (ILK) is a ubiquitously expressed scaffold protein that functions as a central component and mediator of cell-extracellular matrix (ECM) interactions (Novak et al., 1998). ILK binds the cytoplasmic tail of $\beta 1$ integrin and consists of three structural and functional domains (Dedhar and Hannigan, 1996): five ankyrin repeats at the N terminus, which allow interaction with PINCH; a Pleckstrin-homology (PH) domain; and a C-terminal kinase-like domain (Wickström et al., 2010b). By targeting of the PINCH-Parvin complex to integrin adhesion sites, ILK regulates the engagement and remodeling of the actin cytoskeleton downstream of integrin adhesion (Wickström et al., 2010a; Wickström et al., 2010b). Moreover, there is evidence for direct interactions of ILK with tyrosine kinase receptors (RTKs) via PINCH and the NCK2 adaptor protein (Tu et al., 1998). Thus, ILK links cell-matrix interactions with signals modulating remodeling of the cytoskeleton and is therefore involved in central cell biological processes such as cell adhesion, migration, proliferation, survival and differentiation (Hannigan et al., 2007).

ILK has been also reported to affect endothelial cell (EC) apoptosis, proliferation and migration as well as vascular

development *in vitro* (Friedrich et al., 2004; Vouret-Craviari et al., 2004). In addition, defects in vascular development were observed *in vivo* in ILK-deficient mice (Friedrich et al., 2004). However, despite the EC-specific deletion of ILK, the mice died at an early embryonic stage and, therefore, the molecular defects underlying the observed delay of vascular development could not be determined (Friedrich et al., 2004). A recent publication in keratinocytes has provided new mechanistic insight into the cell biological role of ILK by illustrating its direct involvement in trafficking and its integration into the plasma membrane (Wickström et al., 2010a; Wickström et al., 2010b). Caveolae are present in most cell types, but are particularly abundant in ECs and are known to play a crucial role in EC biology (Cho et al., 2004). The principal component of caveolae in ECs is caveolin 1 and this molecule is known to cluster a great variety of different signaling molecules, e.g. RAS, nitric oxide, G-proteins and growth factors such as vascular endothelial growth factor (VEGF) (Krajewska and Maslowska, 2004). Caveolin 1 assists compartmentalization of signaling pathways by establishing specific lipid microdomains that act as specialized signaling hubs (Balijepalli et al., 2006; Saliez et al., 2008). Integrin-based adhesion has been shown to regulate multiple signaling cascades and to provide crosstalk with growth factors. Therefore, we hypothesized that the involvement of ILK in the formation of lipid rafts and/or caveolin 1 microdomains could be important for this crosstalk (Head et al., 2005; Head et al., 2006). In order to understand the potential relevance of ILK for EC biology, we have investigated EC development and function in *Ilk*^{-/-} embryonic stem (ES) cells. Our study revealed strongly reduced formation of vessel-like structures in *Ilk*^{-/-} embryoid bodies (EBs) because of defective EC signaling. This striking alteration is due to perturbed caveolin 1 positioning in vicinity of the plasma membrane.

¹Institute of Physiology I, Life and Brain Center, University of Bonn, Bonn, NRW, 53105, Germany. ²Department of Molecular and Cellular Sport Medicine, German Sport University, Cologne, NRW, 50933, Germany. ³Paul Gerson Unna Group 'Skin homeostasis and ageing', Max-Planck Institute for Biology of Ageing, Cologne, NRW, 50931, Germany. ⁴Department of Dermatology, University of Cologne, Cologne, NRW, 50931, Germany.

* Authors for correspondence (bernd.fleischmann@uni-bonn.de; w.bloch@dshs-koeln.de)

MATERIALS AND METHODS

Cell culture

The mouse ES cell lines D3 (wild type) and *Ilk*^{-/-} were derived and maintained in culture in hanging drops (Malan et al., 2010). Time after plating was indicated as (5+7) and (5+14) days.

Immunohistochemistry and detection of endothelial cells and vessels

EBs were fixed with 4% paraformaldehyde (PFA) and MACS-sorted ECs (M-ECs) were stained with the antibody rat anti-mouse PECAM-1 (CD31) (1:800; Pharmingen, San Diego, CA, USA). Other antibodies/markers used were: rabbit polyclonal anti-collagen IV (1:500; Acris Antibodies), mouse monoclonal anti-perlecan (1:500; Biotrend, Köln, Germany), mouse monoclonal anti-fibronectin (1:500; Sigma-Aldrich, Munich, Germany), polyclonal rabbit anti-laminin (1:500; Sigma-Aldrich), rabbit polyclonal PLCγ1 (1:50; abcam, Cambridge, UK), rat anti-mouse flk-1 (1:100, BD Pharmingen, Erembodegem Belgium), Alexa Fluor 488 Phalloidin (1:40; Molecular Probes Invitrogen, Karlsruhe, Germany), mouse monoclonal β-tubulin (1:500; Sigma-Aldrich), rabbit polyclonal anti-caveolin 1 (1:500; BD Pharmingen), wheat germ agglutinin conjugate Alexa Fluor 488 (1:500; Molecular Probes Invitrogen). Secondary antibodies were: Cy3- (or Cy2-) conjugated goat anti-rabbit (or goat anti-mouse) Ig (1:1500 and 1:500; Dianova, Hamburg, Germany).

Magnet-associated cell sorting (MACS)

Differentiated ES cells (5+7 days) were dissociated with Accutase (PAA Laboratories, Linz, Austria). The single cells were stained with an endothelial-specific marker, rat anti-mouse-PECAM-1 (also known as CD31), and MACS sorted as previously described (Schmidt et al., 2004). For analysis, the number of cells in 40 defined areas was calculated using a 40× objective on an Axiophot microscope (Zeiss Microimaging, Goettingen, Germany).

Proliferation assay and apoptosis assay

Wild-type and *Ilk*^{-/-} EBs were fixed and stained with rat anti-PECAM-1 as described above. Proliferating cells were detected with the primary antibody rabbit anti-mouse Ki67 (1:150, pAb; Dianova) and apoptotic cells with a rabbit anti-active caspase 3 (1:500, BD Pharmingen). The number of Ki67- or caspase 3-positive-cells within 50 randomly chosen vessel-like tubes was counted as proliferating or apoptotic M-ECs (Müller-Ehmsen et al., 2006).

Morphological analysis, apotome and confocal microscopy

The distribution pattern of extracellular matrix proteins, caveolin 1 and cytoskeletal components, as well as live images, were analyzed by confocal microscopy using the LSM 510 META Zeiss microscope (Zeiss Microimaging) or by an inverted confocal laser scanning microscope (Nikon Eclipse Ti). Alternatively, image stacks were acquired with a fluorescence microscope equipped with the ApoTome (Axiovert 200A, Zeiss Microimaging). Live images were acquired with the confocal laser scanning microscope with one image every second for 50 seconds in total. The analysis of velocity was carried out from the videos with Image J 1.37v (Plug-In: Particle Analysis/Manual Tracking). For every picture, the same caveolin 1-EGFP was marked and the distance was measured. The program assigns to each analyzed particle a random color, which it is not related to the velocity. The velocity was then analyzed with a Gaussian distribution. For evaluation of vascular development, PECAM-positive structures in EBs were counted (Malan et al., 2010). In parallel to the quantification of endothelial tubes we also analyzed the distribution of different PECAM-positive structures in four different EBs at early and late stages. We defined 'endothelial precursors' as single endothelial cell precursors, 'clusters' as aggregates of endothelial precursors and 'vessel-like structures' as a network of tube-like structures with at least five branches. The whole EB was screened and results are given as percentage of all PECAM-positive structures (Malan et al., 2010).

Plastic embedding and electron microscopy

M-ECs were fixed in 4% PFA then treated with 1% uranyl acetate. The specimens were embedded in Araldite (Serva, Heidelberg, Germany). Semi-thin sections (500 μm) were cut and stained with Methylene Blue. Ultrathin

sections (30–60 nm) for electron microscopic observation were processed on a microtome with a diamond knife and placed on copper grids. Transmission electron microscopy was performed using a 902A electron microscope from Zeiss (Zeiss Microimaging).

Protein detection and western blot analysis

For western blotting, samples were submitted to SDS-PAGE and proteins were transferred to PVDF membrane and incubated with specific antibodies. Immunoreactive proteins were detected by the enhanced chemiluminescence detection system (Amersham Biosciences Europe, Freiburg, Germany) and normalized to the actin content. VEGF (PAN Biotech, Aidenbach, Germany) stimulation was achieved by treating the cells for 6 hours with low serum medium (1%), then 20 ng/ml VEGF (PAN Biotech) was applied for 4 minutes. We used a concentration that has been reported to be physiologically relevant in inducing vasculo-angiogenesis (Schmidt et al., 2005; Hagedorn et al., 2004); this concentration also induced a clear Ca²⁺ release from the sarcoplasmic reticulum. Densitometry analysis was carried out using ImageJ software (NIH) and normalized to the actin content. Antibodies used were: rabbit polyclonal anti-caveolin 1 (1:500; Acris Antibodies), rabbit polyclonal anti-GFP (1:500; Santa Cruz Biotechnology, Heidelberg, Germany), rabbit polyclonal anti-VEGFR2 and anti-phosphoY1054-1059VEGFR2 (1:2000; Abcam), mouse monoclonal anti-MAPkinase activated (1:1000; Sigma-Aldrich), rabbit polyclonal anti-MAPkinase (1:1000; Upstate, Merck Millipore, Billerica, MA, USA), rabbit polyclonal anti-phospho-PLCγ1 (Tyr783) antibody (1:500; Cell Signaling Technology, Danvers, MA, USA), rabbit polyclonal anti-PLCγ1 (1:1000; Cell Signaling Technology), mouse monoclonal anti-actin (1:4000; Chemicon Millipore, Billerica, MA, USA).

Migration assay

Migration assay was performed in a modified Boyden chamber. The total number of PECAM-positive migrated cells was counted as well as the number of migrated M-ECs (*n*=6) as described previously (Schmidt et al., 2004).

Generation of transgenic ES cell clones

A pCL-MFG fusion plasmid containing the ILK-EGFP cDNA (provided by R. Fässler, Max Planck Institute of Biochemistry, Department of Molecular Medicine, Martinsried, Germany). By cutting the construct with *EcoRI/NotI*, the EGFP cDNA was excised and subsequently cloned into ABD 15-24 pEGFP-N3/β-actin (BD Biosciences Clontech, Heidelberg, Germany) with ABD 15-24-EGFP excised. The resulting β-actin-ILK-EGFP fusion construct was used for electroporation of ILK-ES cells.

Generation of the caveolin 1-EGFP fusion protein

The caveolin 1 cDNA (*Homo sapiens*, PubMed BC082246) was cloned in-frame upstream of the EGFP cDNA of the pEGFP-1 plasmid (BD Biosciences Clontech), in the *BamHI* restriction site. The CAG promoter from pDRIVE-CAG (InvivoGen, San Diego, CA, USA) was cloned into the *SmaI/SalI* restriction site of the caveolin 1 -EGFP fusion plasmid.

Ca²⁺ imaging

M-ECs were loaded with the intracellular calcium ([Ca²⁺]_i) indicator Fura 2 am (5 μM; Molecular Probes Invitrogen) for 10 minutes at room temperature. The bath solution contained: 140 mM NaCl, 5.4 mM KCl, 1 mM MgCl₂, 1.8 mM CaCl₂, 10 mM HEPES and 10 mM glucose. The emitted fluorescence was monitored using a charge-coupled device cooled camera (TILL Photonics, Planegg, Germany) coupled with an inverted microscope (Axiovert 200M, Zeiss Microimaging). The emission data were analyzed using the Vision software package (TILL Vision 4.0, TILL Photonics). Results are displayed as 340 nm/380 nm ratios after background subtraction. *n* is the number of cells tested. A [Ca²⁺]_i increase of <10% was considered to be 'no response'. M-ECs were in some experiments treated with 2% methyl-beta-cyclodextrin (MbetaCD) for 2 hours at 37°C. All drugs used were from Sigma-Aldrich except for epidermal growth factor (EGF) and VEGF (both from PAN-Biotech) and the PLC activator m-3M3FBS (Calbiochem, Merck Millipore, Darmstadt, Germany).

Statistical analysis

All data are presented as mean±s.e.m. Data analysis was performed using analysis of variance with Bonferroni post-hoc test and/or Student's *t*-test for paired and unpaired data. Significance was considered at a *P*-value <0.05. Calculations of significance were carried out using GraphPad Prism 5 (GraphPad Software, San Diego, CA, USA).

RESULTS

ILK deficiency results in strongly reduced differentiation into endothelial tube-like structures

First, we investigated vascular development in wild-type (WT) and *Ilk*^{-/-} EBs based on the morphological characteristics of endothelial structures at different time points of development. We found a strongly reduced number of PECAM-positive endothelial tubes in the *Ilk*^{-/-} EBs (Fig. 1A) compared with WT controls; *Ilk*^{-/-} ECs were preferentially assembled in clusters (Fig. 1A, middle). Quantitative analysis of the main types of vessel structures (Fig. 1B; see Materials and methods) revealed that WT EBs possessed similar percentages of cells, clusters and vessel-like structures (25%, 33% and 41%, respectively) at 5+7 days (5+7d), whereas in *Ilk*^{-/-} EBs a clearly (*P*=0.002, paired Student's *t*-test) higher proportion of single cells (75.3%, 22.2% and 2.5% for cells, clusters and vessels, respectively) was detected (Fig. 1C). Similarly, at the late differentiation stage (5+14d) lower numbers of vessel-like structures (64.9%, 24.7% and 10.4% for cells, clusters and vessels, respectively) were found in *Ilk*^{-/-} EBs compared with WT EBs (19.4%, 2% and 78.6% for cells, clusters and vessels, respectively; *P*=0.007, paired Student's *t*-test). To prove unequivocally that ILK deficiency caused this defect of vascular development, we generated

stable rescue ES cell lines, in which the CAG promoter drives expression of ILK. In these EBs, the percentage of vessel-like structures increased (30%, 46.9% and 19.3% for cells, clusters and vessels, respectively, at 5+7d; and 10%, 37.5% and 52.5% for cells, clusters and vessels, respectively, at 5+14d), suggesting a partial rescue (see also Fig. 1A, right-hand panel; Fig. 1C).

In order to understand better the observed differences between WT and *Ilk*^{-/-} EBs, we assessed the cell biological properties of the ECs in more detail. We found a significant increase in the rate of apoptosis in *Ilk*^{-/-} ECs at 5+7d (WT: 32.2±12.9, *n*=8 differentiated EBs; *Ilk*^{-/-}: 191.0±38.2, *n*=8), as well as at 5+14d of development (WT: 17.2±3.6, *n*=8; *Ilk*^{-/-}: 124.2±33.6, *n*=8). The proliferation rate was very similar in WT and *Ilk*^{-/-} ECs at the early stage of development (WT: 43.8±6.4, *n*=8; *Ilk*^{-/-}: 38.8±4.2, *n*=8), whereas it was increased in the *Ilk*^{-/-} cells at the late stage (WT: 16.9±4.5, *n*=8; *Ilk*^{-/-}: 59.8±9.5, *n*=8). The migration rate did not differ at 5+7d (WT: 59.2±6.6, *n*=4; *Ilk*^{-/-}: 65.0±13.1, *n*=4), whereas in 5+14d EBs a higher migration of *Ilk*^{-/-} PECAM-positive ECs was seen (WT: 55.0±4.7, *n*=4; *Ilk*^{-/-}: 96.0±16.8, *n*=4). Thus, our data show that ILK deficiency results in a striking impairment of vessel formation. The observed discrepancy between proliferation and apoptosis rates at the late differentiation stage could explain the decreased vessel formation in the *Ilk*^{-/-} EBs.

VEGF signaling is defective in *Ilk*^{-/-} ECs

It is well known that VEGF signaling plays a key role in EC biology and vascular development. The observed phenotype in the *Ilk*^{-/-} EBs prompted us to investigate the expression and distribution pattern of VEGFR2 (KDR – Mouse Genome Informatics) using immunohistochemistry. This analysis did not reveal obvious differences between WT and *Ilk*^{-/-} MACS-sorted endothelial cells (M-ECs) (Fig. 2A). We also quantified VEGFR2 expression by western blotting and found comparable levels in WT and *Ilk*^{-/-} M-ECs (Fig. 2B) [arbitrary optical density (OD)=0.99±0.002 in WT and 0.99±0.01 in ILK, *n*=3]. As normal expression levels of the receptor cannot exclude functional defects, we next assessed the phosphorylation of VEGFR2 in response to VEGF (20 ng/ml). We found that phosphorylation of the receptor occurred in both WT and *Ilk*^{-/-} M-ECs; however, phosphorylation levels before and after stimulation were higher in the mutant cells compared with WT cells (relative expression, arbitrary OD=0.7±0.08 in WT and 0.94±0.08 in WT with VEGF; 1.01±0.07 in *Ilk*^{-/-} and 1.2±0.04 in *Ilk*^{-/-} with VEGF, *n*=3; **P*<0.05), suggesting alterations in the basal regulation of VEGFR2 activity (Fig. 2C).

Because of the preserved VEGF-mediated phosphorylation of the VEGFR2 in *Ilk*^{-/-} M-ECs, we suspected downstream signaling defect(s) and explored the key pathways, namely ERK1/2 (MAPK3/1) and PLC-γ (PLCG1) activation. Similar to VEGFR2, ERK1/2 was phosphorylated in WT and *Ilk*^{-/-} M-ECs (Fig. 2D), but, again, the latter displayed higher phosphorylation levels prior to and post VEGF stimulation (arbitrary OD=0.61±0.03 in WT, 0.81±0.04 in WT with VEGF, 0.78±0.03 in *Ilk*^{-/-} and 0.98±0.07 in *Ilk*^{-/-} with VEGF, *n*=3; **P*<0.05). The overall levels of ERK1/2 remained stable in all conditions (arbitrary OD=1.02±0.01 in WT, 1.01±0.005 in WT with VEGF, 1.03±0.05 in *Ilk*^{-/-} and 0.99±0.04 in *Ilk*^{-/-} with VEGF, *n*=3; supplementary material Fig. S3H).

We determined next the downstream signaling pathway in WT and *Ilk*^{-/-} M-ECs using single-cell [Ca²⁺]_i imaging. The majority (67.1%) of WT M-ECs responded to VEGF (20 ng/ml, applied via a micropipette) with an increase of [Ca²⁺]_i (Fig. 2E, left-hand panel); resting [Ca²⁺]_i was augmented by 57.3±5.8% (*n*=49, Fig. 2E, right-hand panel). By contrast, almost all (99.1%, *n*=90) *Ilk*^{-/-} M-ECs

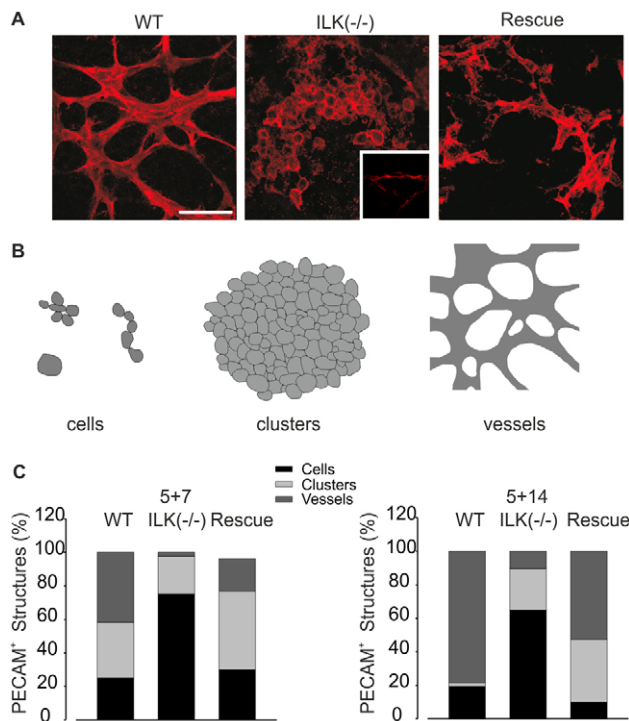


Fig. 1. ILK deficiency results in strongly reduced development and differentiation of endothelial tube-like structures. (A) Endothelial tube-like structures in WT, *Ilk*^{-/-} and ILK-rescued EBs (anti-PECAM staining, red). Inset shows rare, thin, tube-like structure formation. (B) Schematic of different PECAM⁺ structures. (C) Percentage of PECAM⁺ structures at early (5+7) and late (5+14) stages of development. Scale bar: 20 μm.

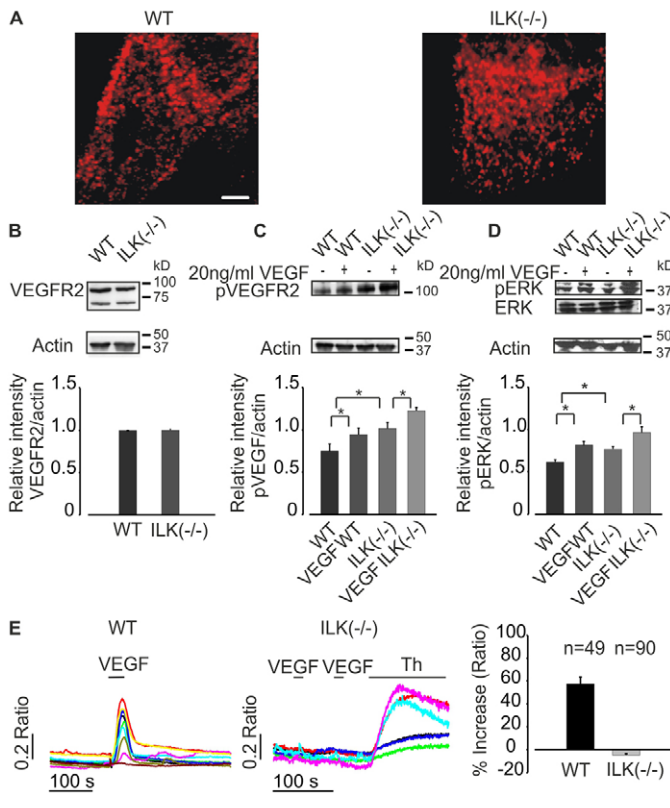


Fig. 2. VEGF signaling is defective in *Ilk*^{-/-} M-ECs. (A) VEGFR2 distribution in WT and *Ilk*^{-/-} M-ECs (anti-VEGFR2 staining, red). (B-D) Western blots of VEGFR2 (B), its phosphorylated form (pVEGFR2) (C) and ERK1/2 as well as its phosphorylated form (pERK) (D) in WT and *Ilk*^{-/-} M-ECs. The densitometric analysis of these western blots is shown below ($n=3$, $*P<0.05$; see also supplementary material Fig. S3H). (E) VEGF (20 nM) evokes an increase of [Ca²⁺]_i in WT (left) but not *Ilk*^{-/-} (middle) M-ECs, whereas thapsigargin (Th; 1 μ M) elevates [Ca²⁺]_i also in M-ECs (middle); representative [Ca²⁺]_i traces are shown, each color labels the 340/380 nm ratio in an individual cell over time. Right: statistical analysis of the percentage increase of [Ca²⁺]_i upon drug application. Error bars represent s.e.m. Scale bar: 5 μ m.

lacked a clear [Ca²⁺]_i response upon application of VEGF (Fig. 2E, middle; the average change in [Ca²⁺]_i was $-4.8 \pm 1.1\%$ ($n=90$, Fig. 2E, right-hand panel). These data suggest that VEGFR2-induced signaling is severely impaired in *Ilk*^{-/-} M-ECs and we therefore explored in more detail the underlying defect.

ILK deficiency causes defective tyrosine kinase signaling

Because of the lack of an increase in [Ca²⁺]_i upon VEGF application in *Ilk*^{-/-} M-ECs, we wondered whether similar signaling defects also occurred with other RTKs in these cells. Indeed, EGF (20 ng) also failed to augment [Ca²⁺]_i in *Ilk*^{-/-} M-ECs in contrast to WT M-ECs; 72.4% of WT cells ($n=21$) showed an EGF-induced increase of [Ca²⁺]_i by $52.2 \pm 10.8\%$, whereas 58 out of 59 *Ilk*^{-/-} cells did not respond to EGF and this is also reflected by the marginal average increase of [Ca²⁺]_i by $2.4 \pm 0.6\%$ (Fig. 3A). Importantly, we could also demonstrate that the defective response to VEGF and EGF was at least partially restored in rescued *Ilk*^{-/-} M-ECs (supplementary material Fig. S1A,B). In fact, the majority of rescued cells (73.3%, $n=33$) responded to EGF and a lower percentage (30.7%, $n=11$) to

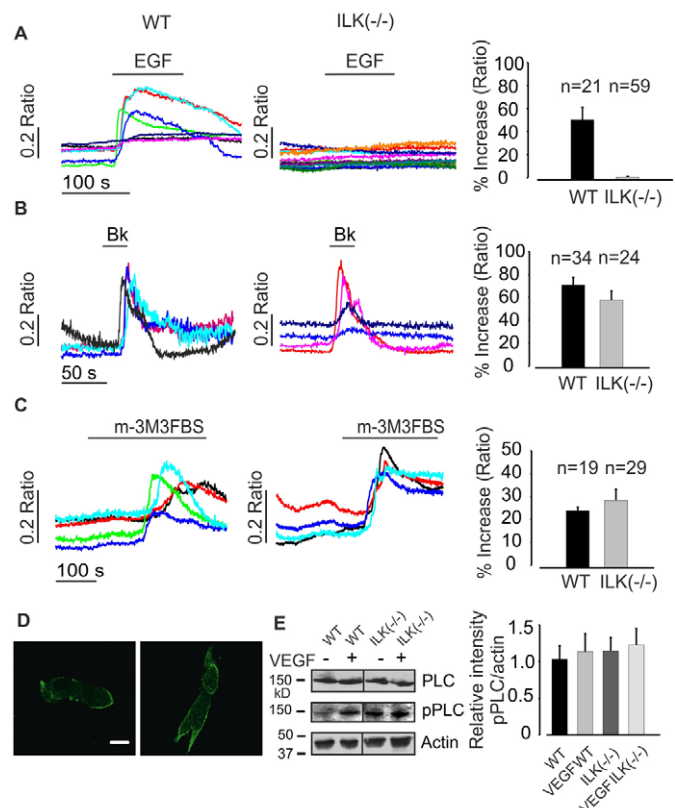


Fig. 3. Tyrosine kinase signaling is defective in *Ilk*^{-/-} M-ECs. (A) EGF (20 nM) evokes an increase of [Ca²⁺]_i in WT but not *Ilk*^{-/-} M-ECs. (B) Bradykinin (Bk, 100 nM) elevates [Ca²⁺]_i in both WT and *Ilk*^{-/-} M-ECs. (C) Direct activation of PLC with m-3M3FBS (25 μ M) also augments [Ca²⁺]_i in WT and *Ilk*^{-/-} M-ECs; each color labels the 340/380 nm ratio in an individual cell over time. For A-C, statistical analyses of the percentage [Ca²⁺]_i increase upon drug application in comparison to control conditions is shown on the right. (D) The cellular distribution of PLC-γ (green) is assessed by immunohistochemistry. (E) Expression analysis of PLC-γ and its phosphorylated isoform (Tyr783) is performed by western blotting (left) and quantified by densitometry (right). Error bars represent s.e.m. Scale bar: 40 μ m. See also supplementary material Fig. S1 and Fig. S3G.

VEGF; the percentage of [Ca²⁺]_i increase amounted to $60.1 \pm 3.1\%$ ($n=33$) and $34.1 \pm 5.4\%$ ($n=11$), respectively (supplementary material Fig. S1C).

Next, we investigated whether other PLC-γ-dependent signaling pathways were also affected by analyzing G_q-coupled agonists. When stimulating M-ECs with bradykinin (100 nM), most of the WT (91.4%, $n=64$) and *Ilk*^{-/-} (67.4%, $n=58$) cells responded with a transient [Ca²⁺]_i response (Fig. 3B) of comparable magnitude. Similar results were also obtained with acetylcholine (ACh; 10 μ M), which showed preserved activation of the [Ca²⁺]_i response in *Ilk*^{-/-} M-ECs (WT: 73.5% of responders, $n=36$; *Ilk*^{-/-}: 69.5% of responders, $n=16$). To pinpoint more precisely the signaling defect, in particular whether it occurred at the receptor level or downstream of the receptor, we used first the direct PLC activator m-3M3FBS. Application of this compound led to an increase of [Ca²⁺]_i in both WT and *Ilk*^{-/-} M-ECs (Fig. 3C), suggesting that PLC-γ and its related downstream signaling components were functional upon direct activation; the percentage of [Ca²⁺]_i increase was $24.7 \pm 1.6\%$ in WT cells ($n=29$) and $29.3 \pm 4.8\%$ in *Ilk*^{-/-} cells ($n=19$) (Fig. 3C, right-hand panel) (WT: 74.4% of responders; *Ilk*^{-/-}: 76% of

responders). We next assessed the PLC- γ distribution pattern in WT and *Ilk*^{-/-} M-ECs by immunocytochemistry and found that it was unchanged (Fig. 3D). Moreover, protein expression analysis of PLC- γ did not reveal significant differences between WT and *Ilk*^{-/-} (Fig. 3E; supplementary material Fig. S3G). In addition, our experiments revealed that VEGF application lead to the phosphorylation of PLC- γ at the Tyr 783 site in WT and *Ilk*^{-/-} M-ECs, indicating intact activation (arbitrary OD pPLC=1.02±0.18 in WT and 1.11±0.24 in WT with VEGF; 1.12±0.18 in *Ilk*^{-/-} and 1.20±0.22 in *Ilk*^{-/-} M-ECs with VEGF; *n*=4; Fig. 3E); the respective numbers are also significantly different (paired *t*-test WT versus WT with VEGF: *P*=0.0117; *Ilk*^{-/-} versus *Ilk*^{-/-} with VEGF: *P*=0.0033). Thus, our experiments showed that ILK plays a crucial role for RTK-dependent signaling in M-ECs.

Caveolin 1 distribution is altered in *Ilk*^{-/-} M-ECs

ILK has been recently reported to play a key role in caveolae formation. As the components of the VEGF/PLC- γ /PtdIns(4,5) P_2 (PIP2) signaling axis are clustered within caveolae in ECs and earlier experiments underscore the crucial role of the clustering of signaling components, we explored the subcellular distribution of components within caveolae. For this purpose, we used double immunohistochemical analysis with the plasma membrane marker wheat germ agglutinin and an antibody against caveolin 1. Caveolin 1 is the main protein component of caveolae in ECs and is essential for caveolae formation (Drab et al., 2001). The stainings illustrated that caveolin 1 is associated with the plasma membrane in WT (Fig. 4A, left-hand panel, see arrow), but not in *Ilk*^{-/-} M-ECs (Fig. 4A, right-hand panel). This important finding was corroborated by electron microscopy. Even though the absolute number of typical caveolar structures is relatively low in cultured M-ECs, we could clearly identify these in close vicinity to the plasma membrane in WT cells, whereas this was not observed at all in any of the *Ilk*^{-/-} M-ECs (60 cells in each preparation were analyzed; *Ilk*^{-/-}: *n*=3 preparations; rescued *Ilk*^{-/-}: *n*=2 preparations; WT: *n*=3 preparations) (Fig. 4B). Interestingly, western blotting experiments showed that the overall expression level of caveolin 1 did not significantly differ between WT and *Ilk*^{-/-} M-ECs (WT: 1.01±0.18 arbitrary OD, *n*=5; *Ilk*^{-/-}: 0.95±0.16, *n*=4; *P*=0.7; Fig. 4D). In addition, even transfection with the caveolin 1-EGFP fusion protein (see also below) did not change the overall expression of caveolin 1 in the cells (WT transfected: 1.01±0.06 arbitrary OD, *n*=7; ILK transfected: 1.02±0.08, *n*=5; *P*=0.7). Because of the lack of caveolin 1 association with the plasma membrane in *Ilk*^{-/-} M-ECs, we investigated whether disruption of caveolin 1 assembly and caveolin 1 microdomain formation in WT M-ECs could reproduce the functional defects observed in the *Ilk*^{-/-} M-ECs. For this purpose, we used beta cyclodextrin (MbetaCD); this compound is a known disruptor of lipid rafts and acts via depletion of cholesterol causing malpositioning of membrane protein complexes (Barbuti et al., 2004; Jang et al., 2001). In agreement with our hypothesis, MbetaCD (2%) prevented VEGF-induced increase of [Ca²⁺]_i in WT M-ECs (*n*=11) (Fig. 4C), whereas, as would be expected (see also Fig. 3B), the bradykinin response was preserved in the MbetaCD-treated *Ilk*^{-/-} M-ECs (Fig. 4C); the percentage of [Ca²⁺]_i increase was 55.5±6.2% in WT cells treated with MbetaCD (*n*=11) with 42.4% of responders, whereas none of the cells tested responded to VEGF stimulation. These data suggest that intact caveolin 1 microdomains in the vicinity of the plasma membrane are required for functional RTK signaling and that deletion of ILK leads to defective caveolin 1 positioning and caveolae formation.

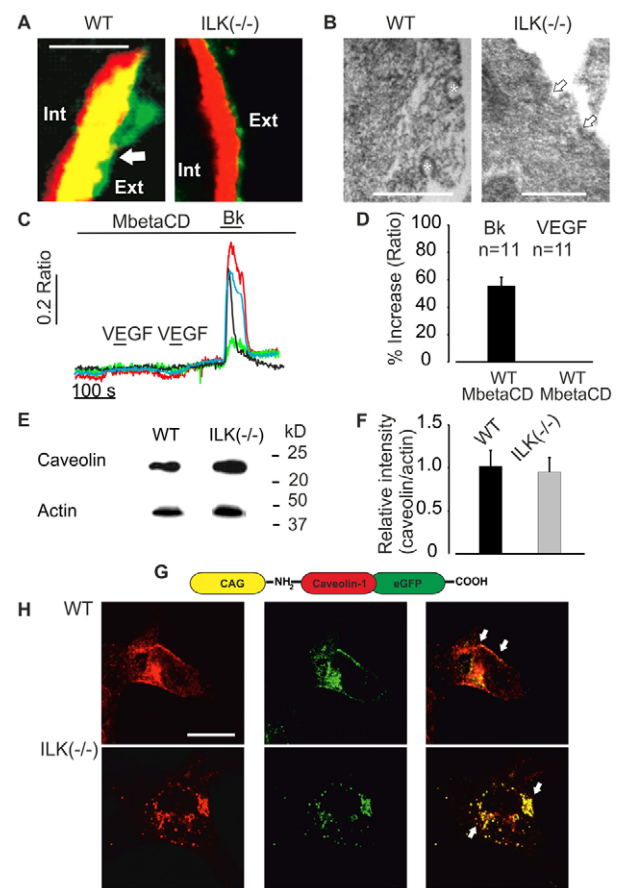


Fig. 4. Caveolin 1 positioning is altered in *Ilk*^{-/-} M-ECs. (A) Caveolin 1 insertion into the plasma membrane in *Ilk*^{-/-} (right) and WT M-ECs (left, arrow) using double staining against wheat germ agglutinin (green) and caveolin 1 (red). Ext, extracellular side; Int, intracellular side. (B) Electron microscopy depicts structures typical for caveolae (asterisks) in WT M-ECs; in *Ilk*^{-/-} M-ECs, only small invaginations of the membrane, but no caveolae, can be detected (arrows, right). (C) VEGF does not evoke an increase of [Ca²⁺]_i in WT M-ECs upon M- β -cyclodextrin (MbetaCD, 2%) treatment, whereas the response to bradykinin remains intact; representative [Ca²⁺]_i traces are shown, each color labels the 340/380 nm ratio in an individual cell over time. (D) Statistical analysis of the percentage of [Ca²⁺]_i increase in WT cells treated with MbetaCD (*n*=11). (E,F) Assessment of caveolin 1 expression using western blotting (E) and its densitometric analysis (F). (G) Scheme of the caveolin 1-EGFP fusion protein under control of the CAG promoter. (H) Immunostaining of native (red) and transfected (green) caveolin 1 in WT (upper) and *Ilk*^{-/-} (lower) cells. Error bars represent s.e.m. Scale bars: 0.5 μ m in A; 4 μ m in B, left; 5 μ m in B, right; 20 μ m in H.

Altered intracellular trafficking and subcellular distribution of caveolin 1 in *Ilk*^{-/-} M-ECs

Because of these findings, we investigated the formation and subcellular localization of caveolae in more detail. To this end, we transfected M-ECs with a caveolin 1-EGFP fusion protein (Fig. 4E). This colocalized with endogenous caveolin 1 in both WT and *Ilk*^{-/-} M-ECs (Fig. 4F, red). We could identify a clear difference in the localization of the caveolin 1-EGFP fluorescence between WT and *Ilk*^{-/-} cells; caveolin 1 had membrane localization in WT cells (Fig. 4H, upper panel, arrows), whereas this was lost in *Ilk*^{-/-} cells (Fig. 4H, lower panel, arrows). This striking difference in the subcellular distribution of caveolin 1 was also confirmed when

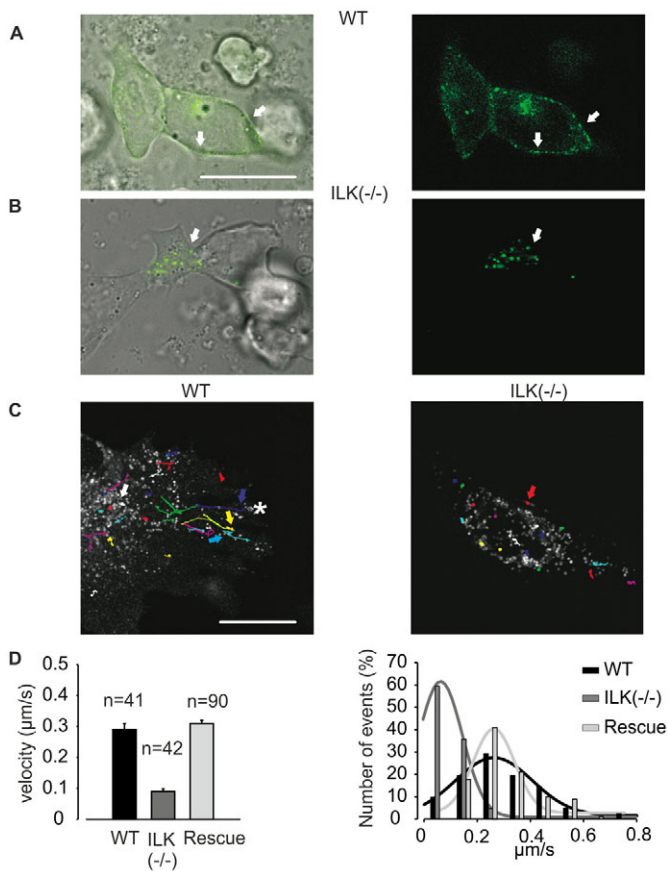


Fig. 5. Defective localization and movement of caveolin 1 in *Ilk*^{-/-} M-ECs. (A,B) Snapshots of WT (A) and *Ilk*^{-/-} (B) M-ECs transfected with caveolin 1-EGFP (green, arrows). (C) Illustration of the movement paths of the caveolin 1-EGFP-positive vesicles. In WT M-ECs ($n=41$ vesicles from four cells), two types of motility are seen: yellow and blue arrows indicate fast long-distance motility in the periphery between the plasma membrane and the cytosol (dark-blue arrow), whereas white arrows indicate slow movement at the center or close to the plasma membrane (asterisk). In *Ilk*^{-/-} M-ECs ($n=42$ vesicles from four cells), the red arrow indicates the typical static movement pattern of fusion proteins in the cytosol and beneath the plasma membrane. (D) Left: average velocities of fusion proteins in WT, *Ilk*^{-/-} and rescue M-ECs. Right: distribution of the different velocities (0 to 0.8 μm/s). Error bars represent s.e.m. The images shown are snapshots taken from supplementary material Movies 1 and 2. Scale bars: 20 μm. See also supplementary material Fig. S2 and Fig. S3E,F.

acquiring with live imaging apotome sections of whole M-ECs. The caveolin 1-EGFP signal was preferentially close to the cell membrane in WT (Fig. 5A, arrows), but was in the center of cells in *Ilk*^{-/-} M-ECs (Fig. 5B, arrows). The idea that ILK determines caveolin 1 formation and its subcellular positioning was further corroborated by analyzing the caveolin 1-EGFP-transduced ILK-rescued M-ECs, in which membrane localization of the fusion protein was similar to that in WT cells (supplementary material Fig S3A-D, arrows). We next investigated the dynamics of caveolin 1 positioning and their subcellular movements using confocal time-lapse microscopy. In WT M-ECs, trafficking of the caveolin 1-EGFP proteins from the cytoplasm to the cell surface was observed (Fig. 5C, left-hand panel; supplementary material Fig. S2A and Movie 1). More detailed analysis of the movement of caveolin 1 revealed that it was slower in the center (Fig. 5C, left-hand panel,

white arrowhead) and faster with curvilinear itineraries in the periphery of M-ECs (see Fig. 5C, left-hand panel, yellow and blue arrowheads), which is consistent with earlier studies (Mundy et al., 2002); occasionally retrograde movement of caveolin 1 protein from the plasma membrane to the center of the cell was observed (Fig. 5C, left-hand panel, dark-blue arrow; supplementary material Fig. S2A, green arrow, and Movie 3). Importantly, most fusion proteins were stationary upon reaching the submembrane localization (Fig. 5C, left-hand panel, asterisk). In clear contrast, in *Ilk*^{-/-} M-ECs the majority of caveolin 1-EGFP molecules were found to be immobile and remained stationary preferentially in the perinuclear region (Fig. 5C, right-hand panel; supplementary material Fig. S2B, red arrowhead, and Movies 2, 4); only very few caveolin 1-positive vesicles reached the plasma membrane. These findings were confirmed by quantifying the movement kinetics of EGFP-tagged caveolin 1. In WT cells, the velocity ranged from 0.06 to 0.72 μm/second whereas in *Ilk*^{-/-} cells it was in the range of 0.003 to 0.28 μm/second (Fig. 5D). Thus, the average velocity of caveolin 1-positive vesicles in *Ilk*^{-/-} M-ECs was significantly lower (0.09 ± 0.01 μm/second for $n=42$ vesicles from four cells) than in WT (0.29 ± 0.02 μm/second for $n=41$ vesicles from four cells). In the rescue M-ECs, movements of the caveolin 1 particles were similar to those in the WT cells, showing curvilinear pathways from the periphery to the central areas of the cells and vice versa (supplementary material Fig. S3F). In addition, treatment with the ryanodine receptor agonist caffeine (2 mM) did not strongly disrupt the movements of caveolin 1-positive particles, excluding the possibility that altered $[Ca^{2+}]_i$ homeostasis was responsible for the disturbed caveolin 1 vesicle movement and positioning. In fact, the average velocity of caveolin 1-positive vesicles in rescue M-ECs was similar to that of WT (0.31 ± 0.01 μm/second for $n=90$ vesicles from ten cells) and of caffeine-treated cells (0.35 ± 0.02 μm/second for $n=65$ vesicles from six cells) (see also supplementary material Movies 5,6). The range of velocities in the rescue cells was 0.12–0.64 μm/second with a similar Gaussian distribution to the WT; also, caffeine-treated cells displayed a similar range of velocities (between 0.14 and 0.88 μm/second) as did the WT and the rescue cells. Thus, these data point to striking defects in caveolin 1 dynamics and positioning in *Ilk*^{-/-} M-ECs.

Deletion of ILK affects the organization of actin filaments and microtubules

Because of the well-known role of ILK for cytoskeletal integrity and its importance for the trafficking of caveolin 1 to the plasma membrane (Wickström et al., 2010a; Wickström et al., 2010b), we explored whether this was also in ECs mechanistically linked to an impaired interaction of microtubules (MTs) with the cortical actin network. We investigated the distribution of actin and MTs in *Ilk*^{-/-} cells and determined whether alterations in the architecture of the cytoskeleton could be detected. In WT cells, the MTs exhibited a clear distribution pattern extending from the center of the cells to sub-plasma membrane regions (Fig. 6A, left-hand panel). By contrast, the MTs in *Ilk*^{-/-} cells (Fig. 6A, right-hand panel) revealed an altered orientation with dense packs of MTs being positioned in the center of M-ECs; in addition, the peripheral density of MTs was decreased. Importantly, we also found that the MT tips in *Ilk*^{-/-} cells were not able to contact and interact with the cortical actin network (Fig. 6B, right-hand panel), whereas the well-organized MTs of WT cells extensively aligned with the cortical actin at the cell periphery (Fig. 6B, left-hand panel, arrows). Together, these data indicate that the interaction of MTs

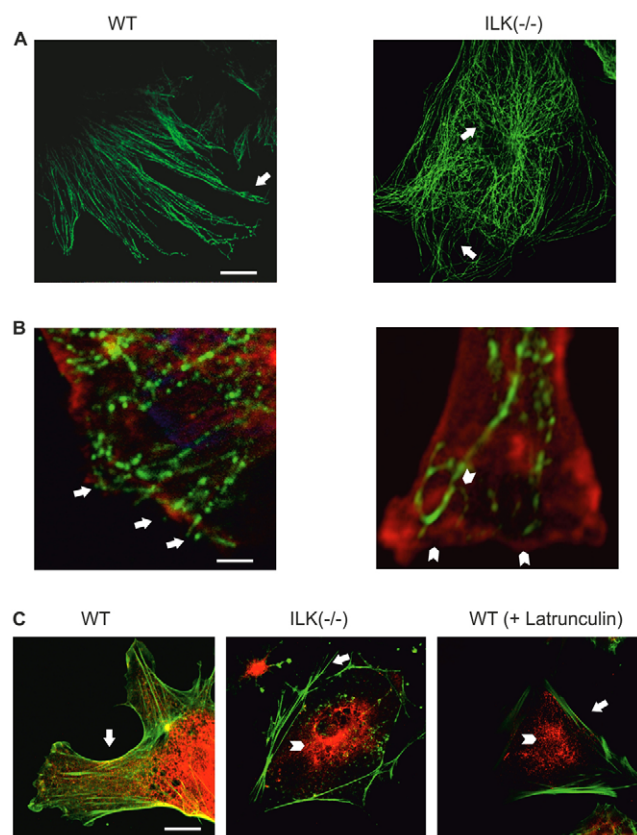


Fig. 6. Loss of ILK affects the subcellular organization of actin filaments and of MTs. (A) Confocal sections of WT and *Ilk*^{-/-} M-ECs stained for tubulin to mark MTs (green). Arrows indicate MT pattern. (B) Double immunostaining with actin (red) and tubulin (green) in WT (arrows) and *Ilk*^{-/-} (arrowheads) M-ECs. (C) Analysis of colocalization of caveolin 1 (red) and actin filaments (phalloidin, green) in WT (left) and *Ilk*^{-/-} M-ECs (middle). Latrunculin (1 μ M, 30 minutes) treatment of WT M-ECs results in re-positioning of caveolin 1 (arrowhead) to the perinuclear area (right). Scale bars: 20 μ m in A; 5 μ m in B, left; 2.5 μ m in B, right; 40 μ m in C, left; 20 μ m in C, middle and right.

with the cortex is impaired in the absence of ILK. In WT M-ECs, a typical regular distribution of stress fibers (Fig. 6C, arrow) was detectable throughout the cell, and caveolin 1 (red in Fig. 6C, left-hand panel) colocalized with the cortical actin fibers. By contrast, in *Ilk*^{-/-} cells (Fig. 6C, right-hand panel) actin was found to be disorganized and to accumulate within the peripheral areas of the cells, whereas caveolin 1 staining displayed a central distribution similar to the native protein (Fig. 4G; Fig. 5B; supplementary material Fig. S2B). Thus, these data reveal that the organization of both MT and actin networks are disrupted in *Ilk*^{-/-} ECs and that the MTs do not interact with the cortical actin. Similar to our functional experiments, we explored next whether disruption of F-actin in WT cells reiterates the phenotype found in *Ilk*^{-/-} M-ECs. For this purpose, we exposed WT cells to latrunculin (1 μ M) for 30 minutes and thereafter investigated actin and caveolin 1 distribution. We observed disrupted actin organization with only a few stress fibers visible and a re-distribution of caveolin 1 molecules to the center of the cells colocalizing with the cortical actin network. These data are reminiscent of those found in *Ilk*^{-/-} M-ECs (Fig. 6C, left-hand panel), indicating a cortical actin- and ILK-dependent subcellular distribution of caveolin 1.

DISCUSSION

Here, we demonstrate that deletion of ILK results in a strong reduction of endothelial tube formation. This prominent EC phenotype is caused by defective trafficking of caveolin 1 to the plasma membrane resulting in defective VEGF signaling. This disturbance of RTK signaling is due to changes in MTs and cortical actin organization giving rise to the destabilization of caveolin 1 microdomains.

Ilk^{-/-} EBs display a striking reduction of endothelial tube formation with alterations of EC proliferation, apoptosis and migration. This phenotype was, as demonstrated by rescue experiments, clearly related to the ILK deficiency. Because key events of EC biology are regulated by VEGF signaling, we have investigated expression and function of VEGF-coupled receptor 2 (VEGFR2) and downstream signaling pathways (Bhattacharya et al., 2009). Ca^{2+} imaging was employed to explore VEGF signaling in single M-ECs and revealed that there was no VEGF-induced $[\text{Ca}^{2+}]_i$ response in mutant cells. This proved to be a more general defect of RTK signaling as EGF was also unable to mobilize $[\text{Ca}^{2+}]_i$ in these cells. Further experiments revealed that VEGFR2 is expressed and functional and that the signaling defect resides downstream. Interestingly, VEGFR2 and ERK1/2 displayed increased basal phosphorylation levels and this is in full agreement with earlier reports on the effects of MbetaCD treatment (Barbuti et al., 2004) or inhibition of ILK activity (Ruiz-Torres et al., 2006). Because of the intact phosphorylation of VEGFR2 and of PLC- γ upon VEGF stimulation and the preserved intracellular Ca^{2+} handling in *Ilk*^{-/-} cells, we suspect that defective crosstalk between signaling components, most likely between PLC- γ and PIP2, underlies the observed phenotype. In fact, in ECs these signaling components are clustered within caveolin 1-enriched microdomains and their disruption inhibits PIP2 turnover. (Jang et al., 2001; Pike and Miller, 1998). Recently, it has been also shown that changes in caveolae density and function, or disruption of the cytoskeletal integrity perturb the compartmentalization of PIP2 signals (Cui et al., 2010). Future experiments are needed to explore the signaling defect in more detail; in particular, activation of PLC- γ and its crosstalk with PIP2 should be assessed using biochemical *in vitro* activity assays. Similarly, the distribution and concentration of PIP2 in the plasma membrane also needs to be explored with and without VEGF activation.

Recently, ILK has been reported to be involved in caveolae organization in keratinocytes (Wickström et al., 2010a). Our present findings reveal that ILK plays a crucial role for the correct subcellular positioning of caveolin 1 in close vicinity of the plasma membrane of M-ECs and illustrate the consequences of its deletion for cytoskeletal integrity, cellular signaling and EC biology. We also mimicked the defective VEGF signaling found in *Ilk*^{-/-} M-ECs by the treatment of WT cells with MbetaCD and these experiments underscore the specific role of lipid rafts in the organization of this signaling pathway. These findings are in line with earlier reports, in which PLC- γ phosphorylation was found to be preserved despite the disruption of plasma membrane microdomains, whereas PIP2 function was reported to be strongly dependent on their clustering and on the integrity of the cytoskeleton (Jang et al., 2001). Although G protein-coupled receptors are known to be coupled with caveolae (Razani et al., 2002), these receptors are affected in a different fashion by caveolar malfunction. In fact, disruption of caveolae by MbetaCD in adult cardiomyocytes affects the β 2- but not the β 1-adrenoceptor-mediated response (Calaghan et al., 2008), possibly explaining why neither acetylcholine nor bradykinin signaling was affected in *Ilk*^{-/-} M-ECs.

As the signaling defects observed in *Ilk*^{-/-} M-ECs were associated with caveolin 1 microdomains, we subsequently explored caveolin 1 positioning and caveolae formation using a variety of cell biological assays. Electron microscopy and high-resolution fluorescence microscopy revealed that *Ilk*^{-/-} M-ECs lacked caveolin 1 at the plasma membrane and sites of caveolae formation, respectively. This was corroborated by time-lapse microscopy of fluorescence-labeled caveolin 1, the central protein component of caveolae (Drab et al., 2001). We observed a clear difference in motility of caveolin 1-positive vesicles of *Ilk*^{-/-} M-ECs compared with WT cells. Rapid trafficking of caveolin 1 between the cytosol and the plasma membrane was observed in WT M-ECs, which is in accordance with previous studies and is associated with the high turnover of this protein in the cytosol (Mundy et al., 2002). This was further corroborated in our rescue M-ECs, in which re-expression of ILK restored caveolin 1 particle movement to that observed in WT cells. By contrast, a strong reduction of caveolin 1 transport to the cell membrane could be observed in *Ilk*^{-/-} M-ECs. Also, in keratinocytes caveolin 1 distribution was found to be dependent on ILK; in addition, its impact on MT stability via mDia1 DIAP1 – Mouse Genome Informatics) and IQGAP1 has been shown (Wickström et al., 2010a). MTs, in concert with the cortical actin network, are assumed to act as tracks for caveolin 1-positive vesicles, and MT-cortical actin crosstalk is required to enable the transfer of caveolin 1 via cortical actin to the plasma membrane, resulting in the formation of caveolae (Mundy et al., 2002; Wickström et al., 2010a). In *Ilk*^{-/-} M-ECs, we found abnormal organization of the actin cytoskeleton and MT network causing reduced MT-actin interactions. To confirm that the defects in the transport of caveolin 1 observed by time-lapse microscopy resulted from abnormal MT-actin crosstalk, we inhibited actin polymerization using latrunculin. Treatment of WT M-ECs with latrunculin led to disruption of the actin cytoskeleton as well as to re-distribution of caveolin 1 and this was reminiscent of the findings in the *Ilk*^{-/-} M-ECs. By contrast, depletion of intracellular Ca²⁺ stores with caffeine did not strongly alter subcellular caveolin 1 dynamics. These data support the view that ILK acts in ECs as a direct scaffolding protein for actin and MT organization, and that ILK-dependent maintenance of cytoskeletal integrity is crucial for the transport, positioning and turnover of caveolin 1 in close vicinity of the plasma membrane; these findings also support those recently reported in keratinocytes (Wickström et al., 2010a). Thus, our data demonstrate that ILK in ECs, through its regulation of caveolin 1 movement and positioning, directly interferes with specific cellular signaling pathways, in particular RTK-mediated signaling, and that intact RTK signaling requires the precise spatial positioning of downstream signaling components.

Acknowledgements

We thank Dr P. Sasse (Institute of Physiology 1, Bonn) for experimental advice; and A. Voß (German Sport University, Cologne) for technical help.

Funding

This work was supported by a grant from the German Research Foundation (DFG) [1086 419/1-2BL to W.B. and B.K.F.].

Competing interests statement

The authors declare no competing financial interests.

Supplementary material

Supplementary material available online at

<http://dev.biologists.org/lookup/suppl/doi:10.1242/dev.091298/-DC1>

References

- Balijepalli, R. C., Foell, J. D., Hall, D. D., Hell, J. W. and Kamp, T. J. (2006). Localization of cardiac L-type Ca(2+) channels to a caveolar macromolecular signaling complex is required for beta(2)-adrenergic regulation. *Proc. Natl. Acad. Sci. USA* **103**, 7500–7505.
- Barbuti, A., Gravante, B., Riolfo, M., Milanesi, R., Terragni, B. and DiFrancesco, D. (2004). Localization of pacemaker channels in lipid rafts regulates channel kinetics. *Circ. Res.* **94**, 1325–1331.
- Bhattacharya, R., Kwon, J., Li, X., Wang, E., Patra, S., Bida, J. P., Bajzer, Z., Claesson-Welsh, L. and Mukhopadhyay, D. (2009). Distinct role of PLCbeta3 in VEGF-mediated directional migration and vascular sprouting. *J. Cell Sci.* **122**, 1025–1034.
- Calaghan, S., Kozera, L. and White, E. (2008). Compartmentalisation of cAMP-dependent signalling by caveolae in the adult cardiac myocyte. *J. Mol. Cell. Cardiol.* **45**, 88–92.
- Cho, C. H., Lee, C. S., Chang, M., Jang, I. H., Kim, S. J., Hwang, I., Ryu, S. H., Lee, C. O. and Koh, G. Y. (2004). Localization of VEGFR-2 and PLD2 in endothelial caveolae is involved in VEGF-induced phosphorylation of MEK and ERK. *Am. J. Physiol.* **286**, H1881–H1888.
- Cui, S., Ho, W. K., Kim, S. T. and Cho, H. (2010). Agonist-induced localization of Gq-coupled receptors and G protein-gated inwardly rectifying K+ (GIRK) channels to caveolae determines receptor specificity of phosphatidylinositol 4,5-bisphosphate signaling. *J. Biol. Chem.* **285**, 41732–41739.
- Dedhar, S. and Hannigan, G. E. (1996). Integrin cytoplasmic interactions and bidirectional transmembrane signalling. *Curr. Opin. Cell Biol.* **8**, 657–669.
- Drab, M., Verkade, P., Elger, M., Kasper, M., Lohn, M., Lauterbach, B., Menne, J., Lindschau, C., Mende, F., Luft, F. C. et al. (2001). Loss of caveolae, vascular dysfunction, and pulmonary defects in caveolin-1 gene-disrupted mice. *Science* **293**, 2449–2452.
- Friedrich, E. B., Liu, E., Sinha, S., Cook, S., Milstone, D. S., MacRae, C. A., Mariotti, M., Kuhlencordt, P. J., Force, T., Rosenzweig, A. et al. (2004). Integrin-linked kinase regulates endothelial cell survival and vascular development. *Mol. Cell. Biol.* **24**, 8134–8144.
- Hagedorn, M., Balke, M., Schmidt, A., Bloch, W., Kurz, H., Javerzat, S., Rousseau, B., Wilting, J. and Bikfalvi, A. (2004). VEGF coordinates interaction of pericytes and endothelial cells during vasculogenesis and experimental angiogenesis. *Dev. Dyn.* **230**, 23–33.
- Hannigan, G. E., Coles, J. G. and Dedhar, S. (2007). Integrin-linked kinase at the heart of cardiac contractility, repair, and disease. *Circ. Res.* **100**, 1408–1414.
- Head, B. P., Patel, H. H., Roth, D. M., Lai, N. C., Niesman, I. R., Farquhar, M. G. and Insel, P. A. (2005). G-protein-coupled receptor signaling components localize in both sarcolemmal and intracellular caveolin-3-associated microdomains in adult cardiac myocytes. *J. Biol. Chem.* **280**, 31036–31044.
- Head, B. P., Patel, H. H., Roth, D. M., Murray, F., Swaney, J. S., Niesman, I. R., Farquhar, M. G. and Insel, P. A. (2006). Microtubules and actin microfilaments regulate lipid raft/caveolae localization of adenylyl cyclase signaling components. *J. Biol. Chem.* **281**, 26391–26399.
- Jang, I. H., Kim, J. H., Lee, B. D., Bae, S. S., Park, M. H., Suh, P. G. and Ryu, S. H. (2001). Localization of phospholipase C-gamma1 signaling in caveolae: importance in EGF-induced phosphoinositide hydrolysis but not in tyrosine phosphorylation. *FEBS Lett.* **491**, 4–8.
- Krajewska, W. M. and Masłowska, I. (2004). Caveolins: structure and function in signal transduction. *Cell. Mol. Biol. Lett.* **9**, 195–220.
- Malan, D., Wenzel, D., Schmidt, A., Geisen, C., Raible, A., Bolck, B., Fleischmann, B. K. and Bloch, W. (2010). Endothelial beta1 integrins regulate sprouting and network formation during vascular development. *Development* **137**, 993–1002.
- Müller-Ehmsen, J., Schmidt, A., Krausgrill, B., Schwinger, R. H. and Bloch, W. (2006). Role of erythropoietin for angiogenesis and vasculogenesis: from embryonic development through adulthood. *Am. J. Physiol.* **290**, H331–H340.
- Mundy, D. I., Machleidt, T., Ying, Y. S., Anderson, R. G. and Bloom, G. S. (2002). Dual control of caveolar membrane traffic by microtubules and the actin cytoskeleton. *J. Cell Sci.* **115**, 4327–4339.
- Novak, A., Hsu, S. C., Leung-Hageteijn, C., Radeva, G., Papkoff, J., Montesano, R., Roskelley, C., Grosschedl, R. and Dedhar, S. (1998). Cell adhesion and the integrin-linked kinase regulate the LEF-1 and beta-catenin signaling pathways. *Proc. Natl. Acad. Sci. USA* **95**, 4374–4379.
- Pike, L. J. and Miller, J. M. (1998). Cholesterol depletion delocalizes phosphatidylinositol bisphosphate and inhibits hormone-stimulated phosphatidylinositol turnover. *J. Biol. Chem.* **273**, 22298–22304.
- Razani, B., Woodman, S. E. and Lisanti, M. P. (2002). Caveolae: from cell biology to animal physiology. *Pharmacol. Rev.* **54**, 431–467.
- Ruiz-Torres, M. P., Pérez-Rivero, G., Rodríguez-Puyol, M., Rodríguez-Puyol, D. and Díez-Marqués, M. L. (2006). The leukocyte-endothelial cell interactions are modulated by extracellular matrix proteins. *Cell. Physiol. Biochem.* **17**, 221–232.
- Saliez, J., Bouzin, C., Rath, G., Ghisdal, P., Desjardins, F., Rezzani, R., Rodella, L. F., Vriens, J., Nilius, B., Feron, O. et al. (2008). Role of caveolar

compartmentation in endothelium-derived hyperpolarizing factor-mediated relaxation: Ca^{2+} signals and gap junction function are regulated by caveolin in endothelial cells. *Circulation* **117**, 1065-1074.

Schmidt, A., Wenzel, D., Ferring, I., Kazemi, S., Sasaki, T., Hescheler, J., Timpl, R., Addicks, K., Fleischmann, B. K. and Bloch, W. (2004). Influence of endostatin on embryonic vasculo- and angiogenesis. *Dev. Dyn.* **230**, 468-480.

Schmidt, A., Wenzel, D., Thorey, I., Werner, S., Fleischmann, B. K. and Bloch, W. (2005). Endostatin down-regulates soluble guanylate cyclase (sGC) in endothelial cells in vivo: influence of endostatin on vascular endothelial growth factor (VEGF) signaling. *Endothelium* **12**, 251-257.

Tu, Y., Li, F. and Wu, C. (1998). Nck-2, a novel Src homology2/3-containing adaptor protein that interacts with the LIM-only protein PINCH and

components of growth factor receptor kinase-signaling pathways. *Mol. Biol. Cell* **9**, 3367-3382.

Vouret-Craviari, V., Boulter, E., Grall, D., Matthews, C. and Van Obberghen-Schilling, E. (2004). ILK is required for the assembly of matrix-forming adhesions and capillary morphogenesis in endothelial cells. *J. Cell Sci.* **117**, 4559-4569.

Wickström, S. A., Lange, A., Hess, M. W., Polleux, J., Spatz, J. P., Krüger, M., Pfaller, K., Lambacher, A., Bloch, W., Mann, M. et al. (2010a). Integrin-linked kinase controls microtubule dynamics required for plasma membrane targeting of caveolae. *Dev. Cell* **19**, 574-588.

Wickström, S. A., Lange, A., Montanez, E. and Fässler, R. (2010b). The ILK/PINCH/parvin complex: the kinase is dead, long live the pseudokinase! *EMBO J.* **29**, 281-291.

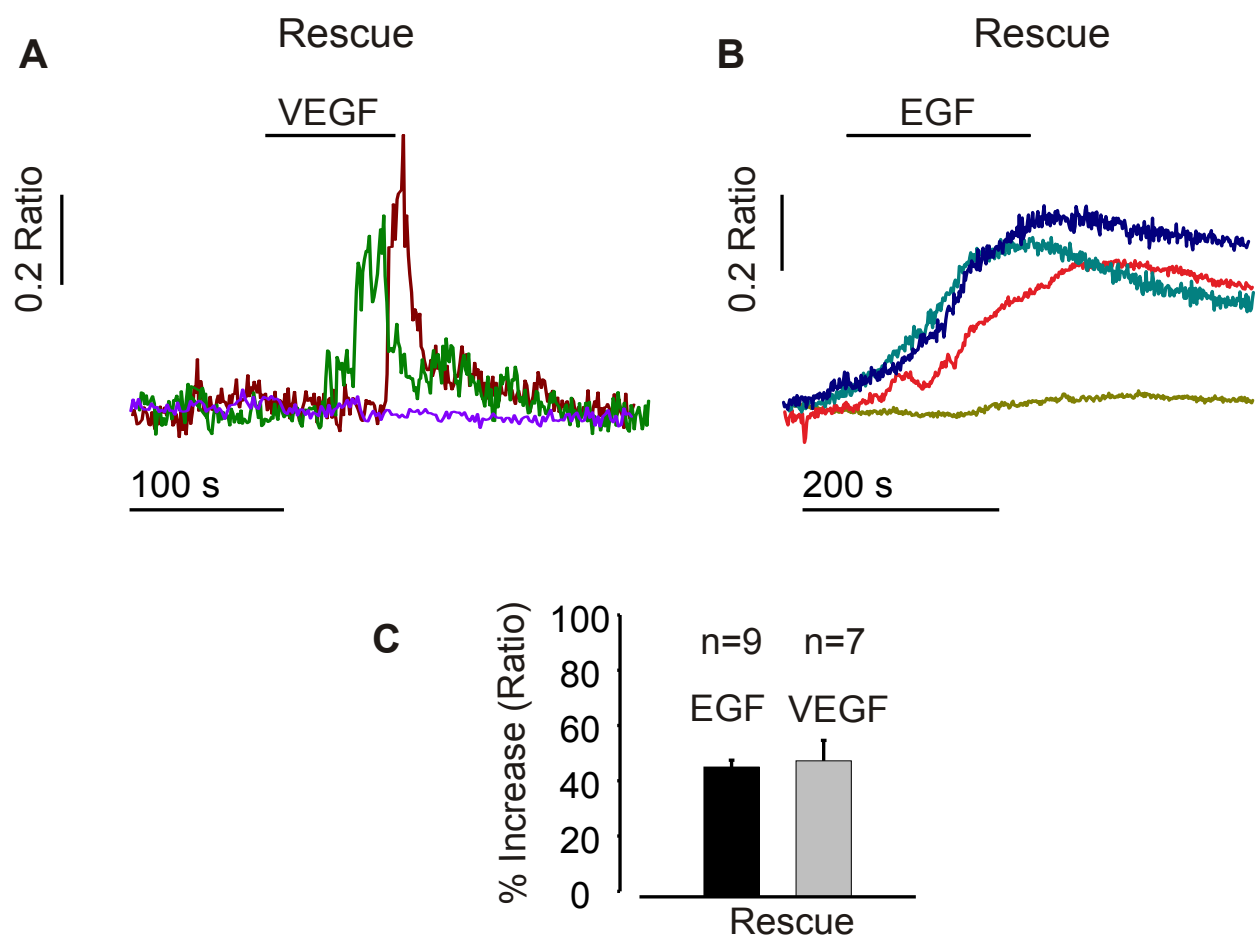


Fig. S1. VEGF and EGF signaling are restored in rescue M-ECs. (A,B) Rescue M-ECs show an increase of $[Ca^{2+}]_i$ upon application of VEGF (A) or EGF (B); representative $[Ca^{2+}]_i$ signals from single cells are depicted, representative $[Ca^{2+}]_i$ traces are shown, each color labels the 340/380 nm ratio in an individual cell over time. (C) Percentage $[Ca^{2+}]_i$ increase with respect to the control value. Error bars represent s.e.m.

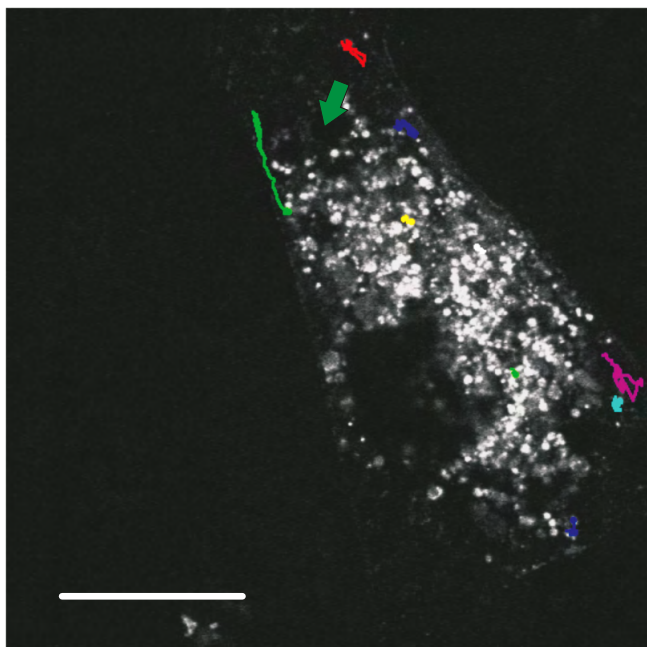
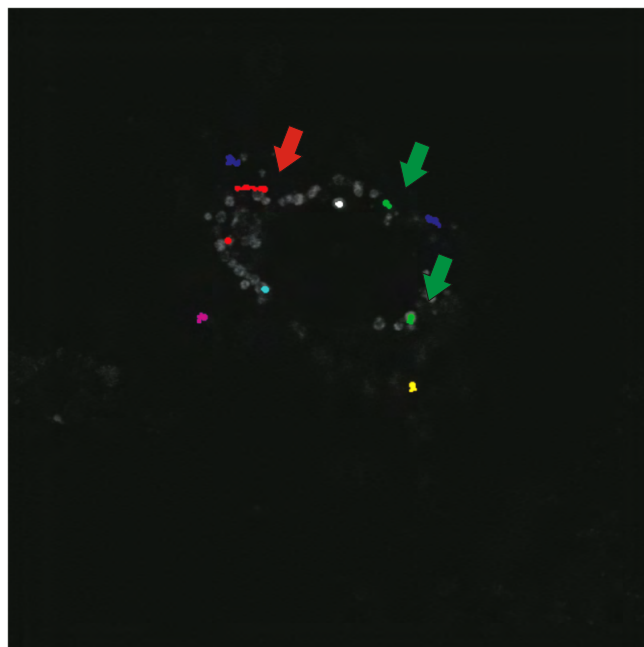
A**B**

Fig. S2. Defective localization and movement of caveolin 1 in *Ilk*^{-/-} M-ECs. (A,B) Dynamics of caveolin 1-EGFP-positive vesicles were analyzed by confocal video microscopy in transfected WT (A) and *Ilk*^{-/-} (B) M-ECs. The images shown are snapshots from supplementary material Movies 3 and 4, acquired at a rate of one image per second for 50 seconds. Arrows indicate appearance and disappearance of caveolin 1 vesicles. In A, the green arrow in WT shows a caveolin 1 vesicle moving fast in proximity to the plasma membrane. In B, the red arrow in the *Ilk*^{-/-} cell depicts the typical slow and short range motility, whereas the green arrows depict static vesicles. Scale bars: 20 μ m.

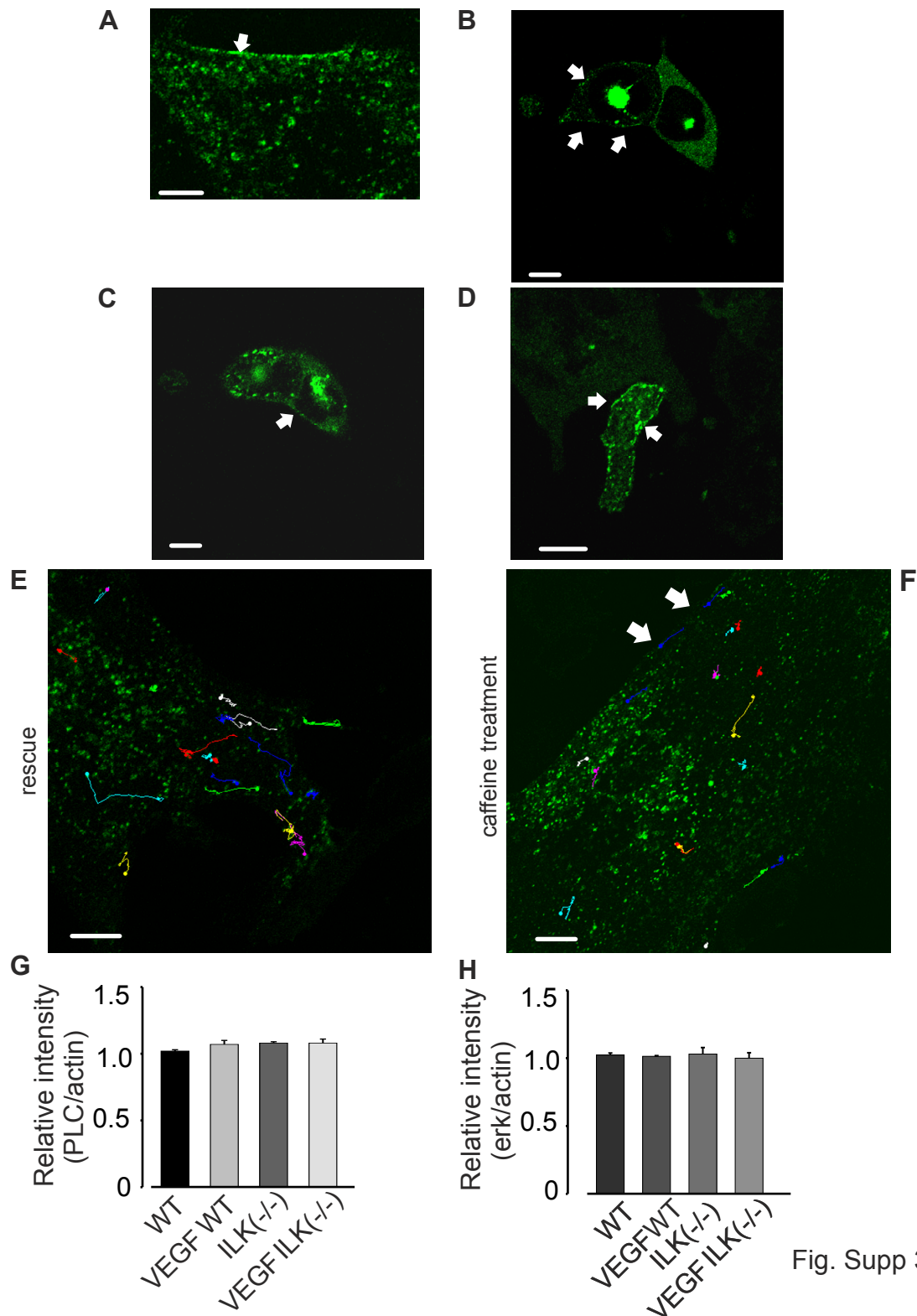
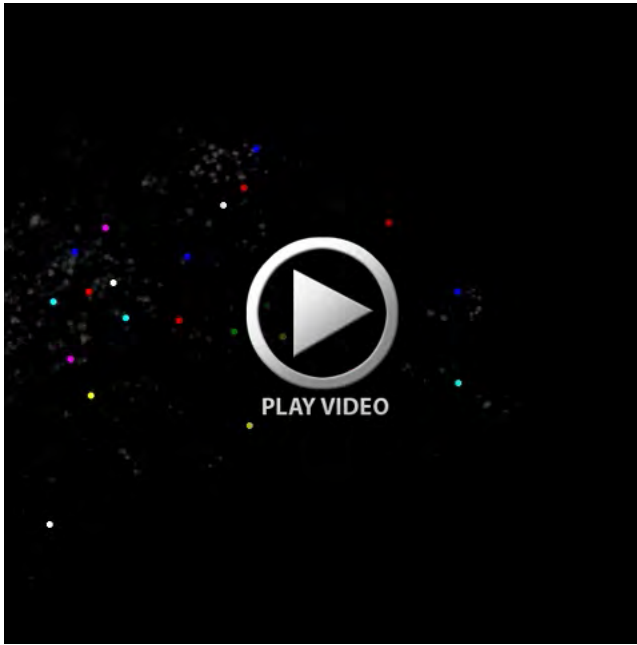
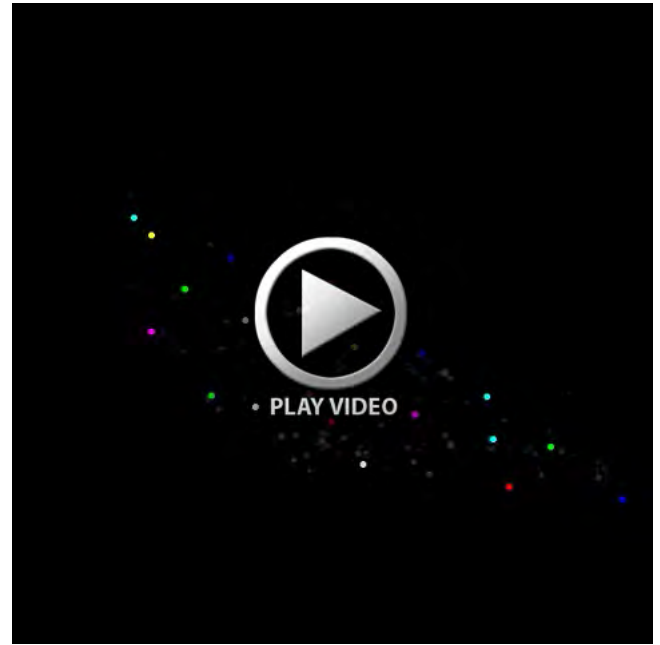


Fig. Supp 3

Fig. S3. Localization and movement of caveolin-1-EGFP transfected rescue M-ECs. (A-D) Snapshots of caveolin-1-EGFP transfected rescue M-ECs (A-C) and caveolin 1-EGFP transfected rescue M-ECs treated with caffeine (2 mM) for 2-4 minutes (D). Arrows depict the plasma membrane distribution of the fusion protein, which is similar to that observed in WT cells. (E,F) Dynamics of caveolin 1-EGFP-positive vesicles were analyzed by confocal video microscopy in transfected rescue M-ECs (E) and transfected rescue M-ECs treated with caffeine for 2-3 minutes (F). The images shown are snapshots from supplementary material Movies 5 and 6, acquired at a rate of one image per second for 50 seconds. Arrows indicate appearance and disappearance of caveolin 1 vesicles. Green, blue and light-blue tracks go from the cell membrane towards the center of the cell. Note also some protein building clusters connecting together and then dividing in different pathways (rosa, pink, yellow tracks). (F) Blue tracks show caveolin 1 vesicles (white arrows) moving fast along in proximity to the plasma membrane despite caffeine treatment. (G,H) Densitometric analysis of western blots of PLC- γ (G) and ERK1/2 (H) proteins in M-ECs in control and upon VEGF treatment conditions (H).



Movie 1



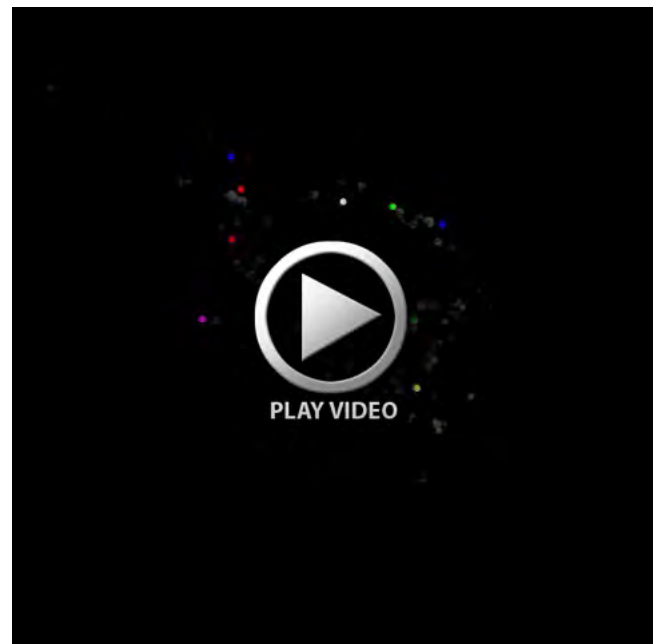
Movie 2

Movies 1 and 2. WT (Movie 1) and *Itk*^{-/-} (Movie 2) M-ECs transfected with the caveolin-1 EGFP construct. Colors depict the different typical kinetic patterns.

<https://journals.biologists.com/dev/article/140/5/987/45953/Deletion-of-integrin-linked-kinase-in-endothelial#supplementary-data>



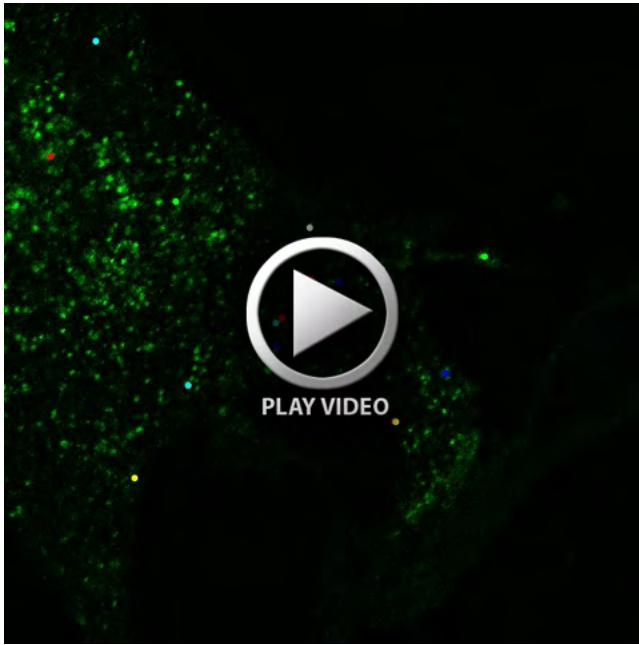
Movie 3



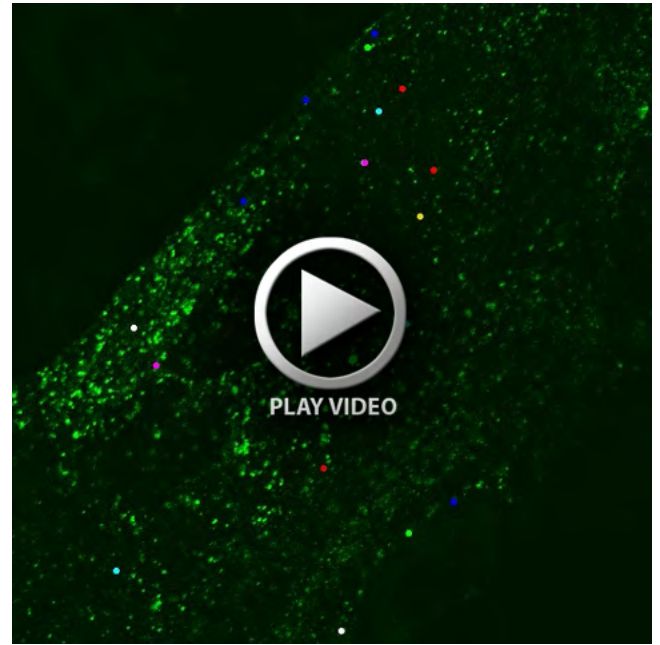
Movie 4

Movies 3 and 4. WT (Movie 3) and *Itk*^{-/-} (Movie 4) M-ECs transfected with the caveolin-1 EGFP construct. Single proteins are tracked with different colors showing the typical kinetic patterns.

<https://journals.biologists.com/dev/article/140/5/987/45953/Deletion-of-integrin-linked-kinase-in-endothelial#supplementary-data>



Movie 5



Movie 6

Movies 5 and 6. Rescue (Movie 5) and caffeine-treated rescue (Movie 6) M-ECs transfected with caveolin-1 EGFP. The different colors depict the various typical kinetic movement patterns.

<https://journals.biologists.com/dev/article/140/5/987/45953/Deletion-of-integrin-linked-kinase-in-endothelial#supplementary-data>

3.1.2 Lack of Laminin γ 1 in embryonic stem cell-derived cardiomyocytes causes inhomogeneous electrical spreading despite intact differentiation and function. Stem Cells. 2009 Jan;27(1):88-99. doi: 10.1634/stemcells.2008-0335. PubMed PMID: 18927478 (IF:7.7).

Aim of the study

Laminin, a heterotrimeric glycoprotein consisting of α , β and γ chains, is a critical ECM component. The laminin γ 1 chain knock-out mouse displayed embryonic lethality at day 5.5 (Smyth et al., 1999), thus unequivocally showing the fundamental role of laminin in embryonic development. The γ 1 chain is ubiquitously present in all basement membranes and highly expressed in heart muscle. The relevance of laminin in cardiovascular disease mechanisms was corroborated by mutations in the laminin LAMA2 and LAMA4 genes (Helbling-Leclerc et al., 1995, Knöll et al., 2007, Wang et al., 2006). These mutations caused severe skeletal muscle pathologies such as congenital muscular dystrophies, and also heart disorders, namely cardiac hypertrophy and malformation of blood vessels leading to a phenotype reminiscent of cardiac ischemia. Lack of laminins in the ECM damages the skeletal muscle fibers which can detach from the surrounding tissues (Smyth 1999). Additionally, laminin helps to regulate cell signaling pathways that are important for muscle growth and repair, as well as for the maintenance of muscle function over time. Laminin α 4 and ILK mutations are also associated with dilated cardiomyopathy due to defects in the development of cardiac and ECs (Knöll et al., 2007). In skeletal muscle, laminins' interaction with the cortical cytoskeleton and integrins assures bidirectional signaling and determines the structural integrity of the cells building basement membranes.

The ubiquitously expressed laminin γ 1 was shown to be critical for embryonic development, and it is highly expressed in cardiac muscle, therefore we were interested to explore the role of laminin in the growth, differentiation and function of cardiac muscle cells.

Methods and Results

Due to early embryonic lethality, using the mouse model to study the fundamental mechanisms of the laminin γ 1 chain in cardiac development and function was impossible. Thus, as

alternative the ES cell in vitro differentiation technique with EBs formation efficiently allowed the investigation of the influence of laminin assembly and basement membrane formation in a condition similar to the in vivo situation. The laminin $\gamma 1$ (-/-) deletion was produced by two sequential targeting events in the cells. The heterozygous and homozygous clones have the same genetic background; therefore, the heterozygous cells were used as control. Using the 3D multicellular EB model, we could study more complex intracellular interactions between cardiomyocytes and other cells of which the heart is composed. Laminin deletion in fibroblasts and ECs may also influence the developmental process differently to if only deleted in cardiomyocytes. Thus, cardiomyocytes were differentiated from the mouse ES cell clones, $\gamma 1$ (+/-) and $\gamma 1$ (-/-), in the EB model. The typical characteristics of cardiac muscle cells, such as beating, morphology and cross-striation, were similar in both genotypes. Interestingly, $\gamma 1$ (-/-) derived cardiomyocytes expressed fewer ECM proteins such as collagen IV or Nidogen, compromising the basement membrane integrity (see Fig 1, page 90, (Malan et al., 2009)).

The correct and organized deposition of ECM proteins is essential in creating cellular structure and integrity but also critical in regulating intra and intercellular communication. The central role of laminin $\gamma 1$ was assessed by rescue experiments incubating EBs with laminin 111, a commonly used substrate for ubiquitous laminins. Application of laminin 111 allowed the recovery of the basement membrane structure with partially restored collagen IV expression indicating the fundamental relationship between laminin $\gamma 1$ assembly and the proper deposition of the various components of the extracellular matrix (see Fig 1, page 90). The alteration in basement membrane deposition could impact the compartmentalization of signaling pathways and proper receptor functioning and affect cardiomyocyte function. Next, the development and functionality of the single cardiomyocytes derived from both clones were investigated. The EBs differentiate into different cardiomyocyte subtypes, namely pacemaker-, ventricular-, and atrial-like cells, as indicated by analysis of the AP characteristic by the current clamp in whole cell modus (Fig 3, page 92 and Table 1, page 93). Interestingly, we found significantly more pacemaker-like cells in the laminin $\gamma 1$ (-/-) EBs compared to the control EBs (+/-). Furthermore,

staining with HCN4, a specific channel marker for pacemaker cells, showed an increase in the ratio of HCN4 positive cells vs. the total number of nuclei of cardiac cells in the laminin $\gamma 1$ (-/-) EBs (Fig 3, page 92), also indicating an increase of this cellular subtype.

To see if disruption of the basement membrane could affect signaling function, I investigated the hormonal regulation of cardiomyocytes by measuring the beating frequency of single cells and the modulation of the L-type calcium current (ICa_L). There was no difference in adrenergic and muscarinic regulation of frequency and ICa_L between the $\gamma 1$ (+/-) and $\gamma 1$ (-/-) cardiomyocytes. Muscarinergic stimulation with the agonist carbachol (CCh) decreased the beating frequency and ICa_L current after β -adrenergic pre-stimulation, indicating integrity of basic functional signaling regulation of cardiomyocytes despite laminin deletion (Fig 4 and Table 1, page 93). To understand whether the ECM can affect the signaling modulation in three-dimensional structures of cardiomyocytes, a condition more similar to that of the in vivo situation, we used the MEA system which allows the recording and analysis of field potentials (FP). The study of electrical impulse generation and conduction velocity propagation on the MEA system showed a regular and stable frequency and coupling of cardiac cells in laminin $\gamma 1$ (+/-) control EBs, whereas the laminin $\gamma 1$ (-/-) EBs presented isolated and competing pacemaker regions. We found several uncoupled beating areas considered independent pacemaker regions in the laminin $\gamma 1$ (-/-) EBs, but not in the laminin $\gamma 1$ (+/-) control EBs. The conduction velocity was slower in the homozygous EBs compared to the heterozygous controls (see Fig 5, page 95). Because changes of conduction velocity can also be due to modification of connexins, we analyzed their expression. Both western blotting and immunofluorescence analysis showed no difference in connexin 43 and 45 expressions between the two genotypes. At the same time, using Van Gieson and collagen VI stainings, we detected a high deposition of ECM proteins between the cells. Defective ECM assembly causes the aggregation of proteins, as we observed by electron microscopy. Accumulations of matrix proteins create electrical isolated areas, potentially leading to the formation of discrete ectopic pacemaking sites. Additionally, these deposits create gaps between cluster of neighboring cells, impeding

their connection and contributing to disruptions in the speed of electrical conduction (Fig 6, page 96).

Conclusion

In this study, we underscore the essential role of laminin $\gamma 1$ in upholding the structural integrity of the basement membrane throughout the developmental process in cardiomyocytes. Lack of laminin $\gamma 1$ induced disruption to the basement membrane and alterations in the distribution of $\beta 1$ integrins; nevertheless, the differentiation and hormonal regulation of cardiomyocytes remained intact. Earlier investigations into $\beta 1$ integrin (-/-) cardiomyocytes indicated a stalling of development at early stages and a complete absence of muscarinic signaling due to the spatial displacement of Gai. We then show that laminin $\gamma 1$ affects $\beta 1$ integrin spatial arrangement; however, the integrin expression remains apparently sufficient to maintain an organized receptor-dependent clustering. On the contrary, disturbances in the basement membrane lead to flawed extracellular matrix assembly, resulting in the accumulation of collagen VI deposits. These appear to hinder basement membrane proper assembly and protein deposits create discrete pacemaker regions, often isolated and only partially connected. These structural changes appear to underlie the disruption of electrical signal propagation and the occurrence of arrhythmicity within the 3D model of cardiomyocytes generated from the laminin $\gamma 1$ (-/-) clones.

Lack of Laminin γ 1 in Embryonic Stem Cell-Derived Cardiomyocytes Causes Inhomogeneous Electrical Spreading Despite Intact Differentiation and Function

DANIELA MALAN,^{a,b} MICHAEL REPPPEL,^c RADOSLAW DOBROWOLSKI,^d WILHELM ROELL,^{a,e} NEIL SMYTH,^{f,g} JUERGEN HESCHELER,^c MATS PAULSSON,^f WILHELM BLOCH,^b BERND K. FLEISCHMANN^a

^aInstitute of Physiology I, Life and Brain Center, ^dInstitute of Genetics, and ^eDepartment of Cardiac Surgery, University of Bonn, Bonn, Germany; ^bDepartment of Molecular and Cellular Sport Medicine, German Sport University, Cologne, Germany; ^cInstitute of Neurophysiology and ^fCenter for Biochemistry, Medical Faculty and Center for Molecular Medicine, University of Cologne, Cologne, Germany; ^gSchool of Biological Sciences, University of Southampton, Southampton, United Kingdom

Key Words. Laminin γ 1 • Extracellular matrix • Embryonic stem-derived cardiomyocytes • Hormonal regulation

ABSTRACT

Laminins form a large family of extracellular matrix (ECM) proteins, and their expression is a prerequisite for normal embryonic development. Herein we investigated the role of the laminin γ 1 chain for cardiac muscle differentiation and function using cardiomyocytes derived from embryonic stem cells deficient in the *LAMC1* gene. Laminin γ 1 ($-/-$) cardiomyocytes lacked basement membranes (BM), whereas their sarcomeric organization was unaffected. Accordingly, electrical activity and hormonal regulation were found to be

intact. However, the inadequate BM formation led to an increase of ECM deposits between adjacent cardiomyocytes, and this resulted in defects of the electrical signal propagation. Furthermore, we also found an increase in the number of pacemaker areas. Thus, although laminin and intact BM are not essential for cardiomyocyte development and differentiation per se, they are required for the normal deposition of matrix molecules and critical for intact electrical signal propagation. STEM CELLS 2009;27:88–99

Disclosure of potential conflicts of interest is found at the end of this article.

INTRODUCTION

Basement membranes (BM) are thin layers of extracellular matrix (ECM) that surround individual cells and cell layers. Laminins, collagen IV, and nidogens are considered critical structural elements of the BM [1], and an intact BM formation is a key prerequisite for normal tissue development and function [2, 3]. Laminin is a heterotrimeric ECM glycoprotein consisting of α , β , and γ chains. Its fundamental importance was unequivocally proven by targeting the *LAMC1* gene encoding the γ 1 chain, resulting in homozygous embryos with very early embryonic lethality at embryonic day 5.5 [4]. The particular biological relevance of laminins for muscle development and differentiation was underscored by the observation that mutations in the *LAMA2* and *LAMA4* genes cause different types of severe skeletal muscle pathologies, such as the congenital muscle dystrophy or the milder limb girdle type 2I in humans [5–7]. A *LAMA4* mutation was also found to result in alterations of endothelial and cardiac cell morphology [8]. Furthermore, the

LAMA4 gene appears to be responsible for changes in heart function due to abnormal cardiovascular ECM, and the resulting phenotype is reminiscent of cardiac ischemia [9]. Studies in C2C12 cells addressed the mechanism of action of laminins in skeletal muscle and revealed that its polymerization and interaction with cell surface receptors were necessary and sufficient to create a cortical cellular architecture wherein the other components of the BM were integrated [1]. Because of these findings, we wondered whether the development and differentiation of cardiac muscle cells, similar to those of skeletal muscle cells, could be greatly altered by the deletion of the predominant laminin subtype. For this purpose we have chosen deletion of laminin γ 1, as this chain is ubiquitous in BM and particularly strongly expressed in heart muscle tissue compared with other types of striated muscle [10]. Indeed, this laminin chain is an obligatory component in most trimeric laminin forms. Because of the early embryonic lethality of the *LAMC1*-deficient mice, we have chosen the embryonic stem (ES) cell in vitro differentiation technique [11, 12] as a suitable model to study the cell biological and functional consequences of the laminin γ 1 dele-

Author contributions: D.M.: collection of data, data analysis and interpretation, manuscript writing; M.R., R.D., and W.R.: collection of data, data analysis and interpretation; N.S.: provision of study material, collection of data, data analysis and interpretation; J.H.: data interpretation; M.P.: provision of study material, data interpretation; W.B. and B.K.F.: conception and design, data interpretation, financial support, manuscript writing, final approval of the manuscript.

Correspondence: Bernd Fleischmann, M.D., Institute of Physiology I, Life & Brain Center, University of Bonn, Sigmund-Freud-Strasse 25, 53105 Bonn, Germany. Telephone: 49-228-6885-200; Fax: 49-228-6885-201; e-mail: bernd.fleischmann@uni-bonn.de; Wilhelm Bloch, M.D., Department of Molecular and Cellular Sport Medicine, German Sport University Cologne, Carl-Diem-Weg 6, 50927 Cologne, Germany. Telephone: 49-221-4982-5380; Fax: 49-221-4982-8370; e-mail: w.bloch@dshs-koeln.de Received April 2, 2008; accepted for publication October 3, 2008; first published online in STEM CELLS EXPRESS October 16, 2008. ©AlphaMed Press 1066-5099/2008/\$30.00/0 doi: 10.1634/stemcells.2008-0335

tion on cardiomyocyte development and differentiation. This approach appeared preferable to a cardiomyocyte-specific knockout strategy because the other cell types present in the heart (i.e., endothelial cells and fibroblasts) also contribute to laminin formation.

Herein, we demonstrate that cardiomyocyte development and differentiation are preserved in laminin $\gamma 1$ ($-/-$) cardiomyocytes despite the complete absence of BM formation. We also show that disturbed BM formation causes defective ECM assembly, matrix deposits, and secondary disturbances in the propagation of the electrical signals.

MATERIALS AND METHODS

ES Cell Preparation

Heterozygous ($+/-$) and homozygous ($-/-$) laminin $\gamma 1$ chain ES cells, generated on an R1 background [4, 13], were cultured and differentiated into spontaneously beating cardiomyocytes as previously described [14]. Single cardiomyocytes were isolated from clusters of spontaneously beating areas [15]. The laminin $\gamma 1$ ($-/-$) deletion was produced by two sequential targeting events in cells. Thus, ($+/-$) and ($-/-$) cells have the same genetic background, and therefore heterozygous ES cells were used as control [4].

Microelectrode Array Mapping Technique

Extracellular recordings on beating laminin ($+/-$) and ($-/-$) ES cell clusters were performed using a microelectrode array (MEA) data acquisition system (Multi Channel Systems, Reutlingen, Germany, <http://www.multichannelsystems.com>) [16, 17]. Standard measurements were performed at 2 kHz (bandwidth, 1–5 kHz) in normal Tyrode solution at 37°C. Data were analyzed off-line with a customized toolbox programmed with MATLAB (MathWorks, Natick, MA, <http://www.mathworks.com>) to detect and characterize field potentials (FPs) as described earlier [17]. The analysis of the interspike intervals, measured as readout for the beating frequency, was used to study the hormonal regulation of the spontaneous electrical activity (also described in [17, 18]). Propagation velocities were calculated as reported earlier [19] (supporting information data).

Electrophysiology

For whole-cell patch-clamp recordings only spontaneously beating, single cardiomyocytes were used. Patch-clamp experiments applying the current- or voltage-clamp mode of the whole-cell configuration were performed as previously reported [20, 21]. Briefly, for measuring peak L-type Ca^{2+} current ($I_{\text{Ca-L}}$), cardiomyocytes were held at a holding potential of -80 millivolt (mV), and depolarizing voltage presteps to -40 mV for 50 milliseconds were applied to inactivate I_{Na} . Thereafter, 100-millisecond voltage steps to 0 mV were applied at a frequency of 0.2 Hz. The pipette solution contained the following (in mM): 120 CsCl, 1 MgCl₂, 5 Mg-ATP, 10 EGTA, and 5 Hepes (pH 7.4; CsOH). The extracellular solution was as follows (in mM): 120 NaCl, 5 KCl, 3.6 CaCl₂, 20 tetraethylammonium-chloride, 1 MgCl₂, and 10 Hepes (pH 7.4; tetraethylammonium-hydroxide). The stimulation or inhibition of $I_{\text{Ca-L}}$ is reported in terms of the percentage of the increase or decrease of $I_{\text{Ca-L}}$ density, respectively. Muscarinic effects on cardiomyocytes were calculated in terms of percentage of variation with respect to isoprenaline (ISO) stimulation. Action potential (AP) recordings were obtained in the current clamp configuration. The pipette solution contained the following (in mM): 50 KCl, 1 MgCl₂, 3 Mg-ATP, 10 EGTA, 80 K⁺ L-aspartate, and 10 Hepes (pH 7.4; KOH). The extracellular solution was as follows (in mM): 140 NaCl, 5.4 KCl, 1.8 CaCl₂, 2 MgCl₂, 10 Hepes, 10 glucose (pH 7.4; NaOH).

Immunocytochemistry

Antibodies included rat anti-mouse actinin (1:500; Sigma-Aldrich, Munich, Germany, <http://www.sigmaaldrich.com>), rabbit

polyclonal anti-collagen IV (1:500; Acris Antibodies GmbH, Herford, Germany, <http://www.acris-antibodies.com>), mouse anti-rat monoclonal perlecan (1:500; Biotrend, Cologne, Germany, <http://www.biotrend.com>), rabbit polyclonal anti-nidogen-1 and -2 (1:1,000 [22]), rabbit polyclonal anti- $\beta 1$ integrin (1:500; Chemicon, Temecula, CA, <http://www.chemicon.com>), rabbit polyclonal anti-connexin 43 (Cx43) (1:400; Alpha Diagnostics, San Antonio, <http://www.4adi.com>), monoclonal anti-laminin $\gamma 3$ (1:1,000, a gift from Dr. Manuel Koch, University of Cologne), rabbit polyclonal anti-N-cadherin (1:250; Zymed Laboratories, South San Francisco, <http://www.invitrogen.com>), monoclonal antibody for mouse reticular fibroblasts, BM4018 (1:500; Acris Antibodies), rabbit anti-hyperpolarization-activated cyclic nucleotide gated potassium channel 4 (HCN4) (Alomone Labs, Jerusalem, <http://www.alomone.com>), and rabbit polyclonal collagen VI (1:2,000; kindly provided by the late Dr. Rupert Timpl, Max Planck Institute for Biochemistry, Martinsried, Germany).

Morphological Analysis, Deconvolution, and Confocal Microscopy

The distribution pattern of some proteins was analyzed by deconvolution fluorescence microscopy (Axiovert 200 M; Carl Zeiss, Göttingen, Germany, <http://www.zeiss.com>) or with an apotome (Carl Zeiss) in laminin $\gamma 1$ ($+/-$) (7 + 6 days of differentiation) and laminin $\gamma 1$ ($-/-$) (7 + 6 days of differentiation) EBs. Alternatively, where indicated, antibody distribution was observed by confocal microscopy using the LSM 510 META Zeiss microscope.

Western Blotting

Proteins from 10 EBs were incubated with rabbit polyclonal anti-serum against $\beta 1$ integrins (Chemicon), rabbit antiserum against fibronectin (raised against highly purified human plasma fibronectin), rabbit collagen I (Quartett, Berlin, <http://www.quartett.com>), collagen III (Abcam, Cambridge, U.K., <http://www.abcam.com>), collagen IV (Acris Antibodies), collagen VI (Fitzgerald Inc., Concord, MA, <http://www.fitzgerald-fii.com>), a rat monoclonal antibody against the nidogen-1 (entactin) G2 domain (MAB 1884; Chemicon), a rabbit antiserum against Cx43 [23], or a rabbit Cx45 antibody [24].

Statistical Analysis

Statistical significance of differences between groups was determined using the paired Student's *t* test for the effects of drugs on $I_{\text{Ca-L}}$, AP, and FP in the same cells and/or EBs and with the analysis of variance with Bonferroni post hoc and/or Student's *t* test for unpaired data between the control and laminin $\gamma 1$ ($-/-$) groups (SPSS 12.0, SPSS Inc., Chicago, IL, <http://www.spss.com>). A Fisher exact test was applied for the analysis of pacemaker cells with GraphPad Prism 5 (GraphPad Software, Inc., San Diego, <http://www.graphpad.com>). A *p* value below .05 was considered statistically significant.

RESULTS

Cardiomyocyte Development and Differentiation

To investigate the influence of BM on the development of cardiac muscle cells and their differentiation, we used laminin $\gamma 1$ ($+/-$) or laminin $\gamma 1$ ($-/-$) ES cells for the in vitro differentiation [14, 25]. Both ES cell lines developed spontaneous beating areas in EBs, although laminin $\gamma 1$ ($-/-$) EBs displayed a lower plating efficiency (approximately 60%). The in vitro differentiation pattern was similar in laminin $\gamma 1$ ($+/-$) and laminin $\gamma 1$ ($-/-$) EBs, start of beating was regularly observed 3–4 days after plating, and beating was seen to continue at least for 7–8 days thereafter. Next, we analyzed the sarcomeric organization of cardiomyocytes in plated whole EBs by immunostaining with cardiac α -actinin. In both control and mutant EBs, normal spindle-shaped

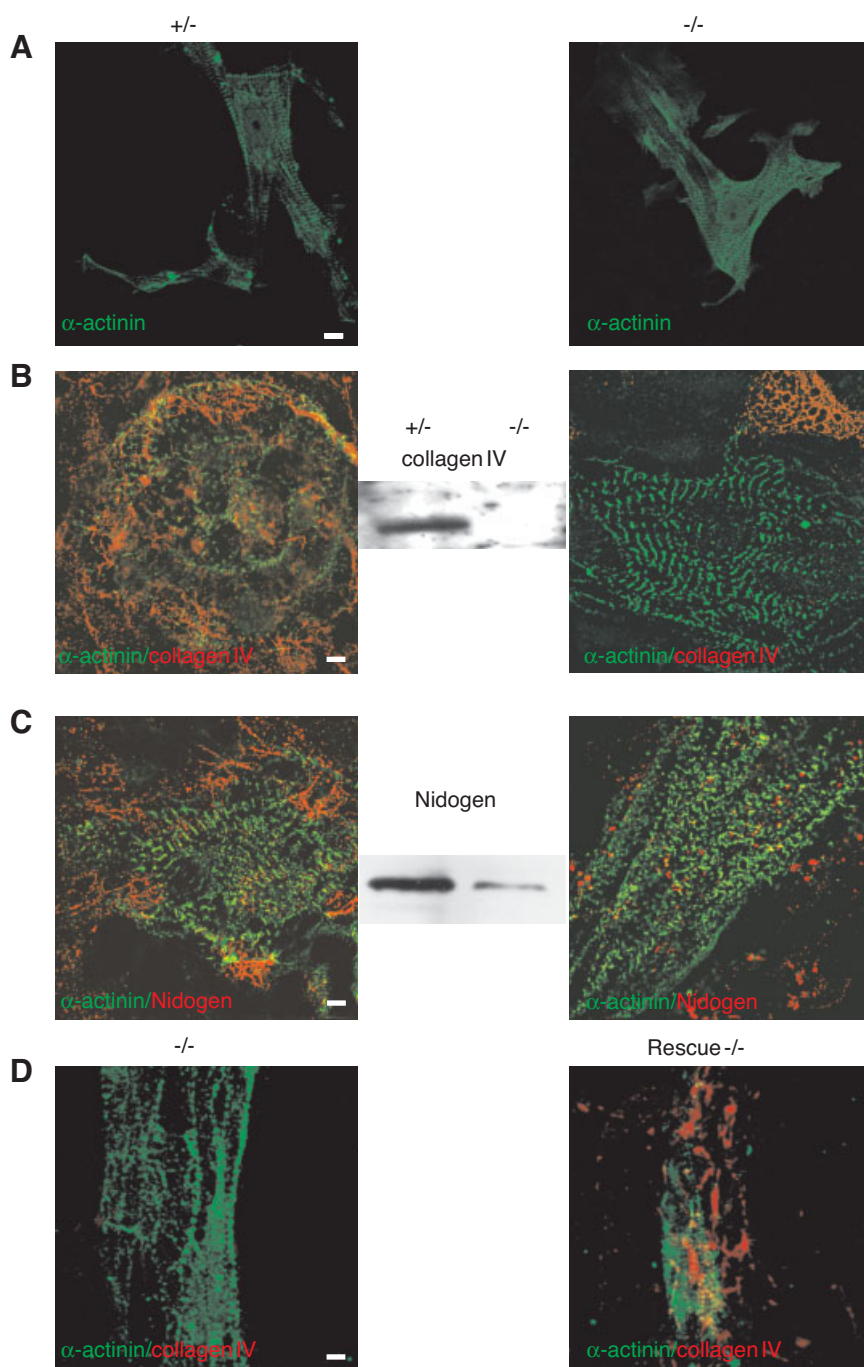


Figure 1. Laminin $\gamma 1$ ($-/-$) EBs differentiate into cardiomyocytes but lack basement membranes (BM). (A): Embryonic stem cell differentiation into α -actinin-positive (green) cross-striated cardiomyocytes in laminin $\gamma 1$ ($+/-$) (left) and ($-/-$) (right) EBs. (B): Laminin $\gamma 1$ ($-/-$) cardiomyocytes (α -actinin, green, right panel) lack the BM protein collagen IV (red), whereas this protein is strongly expressed around laminin $\gamma 1$ ($+/-$) cardiomyocytes (left panel). (B): Middle: Western blot analysis revealed lack of collagen IV expression in laminin $\gamma 1$ ($-/-$) EBs. (C): Nidogen-1 (red) was disrupted in laminin $\gamma 1$ ($-/-$) cardiomyocytes (α -actinin, green, right panel) but was normally distributed around laminin $\gamma 1$ ($+/-$) cardiomyocytes (left panel). (C): Middle: Western blot analysis revealed strong reduction of nidogen-1 content in laminin $\gamma 1$ ($-/-$) EBs. (D): Incubation of laminin $\gamma 1$ ($-/-$) EBs for 5 days with laminin 111 (25 μ g/ml) partially restored collagen IV expression (α -actinin green, collagen IV, red, right panel). Control laminin $\gamma 1$ ($-/-$) EBs without treatment are shown in the left panel. Videos of image stacks from (D) for laminin $\gamma 1$ ($-/-$) and rescued EBs are shown as supporting information Video 1 and 2. Scale bars = 10 μ m (A), 5 μ m (B), 5 μ m (C), and 10 μ m (D).

and triangular cardiomyocytes with intact sarcomeric cytoarchitecture and myofibrillar orientation were observed (Fig. 1A). These findings indicated that the development and differentiation of cardiomyocytes were preserved despite lack of the laminin $\gamma 1$ chain. In addition, we also investigated whether quantitative differences in cardiomyocyte differentiation could be found. For this purpose 20 EBs were dissociated, and the cells were replated and stained with cardiac α -actinin after fixation. We could not detect significant differences in the number of cardiomyocytes, as 18.9 ± 0.3 ($-/-$) ($n = 7$ experiments) and 21.3 ± 1.5 ($+/-$) ($n = 6$ experiments) of the 50,000 cells plated from the dissociated EBs for each experiment were cardiac muscle cells.

BM Formation

As $\gamma 1$ -containing laminins are important for BM formation and architecture [7], we next determined whether BM assembly and organization occurred normally in laminin $\gamma 1$ ($-/-$) cardiomyocytes. Since collagen IV is a reliable indicator of the presence and formation of BM, we studied its distribution in EBs in vicinity of cardiomyocytes using double immunofluorescence labeling for cardiac α -actinin and collagen IV. As expected, collagen IV surrounded cardiomyocytes in control laminin $\gamma 1$ ($+/-$) EBs but was absent in laminin $\gamma 1$ ($-/-$) EBs (Fig. 1B). This finding was corroborated by Western blotting on isolated beating areas where no collagen IV was detected (Fig. 1B, middle panel). Moreover, staining for the BM components ni-

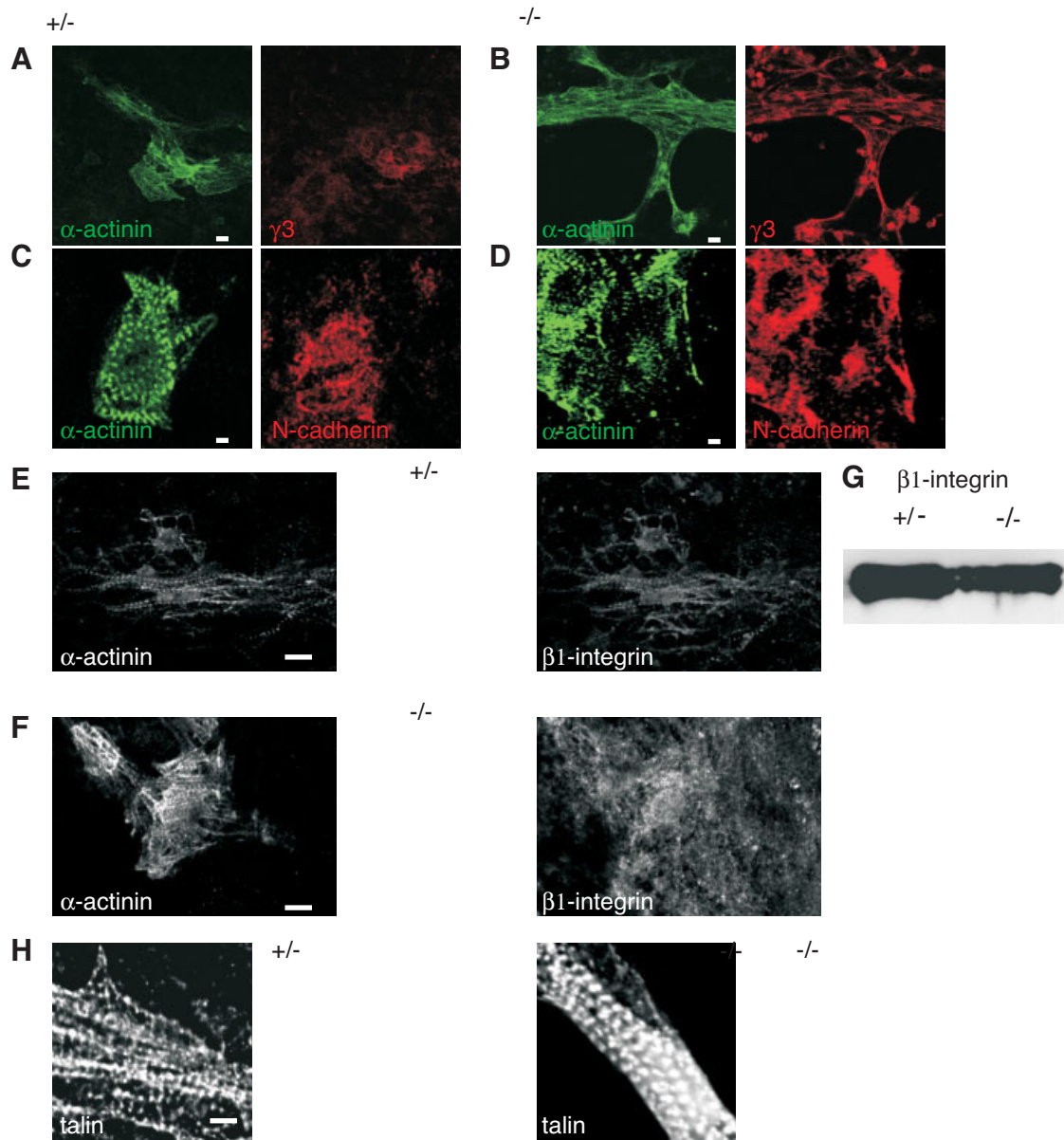


Figure 2. Upregulation of laminin $\gamma 3$ and N-cadherin and normal coronal cytoskeleton in laminin $\gamma 1$ ($-/-$) cardiomyocytes. (**A, B**): Stronger and more organized staining against laminin $\gamma 3$ (red) was detected around laminin $\gamma 1$ ($-/-$) cardiomyocytes (**B**) compared with laminin $\gamma 1$ ($+/-$) cardiomyocytes (**A**). Cardiomyocytes were identified by α -actinin staining ([**A–D**], left panels; [**B**], green). (**C, D**): Upregulation of N-cadherin (red) in laminin $\gamma 1$ ($-/-$) cardiomyocytes (**D**) versus laminin $\gamma 1$ ($+/-$) cardiomyocytes (**C**) (green is α -actinin). (**E, F**): Control cardiomyocytes revealed a close association of $\beta 1$ integrins ([**E**], right) with α -actinin ([**E**], left) in laminin $\gamma 1$ ($+/-$) cardiomyocytes, whereas in the laminin $\gamma 1$ ($-/-$) cells a less stringent association was seen ([**F**], right, $\beta 1$ integrins; left, α -actinin). (**G**): Western blot analysis showed similar content of $\beta 1$ integrins in ($+/-$) and laminin $\gamma 1$ ($-/-$) EBs. (**H**): Talin immunostaining in cardiomyocytes isolated from ($+/-$) ([**H**], left) and laminin $\gamma 1$ ($-/-$) ([**H**], right) EBs; staining at the level of z-line was observed in mutant and control cells. Scale bars = 10 μ m (**A**), 10 μ m (**B**), 5 μ m (**C**), 10 μ m (**D**), 10 μ m (**E**), 10 μ m (**F**), and 5.5 μ m (**H**).

dogan-1 and -2 was disrupted in the laminin $\gamma 1$ ($-/-$) EBs (Fig. 1C), and this correlated well with Western blotting, which revealed a marked reduction in the nidogen-1 ($49\% \pm 6.1\%$ vs. 100% in control) extractable from the matrix surrounding the cardiomyocytes (Fig. 1C, middle panel). We also quantified other ECM molecules in Western blots and found, in accordance with defective BM formation and ECM assembly, an upregulation of fibronectin ($150\% \pm 4.5\%$ vs. 100% in control), collagen I ($100\% \pm 14\%$), and collagen VI ($94\% \pm 1.1\%$) (supporting information Fig. 2), as well as the above-reported downregulation of other components. To rule out clonal aberration and to directly correlate the absence of BM formation with deletion of the laminin $\gamma 1$ chain, we performed reconstitution experiments

by adding 25 μ g/ml laminin 111 protein to laminin $\gamma 1$ ($-/-$) EBs. In the reconstituted EBs a partial recovery of collagen IV and of BM deposits surrounding the cardiomyocytes was detected (Fig. 1D), and this is clearly illustrated in the accompanying stack animations (supporting information Videos 1, 2). We next analyzed whether compensatory mechanisms could be responsible for the surprising finding of the apparently normal cardiac development and differentiation and intact cytoarchitecture of the laminin $\gamma 1$ ($-/-$) cardiomyocytes. One candidate molecule was the laminin $\gamma 3$ chain, known to be present in laminin 213, an isoform reported to be expressed in the heart [26, 27]. Double immunostaining for laminin $\gamma 3$ and cardiac α -actinin revealed a more organized structure of the $\gamma 3$ chain

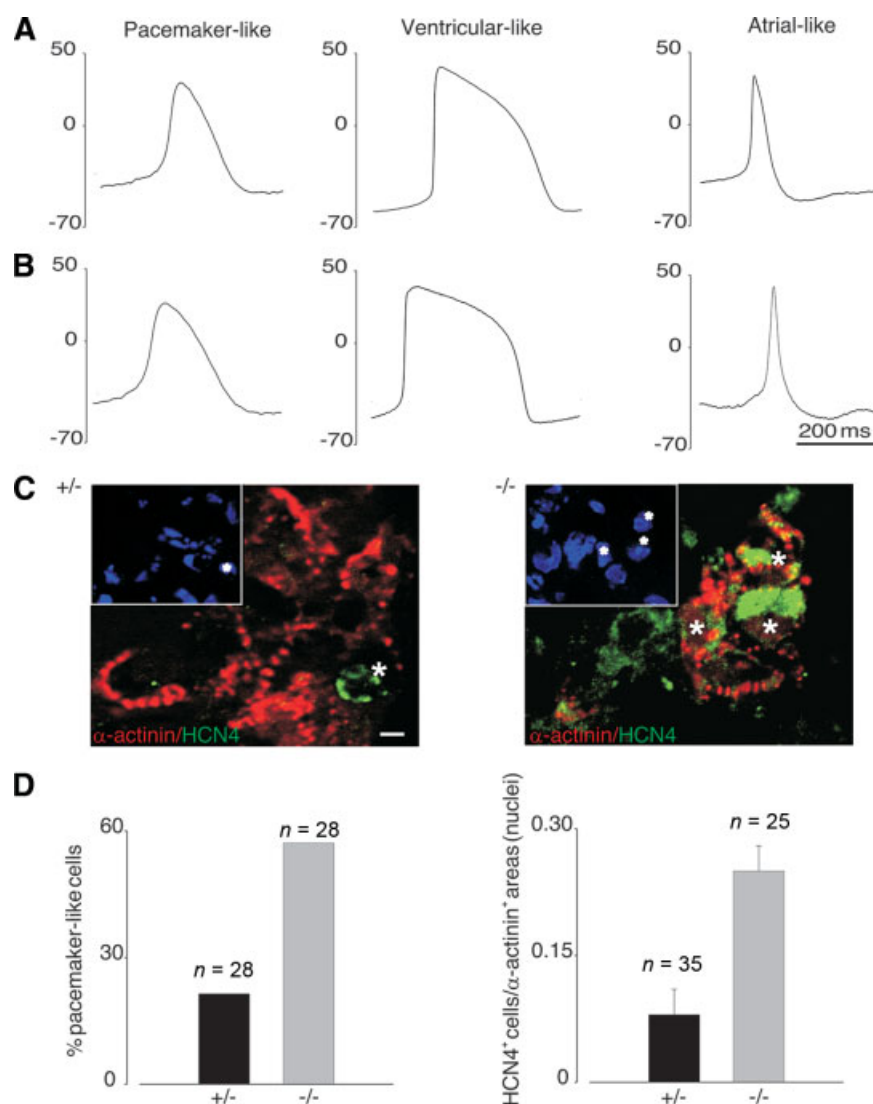


Figure 3. Prevalent differentiation of laminin $\gamma 1$ (-/-) cardiomyocytes into the pacemaker-like subtype. (A, B): Current clamp recordings revealed differentiation of embryonic stem (ES) cell-derived laminin $\gamma 1$ (+/-) (A) and (-/-) (B) cells into all major cardiac subtypes. (C): Immunostainings with the cardiac pacemaker marker HCN4 (green) in cardiac- α -actinin (red)-positive areas revealed very few positive pacemaker cells in laminin $\gamma 1$ (+/-) (left panel) but significantly ($p = .0003$) more in laminin $\gamma 1$ (-/-) (right panel) EB slices. Insets: Nuclear staining with Hoechst dye. Asterisks mark the nuclei of cells in the immunostaining and in the nuclear counterstaining. (D): Bar graph of percentage of pacemaker cells identified by action potential shape in laminin $\gamma 1$ (-/-) versus (+/-) (left) ES cell-derived cardiomyocytes (left panel). Shown is the bar graph of ratio of HCN4-positive pacemaker cells versus total number of nuclei in cardiac- α -actinin-positive areas of EBs (right panel). Scale bar = 5 μ m (C) and 10.5 μ m ([C], inset). Abbreviation: HCN4, hyperpolarization-activated cyclic nucleotide gated potassium channel 4; ms, milliseconds.

surrounding laminin $\gamma 1$ (-/-) cardiomyocytes, suggesting that $\gamma 3$ -containing laminin molecules could act as a new binding partner between cell surface molecules and hence induce cytoskeletal reorganization. However, this rescue was not sufficient to restore intact BM assembly (Fig. 2A, 2B); the $\gamma 3$ chain expression could not be quantified, as the antibody did not work under reducing conditions. Besides the $\gamma 3$ chain, we also investigated N-cadherin expression and found more intense staining at the border of the cardiomyocytes in laminin $\gamma 1$ (-/-) EBs compared with controls (Fig. 2C, 2D). These immunohistological findings suggest a morphological redistribution of cytoskeletal components. Thus, deletion of the laminin $\gamma 1$ chain results in a complete lack of BM formation, whereas the development and structure of cardiomyocytes remained intact, presumably because of the presence of $\gamma 3$ -containing laminins and a compensatory upregulation of cadherins [28, 29].

Expression and Distribution of Integrins and Associated Cytoskeletal Components

Lack or disruption of BM could also affect the distribution and function of $\beta 1$ integrins, which we reported to be important for heart muscle development [12] and function [20]. In fact, our earlier studies in $\beta 1$ integrin (-/-) ES cell-derived cardiomyocytes revealed that specifically muscarinic signaling was miss-

ing. Therefore, we first analyzed the expression of these key molecules with immunocytochemistry and Western blotting. In control cardiomyocytes a close association of $\beta 1$ integrins with the z -line was observed, whereas a less defined distribution pattern was seen in the laminin $\gamma 1$ (-/-) cardiomyocytes (Fig. 2E, 2F). This was caused by a homogeneous redistribution of $\beta 1$ integrins in the absence of intact BM. The densitometric analysis of $\beta 1$ integrin expression revealed only a modest reduction in laminin $\gamma 1$ (-/-) EBs ($75.6\% \pm 4.3\%$ $\beta 1$ integrin expression vs. 100% in control [$n = 2$; $p = .03$; Fig. 2G]). The distribution of talin, a focal adhesion-associated molecule and member of coronary cytoskeletal proteins, revealed an intact and stable cytoskeletal organization (Fig. 2H). This differs from our findings in $\beta 1$ integrin (-/-) cardiomyocytes [20] and suggests that laminin assembly and BM organization are independent processes.

Differentiation into Cardiomyocyte Subtypes

Our findings suggest that cardiomyocyte development is intact in laminin $\gamma 1$ (-/-) ES cells, and we therefore investigated next whether their differentiation into the different cardiomyocyte subtypes was preserved. For this purpose we determined key parameters of AP shape and duration using the patch-clamp technique: maximum diastolic potential (MDP), maximum rate

Table 1. Cell type and AP morphology

Cell type and AP morphology	APD90 ^a (ms)	APD50 ^b (ms)	MDP ^c (mV)	Dv/dt mean ^d (V/second)	Dv/dt max ^e (V/second)
Laminin $\gamma 1$ (+/-), six differentiations					
Atrial-like ($n = 3$)	102 \pm 14.5	32.1 \pm 22.0	-48.0 \pm 4.4	3.7 \pm 1.3	15.6 \pm 4.1
Ventricular-like ($n = 19$)	300.5 \pm 37.5	208.5 \pm 26.7	-52.0 \pm 2.2	2.2 \pm 0.3	10.9 \pm 1.1
Pacemaker-like ($n = 6$)	150.6 \pm 19.2	70.2 \pm 22.4	-40.0 \pm 3.5	1.5 \pm 0.3	3.2 \pm 0.9
Laminin $\gamma 1$ (-/-), seven differentiations					
Atrial-like ($n = 3$)	71 \pm 27.1	28.6 \pm 23.1	-43.0 \pm 2.6	2.1 \pm 0.4	12.1 \pm 0.5
Ventricular-like ($n = 9$)	258 \pm 37.8	198.1 \pm 23.8	-52.0 \pm 3.2	2.1 \pm 0.3	9.8 \pm 1.7
Pacemaker-like ($n = 16$)	126 \pm 12.5	90.7 \pm 22.5	-41.0 \pm 0.3	1.9 \pm 0.3	4.3 \pm 0.8

^aAction potential duration at 90% repolarization.^bAction potential duration at 50% repolarization.^cMaximum diastolic potential.^dMean rate of rise of AP.^eMaximum rate of rise of AP.

Abbreviations: AP, action potential; MDP, maximum diastolic potential; mV, millivolt.

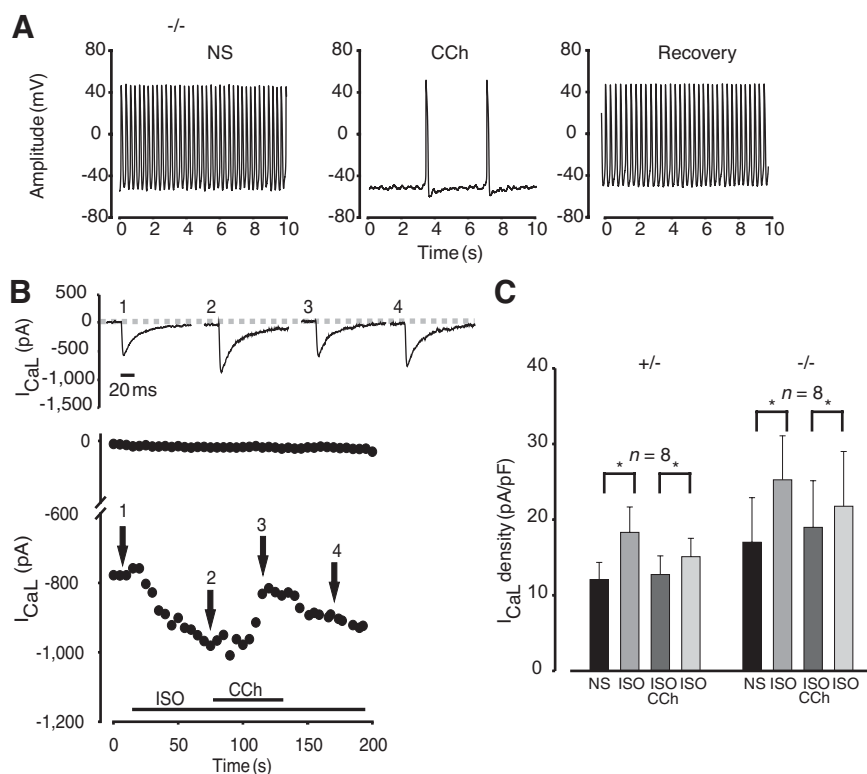


Figure 4. Hormonal regulation is intact in laminin $\gamma 1$ (-/-) cardiomyocytes. (A): Action potentials recorded from a representative laminin $\gamma 1$ (-/-) embryonic stem cell-derived cardiomyocyte (NS). Perfusion with the muscarinic agonist CCh (1 μ M) had a strong negative chronotropic effect that could be reversed upon wash-out (recovery). (B): Left: Time course of peak I_{CaL} in a representative laminin $\gamma 1$ (-/-) cardiomyocyte (numbers correspond with the original traces shown above the line: 1, NS; 2, ISO (1 μ M); 3, CCh (1 μ M); 4, recovery; dotted line shows the holding current). The β -adrenergic agonist ISO stimulated I_{CaL} , the additional application of CCh depressed it, and perfusion of ISO alone restored peak I_{CaL} . (C): Statistics of the hormonal modulation of I_{CaL} revealed similar responses in laminin $\gamma 1$ (+/-) (left) and laminin $\gamma 1$ (-/-) (right) cardiomyocytes. Abbreviations: CCh, carbachol; I_{CaL} , L-type Ca^{2+} current; ISO, isoprenalin; ms, milliseconds; mV, millivolt; NS, normal solution; pA, picoampere; pF, picofarad; s, seconds.

of rise of the AP (dV/dt), and action potential duration at 50% and 90% of repolarization. We tested isolated cardiomyocytes obtained from seven (-/-) and six (+/-) EB preparations (details also given in Fig. 3A, 3B; Table 1). As established earlier [14, 30], we could classify the ES cell-derived cardiomyocytes on the basis of AP shape and duration into three subtypes: pacemaker-, atrial-, and ventricular-like cells. Interestingly, we found in the laminin $\gamma 1$ (-/-) EBs significantly ($p = .0129$) more pacemaker-like cells (Table 1; Fig. 3A, 3B, 3D, left panel) compared with control EBs. To corroborate this important finding with a different methodological approach, we performed double immunohistochemical stainings on slices of whole EBs with the cardiac pacemaker marker HCN4 and with cardiac α -actinin as well as nuclear counterstaining (Fig. 3C). These experiments yielded a significant ($p = .0003$) increase of the ratio of HCN4-positive cells versus the total number of nuclei in cardiac- α -actinin-positive areas of mutant EBs ($0.25 \pm$

0.03 cells; $n = 25$ EBs) (supporting information data) compared with the ratio in control EBs (0.08 ± 0.03 cells; $n = 35$ EBs) (Fig. 3D, right panel). Higher numbers of pacemaker cells were also observed with anti-HCN4 3-3'-diaminobenzidine (DAB) staining (supporting information Fig. 2B).

Hormonal Regulation of Cardiomyocyte Function at the Single-Cell and Multicellular Level

The lack of BM and the accompanying changes of $\beta 1$ integrin distribution prompted us to analyze the hormonal regulation in laminin $\gamma 1$ (-/-) cardiomyocytes. This was determined by measuring the frequency of APs as well as the modulation of the I_{CaL} at the single-cell level using the patch-clamp technique. Carbachol (CCh) (1 μ M) slowed spontaneous beating by $49.0\% \pm 0.50\%$ ($n = 14$) in laminin $\gamma 1$ (-/-) cardiomyocytes, similar to laminin $\gamma 1$ (+/-) cardiomyocytes ($48.5\% \pm 0.50\%$; $n = 9$) (Fig. 4A). The known ISO-induced increase of the AP

frequency [21] was observed to a similar degree in both laminin (+/–) ($61.1\% \pm 1.4\%$; $n = 10$) and laminin (–/–) ($66.6\% \pm 1.0\%$; $n = 14$) cardiomyocytes. In addition, after ISO pretreatment led CCh to a reduction of the beating frequency in both laminin (+/–) ($24.1\% \pm 0.5\%$; $n = 10$) and laminin (–/–) ($24.0\% \pm 0.6\%$; $n = 5$) cardiomyocytes, respectively (supporting information Table 1). As a standard read-out for muscarinic and β -adrenergic signaling [15, 21, 31], we further investigated the regulatory effects of these hormones on I_{Ca-L} amplitude. This yields information concerning the physiological integrity of cardiomyocytes, since I_{Ca-L} is a key determinant of the excitation-contraction machinery. Our experiments showed that the CCh-mediated inhibition of I_{Ca-L} after prestimulation with ISO was present in laminin $\gamma 1$ (–/–) (Fig. 4B) and laminin $\gamma 1$ (+/–) (data not shown) cardiomyocytes. Statistical analysis revealed that the percentage of the inhibition of I_{Ca-L} by CCh was almost identical in heterozygous ($-28.7\% \pm 4.8\%$) and homozygous ($-24.5\% \pm 3.7\%$) cells. The ISO-induced stimulation was comparable in both groups, with $52.6\% \pm 13.6\%$ ($n = 8$) and $44.1\% \pm 12.9\%$ ($n = 8$) for heterozygous and homozygous cardiomyocytes, respectively. Thus, we found at the single-cell level that adrenergic and muscarinic regulation is preserved in laminin $\gamma 1$ (–/–) ES cell-derived cardiomyocytes. Interestingly, a small but statistically significant ($p = .05$) upregulation of the density of I_{Ca-L} (picoampere/picofarad) was noticed in the laminin $\gamma 1$ (–/–) cells (12.1 ± 2.2 , $n = 8$, for (+/–) and 17.0 ± 5.8 , $n = 8$, for (–/–), respectively) (Fig. 4C; supporting information Table 2).

Next we used the MEA system to monitor the hormonal modulation in intact EBs without enzymatic treatment. For this purpose, cardiac clusters were plated and differentiated on MEAs, and the modulation of chronotropy was tested upon CCh (10 μ M) and/or ISO (1 μ M) application. Spontaneously occurring FPs showed a typical physiological response to CCh and ISO, similar to the single-cell AP measurements described above and in earlier work [16, 32]. The percentage of EBs that responded to CCh was 71.4% for the laminin $\gamma 1$ (+/–) ($n = 5$) and 77.7% for the laminin $\gamma 1$ (–/–) ($n = 7$) preparations. Moreover, laminin $\gamma 1$ (–/–) EBs showed a negative chronotropic response to CCh, and this was reversed after wash-out. CCh reduced the FP frequency to $68\% \pm 10.5\%$ ($n = 5$) in (+/–) EBs and to $77\% \pm 10.4\%$ ($n = 7$) in (–/–) EBs. Similarly, muscarinic inhibition slowed after β -adrenergic prestimulation spontaneous activity to a similar degree in (+/–) and (–/–) EBs (supporting information Fig. 1; supporting information Table 3). Thus, the hormonal regulation of chronotropy of cardiac clusters was fully intact.

Electrical Signal Propagation in Beating Clusters

To understand the mechanism(s) whereby laminin disruption and consequent breakdown of the ECM network change conduction and crosstalk between cardiomyocytes, we performed a detailed analysis on EBs by measuring electrical impulse generation and electrical propagation between cardiomyocytes using MEA recordings. In Figure 5A, two original FP traces from different electrodes (26 and 73) show a representative example of the laminin $\gamma 1$ (+/–) EBs ($n = 22$). The gray shaded areas on the left (Fig. 5A–5C) indicate the total area of the plated EBs, and this proved comparable in size between control and the mutant EBs. Interestingly, some of the laminin $\gamma 1$ (–/–) EBs (~40%) did not adhere stably to MEAs; for MEA analysis, only the ones with good attachment providing adequate electrical signals could be used. In a representative control EB, a single pacemaker area was found in vicinity of electrode 26, and the signal was propagated in the direction of electrode 73, as indicated by the delay between the two electrodes (dotted line). Electrical

coupling was proven by the identical frequency and the stable delay. On the contrary, isolated and competing pacemaker regions were found in the laminin $\gamma 1$ (–/–) EBs ($n = 14$; Fig. 5B): the two representative traces show two electrically active areas around electrode 23 (areas 1 and 2), one serving as the pacemaker and one as the driven area as indicated by the stable delay. However, none of these two signals correlate with the FPs around electrode 87 (3), suggesting a second pacemaker area, which was electrically not coupled to the other pacemaker center. Moreover, we conducted functional rescue experiments by plating laminin $\gamma 1$ (–/–) EBs pretreated with laminin 111 (25 μ g/ml). In some (two of four) of the reconstituted EBs a recovery of the wild-type phenotype was evidenced by the presence of only one pacemaker region (region 1) demonstrated by the MEA recordings from electrodes 36 and 83 (Fig. 5C). The videos of these recordings reveal homogeneous contraction in the entire (+/–) rescued EB, whereas several independently beating areas were seen in the (–/–) EB (supporting information Videos 3–5). Our experiments demonstrated that significantly ($p < .05$) more pacemaker areas were found in laminin $\gamma 1$ (–/–) (2.9; $n = 14$) EBs compared with controls (1.27; $n = 22$) EBs (Fig. 5D); pacemaker regions were calculated according to the number of independently beating areas of the EB. Next, we normalized this number with the size of the EBs by dividing the number of pacemaker regions by the number of electrodes being covered by the EBs. This analysis again yielded significantly more pacemaker regions per electrode in laminin $\gamma 1$ EBs (0.16 ± 0.03 ; $n = 14$) compared with controls (0.06 ± 0.007 ; $n = 22$; $p < .05$) EBs. This finding is depicted in detail in Figure 5D (right panel), where the approximate path of the spreading of the electrical excitation was determined using FP delay analysis and is marked with a black line. In the laminin $\gamma 1$ (+/–) EB (left) a functional syncytium can be identified, whereas in the laminin $\gamma 1$ (–/–) EB (right) only some areas were electrically coupled (black circles and line, Fig. 5D left panel), which was proven by the fixed delay between the pacemaker-related electrodes (also described in Fig. 5A, 5B). In addition, a higher incidence of isolated pacemaker areas (black triangles, Fig. 5D left panel) was detected in the (–/–) EB, as indicated by changes of the delay between the respective electrodes.

We also found that the conduction of the signal between individual electrodes was not as homogeneous in the laminin $\gamma 1$ (–/–) as in the laminin $\gamma 1$ (+/–) EBs. The time course shown in Figure 5E depicts strong changes of the delay in the (–/–) EB (right panel), whereas the delay between respective electrodes remained stable in the (+/–) EB (left panel). This finding suggests a high presence of electrically isolated and/or partially coupled pacemaker areas in the laminin $\gamma 1$ (–/–) EBs. In fact, the pacemaker regions proved to some extent isolated in the laminin $\gamma 1$ (–/–) EBs, when using the FP delay analysis. In addition, the apparent conduction velocity in cardiomyocyte clusters of laminin $\gamma 1$ (–/–) EBs was significantly ($p = .014$) lower (0.0139 ± 0.0022 m/s; $n = 11$) versus controls (0.025 ± 0.0019 m/s; $n = 12$). Slowing of the apparent conduction velocity in cardiomyocyte clusters of laminin $\gamma 1$ (–/–) EBs could be due to changes of intracellular conduction, which is governed by Na^+ and/or Ca^{2+} channels. These are reflected in the upstroke velocity of APs, and we therefore analyzed dV/dt max (Table 1). This revealed similar values for cardiomyocytes derived from mutant and control EBs. However, since the average maximal diastolic potential of our cells was found to be relatively depolarized and since this could result in voltage-dependent inactivation of Na^+ channels, we determined dV/dt max in cardiomyocytes with relatively negative (less than -55 mV) MDP. This analysis yielded an average dV/dt max of 14.7 ± 4.4 V/second ($n = 5$; average MDP, -59 ± 4.4) and

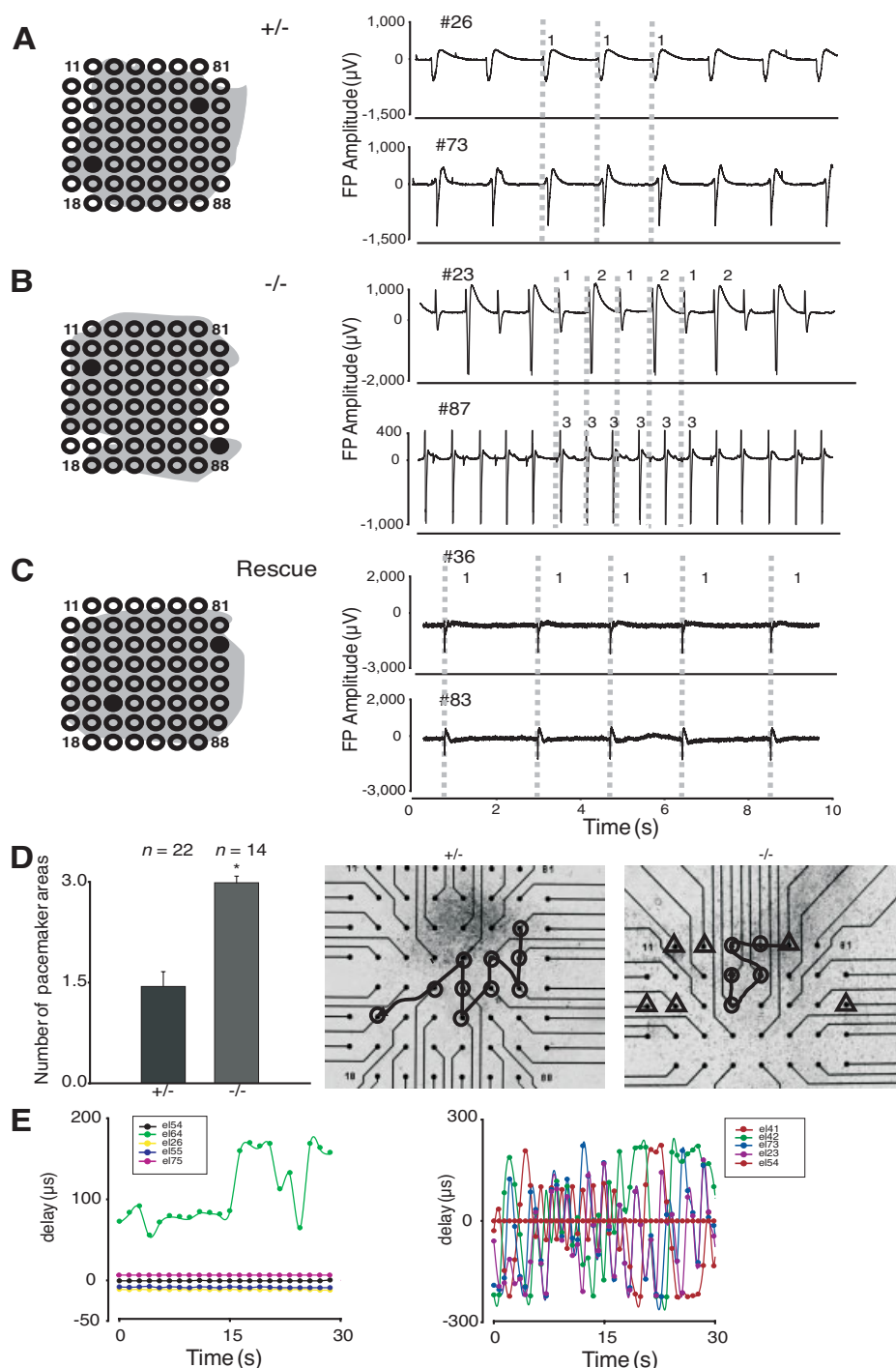


Figure 5. Electrical signal propagation is slowed and the number of pacemaker centers in laminin $\gamma 1$ ($-/-$) EBs. **(A):** FPs recorded from a representative laminin $\gamma 1$ ($+/+$) (right panel) EB with microelectrode array (MEA) from the marked electrode sites (left panel). This EB showed a unique pacemaker region around electrode 26; the stable delay between electrode 26 and 73 is indicated by the dotted lines (1). **(B):** FPs recorded from a representative laminin $\gamma 1$ ($-/-$) EB revealed that the pacemaker around electrode 23 was electrically independent from electrode 87 (3), as no stable delays between these two sites were observed; in contrast, around electrode 23 a stable delay between two electrically active areas (1, 2) was found. **(C):** FPs recorded from a representative laminin $\gamma 1$ ($-/-$) rescued EB pretreated with laminin 111 showed only a single pacemaker region around electrode 36, with a stable delay at electrode 83 (1). **(D):** Left panel: Statistics of the number of pacemaker areas in mutant and control EBs; a significantly ($p = .0001$) higher number of pacemaker areas was observed in laminin $\gamma 1$ ($-/-$) EBs. **(D):** Right panels: overview pictures taken from laminin $\gamma 1$ ($+/+$) (left) and laminin $\gamma 1$ ($-/-$) (right) EBs plated on MEAs. Dark lines with arrows indicate the propagation of the spontaneous electrical FP wave front; black triangles show uncoupled beating areas. **(E):** Time course of the FP delay between individual electrodes allowed to identify the primary pacemaker region in EBs. In the left panel, a laminin $\gamma 1$ ($+/+$) EB with a homogeneous propagation of the FP between different electrodes is shown, whereas the laminin $\gamma 1$ ($-/-$) EB (right panel) was characterized by inhomogeneous delays. The chosen electrodes correspond to the entire area where FPs could be recorded, and these areas are of similar size in these EBs. Abbreviations: FP, field potentials; s, seconds.

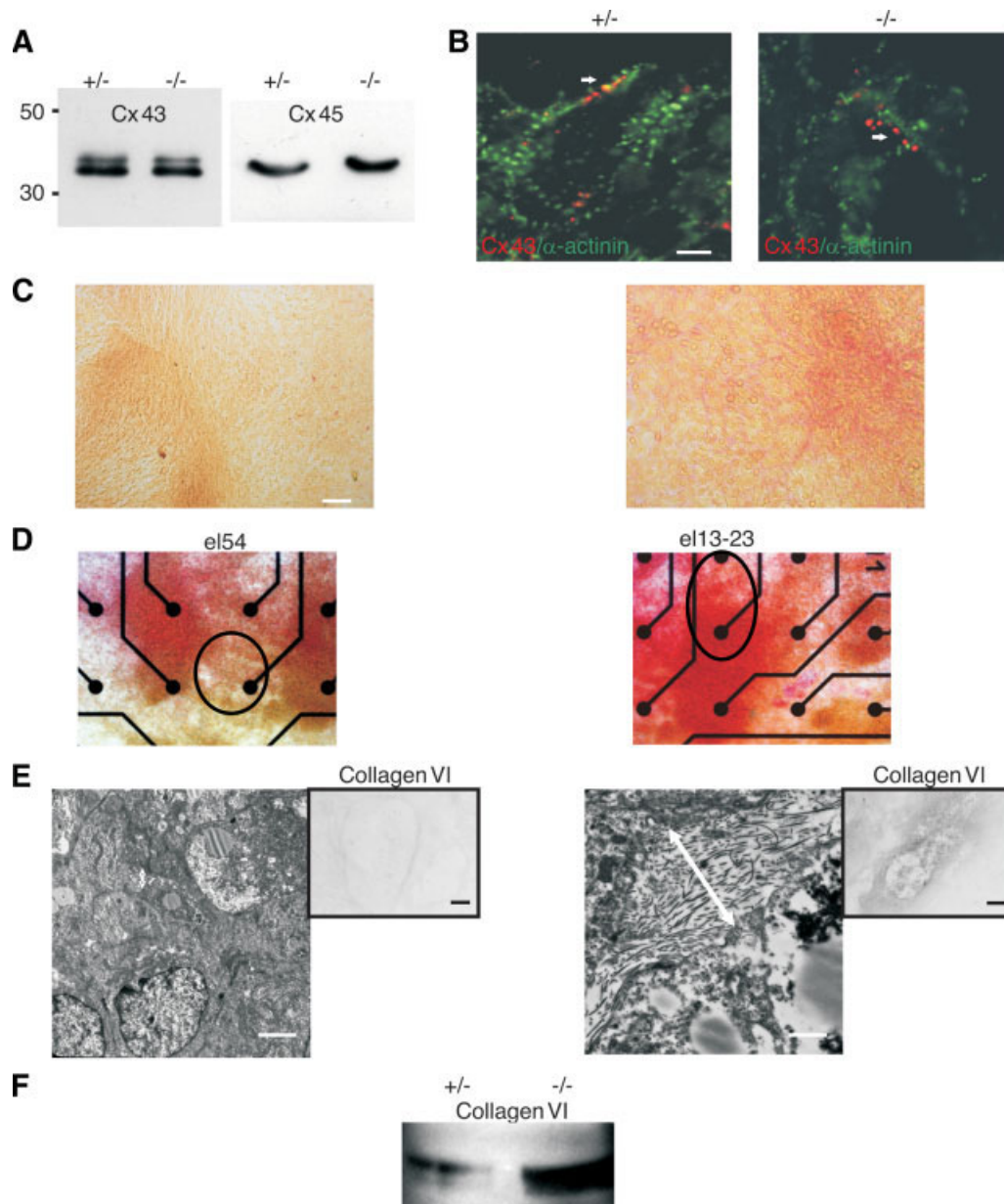


Figure 6. Defective extracellular matrix (ECM) assembly causes deposits of ECM. (A): Western blot analysis showed similar content of Cx43 (left panel) and Cx45 (right panel) proteins in laminin $\gamma 1$ (+/-) and laminin $\gamma 1$ (-/-) EBs. (B): Cx43 immunostaining (red) showed a similar distribution in laminin $\gamma 1$ (+/-) (left panel) and laminin $\gamma 1$ (-/-) (right panel) embryonic stem cell-derived cardiomyocytes (cardiac- α -actinin-positive, green). (C): Van Gieson staining revealed a lower deposition of ECM in a representative laminin $\gamma 1$ (+/-) EB (left panel) compared with a laminin $\gamma 1$ (-/-) EB. (D): Van Gieson staining also evidenced high deposition of ECM between beating areas in a representative (-/-) EB plated on a microelectrode array (MEA); the left panel depicts a representative laminin $\gamma 1$ (+/-), and the right panel depicts a laminin $\gamma 1$ (-/-) MEA EB with the number of electrodes. (E): Electron microscopy detected a high deposition of fibrous collagen in the laminin $\gamma 1$ (-/-) EB (bigger right panel), causing spacing between adjacent cells (indicated by the white arrows); this was not the case in the laminin $\gamma 1$ (+/-) EB (bigger left panel). Scale bars = 1.5 μ m (left) and 0.75 μ m (right). 3-3'-diaminobenzidine detection revealed stronger fibrous collagen VI deposition in the laminin $\gamma 1$ (-/-) EB (smaller right panel) than in control (smaller left panel). (F): Western blotting for collagen VI confirmed the upregulation of this protein in laminin $\gamma 1$ (-/-) beating areas of EBs. Scale bars = 5 μ m (B), 20 μ m (C), 1.5 μ m (E, bigger left), 0.75 μ m (E, bigger right), and 120 μ m (E, inset). Abbreviation: Cx, connexin; el, electrode.

13.5 \pm 8.1 V/second (n = 5; average MDP, -58 \pm 6.3) for control and mutant cardiomyocytes, respectively, ruling out prominent differences of Na⁺ currents. Furthermore, differences in K⁺ channel expression also appear unlikely because of the similar MDPs (Table 1).

Besides ion channels being responsible for intracellular conduction, connexins play a key role for intercellular conduction and spreading of the electrical signal. We have

therefore also investigated the most relevant connexin isoforms in developing heart muscle cells. There was no obvious difference in the distribution of Cx43 in laminin $\gamma 1$ (+/-) and (-/-) EBs (Fig. 6B, arrows); this analysis is somewhat difficult, as the anisotropic alignment of the cardiomyocytes is not preserved in the EBs. Nevertheless, our findings are also supported by the quantitation of connexins using Western blotting, which revealed no differences in expression for

Cx43 (Fig. 6A, left). Similarly, the expression of Cx45 (Fig. 6A, right), the predominant isoform during early cardiac development [33], was also found to be unaltered, making it unlikely that changes in the expression and/or distribution of connexins underlie the observed alterations. Specific staining with BM4018 revealed that fibroblasts and reticular fibroblasts were similarly distributed in wild-type and knockout cardiomyocytes (data not shown), excluding the possibility that interdispersion of electrically isolating cells caused the observed conduction defect.

To understand whether lack of laminin can mechanistically account for the observed disturbances of the electrical signal propagation in the laminin $\gamma 1$ ($-/-$) EBs, Van Gieson staining was performed. This demonstrated deposition of ECM between cells ($-/-$) in EBs (Fig. 6C), presumably due to the lack of an intact BM. This could lead to the isolation of electrically active areas, as these deposits correlated with sites of disturbed electrical spreading on representative ($+/-$) (left) and ($-/-$) (right) EBs (from Fig. 5D) plated on the MEAs (Fig. 6D). Since it was not possible to quantitate the matrix interdispersed between cardiomyocytes, we further underscored our observation by ultrastructural analysis. Electron microscopy depicted collagen-like extracellular structures (Fig. 6E, bigger panel), which caused spacing between adjacent laminin $\gamma 1$ ($-/-$) cells. Such intercellular gaps prevent intercellular coupling via gap junctions despite normal expression of connexins. Furthermore, DAB staining confirmed enhanced extracellular deposits of matrix components, particularly of collagen VI in the knockout EBs (Fig. 6E, inset), and this finding was further corroborated by Western blotting analysis (Fig. 6F). This increased ECM deposition was also shown for other matrix proteins (supporting information Fig. 2). Thus, altered BM formation results in disorganized ECM deposition, leading to disturbed electrical pulse propagation.

DISCUSSION

The aim of our work was to investigate cardiac cells development and function upon deletion of the laminin $\gamma 1$ chain. The biological relevance of laminins for development has been unequivocally evidenced by targeting experiments, as deletion of the laminin $\alpha 1$, $\beta 1$, and $\gamma 1$ [4, 34, 35] chains results in BM defects and early embryonic lethality. Since laminin plays a key role for skeletal muscle biology and since mutations in laminin genes result in prominent muscle pathologies in humans, we wondered about the cell biological and functional consequences on cardiac muscle development and differentiation upon deletion of the laminin $\gamma 1$ chain. We show that this results in a complete absence of BM (collagen IV, nidogen) around cardiomyocytes, whereas cardiomyocyte development and differentiation remain surprisingly unaffected. The observed lack of BM formation is clearly due to the deficiency of laminin, since our rescue approach with soluble laminin led to a partial recovery of BM structure/formation around cardiomyocytes. Our data also demonstrate that the cytoskeleton of cardiomyocytes is in contrast to skeletal muscle [1, 2, 7], relatively independent of ECM structures. This is most likely due to compensatory effects of the laminin $\gamma 3$ chain. This chain is broadly expressed in several tissues [26], has the same modular structure as the laminin $\gamma 1$ chain, and was found to be more organized around laminin $\gamma 1$ ($-/-$) cardiomyocytes, thereby forming a partial molecular substitute. We also observed a higher N-cadherin concentration at the border zones of laminin $\gamma 1$ ($-/-$) car-

diomyocytes, indicating its contribution to the maintenance of cytoskeletal anchorage and cell-cell contacts.

Laminin polymerization is essential, first, to induce reorganization of laminin itself into a BM, and then to form a structured network of the components of the cortical cytoskeleton, such as $\beta 1$ integrin, vinculin, and talin. We showed in our earlier work that $\beta 1$ integrin ($-/-$) cardiomyocytes did only differentiate into primitive cardiac muscle cells [12] and that muscarinic signaling was entirely absent because of spatial displacement of $G\alpha_i$ [20]. However, although the lack of laminin affected the expression and the distribution of $\beta 1$ integrins, the function of laminin $\gamma 1$ ($-/-$) cardiomyocytes at the single-cell level and in whole EBs was preserved [20, 36]. This suggests that the presence of $\beta 1$ integrins, even if not entirely correctly distributed, suffices to preserve an orderly spatial organization of the receptor-dependent actinin-talin clustering, presumably thereby maintaining the cortical cytoskeleton in cardiomyocytes.

Alterations in certain laminin genes result in muscular pathologies but also in severe changes of heart function (i.e., disturbances of heart rate variability), impaired conduction resulting in arrhythmias, and left ventricular failure accompanied by progressive accumulation of connective tissue [37–39]. In line with these observations our MEA results show that the electrical signal is not appropriately propagated in laminin $\gamma 1$ ($-/-$) EBs, and this is supported by the reduced apparent conduction velocity within cardiomyocyte clusters. There are two mechanisms potentially responsible for this disturbed conductance, intracellular and intercellular. We could not detect a significant lowering of Na^+ (dV/dt max measurements), I_{Ca-L} , and/or K^+ (MDP) channels, thereby ruling out the possibility that changes of the intracellular conduction caused the observed slowed conduction in the laminin $\gamma 1$ chain ($-/-$) cardiomyocyte clusters. The intercellular conduction is mediated by connexins, and we therefore investigated cardiac connexins with Western blotting and immunostaining. The experiments yielded no apparent differences in their expression and localization. Furthermore, we could not find an increase in potentially electrically isolating cells interspersed between the cardiomyocytes, a finding supported by the relatively little reduction in apparent conduction velocity in the mutant cardiomyocyte clusters. In fact, in the case of cardiomyocyte-fibroblast coupling the apparent conduction velocity would strongly drop [40]. Rather, we found deposits of ECM between adjacent cells, which presumably caused altered spacing between the cells (also described in Fig. 6E, right) resulting in defective intercellular coupling via gap junctions despite their normal expression pattern. Furthermore, we found in single-cell experiments and in EBs more pacemaker-like cardiomyocytes and ectopic centers, respectively. This suggests that the maintenance of spontaneously active, pacemaker-like cells is enhanced in electrically silent and/or uncoupled areas and/or that there is a compensatory mechanism to overcome the uncontrolled ECM deposition and the alteration of the propagation of electrical excitation. We propose that this mechanism underlies the increased number of pacemaker-like cells rather than the lack of laminin $\gamma 1$ expression directly modulating the subtype differentiation of early cardiomyocytes.

The clearly higher deposits of several ECM proteins (collagen I and VI and fibronectin, among others) in laminin $\gamma 1$ ($-/-$) EBs because of disturbed BM formation (downregulation of collagen IV, nidogen-1, and $\beta 1$ integrins), fit nicely into the pathophysiological sequelae of cardiomyopathies, where remodeling of the heart is followed by deposition of ECM molecules or, eventually, calcifications as well. Our data demonstrate that such deposits can hinder normal spreading of the

electrical signal and consequently result in the in vivo situation, with a propensity toward potentially life-threatening ventricular arrhythmias [41–43].

SUMMARY

Our study demonstrates that the differentiation and function of laminin $\gamma 1$ ($-/-$) cardiomyocytes are intact despite the complete absence of BM. However, disruption of normal BM formation and the resulting deposits of ECM hinder physiological spreading of the electrical propagation wave, leading to slowing of the apparent conduction velocity and an increase of the number of pacemaker areas. Thus, even though laminin is not involved directly in heart muscle development and cardiomyocyte signaling, it plays a key role in the organization of the ECM and hence in the orderly propagation of electrical signals.

REFERENCES

- Colognato H, Winkelmann DA, Yurchenco PD. Laminin polymerization induces a receptor-cytoskeleton network. *J Cell Biol* 1999;145:619–631.
- Colognato H, Yurchenco PD. The laminin alpha2 expressed by dystrophic dy(2J) mice is defective in its ability to form polymers. *Curr Biol* 1999;9:1327–1330.
- Yurchenco PD, Cheng YS, Campbell K et al. Loss of basement membrane, receptor and cytoskeletal lattices in a laminin-deficient muscular dystrophy. *J Cell Sci* 2004;117:735–742.
- Smyth N, Vatansever HS, Murray P et al. Absence of basement membranes after targeting the LAMC1 gene results in embryonic lethality due to failure of endoderm differentiation. *J Cell Biol* 1999;144:151–160.
- Allamand V, Guicheney P. Merosin-deficient congenital muscular dystrophy, autosomal recessive (MDC1A, MIM#156225, LAMA2 gene coding for alpha2 chain of laminin). *Eur J Hum Genet* 2002;10:91–94.
- Helbling-Leclerc A, Zhang X, Topaloglu H et al. Mutations in the laminin alpha 2-chain gene (LAMA2) cause merosin-deficient congenital muscular dystrophy. *Nat Genet* 1995;11:216–218.
- Yurchenco PD, Amenta PS, Patton BL. Basement membrane assembly, stability and activities observed through a developmental lens. *Matrix Biol* 2004;22:521–538.
- Knöll R, Postel R, Wang J et al. Laminin-alpha4 and integrin-linked kinase mutations cause human cardiomyopathy via simultaneous defects in cardiomyocytes and endothelial cells. *Circulation* 2007;116:515–525.
- Wang J, Hoshijima M, Lam J et al. Cardiomyopathy associated with microcirculation dysfunction in laminin alpha4 chain-deficient mice. *J Biol Chem* 2006;281:213–220.
- Yanai I, Benjamin H, Shmoish M et al. Genome-wide midrange transcription profiles reveal expression level relationships in human tissue specification. *Bioinformatics* 2005;21:650–659.
- Bloch W, Forsberg E, Lentini S et al. Beta 1 integrin is essential for teratoma growth and angiogenesis. *J Cell Biol* 1997;139:265–278.
- Fässler R, Georges-Labouesse E, Hirsch E. Genetic analyses of integrin function in mice. *Curr Opin Cell Biol* 1996;8:641–646.
- Lohikangas L, Gullberg D, Johansson S. Assembly of laminin polymers is dependent on beta1-integrins. *Exp Cell Res* 2001;265:135–144.
- Kolossov E, Lu Z, Drobinskaya I et al. Identification and characterization of embryonic stem cell-derived pacemaker and atrial cardiomyocytes. *FASEB J* 2005;19:577–579.
- Ji GJ, Fleischmann BK, Bloch W et al. Regulation of the L-type Ca^{2+} channel during cardiogenesis: Switch from NO to adenylyl cyclase-mediated inhibition. *FASEB J* 1999;13:313–324.
- Banach K, Halbach MD, Hu P et al. Development of electrical activity in cardiac myocyte aggregates derived from mouse embryonic stem cells. *Am J Physiol Heart Circ Physiol* 2003;284:H2114–H2123.
- Reppel M, Boettinger C, Hescheler J. Beta-adrenergic and muscarinic modulation of human embryonic stem cell-derived cardiomyocytes. *Cell Physiol Biochem* 2004;14:187–196.
- Halbach M, Egert U, Hescheler J et al. Estimation of action potential changes from field potential recordings in multicellular mouse cardiac myocyte cultures. *Cell Physiol Biochem* 2003;13:271–284.
- Hescheler J, Halbach M, Egert U et al. Determination of electrical properties of ES cell-derived cardiomyocytes using MEAs. *J Electrocardiol* 2004;37(suppl):110–116.
- Bloch W, Fan Y, Han J et al. Disruption of cytoskeletal integrity impairs

ACKNOWLEDGMENTS

This work was supported by grants from the Deutsche Forschungsgemeinschaft (BL 419/2-2 and SM 65/1-3 within Priority Program 1086 (to B.K.F., W.B., and N.S.). R.D. was supported by a grant (SFB 645, B2) of the Deutsche Forschungsgemeinschaft to K. Willecke. Parts of this study have been reported as abstracts at the annual meeting of the German Physiological Society. We thank Dr P. Sasse for helpful and critical discussion.

DISCLOSURE OF POTENTIAL CONFLICTS OF INTEREST

The authors indicate no potential conflicts of interest.

- Gi-mediated signaling due to displacement of Gi proteins. *J Cell Biol* 2001;154:753–761.
- Malan D, Ji GJ, Schmidt A et al. Nitric oxide, a key signaling molecule in the murine early embryonic heart. *FASEB J* 2004;18:1108–1110.
 - Bader BL, Smyth N, Nedbal S et al. Compound genetic ablation of nidogen 1 and 2 causes basement membrane defects and perinatal lethality in mice. *Mol Cell Biol* 2005;25:6846–6856.
 - Wilgenbus KK, Kirkpatrick CJ, Knuechel R et al. Expression of Cx26, Cx32 and Cx43 gap junction proteins in normal and neoplastic human tissues. *Int J Cancer* 1992;51:522–529.
 - Dedek K, Schultz K, Pieper M et al. Localization of heterotypic gap junctions composed of connexin45 and connexin36 in the rod pathway of the mouse retina. *Eur J Neurosci* 2006;24:1675–1686.
 - Kolossov E, Fleischmann BK, Liu Q et al. Functional characteristics of ES cell-derived cardiac precursor cells identified by tissue-specific expression of the green fluorescent protein. *J Cell Biol* 1998;143:2045–2056.
 - Koch M, Olson PF, Albus A et al. Characterization and expression of the laminin gamma3 chain: A novel, non-basement membrane-associated, laminin chain. *J Cell Biol* 1999;145:605–618.
 - Gersdorff N, Kohfeldt E, Sasaki T et al. Laminin {gamma}3 chain binds to nidogen and is located in murine basement membranes. *J Biol Chem* 2005;280:22146–22153.
 - Hertig CM, Butz S, Koch S et al. N-cadherin in adult rat cardiomyocytes in culture. II. Spatio-temporal appearance of proteins involved in cell-cell contact and communication formation of two distinct N-cadherin/catenin complexes. *J Cell Sci* 1996;109(Pt 1):11–20.
 - Charrasse S, Meriane M, Comunale F et al. N-cadherin-dependent cell-cell contact regulates Rho GTPases and beta-catenin localization in mouse C2C12 myoblasts. *J Cell Biol* 2002;158:953–965.
 - Maltsev VA, Wobus AM, Rohwedel J et al. Cardiomyocytes differentiated in vitro from embryonic stem cells developmentally express cardiac-specific genes and ionic currents. *Circ Res* 1994;75:233–244.
 - Maltsev VA, Ji GJ, Wobus AM et al. Establishment of beta-adrenergic modulation of L-type Ca^{2+} current in the early stages of cardiomyocyte development. *Circ Res* 1999;84:136–145.
 - Reppel M, Pillekamp F, Brockmeier K et al. The electrocardiogram of human embryonic stem cell-derived cardiomyocytes. *J Electrocardiol* 2005;38:166–170.
 - Kumai M, Nishii K, Nakamura K et al. Loss of connexin45 causes a cushion defect in early cardiogenesis. *Development* 2000;127:3501–3512.
 - Shim C, Kwon HB, Kim K. Differential expression of laminin chain-specific mRNA transcripts during mouse preimplantation embryo development. *Mol Reprod Dev* 1996;44:44–55.
 - Murray P, Edgar D. Regulation of programmed cell death by basement membranes in embryonic development. *J Cell Biol* 2000;150:1215–1221.
 - Malan D, Gallo MP, Bedendi I et al. Microtubules mobility affects the modulation of L-type $I(Ca)$ by muscarinic and beta-adrenergic agonists in guinea-pig cardiac myocytes. *J Mol Cell Cardiol* 2003;35:195–206.
 - Tidball JG, Wehling-Henricks M. Evolving therapeutic strategies for Duchenne muscular dystrophy: Targeting downstream events. *Pediatr Res* 2004;56:831–841.
 - Payne TR, Oshima H, Sakai T et al. Regeneration of dystrophin-expressing myocytes in the mdx heart by skeletal muscle stem cells. *Gene Ther* 2005;12:1264–1274.
 - Hainsey TA, Senapati S, Kuhn DE et al. Cardiomyopathic features associated with muscular dystrophy are independent of dystrophin absence in cardiovascular. *Neuromuscul Disord* 2003;13:294–302.
 - Gaudesius G, Miragoli M, Thomas SP et al. Coupling of cardiac elec-

- trical activity over extended distances by fibroblasts of cardiac origin 2. *Circ Res* 2003;93:421–428.
- 41 Kamisago M, Sharma SD, DePalma SR et al. Mutations in sarcomere protein genes as a cause of dilated cardiomyopathy. *N Engl J Med* 2000;343:1688–1696.
- 42 Petrich BG, Eloff BC, Lerner DL et al. Targeted activation of c-Jun N-terminal kinase in vivo induces restrictive cardiomyopathy and conduction defects. *J Biol Chem* 2004;279:15330–15338.
- 43 Herpel E, Singer S, Flechtenmacher C et al. Extracellular matrix proteins and matrix metalloproteinases differ between various right and left ventricular sites in end-stage cardiomyopathies. *Virchows Arch* 2005; 446:369–378.



See www.StemCells.com for supporting information available online.

Lack of Laminin {gamma}1 in Embryonic Stem Cell-Derived Cardiomyocytes Causes Inhomogeneous Electrical Spreading Despite Intact Differentiation and Function

Daniela Malan, Michael Reppel, Radoslaw Dobrowolski, Wilhelm Roell, Neil Smyth, Juergen Hescheler, Mats Paulsson, Wilhelm Bloch and Bernd K. Fleischmann
Stem Cells 2009;27;88-99; originally published online Oct 16, 2008;
DOI: 10.1634/stemcells.2008-0335

This information is current as of February 5, 2009

**Updated Information
& Services**

including high-resolution figures, can be found at:
<http://www.StemCells.com/cgi/content/full/27/1/88>

Supplementary Material

Supplementary material can be found at:
<http://www.StemCells.com/cgi/content/full/2008-0335/DC1>

 **AlphaMed Press**

3.2 Cardiomyocytes differentiated from iPS cells as a model for studying monogenic heart disease:

3.2.1 Cardiomyocytes obtained from induced pluripotent stem cells with Long-QT syndrome 3 recapitulate typical disease-specific features in vitro. Circ Res. 2011 Sep 30;109(8):841-7. DOI: 10.1161/CIRCRESAHA.111.243139. Epub 2011 Jul 28. PubMed PMID: 21799153 (IF:9.48).

Aim of the study

The discovery of iPS cells has opened new horizons in using pluripotent stem cells, as a model for studying congenital diseases in the culture dish in vitro. Cells derived from iPS cells carry the gene mutation responsible for the illness but also the genetic background of the patient. This aspect confers better prediction and accuracy of the mechanisms that cause the disease. In addition, iPS cells have the advantage of ensuring a continuous source of cells. They are, therefore, essential in screening for effective drugs for treating the disease.

Monogenetic diseases are due to mutations in one specific gene which cause in to a specific cell, changes in the function or properties. The cells in culture should exhibit the phenotype expected from the patient and give clear, defined readouts reflecting the disease. Diseases arising from ion channelopathies, characterized by mutations in specific ion channel-encoding genes, present a compelling opportunity for replicating phenotypes within monotypic cell cultures derived from patient-specific iPS cells. The genetic simplicity provides a clear cause-and-effect relationship between the genetic alteration and the resulting disease phenotype.

LQTS are monogenetic diseases causing a delayed repolarization of the membrane potential of cardiomyocytes, which leads to long APD resulting in a prolongation of the QT interval in the ECG. Several mouse models for LQTS were generated. Particularly interesting was the mouse expressing the delta KPQ mutation (Scn5aΔ/+), which consists of the deletion of the amino acids, lysine-proline-glutamine, in the intracellular loop between domain III and IV of the cardiac Na⁺ (Nav1.5, Scn5a) channel (Nuyens et al., 2001). This is the most common gain of function mutation in humans, causing LQTS3, resulting in QT prolongation and arrhythmic events with sudden death during bradycardia in patients. In the Scn5aΔ/+ mouse model, it was

possible to detect the mutation-induced phenotype, namely a prolongation of the AP and a propensity for arrhythmias, as well as a specific dependence of QT prolongation at lower beating frequencies.

The primary motivation of the study on disease-specific cardiomyocytes from iPS cells derived from the fibroblasts of the LQTS3 mouse, was to evaluate whether, following the reprogramming process and subsequent in vitro differentiation, these cells could faithfully reproduce the characteristic phenotype exhibited by the LQTS3 mouse harboring the human mutation. Therefore, after generation as proof of principle disease-specific cardiomyocytes we then looked for the electrophysiological hallmarks of LQTS 3 cardiomyocytes in vitro.

Methods and results

Generation of iPS cells was achieved by retroviral transduction of murine embryonic fibroblasts from heterozygous (*Scn5a* Δ /+) and wild-type mice with the three factors Oct4, Sox-2 and Klf4, or additionally with the fourth factor c-Myc. Successful reprogramming was confirmed, showing pluripotency characteristics such as positive staining for the pluripotent markers Oct4 and SSEA1, and teratoma formation in SCID mice (Fig 1, page 842, (Malan et al., 2011)). In vitro differentiation of iPS cells was obtained via EB formation using the hanging drop method, enabling the generation of cells of all three germ layers and then the differentiation of spontaneously beating cardiomyocytes. Gene expression analysis revealed, as expected, a reduced expression of the pluripotency marker Nanog and Oct4 during differentiation. In contrast, the level of cardiac muscle structural and functional genes (*Myl2*, *Myl7*, *Myh6*, *Myh7*, *Hcn4* and *Scn5a*) increased in both wild-type and *Scn5a* Δ /+ cells after 14 days of cultivation (Fig 2, page 843). These data indicated that generation of cardiomyocytes was possible.

By the enzymatic dissociation of beating areas of EBs, we obtained single cardiomyocytes of wild-type and *Scn5a* Δ /+ iPS cells. We found similar *Scn5a* channel distribution patterns in both clones using immunostainings, and equal peak sodium currents using the patch clamp technique. However, biophysical characterization of the sodium current yielded a significantly faster recovery from inactivation in *Scn5a* Δ /+ cardiomyocytes. Furthermore, the TTX-sensitive late sodium current was also significantly larger in *Scn5a* Δ /+ than in wild-type cardiomyocytes

(see Table 1, page 845, and Fig 3, page 844). Analysis of AP shape at various pacing frequencies showed a prolonged APD in Scn5a Δ /+ cardiomyocytes at low pacing rates (<0.5 Hz). For quantitation, the relationship between the pacing period and APD was determined for each cell by linear regression analysis. This relationship yielded a flat slope in wild-type cardiomyocytes but a steep positive slope in Scn5a Δ /+ cardiomyocytes, indicating a correlation between the APD and the frequency of pacing, specifically with prolonged APD at lower pacing frequencies (see Table 2, page 845 and Fig 4, page 846). Furthermore, at low pacing rates EADs were observed in about half of Scn5a Δ /+ cells (53.8%), but never in wild-type cardiomyocytes. The electrophysiological hallmarks were typical of the LQTS gain of function delta KPQ mutation of the Scn5a Na⁺ channel. Most importantly, the electrophysiological results were similar to those that were obtained from the LQTS3 mouse and patients carrying this mutation.

Conclusion

In this study, we provide evidence that cardiomyocytes derived from iPS cells obtained by reprogramming fibroblasts of a mouse model of a human LQTS3 mutation can recapitulate the typical pathophysiological features in cardiomyocytes upon reprogramming and in vitro differentiation. Most importantly, we observed a prolonged AP at low frequencies with EADs, all typical signs of LQTS3. This data further confirmed the possibility of using iPS-derived cardiomyocytes in the analysis of monogenetic disease mechanisms even though they are not at a terminal maturation stage.

Contribution: designed, performed, and analyzed patch clamp experiments, discussion, and analysis of the data, coauthored the manuscript.

Cardiomyocytes Obtained From Induced Pluripotent Stem Cells With Long-QT Syndrome 3 Recapitulate Typical Disease-Specific Features In Vitro

Daniela Malan,* Stephanie Friedrichs,* Bernd K. Fleischmann, Philipp Sasse

Rationale: Current approaches for the investigation of long-QT syndromes (LQTS) are mainly focused on identification of the mutation and its characterization in heterologous expression systems. However, it would be extremely helpful to be able to characterize the pathophysiological effects of mutations and to screen drugs in cardiomyocytes.

Objective: The aim of this study was to establish as a proof of principle the disease-specific cardiomyocytes from a mouse model with LQTS 3 by use of induced pluripotent stem (iPS) cells and to demonstrate that the mutant cardiomyocytes display the characteristic pathophysiological features in vitro.

Methods and Results: We generated disease-specific iPS cells from a mouse model with a human mutation of the cardiac Na^+ channel that causes LQTS 3. The control and LQTS 3-specific iPS cell lines were pluripotent and could be differentiated into spontaneously beating cardiomyocytes. Patch-clamp measurements of LQTS 3-specific cardiomyocytes showed the biophysical effects of the mutation on the Na^+ current, with faster recovery from inactivation and larger late currents than observed in controls. Moreover, LQTS 3-specific cardiomyocytes had prolonged action potential durations and early afterdepolarizations at low pacing rates, both of which are classic features of the LQTS 3 mutation.

Conclusions: We demonstrate that disease-specific iPS cell-derived cardiomyocytes from an LQTS 3 mouse model with a human mutation recapitulate the typical pathophysiological phenotype in vitro. Thus, this method is a powerful tool to investigate disease mechanisms in vitro and to perform patient-specific drug screening. (*Circ Res.* 2011;109:841-847.)

Key Words: cardiac electrophysiology ■ cell culture ■ induced pluripotent stem cells ■ long QT syndrome ■ SCN5A

Long-QT syndrome (LQTS) is a severe disorder of the electric activity of the heart. It is caused by delayed repolarization of cardiomyocytes, which leads to abnormally long action potential (AP) durations that result in a prolonged QT interval in the ECG.¹ The lifespan of patients with LQTS is often limited because of the development of ventricular tachycardia and sudden cardiac death.^{1,2} Generally, LQTS are caused by loss-of-function mutations, but they can also be caused by gain-of-function mutations, the most common being LQTS 3. The most frequent LQTS 3 mutation is the deletion of the amino acids lysine-proline-glutamine (ΔKPQ) in the intracellular loop between domains III and IV of the cardiac Na^+ channel.^{1,3} This results in reactivation of Na^+ channels during the late phase of the AP, which leads to prolongation of the AP duration and QT interval, as well as dangerous early afterdepolarizations (EADs) at slow heart rates.³ Because of the strong frequency dependence of this effect, patients with LQTS 3 have lethal arrhythmias preferentially at rest and during sleep.^{1,2}

The common pathophysiological feature of LQTS is the prolonged AP duration in cardiomyocytes. This cannot be

investigated directly in vitro because sufficient numbers of human ventricular cardiomyocytes cannot be harvested from patients. Therefore, the properties of mutated ion channels are preferentially investigated in heterologous expression systems that lack the typical cell biological and physiological features of cardiomyocytes.^{2,4}

Induced pluripotent stem (iPS) cells can be propagated to an unlimited extent and have been shown to serve as a source of cardiomyocytes in vitro.⁵ Moreover, it has been shown recently that iPS cells derived from patients with LQTS 1 or 2 can be used to obtain disease-specific cardiomyocytes.^{6,7} In the present study, we provide evidence that cardiomyocytes differentiated from disease-specific iPS cells do recapitulate the typical frequency-dependent features of the LQTS 3 phenotype in vitro.

Methods

An expanded Methods section is available in the Online Data Supplement at <http://circres.ahajournals.org>.

iPS cells were generated by retroviral transduction of murine embryonic fibroblasts (MEFs) from *Scn5a* Δ /+ mice (mice heterozy-

Original received July 13, 2010; resubmission received February 23, 2011; revised resubmission received July 13, 2011; accepted July 14, 2011. In June 2011, the average time from submission to first decision for all original research papers submitted to *Circulation Research* was 14.48 days.

From the Institute of Physiology I, Life & Brain Center, University of Bonn, Germany.

*D.M. and S.F. contributed equally to this work.

Correspondence to Philipp Sasse, MD, or Bernd K. Fleischmann, MD, Institute of Physiology I, Life & Brain Center, University of Bonn, Sigmund Freud Strasse 25, Bonn, 53105, Germany. E-mail philipp.sasse@uni-bonn.de or bernd.fleischmann@uni-bonn.de

© 2011 American Heart Association, Inc.

Circulation Research is available at <http://circres.ahajournals.org>

DOI: 10.1161/CIRCRESAHA.111.243139

Non-standard Abbreviations and Acronyms	
AP	action potential
APD ₉₀	action potential duration at 90% of repolarization
EAD	early afterdepolarization
EB	embryoid body
ES cells	embryonic stem cells
iPS cells	induced pluripotent stem cells
MEF	murine embryonic fibroblast
Scn5aΔ/+	mice heterozygous for KPQ deletion of Scn5a

gous for the KPQ deletion of Scn5a) and wild-type littermates either with the 3 factors Oct4, Sox2, and Klf4 or additionally with the fourth factor c-Myc, as described previously.^{8,9} Teratoma assay was performed by injection of undifferentiated iPS cells into SCID mice. For in vitro differentiation of iPS cells, the hanging drop method was used to generate embryoid bodies as described previously.¹⁰ Immunostainings were performed according to standard protocols,¹⁰ and TaqMan assays (Applied Biosystems, Foster City, CA) were used for quantitative polymerase chain reaction.

Na⁺ currents were recorded and biophysically characterized from differentiated cardiomyocytes by use of the patch-clamp technique as described previously.^{3,4,10,11} For recording of frequency-dependent AP durations, APs were evoked at various pacing periods, and the slope of the AP duration at 90% of repolarization (APD₉₀)–pacing period relationship was analyzed for each individual cell by a linear regression.

Results

Generation of Disease-Specific iPS Cell Lines

iPS cells were generated from MEFs derived from wild-type and Scn5aΔ/+ littermates. For this purpose, MEFs were prepared from single embryos, genotyped (Figure 1B), and infected with retroviruses to express specific “stemness” factors.⁸ Reprogramming efficiency was enhanced by the addition of extracellular signal-regulated kinase and glycogen synthase kinase 3 inhibitors.⁹ Embryonic stem (ES) cell–like colonies appeared after 14 days and were selected on the basis of their ES cell–like morphology. Wild-type and Scn5aΔ/+ iPS cell lines were propagated on irradiated MEF layers and retained the morphology of undifferentiated ES cells (Figure 1A). Both wild-type and Scn5aΔ/+ iPS cells expressed the stem cell markers Oct4 and SSEA1 (Figure 1C). As expected,

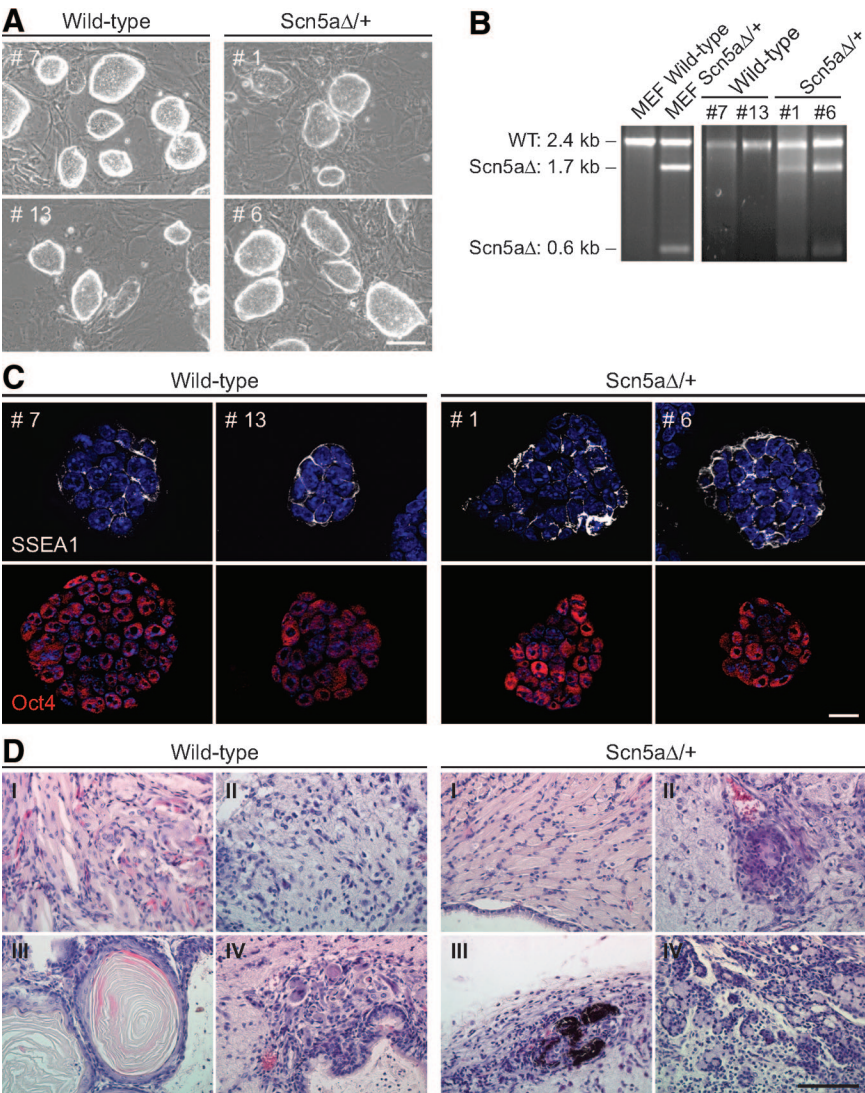


Figure 1. Generation of LQTS 3–specific iPS cell lines. **A**, Phase-contrast images of wild-type (left) and Scn5aΔ/+ (right) iPS cell lines. **B**, Genotyping of MEFs from wild-type and Scn5aΔ/+ embryos (left) used for generation of iPS cell lines and genotyping of established iPS cell clones (right). **C**, Immunostainings of wild-type and Scn5aΔ/+ iPS cell colonies for the pluripotent markers SSEA1 (upper row, white) and Oct4 (lower row, red). **D**, Teratoma derived from wild-type (left) and Scn5aΔ/+ (right) iPS cell lines with cell types from all 3 germ layers: skeletal muscle (I), neurons (II), squamous epithelium (left III), retinal epithelium with pigment (right III), and glandular tissue (IV). Nuclei are shown in blue. Scale bars: 100 μm (A and D), 20 μm (C).

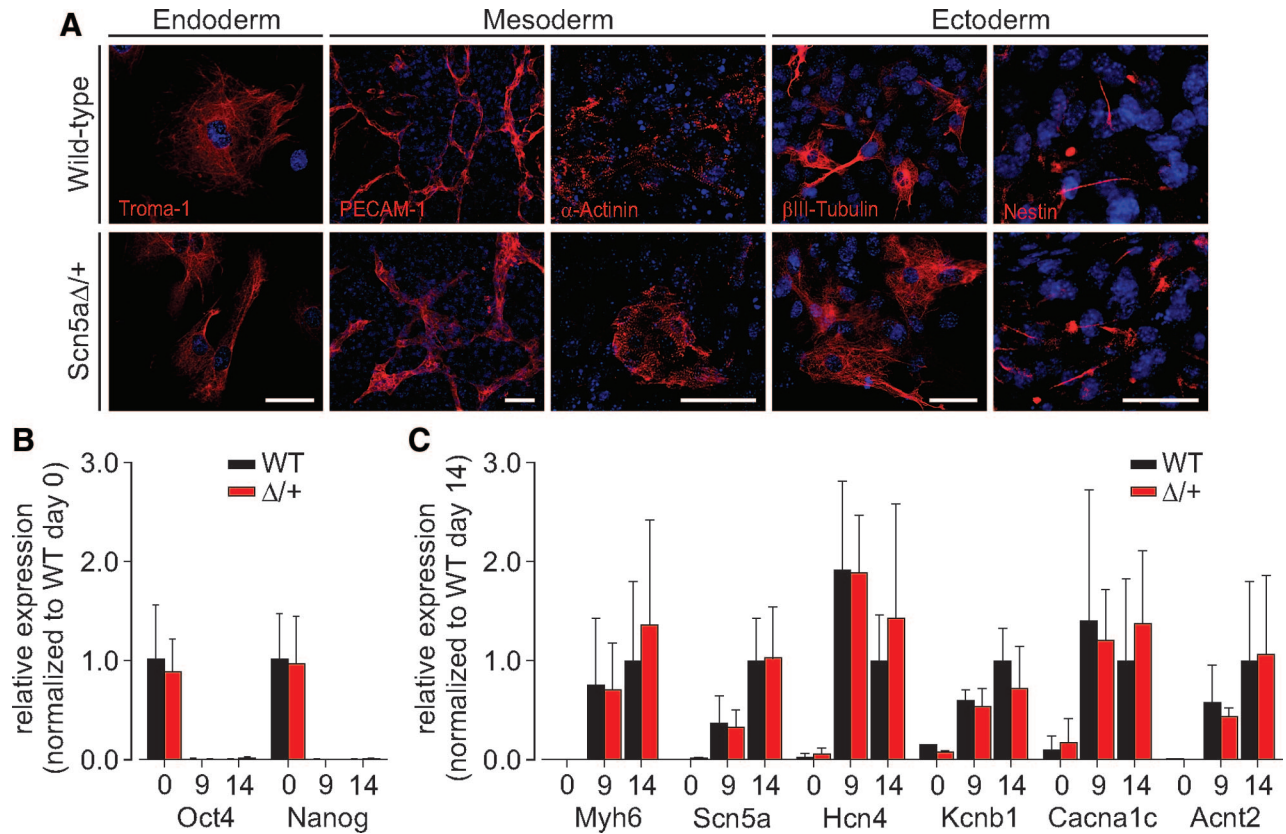


Figure 2. Differentiation potential of iPS cells. **A**, Wild-type (top) and Scn5aΔ/+ (lower) iPS cells were differentiated for 10 days and stained for specific markers (red). PECAM-1 indicates platelet endothelial cell adhesion molecule-1. **B** and **C**, Relative gene expression of the stem cell markers Oct4 and Nanog (**B**) and of cardiac markers (**C**) in wild-type (WT) and Scn5aΔ/+ undifferentiated iPS cells (0) and differentiated embryoid bodies at day 9 (9) and day 14 (14). Nuclei are shown in blue. Scale bars, 50 μm; error bars, SD.

genotyping of iPS cell lines revealed the mutation in the Scn5aΔ/+ but not in the wild-type iPS cells (Figure 1B).

Pluripotency of Wild-Type and Scn5aΔ/+ iPS Cells

The pluripotency of established iPS cell lines was proven by in vivo teratoma formation and in vitro differentiation. After injection of wild-type and Scn5aΔ/+ iPS cells into SCID mice, teratoma developed with tissues from all 3 germ layers (Figure 1D). We also analyzed the in vitro differentiation characteristics and stained embryoid bodies at day 10 for markers of cells from the 3 different germ layers. Both wild-type and Scn5aΔ/+ iPS cell lines showed Troma-1-positive cells, which indicates endodermal differentiation (Figure 2A). Mesodermal differentiation (Figure 2A) was proven on the basis of platelet endothelial cell adhesion molecule-1-positive endothelial cells and α-actinin-positive cardiomyocytes. The presence of nestin- and βIII-tubulin-positive cells highlighted ectodermal differentiation (Figure 2A). Wild-type and Scn5aΔ/+ embryoid bodies showed typical spontaneous beating areas starting around day 7 of differentiation (supplementary Videos I and II). Relative gene expression analysis by quantitative polymerase chain reaction revealed a similar expression of stem cell markers (Oct4 and Nanog) in wild-type and Scn5aΔ/+ iPS cells that decreased on differentiation (Figure 2B). Expression of the cardiac-specific markers α-myosin heavy chain (Myh6), Na_v1.5 Na⁺

channel (Scn5a), hyperpolarization-activated cyclic nucleotide-gated channel 4 (Hcn4), K_v2.1 delayed rectifier K⁺ channel (Kcnb1), Ca_v1.2 L-type Ca²⁺ channel (Cacna1c), and α2-actinin (Acnt2) increased to a similar extent during differentiation of wild-type and Scn5aΔ/+ iPS cells (Figure 2C). Interestingly, expression of the Na⁺ channel (Scn5a) further increased with ongoing differentiation from day 9 to day 14.

Biophysical Characterization of Na⁺ Currents in Disease-Specific and Wild-Type Cardiomyocytes From iPS Cells

To measure Na⁺ currents and APs in single wild-type and Scn5aΔ/+ iPS cell-derived cardiomyocytes, single cells were isolated from beating areas of embryoid bodies and investigated by use of the patch-clamp technique. Cardiomyocytes from both lines were spontaneously beating and showed similar Na⁺ channel distribution and well-organized sarcomeric structures with Scn5a and α-actinin staining (Figure 3A).

Because LQTS 3 is caused by mutated Na⁺ channels, we investigated the functional expression of the voltage-dependent Na⁺ current at early (day 12) and late (late developmental stage, days 19 to 22) stages of differentiation using voltage ramps (data not shown). The percentage of cells with Na⁺ currents was lower in the early developmental stage (66.6% of wild-type [n=12] and 66.6% of Scn5aΔ/+ [n=15] cells) than in the late developmental stage (92.8% of wild-

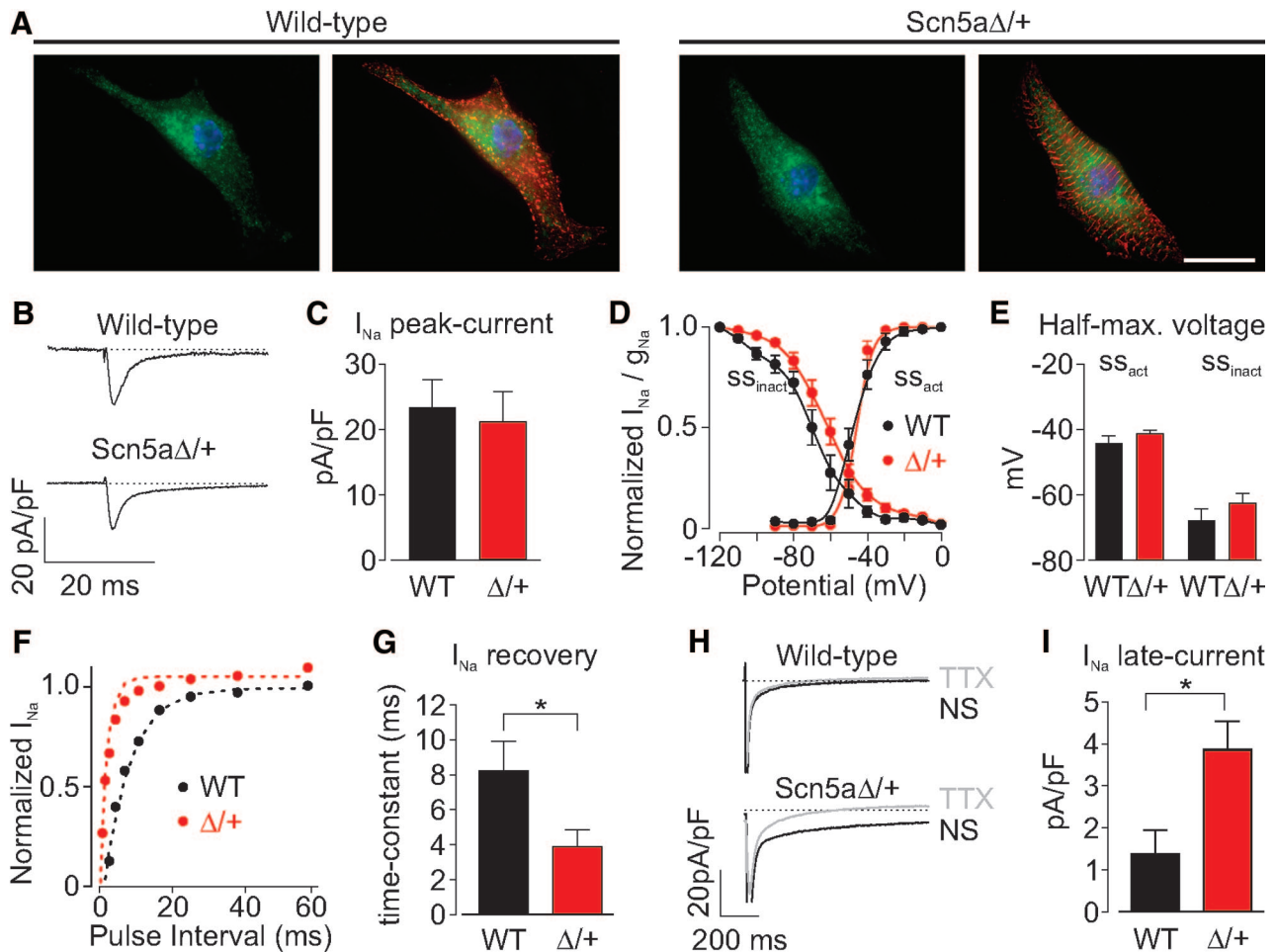


Figure 3. Na⁺ currents in LQTS 3-specific and wild-type cardiomyocytes. **A**, Immunofluorescence images of Scn5a Na⁺ channel distribution (green) and sarcomeric α -actinin structure (red) in a wild-type and Scn5a Δ /+ cardiomyocyte. **B** and **C**, Na⁺ currents (**B**) and average current densities (**C**) in wild-type (WT) and Scn5a Δ /+ iPS cell-derived cardiomyocytes. **D** and **E**, Averaged steady state activation (ss_{act}) and inactivation (ss_{inact}) curves for wild-type and Scn5a Δ /+ cardiomyocytes (**D**) and statistical analysis of the potential of half-maximal (Half-max) activation and inactivation (**E**). **F**, Analysis of recovery from inactivation in a representative wild-type and Scn5a Δ /+ cardiomyocyte (monoexponential fit shown by dashed lines). **G**, Statistical analysis of the time constants of recovery from inactivation. **H**, Representative traces of late Na⁺ current before and after tetrodotoxin (TTX) application (20 μ mol/L) in a wild-type (**top**) and an Scn5a Δ /+ (**lower**) cardiomyocyte. **I**, Statistical analysis of TTX-sensitive late Na⁺ current densities. Nuclei are shown in blue. Scale bar, 20 μ m. Dotted lines indicate zero current; error bars, SEM. * P <0.05.

type [$n=14$] and 76.4% of Scn5a Δ /+ [$n=17$] cells). This is in line with gene expression data of the Na⁺ channel (Figure 2C), and therefore, only cardiomyocytes from the late developmental stage were investigated further. The capacitance of these cells was very similar (Table 1), which excludes the possibility that functional differences were related to cell size. Na⁺ current density at -10 mV was similar in wild-type and Scn5a Δ /+ cells (Figures 3B and 3C; Table 1). We also did not observe differences between genotypes in the steady state activation and inactivation of the Na⁺ current (Figure 3D) or in the potential for half-maximal activation and inactivation (Figure 3E; Table 1). The time constants for the kinetics of deactivation did not differ at -40 mV and at 0 mV between wild-type and Scn5a Δ /+ cardiomyocytes (Table 1). However, recovery from inactivation of the Na⁺ current was significantly faster in Scn5a Δ /+ than in wild-type cells (Figures 3F and 3G; Table 1). Similarly, the tetrodotoxin-sensitive late Na⁺ current was significantly larger in Scn5a Δ /+ than in wild-type iPS cell-derived cardiomyocytes (Figures 3H

and 3I; Table 1). These data revealed that the classic biophysical features of the mutated Scn5a Na⁺ current could be observed in iPS cell-derived late-stage cardiomyocytes.

Characterization of APs From Wild-Type and Scn5a Δ /+ iPS Cell-Derived Cardiomyocytes

Because prolonged duration of APs, especially at low frequencies, is the typical hallmark of LQTS 3, we evoked APs in the current clamp mode and focused primarily on AP duration at different pacing frequencies. Amplitude, upstroke velocity, and resting membrane potential were similar in both genotypes (Table 2); however, clear differences were observed when we analyzed frequency-dependent AP durations. Wild-type cardiomyocytes had similar AP durations at fast and slow pacing rates (Figure 4A). In contrast, Scn5a Δ /+ cardiomyocytes showed prolonged AP durations when paced at slower rates (Figure 4B).

Because of the high variability of AP duration at APD₉₀ between individual cells, only a tendency toward prolonga-

Table 1. Biophysical Parameters of Na⁺ Currents

Parameter	Wild Type	Scn5aΔ/+	P
Capacitance, pF	54.6±8.4, n=33	49.8±7.1, n=27	0.66
<i>I</i> _{Na} peak, pA/pF	23.3±4.4, n=9	21.2±4.6, n=7	0.75
SS _{act} v1/2, mV	−44.3±2.4, n=15	−41.3±1.0, n=7	0.26
SS _{inact} v1/2, mV	−67.8±3.5, n=12	−62.6±3.0, n=11	0.27
τ Deact −40 mV, ms	3.63±0.95, n=14	3.47±1.17, n=8	0.92
τ Deact 0 mV, ms	2.43±0.60, n=13	2.07±0.72, n=6	0.71
τ Recovery, ms	8.23±1.67, n=7	3.90±0.96, n=7	0.0496
<i>I</i> _{Na} late, pA/pF	1.38±0.56, n=7	3.86±0.67, n=8	0.0144

*I*_{Na} peak indicates Na⁺ current density at −10 mV; SS_{act} v1/2, half-maximal voltage of steady state activation; SS_{inact} v1/2, half-maximal voltage of steady state inactivation; τ Deact, time constant of the kinetic of deactivation at −40 mV and 0 mV; τ Recovery, time constant of recovery from inactivation; and *I*_{Na} late, current density of tetrodotoxin-sensitive late Na⁺ current.

Values are mean±SEM.

P determined by Student *t* test.

tion of averaged APD₉₀ was noted in Scn5aΔ/+ cells (Figure 4C). Because of the cell-to-cell variability, we quantified the dependency of AP duration of pacing periods (APD₉₀–pacing period) in individual cardiomyocytes using linear regression analysis (examples in Figure 4D). In wild-type cells, APD₉₀ was hardly affected by pacing frequency, therefore yielding a flat slope in the APD₉₀–pacing period relationship (Figure 4E; Table 2). In contrast, this was significantly different in Scn5aΔ/+ cardiomyocytes, in which the slope was steeply positive (Figure 4E; Table 2). In addition, approximately half of the Scn5aΔ/+ cardiomyocytes developed EADs at low pacing rates (Figures 4F and 4G), which were not observed in any of the wild-type cells (Figures 4F and 4G).

Discussion

The aim of the present study was to investigate whether reprogramming of fibroblasts harvested from a representative LQTS 3 model enabled reproduction of the characteristic electrophysiological features of the disease in vitro. For this purpose, we used a well-established LQTS 3 mouse model carrying the human ΔKPQ mutation of the Na⁺ channel (Scn5aΔ/+) that is known to display typical electrophysio-

logical features of LQTS 3, including specific frequency-dependent changes of the AP duration.^{3,12}

We demonstrated that iPS cells can be generated from wild-type and Scn5aΔ/+ MEFs. The pluripotency of iPS clones was confirmed by gene expression analysis, teratoma formation, and in vitro differentiation assays. Most importantly, wild-type and Scn5aΔ/+ iPS cells could be differentiated into functional intact cardiomyocytes. We investigated different stages of iPS cell differentiation and found that compared with cells in the early developmental stage, late developmental stage cells have higher Scn5a gene expression, and a larger percentage of late developmental stage cardiomyocytes expressed functional Na⁺ currents, which is similar to ES cell–derived cardiomyocytes.¹¹ Therefore, late developmental stage spontaneously beating single cardiomyocytes were analyzed, and the biophysical properties between wild-type and Scn5aΔ/+ cardiomyocytes were compared. Cell capacitance, Scn5a channel distribution, and Na⁺ peak current densities were similar between the 2 genotypes; however, in Scn5aΔ/+ cardiomyocytes, Na⁺ currents had faster recovery from inactivation and larger amplitudes of the late component of the Na⁺ current. These biophysical properties are typical of the ΔKPQ mutation and have been described previously in heterologous expression systems⁴ and in cardiomyocytes from the LQTS 3 mouse model.³ Other biophysical features of the Na⁺ current, such as steady state activation and inactivation, were unaltered, which is in accordance with previous reports on the ΔKPQ mutation.^{3,4} When measuring APs, we observed a tendency toward longer APD₉₀ in Scn5aΔ/+ cardiomyocytes, but this did not reach statistical significance because of high intercellular variability. This variability is most likely because in contrast to investigations of the adult heart in previous studies,³ the developmental stages of iPS and ES cell–derived cardiomyocytes is not identical between individual cells. We therefore determined the APD₉₀ at different pacing rates in the same cell and found that all Scn5aΔ/+ iPS-derived cardiomyocytes had prolonged APD₉₀ at lower stimulation rates and a high incidence of EADs. Thus, cardiomyocytes with the ΔKPQ mutation were characterized by a steep APD₉₀–pacing period ratio, and this clearly differed from iPS cell–derived wild-type cardiomyocytes. The steep positive frequency dependence of AP or QT duration is, in contrast to LQTS 1 and 2, a phenotypic hallmark of LQTS 3 and has been reported in mice³ and patients.¹²

We were able to analyze APD₉₀ in LQTS3-specific iPS cell–derived cardiomyocytes within a broad range (0.5 to 6 seconds) of pacing periods. Although these were substantially lower rates than observed in adult mice, the large pacing range enabled investigations of the frequency-dependent adverse effects of ion channel mutations and of novel compounds, in particular with the use-dependent block of ion channels.

The generation of disease-specific cardiomyocytes from iPS cells represents an important step, because human cardiomyocytes cannot be harvested and expanded in sufficient numbers from patients. Because of this limitation, previous investigations of LQTS used heterologous expression in noncardiomyocytes to unravel the consequences of a mutation on the biophysical properties of the affected ion channel. However, because these cells lack the potential for AP

Table 2. AP Parameters

Parameter	Wild Type	Scn5aΔ/+	P
RMP at 1 Hz, mV	−80.0±3.5, n=6	−83.0±3.3, n=7	0.55
APA at 1 Hz, mV	96.7±4.9, n=6	110.0±3.8, n=7	0.06
Vmax at 1 Hz, V/s	64.6±11.3, n=6	88.6±9.2, n=7	0.13
APD ₉₀ at 2 Hz, ms	48.0±9.7, n=5	83.2±18.0, n=7	0.12
APD ₉₀ at 1 Hz, ms	60.5±12.7, n=6	84.8±21.6, n=7	0.36
APD ₉₀ at 0.17 Hz, ms	63.6±13.2, n=5	113.7±24.8, n=6	0.12
Slope, ms/s	−2.92±1.27, n=9	9.08±3.60, n=11	0.0178
% Cells with EAD	0%, n=10	50%, n=12	0.0152*

RMP indicates resting membrane potential; APA, AP amplitude; Vmax, maximal upstroke velocity; and slope, slope of linear relationship between APD₉₀ and pacing period.

Values are mean±SEM. P determined by Student *t* test except *, which was analyzed by Fisher exact test.

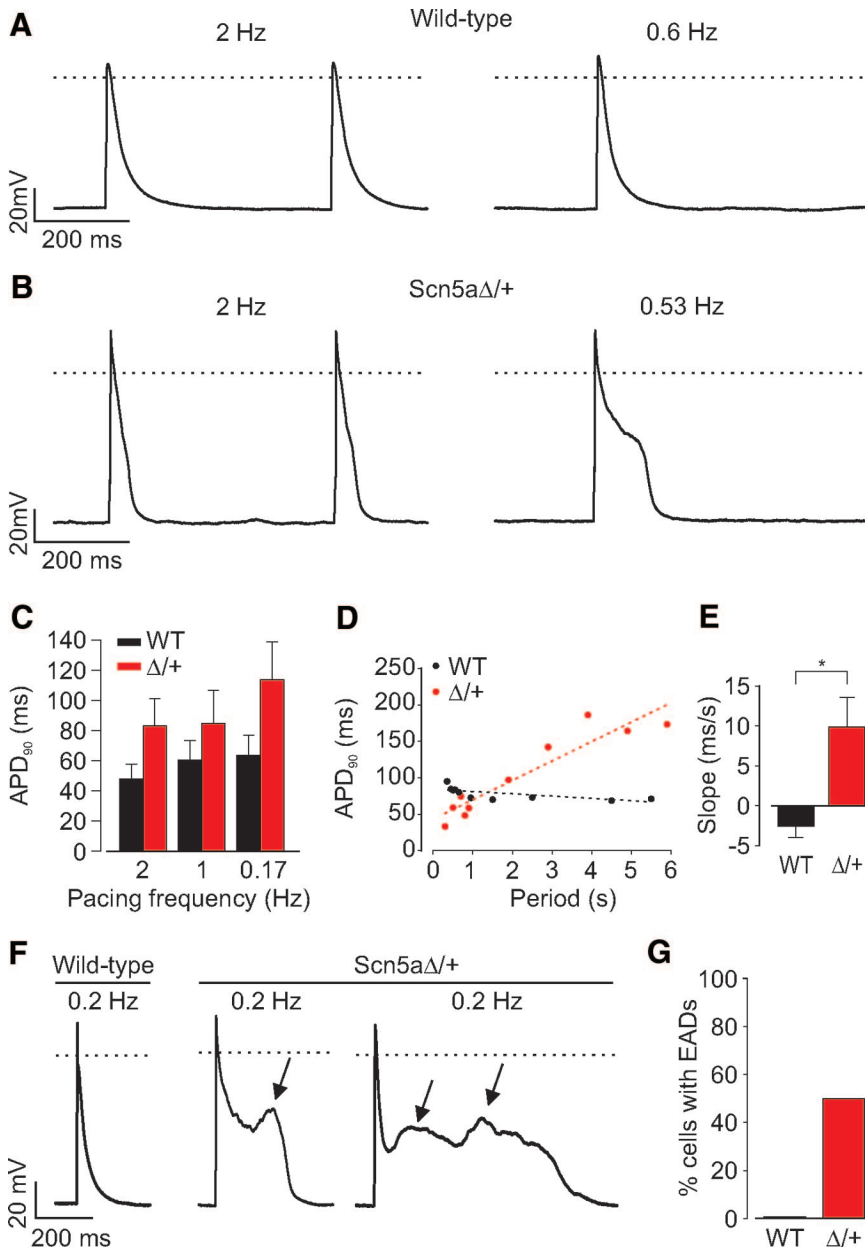


Figure 4. AP characteristics of LQTS 3-specific and wild-type cardiomyocytes. **A** and **B**, Representative traces of APs from wild-type (**A**) and *Scn5a*Δ/+ (**B**) cardiomyocytes at high and low pacing frequencies. **C**, Statistical analysis of APD₉₀ at different pacing periods for wild-type (WT) and *Scn5a*Δ/+ cells. **D**, Relationship between APD₉₀ and pacing period of the wild-type (black) and *Scn5a*Δ/+ (red) cell shown in panels **A** and **B**. Linear regression shown by dashed lines. **E**, Statistical analysis of the slope of APD₉₀-pacing period relationship from individual cells. **F**, Typical EADs were observed at low pacing frequencies only in *Scn5a*Δ/+ cells (**middle and right, arrows**) and never in wild-type cells (**left**). **G**, Percentage of cardiomyocytes displaying EADs. Dotted line indicates 0 mV; error bars, SEM. **P* < 0.05.

generation, such systems can only predict the possible consequences related to AP shape and duration in cardiomyocytes.^{4,13} In addition, heterologous systems do not reflect the influence of potential compensatory pathways, the impact of known and unknown accessory channel subunits, and the variability of cell-specific trafficking aspects, all effects that may be present in functional cardiomyocytes. Although mouse models displaying human LQTS have been generated with success and recapitulate at least in part the phenotype in cardiomyocytes,^{2,3} they are of limited relevance because of striking differences in heart rate² and because they cannot be used to generate unlimited amount of cardiomyocytes for high-throughput screenings in vitro.

Recently, LQTS 1 and 2 disease-specific cardiomyocytes were obtained from reprogrammed fibroblasts of patients.^{6,7} Here, we provide evidence that LQTS 3 disease-specific iPS cells can also be generated and differentiated into cardiomyo-

cytes that maintain the functional hallmarks of the mutation in vitro. This outcome could not be predicted by previous studies, because iPS-derived cardiomyocytes are not terminally differentiated. At the early developmental stage, ES cell-derived cardiomyocytes have primarily Ca²⁺-driven APs, and only at later stages of differentiation does the functional Na⁺ current density increase and the AP become Na⁺ dependent.¹¹ In addition, beating frequencies of iPS- and ES-derived cardiomyocytes are similar to fetal hearts, which are characterized by much lower beating rates than adult cardiomyocytes. It was therefore unclear whether the functional phenotype of the ΔKPQ mutation could be reproduced despite these obvious physiological differences between adult mouse and iPS cardiomyocytes. The present data clearly demonstrate that the pathognomonic functional features of the ΔKPQ mutation, namely, the long AP duration at slower pacing rates and the occurrence of EADs, are identified in LQTS 3-specific iPS-derived cardiomyocytes. In future

studies, it should be possible to measure these effects with a high-throughput patch clamp or extracellular field potential recordings. Such approaches could enable pharmacological screening in vitro on cardiomyocytes, sparing animal experiments. Moreover, it is very likely that the use of iPS cells will allow functional analysis and patient-specific drug development even in patients in whom the specific mutation underlying the disease has not yet been identified. The feasibility of generating iPS cells from skin biopsy samples, keratinocytes, or somatic cell types of humans will enable the establishment of a wide range of relevant human disease models in the culture dish.

Acknowledgments

We thank P. Carmeliet, Flanders Interuniversity Institute for Biotechnology (VIB), Leuven, Belgium, for providing the *Scn5a* Δ /+ mouse line; H.R. Schoeler and H. Zaehres, Max Planck Institute for Molecular Biology, Muenster, Germany, for the help with the iPS technology; and R. Schneider, Rhenish-Westphalian Technical University (RWTH Aachen), Aachen, Germany, for help with the teratoma analysis.

Sources of Funding

This work was supported by a grant from the German Ministry of Education and Research (01GN0813) to P.S. and B.K.F.

Disclosures

None.

References

- Hedley PL, Jorgensen P, Schlamowitz S, Wangari R, Moolman-Smook J, Brink PA, Kanters JK, Corfield VA, Christiansen M. The genetic basis of long QT and short QT syndromes: a mutation update. *Hum Mutat*. 2009; 30:1486–1511.
- Charpentier F, Bourge A, Merot J. Mouse models of SCN5A-related cardiac arrhythmias. *Prog Biophys Mol Biol*. 2008;98:230–237.
- Nuyens D, Stengl M, Dugarmaa S, Rossenbacker T, Compennolle V, Rudy Y, Smits JF, Flameng W, Clancy CE, Moons L, Vos MA, Dew-erchin M, Benndorf K, Collen D, Carmeliet E, Carmeliet P. Abrupt rate accelerations or premature beats cause life-threatening arrhythmias in mice with long-QT3 syndrome. *Nat Med*. 2001;7:1021–1027.
- Chandra R, Starmer CF, Grant AO. Multiple effects of KPQ deletion mutation on gating of human cardiac Na⁺ channels expressed in mammalian cells. *Am J Physiol*. 1998;274:H1643–H1654.
- Mauritz C, Schwanke K, Reppel M, Neef S, Katsirntaki K, Maier LS, Nguemo F, Menke S, Haustein M, Hescheler J, Hasenfuss G, Martin U. Generation of functional murine cardiac myocytes from induced pluripotent stem cells. *Circulation*. 2008;118:507–517.
- Moretti A, Bellin M, Welling A, Jung CB, Lam JT, Bott-Flugel L, Dorn T, Goedel A, Hohnke C, Hofmann F, Seyfarth M, Sinnecker D, Schomig A, Laugwitz KL. Patient-specific induced pluripotent stem-cell models for long-QT syndrome. *N Engl J Med*. 2010;363:1397–1409.
- Itzhaki I, Maizels L, Huber I, Zwi-Dantsis L, Caspi O, Winterstern A, Feldman O, Gepstein A, Arbel G, Hammerman H, Boulos M, Gepstein L. Modelling the long QT syndrome with induced pluripotent stem cells. *Nature*. 2011;471:225–229.
- Takahashi K, Yamanaka S. Induction of pluripotent stem cells from mouse embryonic and adult fibroblast cultures by defined factors. *Cell*. 2006;126:663–676.
- Ying QL, Wray J, Nichols J, Battle-Morera L, Doble B, Woodgett J, Cohen P, Smith A. The ground state of embryonic stem cell self-renewal. *Nature*. 2008;453:519–523.
- Kolosov E, Lu Z, Drobinskaya I, Gassanov N, Duan Y, Sauer H, Manzke O, Bloch W, Bohlen H, Hescheler J, Fleischmann BK. Identification and characterization of embryonic stem cell-derived pacemaker and atrial cardiomyocytes. *FASEB J*. 2005;19:577–579.
- Maltsev VA, Wobus AM, Rohwedel J, Bader M, Hescheler J. Cardiomyocytes differentiated in vitro from embryonic stem cells developmentally express cardiac-specific genes and ionic currents. *Circ Res*. 1994;75:233–244.
- Schwartz PJ, Priori SG, Locati EH, Napolitano C, Cantu F, Towbin JA, Keating MT, Hammoude H, Brown AM, Chen LS. Long QT syndrome patients with mutations of the SCN5A and HERG genes have differential responses to Na⁺ channel blockade and to increases in heart rate: implications for gene-specific therapy. *Circulation*. 1995;92:3381–3386.
- Berecki G, Zegers JG, Bhuiyan ZA, Verkerk AO, Wilders R, van Ginneken AC. Long-QT syndrome-related sodium channel mutations probed by the dynamic action potential clamp technique. *J Physiol*. 2006;570:237–250.

Novelty and Significance

What Is Known?

- The pathophysiological consequences of ion channel mutations that cause long-QT syndrome (LQTS) cannot be analyzed directly in cardiomyocytes from patients.
- Induced pluripotent stem (iPS) cells can be generated from skin biopsy samples of patients and differentiated into cardiomyocytes.

What New Information Does This Article Contribute?

- Disease-specific iPS cells can be generated from murine fibroblasts that carry a human mutation of the Na⁺ channel that causes LQTS 3.
- Cardiomyocytes can be differentiated in the culture dish from LQTS 3-specific iPS cells and show the known biophysical features of the cardiac Na⁺ channel mutation.
- Action potential durations of LQTS 3 cardiomyocytes were found to be prolonged at slow heart rates, which is the pathognomonic feature of LQTS 3.

LQTS are characterized by severe, potentially life-threatening cardiac arrhythmias and are caused by ion channel mutations that

lead to prolongation of the cardiac action potential duration. The pathophysiological features of LQTS have been investigated by identifying the underlying mutation, analyzing mutated ion channels in nonexcitable cells, and predicting the functional consequences on action potential duration in cardiomyocytes. A much more promising approach would be the direct analysis of cardiomyocytes from LQTS patients. Because it is technically not feasible to harvest sufficient numbers of cells from cardiac biopsy samples, we suggest an alternative approach using cardiomyocytes differentiated from iPS cells that can be obtained from skin biopsy samples by reprogramming. We demonstrate as a proof-of-principle that iPS cell-derived cardiomyocytes can be harvested from a mouse model with a human Na⁺ channel mutation that causes LQTS 3. Most importantly, for the first time, we analyzed action potentials of LQTS 3-specific cardiomyocytes from iPS cells and identified prolonged action potential durations and early afterdepolarizations at low pacing rates, which is the typical feature of LQTS 3. We suggest that cardiomyocytes differentiated from disease-specific iPS cells are a powerful tool for the investigation of disease mechanisms in vitro and for patient-specific drug screenings.

Cardiomyocytes Obtained From Induced Pluripotent Stem Cells With Long-QT Syndrome 3 Recapitulate Typical Disease-Specific Features In Vitro

Daniela Malan, Stephanie Friedrichs, Bernd K. Fleischmann and Philipp Sasse

Circ Res. 2011;109:841-847; originally published online July 28, 2011;

doi: 10.1161/CIRCRESAHA.111.243139

Circulation Research is published by the American Heart Association, 7272 Greenville Avenue, Dallas, TX 75231

Copyright © 2011 American Heart Association, Inc. All rights reserved.

Print ISSN: 0009-7330. Online ISSN: 1524-4571

The online version of this article, along with updated information and services, is located on the World Wide Web at:

<http://circres.ahajournals.org/content/109/8/841>

Data Supplement (unedited) at:

<http://circres.ahajournals.org/content/suppl/2011/07/28/CIRCRESAHA.111.243139.DC1.html>

Permissions: Requests for permissions to reproduce figures, tables, or portions of articles originally published in *Circulation Research* can be obtained via RightsLink, a service of the Copyright Clearance Center, not the Editorial Office. Once the online version of the published article for which permission is being requested is located, click Request Permissions in the middle column of the Web page under Services. Further information about this process is available in the [Permissions and Rights Question and Answer](#) document.

Reprints: Information about reprints can be found online at:
<http://www.lww.com/reprints>

Subscriptions: Information about subscribing to *Circulation Research* is online at:
<http://circres.ahajournals.org/subscriptions/>

SUPPLEMENTAL MATERIAL

Malan et al.: Cardiomyocytes from LQTS 3-specific iPS cells

Detailed Methods:

Generation of iPS cells

To obtain *Scn5a* Δ /+ and wild-type mouse embryonic feeder cells (MEFs) *Scn5a* Δ /+ and wild-type littermates were mated and embryos harvested at embryonic day 13.5. MEFs were generated from individual embryos by Trypsin-digestion as reported earlier.¹ MEFs were frozen directly after harvesting and the head of each embryo was used for genotyping (see below).

For iPS cell generation, MEFs with the desired genotype were thawed and cultured in MEF medium (DMEM, 15% FCS, 0.1 mmol/L MEM nonessential amino acids, 0.1 mmol/L 2-mercaptoethanol, 100 U/mL penicillin, and 100 mg/mL streptomycin, all from Invitrogen) for less than three passages and seeded at a density of 5×10^4 cells per well of a 6-well plate one day before transduction. Reprogramming was initiated by transduction with ecotrophic retroviruses either expressing the three factors Oct4, Sox-2, and Klf4, or additionally c-Myc, as previously described.¹ Therefore MEFs were incubated with virus-containing supernatants (250-500 μ l of each virus) supplemented with 6 μ g/mL protamine sulphate (Sigma) for 24 h (day 0 of reprogramming). The next day, the medium was replaced with fresh MEF medium. At day 4 cells were passaged once and from this time on further maintained in mouse ES cell medium (MEF medium supplemented with 1000 U/mL leukemia inhibitory factor (Chemicon), 3 μ mol/L CHIR99021 and 1 μ mol/L PD184352 (Axon Medchem)). The iPS cell colonies with ES cell-like morphology were mechanically isolated from day 14 onwards, dissociated with Trypsin, and replated on irradiated MEF layers in mouse ES cell medium. Genotyping of *Scn5a* Δ /+ embryos, MEFs and iPS cells was performed as reported earlier.²

For retrovirus production pMXs-based retroviral vectors¹ (kindly provided by S. Yamanaka through Addgene) encoding the mouse cDNA of Oct4, Sox-2, Klf4 and c-Myc was used. Each retrovirus was produced individually. Therefore HEK 293 FT cells (Invitrogen) grown to ~70% confluence on a 10 cm dish were co-transfected with a pMXs vector (2 μ g) and a packaging-defective ecotrophic helper plasmid (2 μ g, pCL-Eco, kindly provided by I.M. Verma through Addgene) using Eugene 6 transfection reagent (12 μ l, Roche) according to manufacturer's recommendations. Virus supernatants (10 ml each 10 cm plate) were harvested 48 h after transfection and passed through a 0.45- μ m filter. Retrovirus production and infection was controlled using a pMXs-GFP control virus in parallel.

Culture and differentiation of iPS cells

The iPS cells were cultured in mouse ES cell medium (see above) on irradiated MEF layers and passaged every 2 to 3 days. For cardiomyocyte differentiation the hanging drop method was performed to initiate embryoid body (EB) formation (day 0 of differentiation) as previously described.³ Briefly, EBs were generated by aggregation of 400 cells in 20 μ L of differentiation medium for 2 days and subsequent cultured for another 5 days in differentiation medium (Iscove's modified Dulbecco's medium, 20% FCS, 0.1 mmol/L MEM nonessential amino acids, 0.1 mmol/L 2-mercaptoethanol, 100 U/mL penicillin, 100 mg/mL streptomycin, all Invitrogen). At day 5 or day 7, EBs were plated on glass cover slips or 6-well plates and used for immunocytochemistry at day 10 or dissociated into single cardiomyocytes at early (day 12) and late (day 19-22) developmental stages for patch clamp analysis. Most of the WT and Scn5a Δ /+ iPS clones had comparable cardiac differentiation capabilities and clones #7 (WT) and #6 (Scn5a Δ /+) were used for differentiation experiments in this study.

Genotyping of MEFs and iPS cells

To examine the genotype of the Scn5a Δ /+ MEFs and iPS cells, the Scn5a locus was amplified from genomic DNA using forward (5'-GCAGTGGGAGGACAACCTCTACATG-3') and reverse (5'-GTTCCAGCTGTTGGTGAAGTAATAGTGG-3') primers as previously described.² PCR products were subjected to EcoRV digestion which cuts a silent mutation in the mutated Scn5a allele and results in 1.7 kb and 0.7 kb fragments in contrast to the 2.4 kb fragment of the wild-type allele.²

Teratoma assay

Teratoma assays were performed for each genotype. Undifferentiated murine iPS cells were obtained by trypsin dissociation. Preplating was performed on 0.1% gelatin-coated dishes for 45 min to obtain a pure iPS cell suspension without feeder cells. We injected 100 μ l cell suspensions with 1×10^6 iPS cells subcutaneously into the hind limbs of SCID mice. Four weeks after the injection, tumors were surgically dissected, fixed over night in Z-Fix (Anatech LTD), and embedded in paraffin. 6 μ m sections were cut and stained with haematoxylin and eosin.

Immunocytochemistry

Immunostainings were performed on colonies of undifferentiated iPS cells and EBs at day 10 of differentiation after fixation with 4% paraformaldehyde (Fluka) for 30 min. Cells and EBs were permeabilized with 0.2 % Triton X-100 (Fluka) for 10 min, blocked with 5% normal donkey/goat

serum (Jackson ImmunoResearch) for 30 min, incubated with primary antibodies diluted in 0.5 % normal donkey/goat serum for 2 h and subsequently incubated with secondary antibodies diluted in Hoechst (1 µg/mL; Sigma) for 1 h. Samples were embedded in Polyvinyl alcohol mounting medium (Fluka) and analyzed using an AxioObserver Z1 microscope equipped with an ApoTome optical sectioning device and the AxioVision software (Zeiss). Colonies of iPS cells were stained against Oct4 (rabbit polyclonal IgG, 1:100; Santa Cruz Biotechnologies) and SSEA1 (mouse, 1:80; Developmental Studies Hybridoma Bank). Differentiated EBs were stained against β III-Tubulin (mouse, 1:100; Sigma-Aldrich), Nestin (mouse, 1:100; Chemicon), Troma1 (rat, 1:100, R. Kemler, Freiburg), platelet endothelial cell adhesion molecule-1 (PECAM-1, rat, 1:800; Becton Dickinson), α -Actinin (mouse, 1:400; Sigma) and anti Nav1.5 (rabbit, 1:200; Alomone). Secondary antibodies used in this study were: donkey anti-mouse IgG Cy2-labeled, donkey anti-mouse IgG Cy3-labeled, donkey anti-rat Cy3-labeled, donkey anti-rabbit Cy3-labeled (all 1:400; all from Jackson ImmunoResearch) and goat anti-mouse IgG Alexa647-labeled (1:500; Invitrogen).

Quantitative gene expression analysis

Gene expression was quantified by real time PCR. Total RNA was extracted using the RNeasy plus mini kit (Qiagen) from undifferentiated iPS cells and differentiated EBs at day 9 and day 14 and 300 - 800 ng RNA was reverse transcribed into cDNA with the SuperScript VILO cDNA Synthesis Kit (Invitrogen). Quantitative polymerase chain reaction was performed in triplicates using Tagman Assays and Gene Expression Master Mix (Applied Biosystems) according to manufacturer's instructions on a Rotorgene 6000 realtime polymerase chain reaction machine (Corbett). The following assays were used: Oct4: Mm00658129_gH, Nanog: Mm02019550_s1, Myh6: Mm00440354_m1, Scn5a: Mm00451971_m1, Hcn4: Mm01176086_m1, Kcnb1: Mm00492791_m1, Cacna1c: Mm00437917_m1, Acnt2: Mm00473657_m1, Gapdh: Mn99999915_g1. Raw data were analysed with the Rotor-Gene Q Series Software 1.7. Cycle threshold (C_T) was calculated during the exponential phase at identical threshold values for all runs. C_T values of target genes were subtracted by the C_T value of the housekeeping gene Gapdh to obtain ΔC_T and relative expression was calculated as $2^{\Delta C_T}$. Each analysis was performed with three independent biological replicates from independent differentiations. Relative expression values were normalized to the mean of wild-type undifferentiated iPS cells (for Oct4 and Nanog) or to the mean of wild-type differentiated EBs at day 14 (for all other genes).

Single cardiomyocyte isolation and electrophysiology

For patch-clamp experiments single beating cardiomyocytes from EBs were used at early (day 12) and late (day 19-22) developmental stages of differentiation. Therefore beating areas of 20-40 EBs were dissected under a microscope, collected in PBS and dissociated with 1mg/mL collagenase type B (Roche) for 25 min at 37°C under shaking conditions. Single cells were plated at low densities on gelatine-coated (0.1%) coverslips in differentiation medium in order to obtain isolated single cells. Patch-clamp experiments were performed after 48-72 h on single beating cardiomyocytes using an EPC10 amplifier (Heka) in the whole cell configuration as reported earlier³ with continuously superfusion with extracellular solution at 37°C.

Na⁺ current was measured in the voltage clamp mode. For recording of peak and recovery from inactivation Na⁺ current (Figure 3 B-E) the pipette solution contained (in mmol/L) 3 NaCl, 133 CsCl₂, 2 MgCl₂, 2 NaATP, 2 TEACl, 10 EGTA and 5 HEPES (pH7.3 CsOH) and the external solution: 7 NaCl, 133 CsCl₂, 1.8 CaCl₂, 1.2 MgCl₂, 5 Hepes, 11 glucose, 0.005 nifedipine, pH 7.4 (CsOH). Liquid junction potential of these solutions was 0.2 mV and therefore neglected. For the recovery of inactivation kinetics the peaks Na⁺ current in response to pairs of depolarization pulses from -100 mV to 10 mV were recorded with increasing delays between the two pulses from 1.5 ms to 57 ms). For quantification the Na⁺ current amplitude from the second pulse was normalized to those from the first pulse, plotted against the delay and these values were fitted with a mono-exponential growth (examples see Figure 3 D). The current densities for the peak Na⁺ current were measured from the first pulse of the recovery from inactivation protocol, in response to a -10 mV depolarizing pulse of 40 ms from a holding potential of -100 mV. Steady state fast activation was measured by application of 30 ms pluses of increasing amplitude (10mV steps) from -90 mV to 0 mV from a holding potential of -100 mV. Peak currents were divided by the respective driving force for Na⁺ to obtain the Na⁺ conductance ($g_{Na} = I_{Na} / [V_m - V_{eq}]$). Data from of each individual cell was normalized to maximum conductance and fitted using a Boltzmann distribution to obtain the half maximal voltage of activation. To calculate the time constants of Na⁺ current deactivation, currents at -40 mV and -10 mV were fitted with single exponential function. Steady state inactivation was measured by a double pulse protocol from a holding potential of -100 mV consisting of a 200 ms pulse of increasing amplitude from -120 mV to 0 mV (10 mV steps) followed by a test pulse of 25ms to 0 mV. Na⁺ currents were normalized to the maximum current and each individual cell was fitted with a Boltzmann distribution to obtain the half maximal voltage of inactivation.

Late Na⁺ current was measured using an external solution containing (in mmol/L): 135 NaCl, 5.4 KCl, 1.8 CaCl₂, 1 MgCl₂, 10 Hepes, 10 glucose, 0.005 nifedipine, pH 7.4 (NaOH). The late

tetrodotoxin-sensitive Na^+ current density was measured at the end of a 100ms test pulse to -10mV and 20 sweeps before and after tetrodotoxin (20 μM) application were averaged and subtracted. Currents were normalized to the cell capacitance and expressed in pA/pF.

Recording of membrane potential was performed in the current clamp mode and with a pipette solution containing (in mmol/L) 50 KCl, 80 K-Aspartate, 1 MgCl_2 , 3 MgATP, 10 EGTA, 10 HEPES, pH 7.4 (KOH) and an external solution containing 140 NaCl, 5.4 KCl, 1.8 CaCl_2 , 1 MgCl_2 , 10 Hepes, 10 glucose, pH 7.4 (NaOH). Spontaneous membrane potential without current injection was not significantly different between wild-type (-72.2 \pm 2.7 mV, n=13) and *Scn5a* Δ /+ (-69.5 \pm 5.6 mV, n=15) cardiomyocytes. In cells with resting membrane potential >-70 mV and/or spontaneous action potential (AP) generation, current injection was used to obtain a resting membrane potential of \sim -80 mV. The required current to achieve this and the resulting resting membrane potential (Table 2) was not significantly different between wild-type (14.2 \pm 7.1 pA, n=13) and *Scn5a* Δ /+ (23.2 \pm 8.3 pA, n=15) cardiomyocytes. APs were elicited by a 2.5 ms current injection pulse through the patch pipette and the strength of the pulse was increased stepwise until a stable action potential with an explicit peak was established. The stimulation frequency was controlled by an external Stimulator (Model 2100, A-M Systems) attached to the EPC10 amplifier. To quantify the frequency-dependent AP duration, cardiomyocytes were stimulated at pacing periods between 0.5s and 6s and at each period the average APD at 90% of repolarization was determined. For each individual cell the APD90 values were plotted against the periods and a linear regression analysis was used to determine the slope of this relationship (examples see Figure 4C).

Data were acquired at a sampling rate of 10-20 kHz (voltage clamp) or 5 kHz (current clamp), filtered at 1 KHz, digitized with the Patchmaster software (HEKA) and analyzed offline using the Fitmaster (HEKA) or the Labchart software (AD Instruments). Membrane potentials were not corrected for liquid junction potentials. AP parameters were analyzed with the cardiac action potential analysis module of Labchart. The maximal AP upstroke velocity was determined in the region from 30% to 100% of action potential amplitude in order to minimize the current injection effects in the initial phase of the AP. APD90 was calculated from the peak of the AP to the point where the AP has dropped by 90% of its amplitude.

Statistical tests were performed using unpaired Student's t-Test for all data except percentage of cells with early afterdepolarizations which was analyzed by Fisher's exact test. A *P*-value of <0.05 was considered significant and is indicated by a * in the figures. All data is expressed as mean \pm SEM.

Legends for Movie files

Supplementary Movie 1. Movie of a representative embryoid body derived from wild-type iPS cells with a spontaneous beating area. Recording and playback speed is 15 fps.

Supplementary Movie 2. Movie of a representative embryoid body derived from Scn5a Δ /+ with a spontaneous beating area. Recording and playback speed is 15 fps.

References

1. Takahashi K, Yamanaka S. Induction of pluripotent stem cells from mouse embryonic and adult fibroblast cultures by defined factors. *Cell*. 2006;126:663-676.
2. Nuyens D, Stengl M, Dugarmaa S, Rossenbacker T, Compennolle V, Rudy Y, Smits JF, Flameng W, Clancy CE, Moons L, Vos MA, Dewerchin M, Benndorf K, Collen D, Carmeliet E, Carmeliet P. Abrupt rate accelerations or premature beats cause life-threatening arrhythmias in mice with long-QT3 syndrome. *Nat Med*. 2001;7:1021-1027.
3. Kolossov E, Lu Z, Drobinskaya I, Gassanov N, Duan Y, Sauer H, Manzke O, Bloch W, Bohlen H, Hescheler J, Fleischmann BK. Identification and characterization of embryonic stem cell-derived pacemaker and atrial cardiomyocytes. *FASEB J*. 2005;19:577-579.

3.2.2 Scalable electrophysiological investigation of iPS cell-derived cardiomyocytes obtained by a lentiviral purification strategy. J. Clin. Med. 2015, 4(1), 102-123; doi:10.3390/jcm4010102 (IF:1.10)

Aim of the study

In the previous study, we demonstrated the generation of cardiomyocytes from murine fibroblasts that carry the human Δ KPQ mutation of the Scn5a Na⁺ channel causing LQTS3. The main message of the study is that the derived cardiomyocytes take on the phenotypic characteristics of the mutation, and analysis of their AP provides a clear interpretation of the pathology.

However, the production of cardiomyocytes for use in a mid- to high- throughput setting requires specific qualities. Firstly, many cells are needed, therefore demanding upscaling methods. Further, the procedure to obtain several individual clones require intensive, laborious picking and the characterization of each clone. Also needed is the production of a pure cardiomyocyte population, because other cells are also generated during differentiation. Purity is critical in the screening of drug compound libraries that require the use of automated assays. Automated planar patch clamp methods have been developed in the field of electrophysiological analysis, which is necessary for screening substances acting at the level of ion channels or signal pathways. A fast and efficient system to obtain iPS cells and a pure cardiomyocyte population would be essential for phenotype-specific characterization and pharmacological screening using automated assays. This study aimed to establish a novel strategy to obtain iPS cells without clone picking, using lentivirus gene transfer, promoting a neomycin selection, the maintenance of undifferentiated iPS cells and a puromycin selection for purification of cardiomyocytes from iPS cell lines reproducing a cardiac disease.

Methods and results:

The strategy to generate non-clonal murine iPS cell lines and thereafter a pure cardiomyocyte population consisted of infection of undifferentiated iPS cells with a lentiviral plasmid (α PaG-RexNeo), with a neomycin resistance gene expressed under the control of the pluripotency promoter Rex-1. After infection of murine wild-type and LQTS3 carrying the KPQ mutation iPS cells, undifferentiated stem cells with stable integration of the lentivirus can be selected by

cultivation in the presence of neomycin. The time of generation of patient-specific disease iPS cell lines should be optimized if we consider patient-tailored medicine. Therefore, we decided to develop a strategy in which we pooled all iPS cells that survived the neomycin selection, and generated non-clonal iPS cell lines. This avoids the selection of single-cell clones, which is very time-consuming. In addition, the lentiviral plasmid contained a short version of the cardiac-specific alpha myosin heavy chain (α -MHC), driving a puromycin resistance gene and the green fluorescence protein. The introduction of the 2A self-cleaving peptide sequence achieved the parallel expression of both promoter and fluorescence protein to visualize cardiomyocyte formation. The α -MHC promoter was expressed when cardiomyocytes differentiated and they could be selected due to the puromycin resistance (see Fig 1, pages 108-9, (Friedrichs et al., 2015). Application of puromycin to differentiated iPS cells led to the death of non-cardiomyocytes and resulted in a nearly pure cardiomyocyte population (Fig 2, page 110). Purified LQTS3-specific cardiomyocytes were electrophysiologically characterized by manual patch clamp and showed, as did the original clones from the previous paper (Malan et al., 2011), prolonged APDs and EADs at low pacing rates (Fig 3 c-e, page 111). These electrophysiological features were not detected in the purified wild-type cardiomyocytes. Thus, the disease phenotype's hallmarks were maintained despite genetic modification of the original iPS cells, the non-clonal pool of iPS and puromycin selection.

To prove that this pure population of cardiac cells could be used for drug screening, we tested these cells in two automated assays which have the potential for higher throughput analysis compared to manual patch clamp: the planar patch-clamp technique and microelectrode arrays (MEA). The planar patch clamp (Patchliner, Nanion Technology) involves a chip with a small hole in it, and when cells placed by a robot arm are aspirated into the chip, a gigaseal is formed. The system can record up to 384 cells simultaneously, making it a high-throughput method for ion channel screening, drug discovery and faster data collection and analysis. MEA is a technique that allows for the measurement of the electrical activity of cells placed on multiple electrodes. The electrical signals give origin to field potentials which can be correlated to AP

recordings. MEA is also a powerful tool for drug discovery and the study of cardiac disease as it allows for the rapid and high-throughput screening of compounds or therapies.

We were able to measure APs automatically with enzymatically dissociated cardiomyocytes in suspension using an automated stimulus finder for the current injection needed to elicit the AP (Fig 4b, page 114). The automatic planar patch clamp analysis with purified wild-type and LQTS3-specific cardiomyocytes showed typical inward and outward currents when applying voltage ramps (see Fig 4a, page 114). We also performed some pharmacology by testing the effect of 4-Aminopyridine (2mM). This drug inhibits repolarizing K^+ channels, and, as expected, led to a prolongation of the APD90, thus confirming the reliability of the automated measurements (Fig 4 d-e, page 114). Next, we recorded APs of purified wild-type and LQTS3 cardiomyocytes at different pacing frequencies to prove the capability of automated assays to detect the specific LQTS3 phenotype. Indeed, APs showed the characteristic prolongation at low heart rates and EADs (Fig 5, c-e, page 115). The possibility of using purified cardiomyocytes from antibiotic selection in scalable screening methods has been proven by analysis with MEA. The field potential, which can be compared to the AP, is recorded with this assay using a monolayer of cardiomyocytes. We tested the capability of this technique to detect the phenotypical features of diseased cardiomyocytes using simultaneous 6-well recordings of the field potential. Two different frequencies were induced by changing from room temperature to 37°C, which increased the spontaneous beating frequency from 1Hz to 1.6 or 1.8 Hz, for wildtype and LQTS3, respectively. As expected, field potentials depicted a prolongation of the QT-Interval at lower frequencies only in LQTS3-specific cardiomyocytes (Fig 6 c-d, page 116). Thus, the disease-specific principle of the frequency dependence of the field potential duration was observed in purified cardiomyocytes with a scalable screening method.

Conclusion:

LQTS3-specific cardiomyocytes can be purified from disease iPS cells with a lentiviral non-clonal gene transfer strategy by antibiotic selection. The non-clonal approach could be applied

to speed up the generation of cardiomyocytes from different somatic cell sources. Importantly cardiomyocytes generated by these genetically modified iPS cell clones maintain the specific cellular hallmarks of the disease. Thus, they are suitable for automated drug screening like planar patch clamp analysis and scalable microelectrode array technologies.

Contribution: designed the study, performed the single cell and automated patch clamp experiments, analyzed the data, wrote the manuscript.

Article

Scalable Electrophysiological Investigation of iPS Cell-Derived Cardiomyocytes Obtained by a Lentiviral Purification Strategy

Stephanie Friedrichs ^{1,†}, Daniela Malan ^{1,†}, Yvonne Voss ^{1,2} and Philipp Sasse ^{1,*}

¹ Institute of Physiology I, Life and Brain Center, University of Bonn, Bonn 53127, Germany; E-Mails: sfriedri@uni-bonn.de (S.F.); dmalan@uni-bonn.de (D.M.); voss@chemie.uni-siegen.de (Y.V.)

² Physical Chemistry I, University of Siegen, Siegen 57076, Germany

† These authors contributed equally to this work.

* Author to whom correspondence should be addressed; E-Mail: philipp.sasse@uni-bonn.de; Tel.: +49-228-6885-200; Fax: +49-228-6885-201.

Academic Editor: Michael J. Edel

Received: 20 August 2014 / Accepted: 9 December 2014 / Published: 7 January 2015

Abstract: Disease-specific induced pluripotent stem (iPS) cells can be generated from patients and differentiated into functional cardiomyocytes for characterization of the disease and for drug screening. In order to obtain pure cardiomyocytes for automated electrophysiological investigation, we here report a novel non-clonal purification strategy by using lentiviral gene transfer of a puromycin resistance gene under the control of a cardiac-specific promoter. We have applied this method to our previously reported wild-type and long QT syndrome 3 (LQTS 3)-specific mouse iPS cells and obtained a pure cardiomyocyte population. These cells were investigated by action potential analysis with manual and automatic planar patch clamp technologies, as well as by recording extracellular field potentials using a microelectrode array system. Action potentials and field potentials showed the characteristic prolongation at low heart rates in LQTS 3-specific, but not in wild-type iPS cell-derived cardiomyocytes. Hence, LQTS 3-specific cardiomyocytes can be purified from iPS cells with a lentiviral strategy, maintain the hallmarks of the LQTS 3 disease and can be used for automated electrophysiological characterization and drug screening.

Keywords: induced pluripotent stem cells; cardiomyocytes; purification; long QT syndrome; planar patch clamp; microelectrode array

1. Introduction

Long QT syndrome (LQTS) is an inherited cardiac disease caused by mutations of cardiac ion channels or accessory subunits, which leads to the loss of function of repolarizing currents or the gain of function of depolarizing currents. Clinically, this disease is characterized by abnormal prolonged QT intervals in the ECG, and the patients affected can develop Torsades de Pointes ventricular tachycardia, which causes syncope and sudden cardiac death [1]. One of the most common LQTS gain of function mutations in humans is the deletion of three amino acids (Δ KPQ) in the α -subunit of the cardiac sodium channel (SCN5A) [2], which is classified as LQTS Type 3 (LQTS 3). This mutation results in faster recovery from inactivation of the sodium current and enhanced late sodium currents, which both lead to prolonged action potentials (APs) and early afterdepolarizations (EADs). Because the impact of this mutation is strongest at a low heart rate, lethal cardiac events mostly occur at rest or during sleep [1].

In the past, LQTSs were studied on heterologous expression systems that lack the typical cell biological and physiological features of cardiomyocytes and that do not generate APs [3,4]. Recently, we have shown that LQTS 3-specific cardiomyocytes can be generated from mouse iPS cells carrying the human Δ KPQ mutation and recapitulated the disease-specific biophysical effects of the mutation, as well as prolonged APs and EADs at low heart rates [5]. Furthermore, other groups have successfully generated iPS cells from LQTS 1, 2 and 3 patients, and the cardiomyocytes differentiated from these cells recapitulated the typical characteristics of the respective disease [6–11]. Therefore, human iPS cell-derived cardiomyocytes are a great advance for the understanding of LQTS, especially because “real” cardiomyocytes provide a model that is close to the patient’s heart cells.

The unlimited proliferation of personalized iPS cells and the differentiation into cardiomyocytes would allow disease- or even patient-specific drug testing. In order to find new drugs to treat LQTS, pharmaceutical compound libraries have to be screened with scalable automatic assays. Potential automatic electrophysiological screening methods are planar patch clamp systems [12] or microelectrode array technologies [13]. One big challenge for all automated assays is the generation of a pure cardiac population, because during iPS cell differentiation, also non-cardiomyocytes are generated.

To date, several purification methods have been used to enrich cardiac cells. Fluorescence-activated cell sorting of cardiomyocytes with cardiac-specific GFP expression or after labeling with mitochondrial dyes can be used, but these methods result only in low amounts of pure cardiac cells and are difficult to scale up [14,15]. Better yields are achieved with scalable antibiotic selection of cardiomyocytes, which express a resistance gene under a cardiac-specific promoter [16,17]. For antibiotic selection, cells must be genetically modified, and here, we report a highly efficient and straightforward lentiviral gene transfer for the selection of cardiomyocytes by an antibiotic resistance gene without a time-consuming screening of individual clones. We have applied this method to obtain pure populations of cardiomyocytes from LQTS 3-specific iPS cells with the human Δ KPQ mutation and

wild-type controls. Furthermore, we proved that purified cardiomyocytes showed the typical features of LQTS 3 in manual patch clamp, automatic planar patch clamp and scalable microelectrode array recording technologies.

2. Experimental Section

2.1. Generation of the Lentiviral α PaG-RexNeo Plasmid and Lentivirus Production

The lentiviral α PaG-RexNeo plasmid is based on a pRRLSIN lentiviral backbone from pRRLSIN.cPPT.PGK-GFP.WPRE (kindly provided by Didier Trono through Addgene #12252). Multiple cloning steps according to standard procedures were used to create an insert containing a short version of the cardiac-specific alpha myosin heavy chain (α -MHC) promoter, a puromycin resistance gene, the green fluorescence protein (GFP) and a fragment with the Rex-1 promoter driving a neomycin resistance gene. The short α -MHC promoter was excised from the α -MHC-pBK plasmid (kindly provided by Jeffrey Robbins) and contained 1745 bp from the 3' part of the full α -MHC promoter. Parallel expression of puromycin and GFP was achieved by the introduction of the 2A self-cleaving peptide sequence (APVKQTLNFDLLKLAGDVESNPGP) [18] that was generated by annealing and in-frame ligation of appropriate oligonucleotides (MWG-Biotech, Ebersberg, Germany). The Rex-1-neomycin sequence was cut from the α -MHC-puro Rex-neo plasmid (kindly provided by Mark Mercola through Addgene #21230). Successful cloning was confirmed by restriction enzyme digestion and DNA sequencing (MWG-Biotech, Ebersberg, Germany). All enzymes for cloning were from Life Technologies (Darmstadt, Germany) and Thermo Scientific Fermentas. For the preparation of lentivirus, 40 μ g of the α PaG-RexNeo plasmid, 8.5 μ g of the pMD2.G plasmid (for the VSV-G envelope, Addgene #12259), 16 μ g of the pMDLg/pRRE plasmid (for Gag/Pol expression, Addgene #12251) and 7 μ g of the pRSV-Rev plasmid (for Rev expression, Addgene #12253, all kindly provided by Didier Trono through Addgene), were cotransfected into 7×10^6 HEK293FT cells (ATCC) in a T75 culture flask, as previously described [19]. After 24 h, the medium was changed with fresh HEK cell medium that consisted of Dulbecco's Modified Eagle Medium (DMEM), 15% fetal calf serum (FCS), 0.1 mmol/L MEM nonessential amino acids, 0.1 mmol/L 2-mercaptoethanol, 100 U/mL penicillin and 100 mg/mL streptomycin (all from Invitrogen/Bernardi). Virus-containing supernatants were collected at Days 3 and 4 after transfection, passed through a 0.45- μ m filter (Sigma-Aldrich, Taufkirchen, Germany) and concentrated by ultracentrifugation at 19,400 rpm for 2 h at 17 °C using an Optima L-90K ultracentrifuge with an SW 32 Ti rotor (Beckman Coulter, Krefeld, Germany). The pellet was resuspended in 50 μ L HBSS without Ca^{2+} and Mg^{2+} (Life Technologies, Darmstadt, Germany) and stored frozen at -80 °C.

2.2. Cell Culture and Lentiviral Gene Transfer of iPS Cells

The iPS cells were cultured as reported before [5] on irradiated mouse embryonic feeder (MEF) layers (PMEF-NL; Millipore, Schwalbach, Germany) in iPS cell medium containing DMEM, 15% FCS, 0.1 mmol/L nonessential amino acids, 0.1 mmol/L 2-mercaptoethanol, 100 U/mL penicillin, 100 mg/mL streptomycin (all from Invitrogen/Life Technologies), 1000 U/mL leukemia inhibitory factor (Chemicon/Millipore), 3 μ mol/L CHIR99021 and 1 μ mol/L PD184352 (Axon Medchem,

Groningen, The Netherlands). Every 2 to 3 days, iPS cells were passaged and seeded at a density of 0.1 to 0.2×10^6 cells in a T75 culture flask.

For gene transfer of α PaG-RexNeo, 0.2×10^6 iPS cells were plated on a T25 culture flask on irradiated MEFs, and 24 h later, the α PaG-RexNeo lentivirus from the production described in section 2.1 was added in 5 mL of iPS cell medium in the presence of 6 μ g/mL protamine sulfate (Sigma-Aldrich) to enhance infection. The next day, fresh iPS cell medium was applied, and the selection of iPS cells with lentivirus integration was initiated 24 h to 48 h later by the addition of 300 μ g/mL neomycin (G418, Invitrogen/Life Technologies). The genetically-engineered wild-type and *Scn5a* Δ /+ iPS cells were further cultivated and passaged in iPS cell medium in the presence of 300 μ g/mL neomycin to avoid lentivirus silencing.

2.3. Differentiation of iPS Cells and Purification of Cardiomyocytes

Cardiomyocyte differentiation was induced using embryoid body (EB) formation with the hanging drop method in combination with a suspension protocol, as previously described [16]. Briefly, EBs were generated by aggregation of 400 cells in 20 μ L differentiation medium for 2 days and subsequently cultured in suspension in 10-cm bacteriological dishes on a horizontal shaker in differentiation medium containing Iscove's Modified Dulbecco's Medium, 20% FCS, 0.1 mmol/L MEM nonessential amino acids, 0.1 mmol/L 2-mercaptoethanol, 100 U/mL penicillin, 100 mg/mL streptomycin (all from Invitrogen/Life Technologies). EBs started to beat at day 10 to 12 of differentiation and 10 μ g/mL puromycin (Sigma-Aldrich) was added at that time point to initiate the selection of cardiomyocytes. One day later, EBs were pooled, washed with PBS and dissociated with 1 mg/mL collagenase B (Roche Diagnostics, Mannheim, Germany) in 1.6 mL in a 50-mL falcon tube for 60 min at 37 °C under shaking condition. The enzymatic reaction was stopped with the addition of 30 mL of differentiation medium. In order to avoid a centrifugation step that was found to be lethal for the freshly-dissociated cardiomyocytes, a subsequent passive sedimentation step was performed for 60 min in the incubator. The supernatant was removed except ~10 mL, in which the cardiomyocytes were resuspended and collected. For further selection and cultivation, cells were seeded on 0.01% fibronectin-coated (Sigma-Aldrich) 10-cm cell culture dishes in differentiation medium supplemented with 2.5 to 5 μ g/mL puromycin. To obtain a more mature stage for electrophysiological analysis, single purified cardiomyocytes were kept in culture for an additional 6 to 10 days, because we have shown that longer differentiation leads to more cells with functional Na^+ currents [5].

2.4. Immunocytochemistry

For immunostainings, cells were fixed with 4% paraformaldehyde for 30 min, permeabilized with 0.2% Triton X-100 for 10 min (both from Sigma-Aldrich) and blocked with 5% donkey or goat serum for 30 min (Jackson ImmunoResearch, Suffolk, England). The primary antibodies were diluted in 0.5% donkey or goat serum, and cells were incubated for 2 h. Colonies of iPS cells were stained against Oct3/4 (rabbit, 1:100; Santa Cruz Biotechnology, Heidelberg, Germany) and SSEA1 (mouse, 1:80; Developmental Studies Hybridoma Bank, Iowa, USA). Single cardiomyocytes were stained against α -actinin (mouse, 1:400; Sigma-Aldrich) and the cardiac Na^+ channel (Nav1.5, rabbit, 1:400; Alomone Labs, Jerusalem, Israel). The appropriate fluorescence-conjugated secondary antibodies,

donkey anti-mouse Cy2-labeled, donkey anti-rabbit Cy3-labeled (both 1:400; Jackson ImmunoResearch) and goat anti-mouse Alexa647-labeled (1:500; Invitrogen/Life Technologies), were diluted in 1 µg/mL of Hoechst 33342 (Sigma-Aldrich) and applied for 1 h. Samples were embedded in polyvinyl alcohol mounting medium (FLUKA; Sigma-Aldrich) and analyzed using an AxioObserver Z1 microscope equipped with an ApoTome optical sectioning device and the AxioVision software (Zeiss, Jena, Germany).

To analyze the purity of iPS cell-derived cardiomyocytes, purified cells at Days 13 to 15 of differentiation from 4 to 5 independent biological replicates were stained against α -actinin. The ratio of α -actinin-positive cells to the total cell number analyzed by nucleus labeling was quantified from large overview pictures that were acquired with the MosaiX function of the AxioVision software (Zeiss).

2.5. Conventional Manual Patch Clamp Analysis

Purified wild-type and Scn5a Δ /+ cardiomyocytes were dissociated and replated for 48 to 72 h at low densities on fibronectin-coated (0.01%) coverslips. Patch clamp experiments were performed after 48 to 72 h using an EPC10 amplifier (HEKA Elektronik, Lambrecht, Germany) in the whole cell configuration and the current clamp mode, as reported earlier [5], with continuous superfusion with extracellular solution at 37 °C containing (in mmol/L) 140 NaCl, 5.4 KCl, 1.8 CaCl₂, 1.2 MgCl₂, 10 Hepes and 10 glucose, pH 7.4 (NaOH), and an internal solution containing (in mmol/L) 50 KCl, 80 K-aspartate, 1 MgCl₂, 3 MgATP, 10 EGTA and 10 HEPES, pH 7.2 (KOH) (all from Sigma-Aldrich). APs were elicited by 2.5 ms-long current injections, and the strength of the pulse was increased stepwise until a stable action potential with a peak over the 0 mV line was reached. The stimulation frequency and amplitude was controlled by an external stimulator (Model 2100, A-M Systems) attached to the EPC10 amplifier.

2.6. Automated Planar Patch Clamp Analysis

For automated planar patch clamp measurements, single dissociated cardiomyocytes are required in suspension without damage of the cell membrane or transmembrane ion channels. Therefore, purified wild-type and Scn5a Δ /+ cardiomyocytes in a 10-cm cell culture dish were washed with 5 mL PBS containing EDTA (2 mM) and stored for 10 min at 4 °C in order to facilitate the detachment of cells by subsequent incubation with 2 mL 0.05% Trypsin in 4 mM EDTA (Gibco/Life Technologies) for 3 to 8 min. Cells were collected in 10 mL of differentiation medium, gently centrifuged for 3 min at 500 rpm, resuspended in 200 to 500 µL external solution and incubated at room temperature for at least 2 h to recover from dissociation. Automated electrophysiological recording was performed with a planar patch clamp robot (Patchliner, Nanion Technologies, Munich, Germany) equipped with an EPC-10 quadro patch clamp amplifier (HEKA Elektronik) for parallel recording of 4 cardiomyocytes in the whole cell configuration. Single-use borosilicate glass chips with medium resistance (1.8 to 3 M Ω , NPC-16, Nanion Technologies) were used for all recordings. The PatchControlHT software (Nanion Technologies) in combination with the PatchMaster software (HEKA Elektronik) was used for cell capture, seal formation, whole-cell access and subsequent recording of voltage ramps, automated determination of AP stimulus thresholds and AP measurements at different stimulation frequencies. The internal solution used contained (in mmol/L) 50 KCl, 60 K-fluoride, 10 NaCl, 20 EGTA and 10

HEPES, pH 7.2 (KOH), and the external solution 140 NaCl, 4 KCl, 2 CaCl₂, 5 Glucose and 10 HEPES, pH 7.4 (NaOH) (all from Sigma-Aldrich). A seal enhancer solution containing (in mmol/L) 80 NaCl, 3 KCl, 10 MgCl₂, 35 CaCl₂ and 10 HEPES (Na⁺ salt), pH 7.4 (HCl) (all from Sigma-Aldrich), was automatically applied to the extracellular channel after cell capture in order to achieve better GΩ-seals and replaced with external solution when the whole cell configuration was established.

In order to identify mature cardiomyocytes, depolarizing voltage ramps (−100 mV to +60 mV in 250 ms) were applied, and the responding current was analyzed to identify the fast spike of Na⁺ currents. APs were recorded in current clamp mode and to avoid spontaneous activity, and to record APs from a stable resting potential, the membrane potential was adjusted to −70 mV by current injection using the low frequency voltage clamp circuit of the amplifier. Before each AP recording, the low frequency voltage clamp was switched off, and the actual current was continuously injected to maintain the resting membrane potential. To determine the current injection threshold for AP generation for each cell individually, an automated macro was programmed and executed. This generated a 2-ms current injection of stepwise (100 pA) increasing intensities and automatically monitored the voltage responses. Leak subtraction was used to subtract the passive capacitive responses to the stimulus. Once the stimulus generates voltage responses with an amplitude of >30 mV above the resting membrane potential, this value was used, and 80 pA was added for safety. Subsequently, APs were automatically evoked and recorded for 30 to 60 s at 0.5 Hz, 1 Hz and 2 Hz by a protocol in the Patchmaster software (HEKA Elektronik).

Data from both conventional and planar patch clamp were acquired with the Patchmaster software and analyzed offline using the Fitmaster (HEKA Elektronik) and the Labchart software (AD Instruments, Oxford, England). The action potential duration at 90% of repolarization (APD₉₀) was analyzed with the peak analysis module of Labchart software (AD Instruments). To quantify the frequency-dependent AP duration, cardiomyocytes were stimulated at different pacing periods (0.5 to 6 s for manual patch clamp and 0.5 to 2 s for automatic patch clamp), and at each period, the average APD₉₀ was determined. For each individual cell, the APD₉₀ values were plotted against the period between stimulation (1/frequency), and a linear regression analysis was used to determine the slope of this relationship.

2.7. Microelectrode Array Analysis

For the microelectrode array (MEA) measurements, purified cardiomyocytes from wild-type and Scn5aΔ/+ iPS cells were detached with 0.05% Trypsin in 0.5 mM EDTA (Gibco/Life Technologies) for 5 min at 37 °C, centrifuged for 5 min at 1000 rpm and resuspended in differentiation medium. Then, 20,000 to 40,000 cells were plated in each well of a 6-well MEA (60-6wellMEA200/30iR-Ti-ter, Multi Channel Systems, Reutlingen, Germany) coated with 0.01% fibronectin (Sigma-Aldrich). After 24 to 72 h, the medium was replaced with external solution (see Section 2.5), and field potentials were recorded at a sampling rate of 10 kHz with the MC-Rack software at room temperature (22 °C) and at 37 °C by switching on the TC02 2-channel temperature controller (both from Multi Channel Systems). Triggered field potentials were averaged over 50 s, and the mean of all 9 electrodes in one well was calculated (OriginPro8G, OriginLab) to obtain one averaged field potential for further analysis. The

field potential duration was manually measured from the minimum of the sharp negative spike to the following maximum (Figure 6c, right).

2.8. Statistics

Data are expressed as the mean \pm S.E.M. Statistical tests were performed using appropriate unpaired or paired Student's *t*-test with Welch's correction for data with unequal variance using Prism (GraphPad software). A *p*-value of <0.05 was considered significant and is indicated by an asterisk (*) in the figures. Because of high variations in temperature-induced frequency between Scn5a Δ /+ and wild-type cardiomyocytes using MEA recordings (Scn5a Δ /+: high 1.4–1.8 Hz, low 0.7–1.0 Hz; wild-type: high 1.6–4.7 Hz, low 1.0–3.5 Hz), in these experiments, only paired Student's *t*-tests within individual genotypes were performed (Figure 6d).

3. Results

3.1. Lentiviral Strategy for Purification of iPS Cell-Derived Cardiomyocytes

In order to obtain a pure cardiomyocyte population from iPS cell differentiation, we have modified a previously-reported antibiotic resistance strategy [16] and used high efficiency lentiviral gene transfer [17]. Therefore, we have generated a lentiviral plasmid (α PaG-RexNeo) for the expression of a puromycin resistance gene and the green fluorescent protein (GFP) reporter gene under the control of a short (1.7 kb) version of the cardiac-specific alpha myosin heavy chain (α -MHC) promoter (Figure 1a). In addition, the plasmid contained a fragment with a neomycin resistance gene expressed under the control of the pluripotency promoter Rex-1 [20]. After infection of cells with this lentiviral plasmid, undifferentiated stem cells with stable integration of the lentivirus can be selected by cultivation in the presence of neomycin [17]. Upon differentiation, cardiomyocytes can be purified by puromycin application and used for electrophysiological investigations (Figure 1b). To test this strategy for the investigation of a clinically relevant cardiac disease, we have purified LQTS 3-specific cardiomyocytes from previously-reported Scn5a Δ /+ iPS cells [5] with the human Δ KPQ mutation in the cardiac sodium channel.

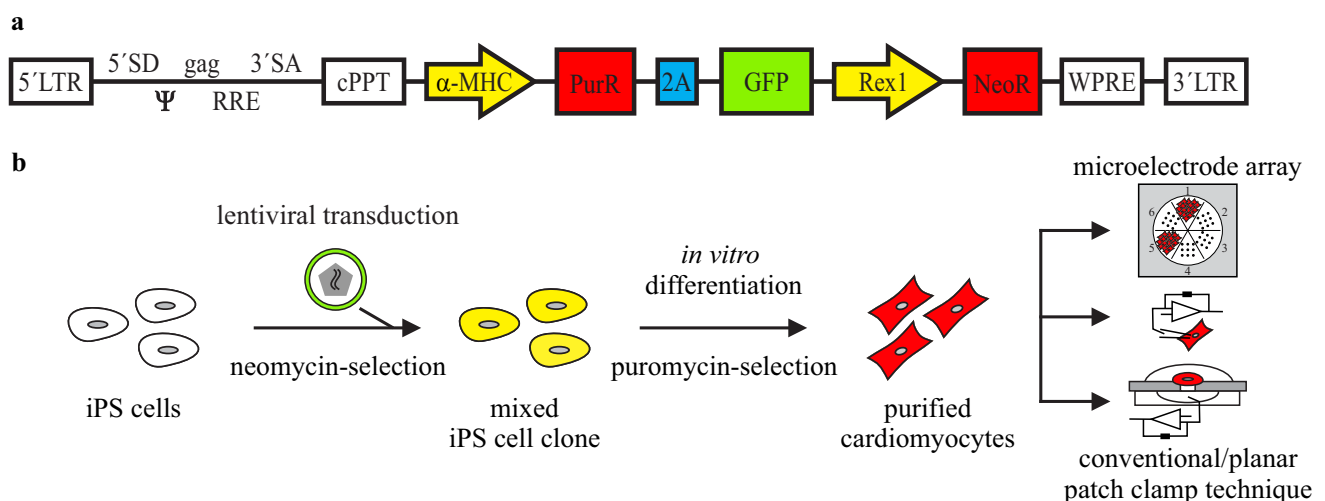


Figure 1. Cont.

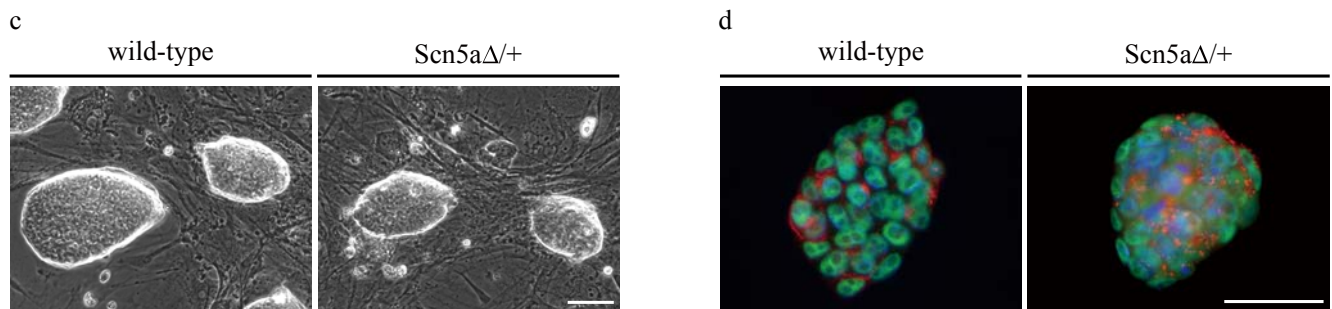


Figure 1. Lentiviral strategy for the purification of iPS cell-derived cardiomyocytes. (a) The lentiviral construct contains a puromycin resistance gene (*PurR*) and a GFP reporter gene separated by a 2A self-cleaving peptide sequence (2A) under the control of the cardiac α -MHC promoter, as well as a neomycin resistance gene (*NeoR*) under the control of the Rex1 promoter; (b) strategy of lentivirus gene transfer into iPS cells and purification of cardiomyocytes for electrophysiological analysis; (c,d) after lentiviral gene transfer and selection, wild-type and *Scn5a* Δ /+ iPS cell lines maintained the characteristic embryonic stem cell-like morphology (c) and expressed the embryonic stem cell-specific markers, Oct3/4 (d, green) and SSEA1 (d, red). Nuclei are shown in blue. Scale bars: 50 μ m.

Therefore, a monolayer of undifferentiated *Scn5a* Δ /+ and wild-type iPS cells were infected with the α PaG-RexNeo lentivirus and further kept under neomycin selection for the isolation of cells with a stable integration. The surviving iPS cells were collected and pooled for each genotype. Although this non-clonal strategy results in a mixture of individual cell clones with uncontrolled variations in the number and location of lentiviral integrations, it does not require the very laborious picking and characterization of several individual clones. Importantly, after α PaG-RexNeo gene transfer and selection, we found that both wild-type and LQT 3-specific iPS cells maintained their characteristic embryonic stem cell morphology (Figure 1c) and expressed the stem cell-specific markers Oct3/4 and SSEA1 (Figure 1d).

3.2. Purification of α PaG-RexNeo iPS Cell-Derived Cardiomyocytes

In vitro differentiation of α PaG-RexNeo wild-type and *Scn5a* Δ /+ iPS cells was performed using the hanging drop method for embryoid body (EB) generation [21] followed by a mass culture protocol (Figure 2a) [16]. EBs showed spontaneously beating areas at Days 10 to 12 of differentiation with weak GFP signals. At this stage, cardiomyocyte selection was started by puromycin application for one day, and single cells were re-plated on fibronectin-coated culture dishes. Longer selection at the EB stage was inefficient, because dissociation of older and more compact EBs with enhanced extracellular matrix failed, resulting in a low number of single cardiomyocytes. Single dissociated cardiomyocytes were spontaneously beating and weakly GFP-positive (Figure 2b).

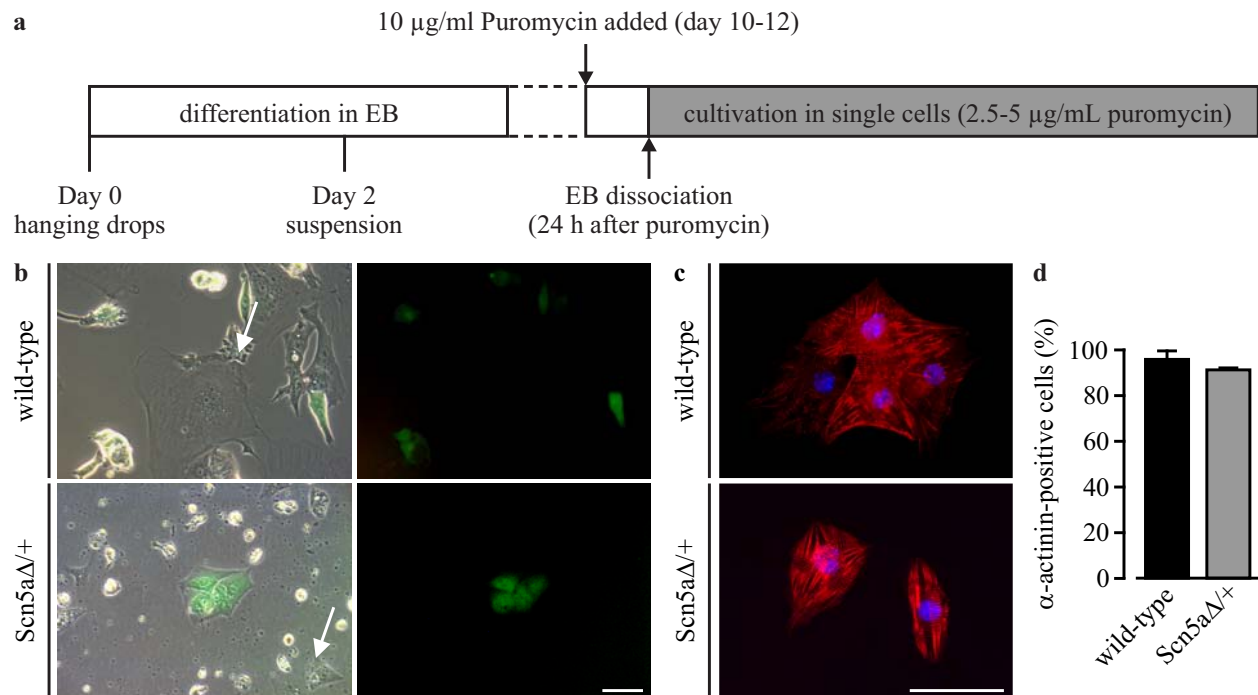


Figure 2. Purification of iPS cell-derived cardiomyocytes. **(a)** The cardiac differentiation protocol used in this study; **(b)** single dissociated cardiomyocytes were GFP-positive and beating, but some non-contracting and GFP-negative cells remained (arrows) after the puromycin selection for 24 h; **(c)** after further purification of single cells, mostly α -actinin-positive cardiomyocytes survived (red); **(d)** cell counting at Days 13 to 15 of differentiation showed the very high purity of wild-type and Scn5a Δ /+ cardiomyocytes. Scale bars: 50 μ m. Error bars: S.E.M. EB, embryoid body.

Because cells without GFP expression or contractions were still present (Figure 2b, arrows), cultures were maintained under a low dose of puromycin selection, which led to further purification. Subsequently, the purity of cardiomyocytes was assessed by staining against cardiac α -actinin and cell nuclei (Figure 2c), and quantitative cell counting showed an almost pure population of cardiomyocytes (Figure 2d) from wild-type ($92.8\% \pm 6.2\%$, $n = 5$) and Scn5a Δ /+ iPS cells ($87.7\% \pm 9.7\%$, $n = 4$).

3.3. Phenotyping of Purified LQTS 3-Specific Cardiomyocytes from Scn5a Δ /+ iPS Cells

Purified cardiomyocytes from wild-type and Scn5a Δ /+ iPS cells showed no obvious difference in cardiac sodium channel distribution or sarcomeric structure (Figure 3a). To exclude that the lentivirus integration, the non-clonal strategy or the purification affect the LQTS 3-specific phenotype we characterized purified cardiomyocytes by classical manual patch clamp techniques.

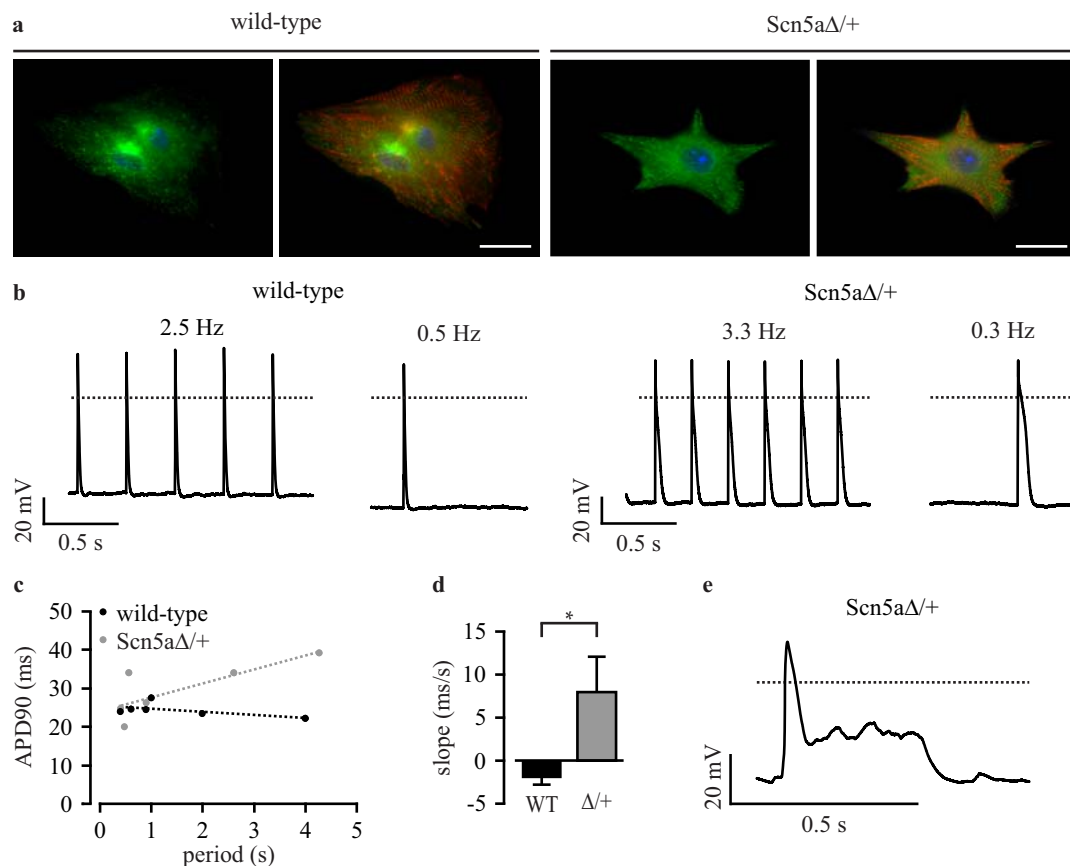


Figure 3. Patch clamp analysis of purified iPS-derived cardiomyocytes. **(a)** Cardiomyocytes from wild-type and Scn5aΔ/+ iPS cells showed a similar cardiac sodium channel distribution (green) and sarcomeric α-actinin pattern (red); **(b)** representative examples of action potentials (APs) from purified wild-type and Scn5aΔ/+ cardiomyocytes at high and low pacing frequencies; **(c)** relationship between action potential duration at 90% of repolarization (APD90) and pacing period from a representative wild-type and Scn5aΔ/+ cardiomyocyte with the analysis of the slope by linear fit (dashed lines); **(d)** statistical analysis of the slope of APD90 to the pacing period relationship from individual wild-type (WT) and Scn5aΔ/+ cardiomyocytes (Δ/+); **(e)** typical long QT syndrome 3 (LQTS 3)-specific early afterdepolarizations (EADs) observed in a Scn5aΔ/+ cardiomyocyte. Scale bar: 20 μm. Error bars: S.E.M. Dotted lines indicate 0 mV.

APs were evoked at various frequencies by current injection, and the frequency-dependent action potential duration at 90% repolarization (APD90) was analyzed. In Scn5aΔ/+ cardiomyocytes, but not in wild-type cells, we found a prolongation of APD90 at lower heart rates (Figure 3b, Table 1), which did not reach statistical significance because of the high variability of APD90 between individual cells. The high variability was not due to the non-clonal purification approach, because it was similarly observed in non-purified cardiomyocytes from the original iPS cell clones [5]. To compensate for this variability, we performed a longitudinal analysis for each individual cell and determined the slope of the relationship between APD90 and basic cycle length (APD restitution) using a linear fit (examples shown in Figure 3c), as reported before [5,22]. This analysis showed almost no influence of cycle length on APD90 in purified wild-type cardiomyocytes yielding flat slopes of APD restitution

(-1.85 ± 0.73 ms/s, $n = 10$, Figure 3d). In contrast, purified Scn5aΔ/+ cardiomyocytes had a significant different positive slope (7.94 ± 4.05 ms/s, $n = 18$, Figure 3d) highlighting the prolongation of APD90 with a longer cycle length. This is the characteristic feature of LQTS 3 in patients [22] and is fully in line with previous reports on non-purified cardiomyocytes from Scn5aΔ/+ iPS cells [5], as well as on cardiomyocytes from the ΔKPQ LQTS 3 mouse model [23]. Importantly, these slope values are almost identical to those obtained from the non-purified original iPS cell clones (wild-type: -2.92 ± 1.27 ms/s; Scn5aΔ/+: 9.08 ± 3.60 ms/s; see Table 2 in Malan *et al.* [5]). Moreover, we detected EADs in some purified Scn5aΔ/+ cardiomyocytes (10.5%, $n = 19$, Figure 3e), but never in wild-type cells (0%, $n = 10$). Resting membrane potential, action potential amplitude and maximum upstroke velocity were not different between wild-type and Scn5aΔ/+ cardiomyocytes (Table 1).

Table 1. Action potential parameters determined by manual and automated planar patch clamp analysis. RMP, resting membrane potential; APA, action potential amplitude; Vmax, maximum upstroke velocity; APD90, APD at 90% of repolarization; Slope, slope of the linear relationship between APD90 and the pacing period. Values are the means \pm S.E.M.

Method Genotype	Manual Patch Clamp			Automated Planar Patch Clamp		
	Wild-Type	Scn5aΔ/+	p-Value	Wild-Type	Scn5aΔ/+	p-Value
RMP at 1 Hz (mV)	-77.4 ± 4.9 $n = 10$	-74.7 ± 3.5 $n = 17$	0.6589	-69.4 ± 6.4 $n = 7$	-78.2 ± 3.0 $n = 9$	0.2040
APA 1 Hz (mV)	106.2 ± 5.7 $n = 10$	103.3 ± 5.7 $n = 17$	0.7207	81.1 ± 13.2 $n = 7$	85.8 ± 10.1 $n = 9$	0.7746
V max at 1 Hz (V/s)	93.7 ± 11.1 $n = 10$	71.6 ± 9.6 $n = 17$	0.1484	56.6 ± 15.5 $n = 7$	52.6 ± 10.2 $n = 9$	0.8248
APD90 at 2 Hz (ms)	36.2 ± 3.5 $n = 10$	39.5 ± 5.1 $n = 14$	0.6004	78.0 ± 28.7 $n = 7$	64.9 ± 17.1 $n = 7$	0.7019
APD90 at 1 Hz (ms)	35.5 ± 3.3 $n = 10$	45.8 ± 6.8 $n = 15$	0.1913	70.1 ± 26.6 $n = 7$	76.7 ± 20.4 $n = 9$	0.8454
APD90 at 0.2 Hz (manual) or 0.5 Hz (automated) (ms)	39.7 ± 2.2 $n = 5$	46.8 ± 6.7 $n = 5$	0.1761	69.6 ± 24.3 $n = 7$	91.5 ± 25.0 $n = 8$	0.5440
Slope (ms/s)	-1.85 ± 0.73 $n = 10$	7.94 ± 4.05 $n = 18$	0.0287	-5.39 ± 4.82 $n = 7$	4.13 ± 1.20 $n = 9$	0.0494

Importantly, we did not find differences in action potential parameters between early and late passages of the non-clonal iPS cell clones (Table 2).

Table 2. Action potential parameters at early (P12–P18) and late (P19–P35) passages determined by manual patch clamp recordings (the abbreviations are as in Table 1).

Genotype	Wild-Type			Scn5aΔ/+		
Passage	Early Passage	Late Passage	<i>p</i> -Value	Early Passage	Late Passage	<i>p</i> -Value
RMP at 1 Hz (mV)	−71.8 ± 2.3 <i>n</i> = 4	−68.3 ± 9.7 <i>n</i> = 3	0.7061	−71.5 ± 7.3 <i>n</i> = 4	−67.3 ± 5.6 <i>n</i> = 7	0.6593
APA 1 Hz (mV)	105.5 ± 6.9 <i>n</i> = 4	99.7 ± 16.5 <i>n</i> = 3	0.7312	97.3 ± 9.0 <i>n</i> = 4	91.3 ± 8.1 <i>n</i> = 7	0.6513
V max at 1 Hz (V/s)	98.8 ± 6.8 <i>n</i> = 4	88.3 ± 31.7 <i>n</i> = 3	0.7215	81.8 ± 15.6 <i>n</i> = 4	59.6 ± 17.6 <i>n</i> = 7	0.4230
APD90 at 1 Hz (ms)	33.1 ± 3.6 <i>n</i> = 4	27.7 ± 0.7 <i>n</i> = 3	0.2657	49.1 ± 15.7 <i>n</i> = 4	52.8 ± 11.3 <i>n</i> = 7	0.8499
Slope (ms/s)	−1.10 ± 0.32 <i>n</i> = 4	−1.10 ± 0.57 <i>n</i> = 3	1.00	14.75 ± 13.12 <i>n</i> = 4	8.94 ± 6.68 <i>n</i> = 8	0.7106

3.4. Automated Electrophysiological Investigation and AP Measurements of Purified Cardiomyocytes with a Planar Patch Clamp System

In order to implement the use of purified wild-type and Scn5aΔ/+ cardiomyocytes for automated screenings, we performed electrophysiological analysis with a planar patch clamp robot (Patchliner, Nanion Technologies). For this technique, freshly dissociated single cells in suspension are required. Therefore, a new and gentle dissociation procedure was used to minimize cell stress and to avoid partial digestion of ion channels, which are required for intact AP generation. Dissociation was facilitated by removal of Ca²⁺ and cooling of cells at 4 °C, which allowed subsequent dissociation with the very short application of Trypsin. After dissociation, cells were gently centrifuged and carefully resuspended in external solution. In order to let cardiomyocytes recover from the dissociation process, cells remained at least 2 h at room temperature before planar patch clamp experiments were performed. To verify the dissociation efficiency, single cells were counted, and the cell concentration was adjusted to 0.1 to 1 × 10⁶ cells/mL to ensure a good catch rate by the planar patch clamp robot. For planar patch clamp measurements, 20 µL containing 2000 to 20,000 purified cardiomyocytes, was automatically pipetted into each recoding unit of the planar patch clamp chip. Once a cell was caught, a negative pressure was automatically applied and a seal enhancer was injected to form a good GΩ-seal for stable recording without leaks.

To estimate the quality of recording and the differentiation stage of cardiomyocytes, depolarizing voltage ramps were applied in the voltage clamp mode. This allowed determination of the intact seal without major leak conductance, as well as the detection of typical inward and outward currents of voltage-dependent ion channels (Figure 4a). Voltage ramps were also used to classify cardiomyocytes in immature cells with a slow inward Ca²⁺ current peak (Figure 4a, left, arrow) and in more mature cells with an additional fast Na⁺ current component (Figure 4a, right, arrow). Because we wanted to characterize a disease based on a Na⁺ channel mutation, only cardiomyocytes with a clear Na⁺ current peak were subsequently used to record APs. APs were evoked by current injection in the current clamp mode (Figure 4c). To identify the minimal current required, a special protocol was executed by the PatchControlHT software (Nanion Technologies). Briefly, stepwise (100 pA steps) increasing

2 ms-long current stimuli were applied, and the voltage responses were analyzed (Figure 4b). As soon as the resulting amplitude was >30 mV above the resting membrane potential, the applied current was defined as the threshold-current and 80 pA was added for safety.

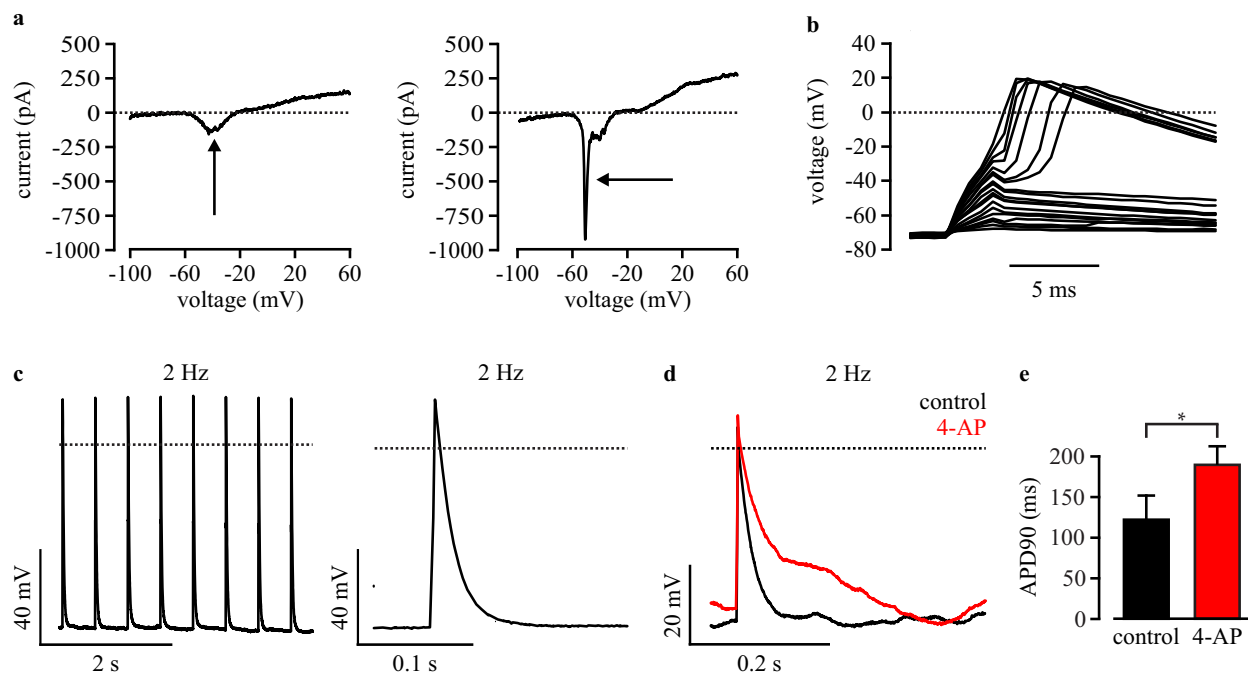


Figure 4. Automated planar patch clamp analysis of purified wild-type iPS-derived cardiomyocytes. **(a)** Examples of voltage ramps of an immature cardiomyocyte with Ca^{2+} current (left, arrow) and of a more mature cell with an additional fast Na^{+} current (right, arrow); **(b)** Representative membrane potential changes in response to stepwise increasing current pulses during the protocol for finding the AP threshold; **(c)** Example of automated AP recording at fixed pacing rate (**left**) with magnification (**right**); **(d)** representative APs before (black) and after blocking of K^{+} channels with automated application of 4-AP (red); **(e)** Statistical analysis of APD90 measured under control conditions and after 4-AP application. Error bars: S.E.M. Dotted lines indicate 0 mV or 0 pA.

To determine if AP recordings with a planar patch clamp system are useful to investigate LQTSs that mainly affects cardiac repolarization, we inhibited the repolarizing K^{+} channels by automated application of 4-aminopyridine and measured the effect on APD90. As expected, we found AP prolongation in purified wild-type cardiomyocytes from 120.1 ± 30.5 ms to 188.9 ± 24.0 ms ($n = 4$, AP evoked at 2 Hz, Figure 4d,e).

3.5. Automated Phenotypic Characterization of LQTS 3-Specific Purified Cardiomyocytes from *Scn5a* Δ /+ iPS Cells with a Planar Patch Clamp Robot

To proof the feasibility to characterize LQTSs with automated electrophysiological analysis, we recorded APs from purified cardiomyocytes using the planar patch clamp system. Frequency dependence was determined with APs elicited at 2, 1 and 0.5 Hz pacing frequencies using the automatically determined current threshold (see the above Section 3.4). Similar to the results from manual patch

clamp recordings (Figure 3), we found prolonged APs at low heart rates in *Scn5a* Δ /+ cardiomyocytes, but not in wild-type cells (Figure 5a,b). Furthermore, the longitudinal analysis of APD restitution in individual cells (examples shown in Figure 5c) showed a positive slope in *Scn5a* Δ /+ cardiomyocytes (4.13 ± 1.20 ms/s, $n = 9$) and a significant different negative slope in wild-type cells (-5.39 ± 4.82 ms/s, $n = 7$, Figure 5d, Table 1). Finally, we observed EADs in 30% of purified *Scn5a* Δ /+ cardiomyocytes (Figure 4e, $n = 10$), but none in wild-type cells ($n = 7$).

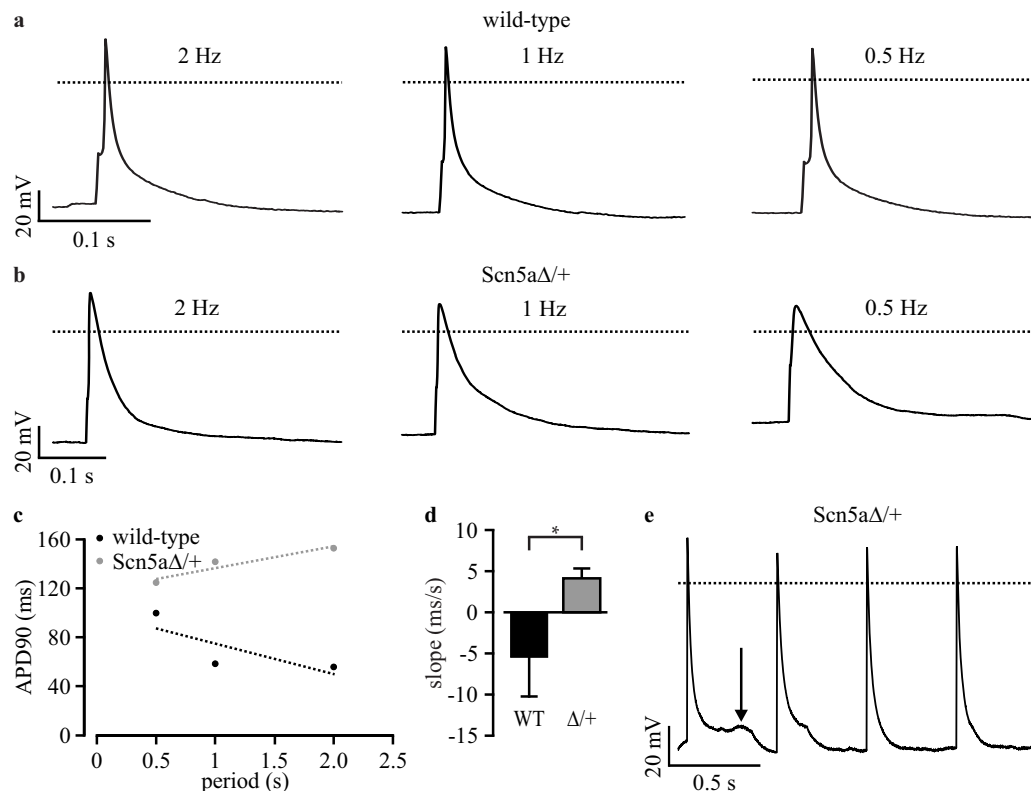


Figure 5. Automated characterization of LQTS 3-specific cardiomyocytes by planar patch clamp. **(a,b)** Representative traces of APs from wild-type **(a)** and *Scn5a* Δ /+ **(b)** cardiomyocytes at high and low pacing frequencies; **(c)** relationship between APD90 and the pacing period from a representative wild-type and a *Scn5a* Δ /+ cardiomyocyte with analysis of the slope by linear fit (dashed lines); **(d)** statistical analysis of the slope of APD90 to the pacing period relationship from individual wild-type (WT) and *Scn5a* Δ /+ cardiomyocytes (Δ /+); **(e)** typical LQTS 3-specific EADs observed in a *Scn5a* Δ /+ cardiomyocyte (arrow). Error bars: S.E.M. Dotted lines indicate 0 mV.

3.6. Analysis of Field Potentials from Purified iPS Cell-Derived Cardiomyocytes with Microelectrode Arrays

The duration of APs can not only be determined by patch clamp analysis, but can also be estimated indirectly from extracellular field potential recordings with microelectrode arrays, because of the good correlation of field potential duration to APD [24]. To prove the functionality of this technology for the characterization of LQTS 3, we plated purified cardiomyocytes obtained from wild-type and *Scn5a* Δ /+ iPS cells on six-well microelectrode arrays on which they formed a monolayer of synchronously

beating cells (Figure 6a). This allowed recordings of field potentials from nine electrodes in six individual wells (example recording in Figure 6b). To determine frequency-dependent field potential duration, measurements were performed at 22 °C and at 37 °C, which accelerated the spontaneous beating frequency.

Field potential duration was analyzed after trigger-based averaging over 50 s and calculation of the mean field potential from all nine electrodes (for details, see Section 2.7), resulting in one averaged field potential for each well (examples in Figure 6c). *Scn5a* Δ /+ cardiomyocytes showed a significantly ($p = 0.011$) longer field potential duration at low frequencies (132.4 ± 25.2 ms, $n = 3$) compared to high frequencies (88.0 ± 22.6 ms, $n = 3$, Figure 6d). Importantly, such a frequency-dependent effect was not observed in wild-type cardiomyocytes (low frequency: 45.5 ± 9.5 ms, $n = 3$; high frequency: 42.1 ± 10.5 ms, $n = 3$; $p = 0.78$). Thus, also field potential analysis with a microelectrode array showed the disease-specific frequency dependence of prolonged AP durations in purified *Scn5a* Δ /+ cardiomyocytes.

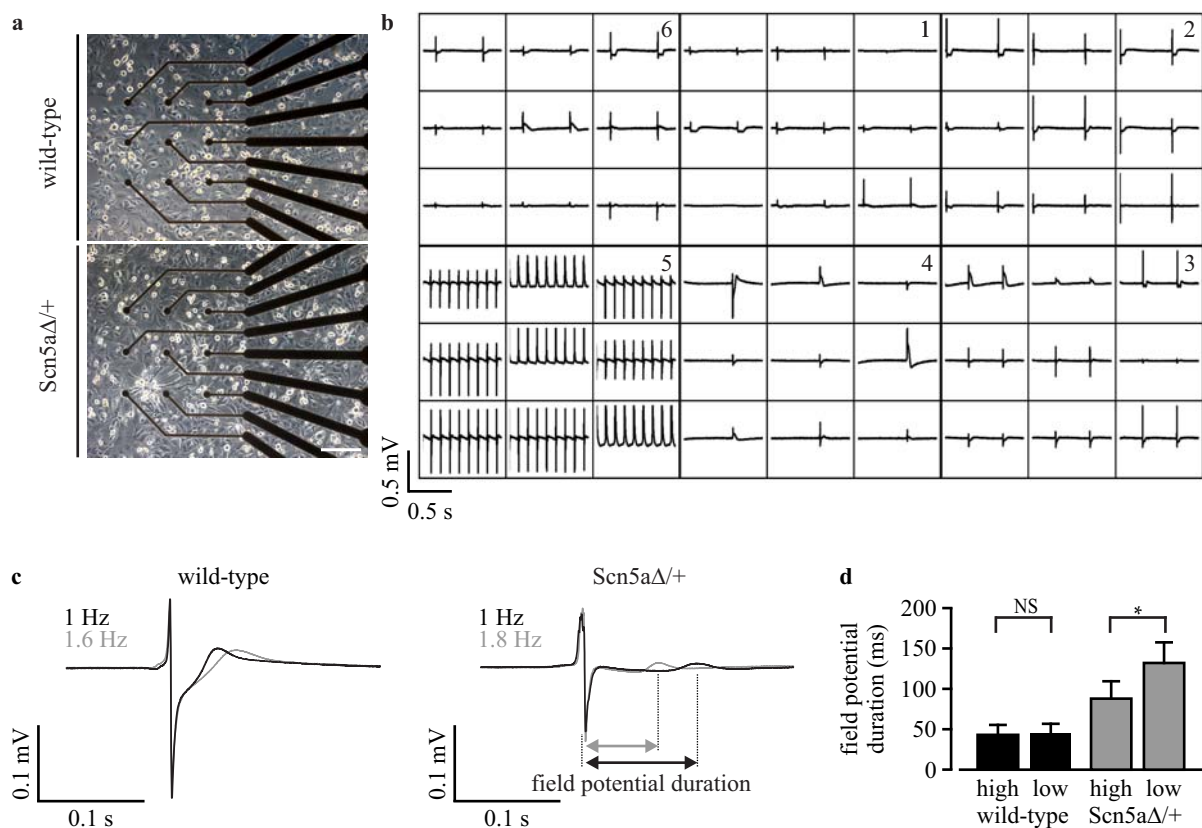


Figure 6. Field potential analysis with microelectrode arrays. (a) Image of the recording electrodes of a six-well microelectrode array with a monolayer of purified cardiomyocytes; (b) overview of field potential recordings from three wells with purified wild-type (bottom) and three wells with *Scn5a* Δ /+ cardiomyocytes (top); (c) examples of averaged field potentials with slow beating at 22 °C (black) and faster beating at 37 °C (grey) from purified wild-type and *Scn5a* Δ /+ cardiomyocytes. The analysis of the field potential duration is shown in the *Scn5a* Δ /+ recording; (d) statistical analysis of the field potential durations at low and high spontaneous beating frequencies from wild-type and *Scn5a* Δ /+ cardiomyocytes. Scale bar: 200 μ m. Error bars: S.E.M. NS, not significant.

4. Discussion

In this study, we present a novel, simple and fast lentiviral strategy for the purification of cardiomyocytes from iPS cells and show the feasibility of using these cells for automated electrophysiological investigations. The adverse effects of the random lentivirus integration, the non-clonal cell selection and the antibiotic purification on the pluripotency of iPS cells or the electrophysiological characteristics of cardiomyocytes were not detected. Importantly, purified cardiomyocytes had fast depolarizing Na^+ currents, AP generation and intact repolarization by K^+ currents and, therefore, were well suited to investigate LQTS in which these parameters are affected. We have proven this by showing the intact electrophysiological phenotype of purified LQTS 3-specific cardiomyocytes from previously published *Scn5a* Δ /+ iPS cells [5]. Furthermore, we have characterized purified cells with the automated planar patch clamp recordings and scalable microelectrode array analysis, which highlights the usefulness of these technologies for drug screening. Following, we discuss the achievements so far and the hurdles to overcome for large-scale purification and electrophysiological screening of cardiomyocytes.

4.1. Lentiviral Non-Clonal Gene Transfer Strategy

We have chosen cardiac-specific expression of an antibiotic resistance gene in order to kill all non-cardiomyocytes by antibiotic application. In contrast to low throughput single-cell sorting of labeled cardiomyocytes [14,15], this strategy enables the large-scale purification of cells. Because transfection of plasmid with common chemical, electroporation or lipofection methods suffers from poor efficiency in undifferentiated iPS cells, viral gene transfer methods are suitable alternatives [25,26]. We have used a lentivirus strategy that allows not only high efficient gene transfer, but also stable integration into the genome [25]. In addition to the cardiac-specific antibiotic resistance, we have employed a neomycin resistance gene under the control of the stem cell-specific promoter, Rex-1 [20], which was shown before to be useful for the selection of embryonic stem cell clones [17]. Thus, neomycin treatment allowed the selection of undifferentiated cells with stable lentivirus integration and without silencing or adverse positional effects of the surrounding host chromatin. One further advantage of using Rex-1-neomycin is that the continuous selection pressure at undifferentiated stages prevents iPS cell differentiation or lentiviral silencing at higher passages.

Usually, after classical or viral gene transfer into pluripotent stem cells, several single-cell clones are picked, propagated and characterized individually [16], a very time-consuming procedure and, therefore, an expensive task. In contrast to previous work, we decided to pool all iPS cells that survived the neomycin selection and generated one non-clonal iPS cell line for each genotype. This strategy harbors the risk that a single iPS cell clone with enhanced proliferation by lentivirus-induced mutations or chromosomal aberrations could overgrow the mixed population. However, the intact stem-cell morphology, the expression of stem cell markers, the normal proliferation of the mixed clones and the high similarity of all electrophysiological parameters in cardiomyocytes from early and late passages of the non-clonal iPS cell lines suggest no adverse effects of this strategy. Importantly, the phenotypical fingerprint of LQTS 3 (APD prolongation at slow rates) was only observed in *Scn5a* Δ /+

cardiomyocytes, both at early and late passages. Furthermore, the slope values of cardiomyocytes from the non-clonal iPS cells were almost identical to those from the original iPS cell clones [5].

The novel possibility to work with non-clonal iPS cells is also supported by a previous report on the successful generation of iPS cell clones in bulk culture without clone picking, which did not reveal differences with clonal selected iPS cell lines regarding pluripotency, gene expression profiles or differentiation potential [27]. Because a non-clonal strategy avoids manual clone picking and could be applied in 96-well or scalable formats, it enables the parallel generation and genetic modification of iPS cell lines from different patients at once. This would allow the purification of cardiomyocytes from many different patients for parallel and comparative electrophysiological screening.

The non-clonal lentiviral cardiomyocyte purification strategy might also have limitations and variations in efficacy because of uncontrolled variations in copy numbers and integration sites between iPS cells. High concentrations of neomycin could be used for selecting clones with the highest copy numbers, and this should be investigated in the future. Because lentiviruses have the tendency to integrate into euchromatin [28], infection at the stem cell level could lead to clones that are neomycin resistant at undifferentiated stages, but encounter lentiviral silencing upon differentiation and, therefore, fail to express puromycin for cardiomyocyte purification. Furthermore, the random integration of lentiviruses could cause insertional mutagenesis; however, this seems not to be frequent, because they tend to integrate away from promoters [29].

Recently, metabolic selection by the cultivation of stem-cell-derived cells in glucose-depleted medium containing only lactate as the energy source was described to be an efficient non-genetic method for the purification of cardiomyocytes [30]. Although the authors report a purity of 99% cardiomyocytes, this method seems to be highly dependent on the cell line used. In fact, although we have extensively tried to reproduce these purity values, we only obtained 45%–80% cardiomyocytes from mouse embryonic stem and human iPS cell lines using identical metabolic selection procedures [31].

4.2. Choice of a Cardiac-Specific Promoter

For cardiac-specific expression of the puromycin resistance gene, we have used the α -MHC promoter, which was shown to enable high efficient purification of cardiomyocytes from mouse and human iPS and embryonic stem cells [16,17,32,33]. Because of the size limitation for gene transfer using lentivirus (~9–10 kb between LTRs [27]), we had to use a short version (~1.7 kb) of the 3' end of the classical 6.5 kb-long α -MHC promoter. Although this fragment contained important gene expression regulatory elements (TATA box, MEF-1 MEF-2 and Nkx2.5 binding sites) [34], it is likely that unidentified enhancing elements were not present explaining the weak GFP expression. Nevertheless, purification of cardiomyocytes was unharmed, indicating sufficient expression of the puromycin resistance gene. This indicates a lower threshold for puromycin resistance than for GFP fluorescence, because the use of a 2A self-cleaving peptide should result in equimolar expression of both proteins [18].

In the future, the use of other promoters should be considered. Although the α -MHC promoter is labeling mature cardiomyocytes in mice, β -MHC is the predominant isoform in the human ventricle, and α -MHC is a marker rather for atrial or failing human cardiomyocytes [35]. Therefore, mature

cardiomyocytes from human iPS cells should be selected with the β -MHC promoter. Furthermore, the choice of other subtype-specific promoters could be very useful to obtain the cardiomyocyte population of interest. For instance, LQTS could be best investigated in ventricular cardiomyocytes that have long AP durations and could be selected using the MLC2v promoter. Moreover, mutations inducing atrial fibrillation might be better investigated with atrial cell selection by the MLC2a promoter, and for studying inherited sick sinus syndromes, pacemaker cells could be purified with sinus node-specific HCN or Tbx promoters.

4.3. Automatable and Scalable Electrophysiological Screening

The use of screening procedures to analyze APs of iPS cell-derived cardiomyocytes is particularly important to identify drugs that induce LQTS or to screen compounds that could treat inherited LQTS. For the systematic screening of many compounds, the classical manual patch clamp is not suitable, and automated and scalable systems are mandatory. For instance, the planar patch clamp technique [12] or the microelectrode array system [24,36] allow the acquisition of more data points per day (planar patch clamp: 200–1000; microelectrode array: 500) than the conventional patch clamp (50 data points/day) [36].

The planar patch clamp system that we have used in this study allows the automated recording of up to eight cells in parallel, as well as the automated application of several compounds. Because cells must be measured in suspension, very gentle dissociation methods have to be further optimized to avoid digestion of transmembrane ion channels.

We found that most action potential parameters were similar between manual and planar patch clamp recordings; however, APD90 tends to be longer (statistically not significant) in the latter (Table 1). We speculate that when using the automated planar patch clamp method, the dissociation procedure or the suction process onto the small holes of the borosilicate glass chips could kill smaller atrial or pacemaker cells with shorter APD or might favor larger ventricular cells with longer APD. However, although absolute APD values seem to vary with the method, the phenotypical fingerprint of LQTS 3-specific cardiomyocytes (positive slopes in the longitudinal regression analysis) can be similarly detected with both patch clamp methods (Table 1).

Similar to the conventional patch clamp, also during automated planar patch clamp analysis, the intracellular milieu is dialyzed against the internal solution, which leads to the wash out of important intracellular components and, therefore, reduces the stability of long-term recordings. This limits the duration of electrophysiological recording of one cell and, therefore, also the number of different compounds and dosages. Thus, this technology seems to be not suited for real high throughput analysis of several thousands of compounds.

Although, here, we only performed six recordings on a microelectrode array in parallel, scalable and automatable systems were developed (QT screen Multi Channel Systems) for parallel field potential recording and compound testing on 96 channels. In contrast to conventional microelectrode measurements (500 data points/day), such systems allow the recording of 6000 data points/day [36]. One remaining challenge is the almost impossible electrical stimulation of cardiomyocytes on microelectrode arrays for standardized recordings and to determine frequency-dependent effects. This

could be solved by using optogenetic technology, which was shown to be effective for the stimulation of purified cardiomyocytes on microelectrode arrays [37].

5. Conclusions

The herein reported non-clonal lentiviral strategy for the purification of cardiomyocytes from iPS cells is simple, fast and cheap and could be applied to large numbers of different iPS cell lines at once. In contrast to the picking of classically-transfected iPS cell clones, this strategy would allow the parallel purification of cardiomyocytes from many different patients for comparative electrophysiological analysis. Because the disease-specific phenotype of purified iPS cell-derived cardiomyocytes was retained and could be analyzed with automated planar patch clamp and scalable microelectrode array technologies, these assay systems will be useful for patient-specific drug screening in the future.

Acknowledgments

We thank Frank Host (University Bonn) for technical assistance and Sonja Stoelzle-Feix (Nanion Technologies) for protocols and technical support on the planar patch clamp system. This work was supported by the German Research Foundation (SA 1785/5-1) and the “StemCellFactory” project, which is co-funded by the European Union (European Regional Development Fund-Investing in your future) and the German federal state, North Rhine-Westphalia (NRW).

Author Contributions

Stephanie Friedrichs and Daniela Malan contributed equally to the work. Stephanie Friedrichs, Daniela Malan and Yvonne Voss performed the experiments and analyzed the data. Stephanie Friedrichs, Daniela Malan and Philipp Sasse designed the study and wrote the manuscript.

Conflicts of Interest

The authors declare no conflict of interest.

References

1. Schwartz, P.J.; Priori, S.G.; Spazzolini, C.; Moss, A.J.; Vincent, G.M.; Napolitano, C.; Denjoy, I.; Guicheney, P.; Breithardt, G.; Keating, M.T.; *et al.* Genotype-phenotype correlation in the long-QT syndrome: Gene-specific triggers for life-threatening arrhythmias. *Circulation* **2001**, *103*, 89–95.
2. Bennett, P.B.; Yazawa, K.; Makita, N.; George, A.L., Jr. Molecular mechanism for an inherited cardiac arrhythmia. *Nature* **1995**, *376*, 683–685.
3. Chandra, R.; Starmer, C.F.; Grant, A.O. Multiple effects of KPQ deletion mutation on gating of human cardiac Na⁺ channels expressed in mammalian cells. *Am. J. Physiol.* **1998**, *274*, H1643–H1654.
4. Charpentier, F.; Bourge, A.; Merot, J. Mouse models of SCN5A-related cardiac arrhythmias. *Prog. Biophys. Mol. Biol.* **2008**, *98*, 230–237.

5. Malan, D.; Friedrichs, S.; Fleischmann, B.K.; Sasse, P. Cardiomyocytes obtained from induced pluripotent stem cells with long-QT syndrome 3 recapitulate typical disease-specific features *in vitro*. *Circ. Res.* **2011**, *109*, 841–847.
6. Itzhaki, I.; Maizels, L.; Huber, I.; Zwi-Dantsis, L.; Caspi, O.; Winterstern, A.; Feldman, O.; Gepstein, A.; Arbel, G.; Hammerman, H.; *et al.* Modelling the long QT syndrome with induced pluripotent stem cells. *Nature* **2011**, *471*, 225–229.
7. Matsa, E.; Rajamohan, D.; Dick, E.; Young, L.; Mellor, I.; Staniforth, A.; Denning, C. Drug evaluation in cardiomyocytes derived from human induced pluripotent stem cells carrying a long qt syndrome type 2 mutation. *Eur. Heart J.* **2011**, *32*, 952–962.
8. Lahti, A.L.; Kujala, V.J.; Chapman, H.; Koivisto, A.P.; Pekkanen-Mattila, M.; Kerkela, E.; Hyttinen, J.; Kontula, K.; Swan, H.; Conklin, B.R.; *et al.* Model for long QT syndrome type 2 using human iPS cells demonstrates arrhythmogenic characteristics in cell culture. *Dis. Model. Mech.* **2012**, *5*, 220–230.
9. Davis, R.P.; Casini, S.; van den Berg, C.W.; Hoekstra, M.; Remme, C.A.; Dambrot, C.; Salvatori, D.; Oostwaard, D.W.; Wilde, A.A.; Bezzina, C.R.; *et al.* Cardiomyocytes derived from pluripotent stem cells recapitulate electrophysiological characteristics of an overlap syndrome of cardiac sodium channel disease. *Circulation* **2012**, *125*, 3079–3091.
10. Egashira, T.; Yuasa, S.; Suzuki, T.; Aizawa, Y.; Yamakawa, H.; Matsuhashi, T.; Ohno, Y.; Tohyama, S.; Okata, S.; Seki, T.; *et al.* Disease characterization using LQTS-specific induced pluripotent stem cells. *Cardiovasc. Res.* **2012**, *95*, 419–429.
11. Moretti, A.; Bellin, M.; Welling, A.; Jung, C.B.; Lam, J.T.; Bott-Flugel, L.; Dorn, T.; Goedel, A.; Hohnke, C.; Hofmann, F.; *et al.* Patient-specific induced pluripotent stem-cell models for long-QT syndrome. *N. Engl. J. Med.* **2010**, *363*, 1397–1409.
12. Stoelzle, S.; Haythornthwaite, A.; Kettenhofen, R.; Kolossov, E.; Bohlen, H.; George, M.; Bruggemann, A.; Fertig, N. Automated patch clamp on mesc-derived cardiomyocytes for cardiotoxicity prediction. *J. Biomol. Screen.* **2011**, *16*, 910–916.
13. Mauritz, C.; Schwanke, K.; Reppel, M.; Neef, S.; Katsirtaki, K.; Maier, L.S.; Nguemo, F.; Menke, S.; Haustein, M.; Hescheler, J.; *et al.* Generation of functional murine cardiac myocytes from induced pluripotent stem cells. *Circulation* **2008**, *118*, 507–517.
14. Huber, I.; Itzhaki, I.; Caspi, O.; Arbel, G.; Tzukerman, M.; Gepstein, A.; Habib, M.; Yankelson, L.; Kehat, I.; Gepstein, L. Identification and selection of cardiomyocytes during human embryonic stem cell differentiation. *FASEB J.* **2007**, *21*, 2551–2563.
15. Hattori, F.; Chen, H.; Yamashita, H.; Tohyama, S.; Satoh, Y.S.; Yuasa, S.; Li, W.; Yamakawa, H.; Tanaka, T.; Onitsuka, T.; *et al.* Nongenetic method for purifying stem cell-derived cardiomyocytes. *Nat. Methods* **2010**, *7*, 61–66.
16. Kolossov, E.; Bostani, T.; Roell, W.; Breitbach, M.; Pillekamp, F.; Nygren, J.M.; Sasse, P.; Rubenchik, O.; Fries, J.W.; Wenzel, D.; *et al.* Engraftment of engineered ES cell-derived cardiomyocytes but not bm cells restores contractile function to the infarcted myocardium. *J. Exp. Med.* **2006**, *203*, 2315–2327.

17. Kita-Matsuo, H.; Barcova, M.; Prigozhina, N.; Salomonis, N.; Wei, K.; Jacot, J.G.; Nelson, B.; Spiering, S.; Haverslag, R.; Kim, C.; *et al.* Lentiviral vectors and protocols for creation of stable hesc lines for fluorescent tracking and drug resistance selection of cardiomyocytes. *PLoS One* **2009**, *4*, e5046.
18. Fang, J.; Qian, J.J.; Yi, S.; Harding, T.C.; Tu, G.H.; VanRoey, M.; Jooss, K. Stable antibody expression at therapeutic levels using the 2A peptide. *Nat. Biotechnol.* **2005**, *23*, 584–590.
19. Pfeifer, A.; Hofmann, A. Lentiviral transgenesis. *Methods Mol. Biol.* **2009**, *530*, 391–405.
20. Hosler, B.A.; LaRosa, G.J.; Grippo, J.F.; Gudas, L.J. Expression of REX-1, a gene containing zinc finger motifs, is rapidly reduced by retinoic acid in F9 teratocarcinoma cells. *Mol. Cell. Biol.* **1989**, *9*, 5623–5629.
21. Wobus, A.M.; Wallukat, G.; Hescheler, J. Pluripotent mouse embryonic stem cells are able to differentiate into cardiomyocytes expressing chronotropic responses to adrenergic and cholinergic agents and Ca²⁺ channel blockers. *Differentiation* **1991**, *48*, 173–182.
22. Friedrichs, S.; Malan, D.; Sasse, P. Modeling long QT syndromes using induced pluripotent stem cells: Current progress and future challenges. *Trends Cardiovasc. Med.* **2013**, *23*, 91–98.
23. Nuyens, D.; Stengl, M.; Dugarmaa, S.; Rossenbacker, T.; Compennolle, V.; Rudy, Y.; Smits, J.F.; Flameng, W.; Clancy, C.E.; Moons, L.; *et al.* Abrupt rate accelerations or premature beats cause life-threatening arrhythmias in mice with long-QT3 syndrome. *Nat. Med.* **2001**, *7*, 1021–1027.
24. Halbach, M.; Egert, U.; Hescheler, J.; Banach, K. Estimation of action potential changes from field potential recordings in multicellular mouse cardiac myocyte cultures. *Cell. Physiol. Biochem.* **2003**, *13*, 271–284.
25. Ma, Y.; Ramezani, A.; Lewis, R.; Hawley, R.G.; Thomson, J.A. High-level sustained transgene expression in human embryonic stem cells using lentiviral vectors. *Stem Cells* **2003**, *21*, 111–117.
26. Fontes, A. Cloning technologies. *Methods Mol. Biol.* **2013**, *997*, 253–261.
27. Willmann, C.A.; Hemeda, H.; Pieper, L.A.; Lenz, M.; Qin, J.; Joussen, S.; Sontag, S.; Wanek, P.; Denecke, B.; Schuler, H.M.; *et al.* To clone or not to clone? Induced pluripotent stem cells can be generated in bulk culture. *PLoS One* **2013**, *8*, e65324.
28. Mitchell, R.S.; Beitzel, B.F.; Schroder, A.R.; Shinn, P.; Chen, H.; Berry, C.C.; Ecker, J.R.; Bushman, F.D. Retroviral DNA integration: ASLV, HIV, and MLV show distinct target site preferences. *PLoS Biol.* **2004**, *2*, e234.
29. Vannucci, L.; Lai, M.; Chiuppesi, F.; Ceccherini-Nelli, L.; Pistello, M. Viral vectors: A look back and ahead on gene transfer technology. *New Microbiol.* **2013**, *36*, 1–22.
30. Tohyama, S.; Hattori, F.; Sano, M.; Hishiki, T.; Nagahata, Y.; Matsuura, T.; Hashimoto, H.; Suzuki, T.; Yamashita, H.; Satoh, Y.; *et al.* Distinct metabolic flow enables large-scale purification of mouse and human pluripotent stem cell-derived cardiomyocytes. *Cell Stem Cell* **2013**, *12*, 127–137.
31. Malan, D.; Sasse, P. University of Bonn, Bonn, Germany. Unpublished work, 2014.
32. Zandstra, P.W.; Bauwens, C.; Yin, T.; Liu, Q.; Schiller, H.; Zweigerdt, R.; Pasumarthi, K.B.; Field, L.J. Scalable production of embryonic stem cell-derived cardiomyocytes. *Tissue Eng.* **2003**, *9*, 767–778.

33. Xu, X.Q.; Zweigerdt, R.; Soo, S.Y.; Ngoh, Z.X.; Tham, S.C.; Wang, S.T.; Graichen, R.; Davidson, B.; Colman, A.; Sun, W.; *et al.* Highly enriched cardiomyocytes from human embryonic stem cells. *Cytotherapy* **2008**, *10*, 376–389.
34. Jin, D.; Ni, T.T.; Hou, J.; Rellinger, E.; Zhong, T.P. Promoter analysis of ventricular myosin heavy chain (VMHC) in zebrafish embryos. *Dev. Dyn.* **2009**, *238*, 1760–1767.
35. Reiser, P.J.; Portman, M.A.; Ning, X.H.; Schomisch Moravec, C. Human cardiac myosin heavy chain isoforms in fetal and failing adult atria and ventricles. *Am. J. Physiol. Heart Circ. Physiol.* **2001**, *280*, H1814–H1820.
36. Meyer, T.; Leisgen, C.; Gonser, B.; Gunther, E. QT-screen: High-throughput cardiac safety pharmacology by extracellular electrophysiology on primary cardiac myocytes. *Assay Drug Dev. Technol.* **2004**, *2*, 507–514.
37. Bruegmann, T.; Malan, D.; Hesse, M.; Beiert, T.; Fuegemann, C.J.; Fleischmann, B.K.; Sasse, P. Optogenetic control of heart muscle *in vitro* and *in vivo*. *Nat. Methods* **2010**, *7*, 897–900.

© 2015 by the authors; licensee MDPI, Basel, Switzerland. This article is an open access article distributed under the terms and conditions of the Creative Commons Attribution license (<http://creativecommons.org/licenses/by/4.0/>).

3.2.3 Human iPS cell model of type 3 long QT syndrome recapitulates drug-based phenotype correction. Basic Res Cardiol. 2016 Mar;111(2):14. doi: 10.1007/s00395-016-0530-0 (IF:6.03)

Aim of the study

In this study, we investigated patient-specific iPS cell-derived cardiomyocytes with a heterozygous p.R1644H mutation in the cardiac Na⁺ channel (Scn5a). This particular mutation was identified in one family branch in which a sudden infant death occurred, and the mother and sister showed QT prolongation in the ECG as signs of LQTS.

This mutation allowed us to explore whether human disease-specific cardiomyocytes also recapitulated the electrophysiological hallmarks of the LQTS3, such as faster recovery from inactivation of the Na⁺ current, and AP prolongation with EADs at low frequency stimulation. If this was the case, we could use these patient-derived cells to test the effectivity of different drugs. Such an analysis could be very beneficial for the patient because several mutations in the Scn5a gene were found, and drug efficacy as well as potential side-effects may be mutation specific.

Methods and results

Fibroblasts derived from skin biopsies from a patient with congenital LQTS carrying a c.4931G>A missense mutation were used to generate human iPS cells (LQTS3), and fibroblasts from a control patient to generate human iPS wild-type cells. Due to the missense mutation, there is an arginine-to-histidine exchange at the cytoplasmic face of the D4S4 transmembrane domain (p.R1644H) of Na⁺ channels, impairing their inactivation and giving rise to a persistent late Na⁺ current. This mutation causes an early recovery from the inactivation of the Na⁺ current, which opposes repolarization, inducing a prolonged QT interval (Wang et al., 1996).

Human iPS cell colonies from LQTS3 and wild-type patients were derived by retroviral reprogramming with the four factors Oct4, Sox2, Klf4 and c-Myc, and characterized for pluripotency through the SEE4 marker. Pluripotency was confirmed by analyzing their differentiation potential, giving rise to cell types of all three germ layers (Fig 1 d-h, page 6,

Malan et al., 2016). Differentiation into cardiomyocytes was achieved by generating EB-like 3D clusters and biphasic modulation of the Wnt signaling pathway (Zhang et al., 2015). EBs started to beat around day 6 of differentiation and expressed cardiac troponin-t positive cells. (Fig 1 i-j, page 6). Cardiomyocytes older than four weeks were used for further characterization since the *Scn5a* expression was increased at that stage, as seen by the RT-qPCR time course (Fig 1 k, page 6). LQTS3-derived cardiomyocytes showed a significant increase in the recovery from the inactivation of the Na^+ current and longer APD. The APD restitution slope (dependence of APD on the pacing period) was steeper in LQTS3 cardiomyocytes compared to wild-type-derived cardiomyocytes, indicating prolonged APD at low stimulation rates in LQTS3, whereas frequency dependency was not seen in the wild-type cardiac cells (Fig 3 c-d, page 7). Thus, the characteristic electrophysiological features of the R1644H mutation were found in the disease human LQTS3 cardiomyocytes. We next used an independent assay based on field potential recording to further prove the ability of detecting the disease phenotype. Frequency-corrected field potential recorded on multi-electrode arrays showed prolonged duration and a notched T wave-like signal probably due to EADs in the LQTS3 cardiomyocytes, thus again revealing typical LQTS3 features. (Fig 3 e-g, page 7).

We further tested whether the cellular model is suitable to assess drug efficacy by applying mexiletine, a common drug for LQTS3 therapy which inhibits preferentially the sustained late Na^+ current rather than the peak current density. This drug acts preferentially on the pathogenic feature of mutant channels, and was given to the patients in this study to prevent arrhythmic events. Both APD investigated by patch clamp analysis and field potential duration were reduced by mexiletine (Fig 4 a-d, page 9). Moreover, mexiletine suppressed in a dose-dependent manner early after afterdepolarizations. We tested alternative drugs that are known to counteract the late sodium current, phenytoin and ranolazine. Also, these drugs reduced APD and field potential duration in our model. This was in line with the clinical observation that phenytoin was a successfully alternative to mexiletine to treat several affected members of the LQTS3 family in this study (Supplemental Fig 2).

Conclusion:

The generation of LQTS3 human iPS cell-derived cardiomyocytes from patients with a heterozygous p.R1644H mutation recapitulated pathophysiological features of the disease. We showed that the human iPS-derived cardiomyocytes could be used to assess the pharmacological responses to drugs used for LQTS3 therapy. Investigation of field potential with EADs and analysis of APs provides integrated readouts that might be most robust and predictive for investigating candidate drug responses. Drugs like mexiletine and ranolazine which inhibit late Na⁺ current were effective in inhibiting the characteristic features of LQTS3 in the cardiomyocyte disease model. The effect was in line with the clinical observations that mexiletine and ranolazine were successfully used in patients. This concordance between iPS cells and clinical data is noteworthy because mexiletine treatment is not effective in all LQTS3 patients with different point mutations. Thus, iPS cell-derived cardiomyocytes from LQTS3 patients can be used as screening tools to predict and prove therapeutically effective drugs.

Contribution: Designed, performed, analyzed the patch clamp data, wrote part of the manuscript.

Human iPS cell model of type 3 long QT syndrome recapitulates drug-based phenotype correction

Daniela Malan¹ · Miao Zhang^{2,3} · Birgit Stallmeyer⁴ · Jovanca Müller⁴ ·
Bernd K. Fleischmann¹ · Eric Schulze-Bahr⁴ · Philipp Sasse¹ · Boris Greber^{2,3}

Received: 16 June 2015 / Accepted: 7 January 2016 / Published online: 23 January 2016
© The Author(s) 2016. This article is published with open access at Springerlink.com

Abstract Long QT syndrome is a potentially life-threatening disease characterized by delayed repolarization of cardiomyocytes, QT interval prolongation in the electrocardiogram, and a high risk for sudden cardiac death caused by ventricular arrhythmia. The genetic type 3 of this syndrome (LQT3) is caused by gain-of-function mutations in the *SCN5A* cardiac sodium channel gene which mediates the fast $\text{Na}_v1.5$ current during action potential initiation. Here, we report the analysis of LQT3 human induced pluripotent stem cell-derived cardiomyocytes (hiPSC-CMs). These were generated from a patient with a heterozygous p.R1644H mutation in *SCN5A* known to interfere with fast channel inactivation. LQT3 hiPSC-CMs recapitulated pathognomonic electrophysiological features of the disease, such as an accelerated recovery from inactivation of sodium currents as well as action potential

prolongation, especially at low stimulation rates. In addition, unlike previously described LQT3 hiPSC models, we observed a high incidence of early after depolarizations (EADs) which is a trigger mechanism for arrhythmia in LQT3. Administration of specific sodium channel inhibitors was found to shorten action and field potential durations specifically in LQT3 hiPSC-CMs and antagonized EADs in a dose-dependent manner. These findings were in full agreement with the pharmacological response profile of the underlying patient and of other patients from the same family. Thus, our data demonstrate the utility of patient-specific LQT3 hiPSCs for assessing pharmacological responses to putative drugs and for improving treatment efficacies.

Keywords Human iPS cells · Cardiac disease modeling · Type 3 long-QT syndrome · Drug testing

D. Malan and M. Zhang contributed equally to this work.

Electronic supplementary material The online version of this article (doi:10.1007/s00395-016-0530-0) contains supplementary material, which is available to authorized users.

✉ Philipp Sasse
philipp.sasse@uni-bonn.de

✉ Boris Greber
boris.greber@mpi-muenster.mpg.de

¹ Institute of Physiology I, Life & Brain Center, University of Bonn, Sigmund-Freud-Str. 25, 53127 Bonn, Germany

² Human Stem Cell Pluripotency Group, Max Planck Institute for Molecular Biomedicine, 48149 Münster, Germany

³ Chemical Genomics Centre of the Max Planck Society, 44227 Dortmund, Germany

⁴ Department of Cardiovascular Medicine, Institute for Genetics of Heart Diseases (IfGH), University Hospital Münster, 48149 Münster, Germany

Introduction

A diagnostic hallmark of LQTS is a prolonged QT interval in the electrocardiogram (ECG) of patients, resulting from impaired myocellular repolarization during action potential (AP) generation. Approximately 5–10 % of LQTS patients are carriers of a gain-of-function mutation in *SCN5A*, the gene encoding the α -subunit of the cardiac sodium channel (LQT3 subtype). These mutations result in an enhanced recovery from channel inactivation and re-activation during the plateau phase of the action potential [2, 21, 27]. Thus, the persistent inward sodium current counteracts cardiac repolarization resulting in prolonged action potentials as well as in the induction of EADs which are key triggers of ventricular tachycardia [4, 12, 18, 30].

In clinical terms, LQT3 patients often exhibit QT interval prolongation at lower heart rates and, consequently, have an increased risk for cardiac events during rest or sleep [23]. This is in contrast to other LQTS subtypes such as LQT1, where cardiac events typically occur at increased heart rates, that is, during physical or emotional (i.e. adrenergic) stress [5, 24]. Therefore, while β -blocker therapy alone can be sufficient for treating LQT1 patients, effective treatment options in LQT3 patients may require additional measures and hence, the best suited pharmacological treatments are still being explored [20]. Moreover, numerous mutations in *SCN5A* have been identified to cause distinct disease phenotypes [18, 22], and drug efficacy may be mutation-specific, suggesting that treatments need to be tailored to a given specific gene defect [19]. In vitro drug screening systems may therefore aid in predicting therapeutic efficacy. LQT3 models based on patient-specific hiPSCs have been shown to recapitulate key electrophysiological disease features such as increased late Na^+ currents and prolonged action potentials at the single-cell level [15, 29]. However, more macroscopic phenotypes like induced arrhythmia or spontaneous EADs have not been reported in these or related studies [6, 9].

To re-investigate this latter point and potentially assess pharmacological response profiles, we have established a patient-derived hiPSC model harbouring a heterozygous *SCN5A* mutation (p.R1644H) mutation that is known to cause LQT3 [31]. Disease pathogenesis of this typical LQT3 mutation is due to disperse sodium channel reopenings following fast initial inactivation [2, 7, 30]. The amplitude of the late Na^+ current is small (<5 %) when compared to that of the initial inward one. Nonetheless, the premature recovery from inactivation of the Na^+ current will counteract cardiomyocyte repolarization, to macroscopically cause a long QT phenotype [2]. Interestingly, besides displaying corresponding electrophysiological phenotypes, cardiac syncytia of R1644H hiPSC-CMs showed spontaneous EADs which are key triggers of arrhythmia in LQT3 patients [12]. EADs could be abolished by treating mutant hiPSC-CMs with the same drug that was successfully used to treat the underlying patient. Our data hence suggest patient-specific hiPSC-CMs may serve as a predictive system for drug assessment in LQT3 personalized medicine.

Materials and methods

Clinical patient history and data generation

In 2006, members of a large family ($n = 23$) with congenital LQTS presented first in our outpatient service. In one family branch, a sudden infant death occurred during

the second month of age. Despite lack of pathological investigation or molecular autopsy, a sudden infant death syndrome (SIDS) caused by LQTS seemed likely, since her mother and a sister were also affected by LQTS. Genotyping and family cascade screening of all family members was then initiated. All family members who participated in the study gave written informed consent before genetic and clinical investigations, in accordance with the last version of the Declaration of Helsinki (World Medical Association and R281) and with recommendations by the local ethics committee. Briefly, ECG analysis was performed using conventional 12-lead ECG recordings and standard lead positions (paper speed: 50 mm/s). Heart rate-corrected QT intervals (QTc) were calculated using Bazett's formula. Genomic DNA was isolated from blood lymphocytes by standard semiautomatic procedures (QIAcube, Qiagen). Locus-specific DNA sequencing was carried out by investigating the major genes relevant for LQTS, *KCNQ1* (LQT1), *KCNH2* (LQT2) and, subsequently, *SCN5A* (LQT3). The patients' sequence data were compared to the genomic reference (NM_198056.2). Amino acid annotations were based on the corresponding human protein sequences (Locus Reference Genome: LRG_289p1). Alamut annotation software (Interactive Biosoftware) was used for mutation nomenclature.

Generation and characterization of hiPSCs

Skin punch biopsies were obtained from one affected LQT3 patient of this family as well as from a healthy control individual, following written informed consent and approval by the medical ethics committee of the University of Münster. Fibroblasts that grew out from the dermal tissue were expanded in conventional serum-containing culture media, and subjected to cellular reprogramming following Melton's protocol [13]. Retroviruses were produced in 293T cells using Fugene 6 transfection with Addgene plasmids 8454 (VSV-G envelope), 8449 (packaging plasmid), 17217 (OCT4), 17218 (SOX2), and 17219 (KLF4) [28]. After retroviral infection of fibroblasts and culture in conventional hESC media with 0.5 mM of valproic acid, emerging colonies were manually picked and expanded. Several cell lines displaying typical hESC morphology and growth characteristics were further characterized according to standard assays [11]. In brief, the heterozygous LQT3 mutation was confirmed using conventional gPCR, cloning and sequencing (Table S2). Transgene silencing was monitored using primers given in Table S2. Karyotypes were assessed based on chromosome counting using standard procedures. The surface marker SSEA4 was detected using standard immunocytochemistry procedures (Millipore #90231, 1:50). hESC marker gene expression was monitored using RT-qPCR analysis as

described [11], using M-MLV (Affymetrix #78306) with dT₁₅ priming, iTaqTM Universal SYBR Green Supermix (BioRad #172-5853), and RPS16/RPL37A as housekeeping controls (Table S2). Global transcriptome profiling in comparison to hESCs was performed using TotalPrepTM RNA Amplification kits (Life Technologies #AMIL1791) and Illumina human-12 V3 arrays, following the manufacturer's instructions and using default settings for hybridization, and performing background subtraction, normalization, and scatter plot analysis in GenomeStudio. Spontaneous in vitro differentiation into derivatives of the three germ layers was performed using conventional embryoid body differentiation as described [10]. Immunocytochemistry was carried out using standard procedures with paraformaldehyde fixation and using appropriate Alexa-conjugated secondary antibodies (Life Technologies). Primary antibodies used were anti-SMA (Dako #M0851, 1:100), anti-AFP (Dako #A0008, 1:300), and anti- β III-tubulin (Sigma #T8660, 1:1000). One LQT3 and one WT hiPSC line showing near-complete transgene silencing and overall hESC-like characteristics according to these assays were used for further investigation.

Maintenance of hiPSCs

hiPSCs were routinely cultured in 6-well plates on 1:75 diluted MatrigelTM HC (Corning #354263), in FTDA medium [10]. FTDA consisted of DMEM/F12, 1× PenStrep/L-glutamine, 1× defined lipids (Life Technologies #21331020, #10378016, and #11905031, respectively), 0.1 % human serum albumin (Biological Industries #05-720-1B), 1× ITS (BD #354350), 10 ng/ml FGF2 (PeproTech #100-18B), 0.2 ng/ml TGF β 1 (eBioscience #34-8348-82), 50 nM Dorsomorphin (Santa Cruz #sc-200689), and 5 ng/ml Activin A (eBioscience #34-8993-85). Cells were routinely passaged as single cells or, initially, as clumps of cells. For single cell splitting, cells were grown to full confluence (until cultures seemingly appeared syncytial), digested for 10–15 min using AccutaseTM (Millipore #SCR005) with 10 μ M Y27632 (abcamBiochemicals #ab120129), and replated in the presence of 10 μ M Y27632 at 400,000–600,000 cells per well of a 6-well plate. hiPSCs reached confluence after 3 days under these conditions and were subsequently harvested as above, for continuous maintenance or for the induction of differentiation. hiPSCs were kept in culture for a maximum of 30 passages. Cell lines were tested negative for mycoplasma.

Directed CM differentiation of hiPSCs

In some experiments, cardiomyocyte differentiation was induced using END-2 co-culture [17], by plating clusters of

undifferentiated hiPSCs onto confluent END-2 feeders in KnockoutTM DMEM (Life Technologies #10829018), 1× ITS (insulin/transferrin/selenium, BD #354350), 250 μ M 2-phospho-L-ascorbic acid, and PenStrep/L-glutamine. For most experiments, hiPSCs were differentiated using a directed differentiation protocol [33]: fully confluent hiPSCs were digested with Accutase and 10 μ M Y27632 for 10–15 min at 37 °C, and dissociated into single cells using a 1 ml pipette. Cells were pelleted and resuspended in d0 differentiation medium. d0 medium was composed of Knockout DMEM, 0.4 % polyvinyl alcohol (Sigma #363170), 10 μ M Y27632, 1× ITS, 1× PenStrep/L-glutamine, 5 ng/ml FGF2, 0.5–2 ng/ml BMP4 (R&D #314-BP-050), and 1–2 μ M CHIR99021 (AxonMedchem #Axon 1386). Cell concentration was adjusted to 40,000–80,000 cells per ml. 100 μ l were added to each well of a 96 well V-bottom plate (Nunc #277143). EBs were allowed to form over night after a 1 min plate centrifugation step at 400 g. Next day (d1), EBs were washed in TS medium and transferred into ultra-low attachment 96 well U-bottom plates (Corning #7007). TS medium contained KO-DMEM, 1× TS, 1× lipid additive (Sigma #L5146), and 1× PenStrep/L-glutamine. 100× TS stock was prepared in advance by dissolving 55 mg transferrin (Sigma #T8158) in 100 ml PBS containing 0.067 mg sodium selenite (Sigma #S5261). On days 2–3, the EBs were incubated in TS medium together with 2 μ M IWP-2 (Santa Cruz #sc-252928), followed by incubation in TS medium w/o IWP-2 hence after. Daily media changes were carried out under a stereo microscope using 200 μ l pipettes with a wide opening. Spontaneous beating was commonly observed from day 6 onwards and scored in the 96-well plates. After the initial differentiation in multi-well plates, beating EBs were usually pooled and further matured in 6-well plates with ultra-low attachment surface (Corning #3471). CM maintenance medium consisted of KO-DMEM, 2 % FCS, and 1× PenStrep/L-glutamine. Cardiomyocytes were typically analysed approximately 4 weeks after the initiation of differentiation.

FACS analysis of differentiated cultures was performed on Beckman Coulter Gallios instrumentation as described [33], following dissociation with 1× TrypLE Select (Life Technologies #12563011) and using PBS/0.5 % saponin/ 5 % FCS for all incubation steps (anti-CTNT, Labvision #MS-295-P, 1:150/Alexa-488-conjugated anti-mouse, Life Technologies #A11001). SCN5A expression in cardiomyocytes was monitored using RT-qPCR analysis (Table S2) or standard immunocytochemistry of dissociated hiPSC-CMs replated onto gelatin-coated dishes (anti-SCN5A, alomone labs #ASC-005, 1:150). Additional antibodies used were anti- α -actinin (Sigma #A7811, 1:800), and anti-NKX2.5 (R&D #AF2444, 1:100).

Patch clamp analysis

For patch-clamp experiments beating aggregates after 4 weeks of differentiation were collected in PBS and dissociated with 1 mg/mL collagenase type B (Roche) for 60 min at 37 °C under shaking conditions. Isolated single cells were plated at low densities on fibronectin-coated (0.1 %) coverslips in differentiation medium. Patch-clamp recordings were performed after 48–72 h on single beating cardiomyocytes using an EPC10 amplifier (Heka) in the whole cell configuration.

Na⁺ current was measured in the voltage clamp mode. For recording of Na⁺ current peak and recovery from inactivation the internal solution contained (in mM) 3 NaCl, 133 CsCl₂, 2 MgCl₂, 2 NaATP, 2 TEACl, 10 EGTA and 5 Hepes, pH 7.3 (CsOH) and the external solution: 7 NaCl, 133 CsCl₂, 1.8 CaCl₂, 1.2 MgCl₂, 5 Hepes, 11 glucose, 0.005 nifedipine, pH 7.4 (CsOH). Peak Na⁺ currents were measured in response to a −10 mV depolarizing pulse of 40 ms from a holding potential of −100 mV, normalised to the cell capacitance and expressed in pA/pF. For analysis of the recovery from inactivation kinetics, pairs of depolarization pulses from −100 to 10 mV were applied with increasing delays between the two pulses (from 1.5 to 57 ms) and the second peak Na⁺ current was normalized to the first, plotted against the delay and these values were fitted with a mono-exponential growth to obtain the time constant of recovery.

Action potential recordings were performed in the current clamp mode with an internal solution containing (in mM) 50 KCl, 80 K-Asparatate, 1 MgCl₂, 3 MgATP, 10 EGTA, 10 Hepes, pH 7.4 (KOH) and an external solution containing 140 NaCl, 5.4 KCl, 1.8 CaCl₂, 1 MgCl₂, 10 Hepes, 10 glucose, pH 7.4 (NaOH). APs were elicited by 2.5 ms long current injection pulses through the patch pipette and the strength of the pulse was increased stepwise until stable action potential generation was established. The current injections were controlled by an external Stimulator (Model 2100, A-M Systems) attached to the EPC10 amplifier. To quantify the frequency-dependent AP duration, cardiomyocytes were stimulated at different pacing periods and at each pacing period the average action potential duration at 90 % of repolarization (APD₉₀) was determined. APD₉₀ values were plotted against pacing periods and a linear regression analysis was used to determine the slope of this relationship for each individual cell. The effects of mexiletine (100 μM), ranolazine (20 μM) and phenytoin (10 μM) on APD were recorded at a constant stimulation frequency of 0.6, 0.2, and 0.2 Hz, respectively. Data were acquired at a sampling rate of

10–20 kHz (voltage clamp) or 5 kHz (current clamp), digitized with the Patchmaster software (HEKA) and analysed offline using Fitmaster (HEKA) or Labchart software (AD Instruments). AP parameters were analysed with the cardiac action potential analysis module of Labchart. APD₉₀ was calculated from the peak of the AP to the point where the AP had dropped by 90 % of its amplitude.

Electrophysiological analysis on microelectrode arrays (MEAs)

Electrophysiological analysis on microelectrode arrays (USB-MEA256 system, Multichannel Systems) was performed essentially as previously described [32]. 9-well MEAs were coated with a small volume of 1:150 pre-diluted Matrigel/0.1 % gelatin solution in KO-DMEM for approximately 2 h at room temperature. hiPSC-CMs were dissociated from maintenance cultures using a 1× or 10× TrypLE Select digestion to obtain a single-cell suspension or small cell aggregates. Approximately 20,000 cells were plated onto the MEA surfaces in a ~3 μl droplet and allowed to attach for ~1 h. MEA chambers with attached cells were then filled with 200 μl of CM maintenance medium. Two days later, baseline recordings were performed at 37 °C. Only FP spectra showing a clear T_{\max} -like signal were considered. T_{\max} and peak-to-peak finding algorithms were implemented in MC Rack software v4.5.7. Field potential durations (FPDs, QT_{max} intervals) and beating frequencies (RR intervals) were averaged from five consecutive measurements from independent recordings. Data were processed in MS Excel using Bazett's formula for frequency correction: $FPD (cQT_{\max}) = QT_{\max} (ms) / (RR (s))^{0.5}$. Only samples showing beat intervals in the range of ~700–2300 ms were considered for QT_{max} quantification. Recordings of drug-treated cells were initiated after a wash-in time of about 10 min. Wash-out recordings were performed after three to five media changes. FP curves monitoring drug responses were overlaid using Adobe Photoshop. Mexiletine was administered at 5–20 μM, as indicated in figures. Ranolazine was used at 20 μM.

Statistics

Electrophysiological data are presented as mean values from biological replicates ± SEM. ECG-based data are presented as mean values ± SD. Statistical analysis was performed using appropriate paired and unpaired 2-sided Student's *t* test or Fisher's exact test *F*. A *p* value of <0.05 was considered statistically significant. * In figures indicates *p* < 0.05, and ** denotes *p* < 0.01.

Results

Clinical history of a family with LQT3 syndrome

Following a case of sudden infant death in a large family with congenital LQTS, 15 of 23 available family members were identified as heterozygous carriers of a c.4931G>A missense mutation in the *SCN5A* gene, a previously described LQT3-causing defect. In the sodium channel protein, this mutation promotes an arginine-to-histidine exchange at the cytoplasmic face of the D4S4 transmembrane segment (p.R1644H; Fig. 1b) [2]. R1644H was one of the first LQT3-causing mutations identified and has been shown to impair fast Na^+ channel inactivation, thereby giving rise to the a persistent late sodium inward current [12, 30, 31].

The mean baseline QTc interval of LQT3 mutation carriers in this family was 478 ± 35 ms ($n = 14$), including two patients with normal QTc values (410 and 424 ms; Table S1). There were no clinical signs for conduction disease or Brugada syndrome in the affected family members. Apart from the sudden cardiac death victim (2 month-old, unknown genotype), six LQT3 patients had syncope before medical treatment (mean age of first event: 24 years). 10 of the patients were treated with β -blockers, and six were given class I antiarrhythmics (mexiletine or phenytoin—three of these with concomitant β -blocker medication). Cardiac devices were implanted in two LQT3 patients that refused oral therapy due to bradycardia and/or orthostatic intolerance (Table S1) [34].

Generation and characterization of LQT3 hiPSCs

One affected family member presenting with QT interval prolongation was selected for hiPSC derivation (Fig. 1a; #5-3 in Table S1). Primary fibroblasts were derived from a skin biopsy taken from the patient following ethical approval and informed written consent. The presence of the mutation was confirmed by DNA sequencing in the cultured cells (Fig. 1b). hiPSCs were derived from these using standard retroviral reprogramming methodology [13, 28]. An hiPSC clone with normal karyotype (Fig. 1b, c) was selected for further characterization. Transgenes of the four reprogramming factors were silenced to negligible levels in LQT3 hiPSCs (Fig. 1d). LQT3 hiPSC colonies under stem cell maintenance conditions stained positive for the surface human embryonic stem cell (hESC) marker SSEA4 (Fig. 1e). RT-qPCR analysis suggested full activation of endogenous hESC marker gene expression (Fig. 1f). Global expression profiling revealed that the transcriptome of LQT3 hiPSCs was virtually indistinguishable from that of hESCs (Fig. 1g). Spontaneous in vitro differentiation gave rise to derivative cell types of the three germ layers suggesting

acquired pluripotency (Fig. 1h). Using a directed differentiation protocol [33], LQT3 hiPSCs robustly converted into spontaneously contracting cardiomyocytes, as evidenced by high percentages of beating embryoid bodies (EBs) as well as FACS analysis for cardiac troponin C (Fig. 1i, j; Movies S1, S2). Finally, because early hiPSC-derived cardiomyocytes tend to be immature in their physiological properties [33], a time-course expression analysis of *SCN5A* was performed. This revealed that *SCN5A* was expressed at lower levels in early (~ 2 week-old) hiPSC-CMs, but at higher and stable levels after approximately 4 weeks of culture (Fig. 1k). These data suggested that LQT3 hiPSCs had acquired a fully reprogrammed hESC-like state and that hiPSC-CMs could be functionally analysed following several weeks of in vitro culture.

As control, wild-type (WT) hiPSCs were derived from an unrelated, healthy donor and characterized in a similar manner. Briefly, WT hiPSCs displayed a hESC-like morphology and karyotype under stem cell maintenance conditions (Fig. S1a, b), had fully silenced the exogenous transgenes (Fig. S1c), and expressed endogenous marker genes at hESC-like levels (Fig. S1d). WT hiPSCs differentiated into derivatives of the three germ layers upon spontaneous in vitro differentiation (Fig. S1e), and readily formed cardiomyocytes using independent differentiation protocols (Fig. S1f, g; Movies S3, S4). Hence, based on these assays, WT hiPSCs shared key pluripotency features with LQT3 hiPSCs and differentiated into cardiomyocytes at comparable efficiencies.

Electrophysiological phenotypes of R1644H hiPSC-CMs

We next investigated the electrophysiological characteristics of LQT3 and WT hiPSC-CMs. The *SCN5A* protein could be detected by immunocytochemistry in a large fraction of cardiomyocytes from both cell lines (Fig. 2a). Peak Na^+ current density measurements at -10 mV using patch clamp recordings confirmed that the channel was functionally active in both WT and LQT3 hiPSC-CMs. Peak current amplitudes tended to be slightly increased in LQT3 cardiomyocytes, but this difference was not statistically significant (Fig. 2b, WT: 12.2 ± 1.8 pA/pF, $n = 11$; LQT3: 19.9 ± 5.5 pA/pF, $n = 6$). A clear increased recovery from inactivation of the sodium current was found in LQT3 compared to WT-CMs (Fig. 2c; time constant τ of recovery from inactivation: WT 10.8 ± 1.8 ms, $n = 13$; LQT3: 3.6 ± 0.6 ms, $n = 5$, $p < 0.05$). These data demonstrate that the pathognomonic electrophysiological feature of the R1644H mutation was found in our LQT3 disease model [30].

Next, we explored action potential durations (APD) in the current clamp mode. APDs measured at a stimulation

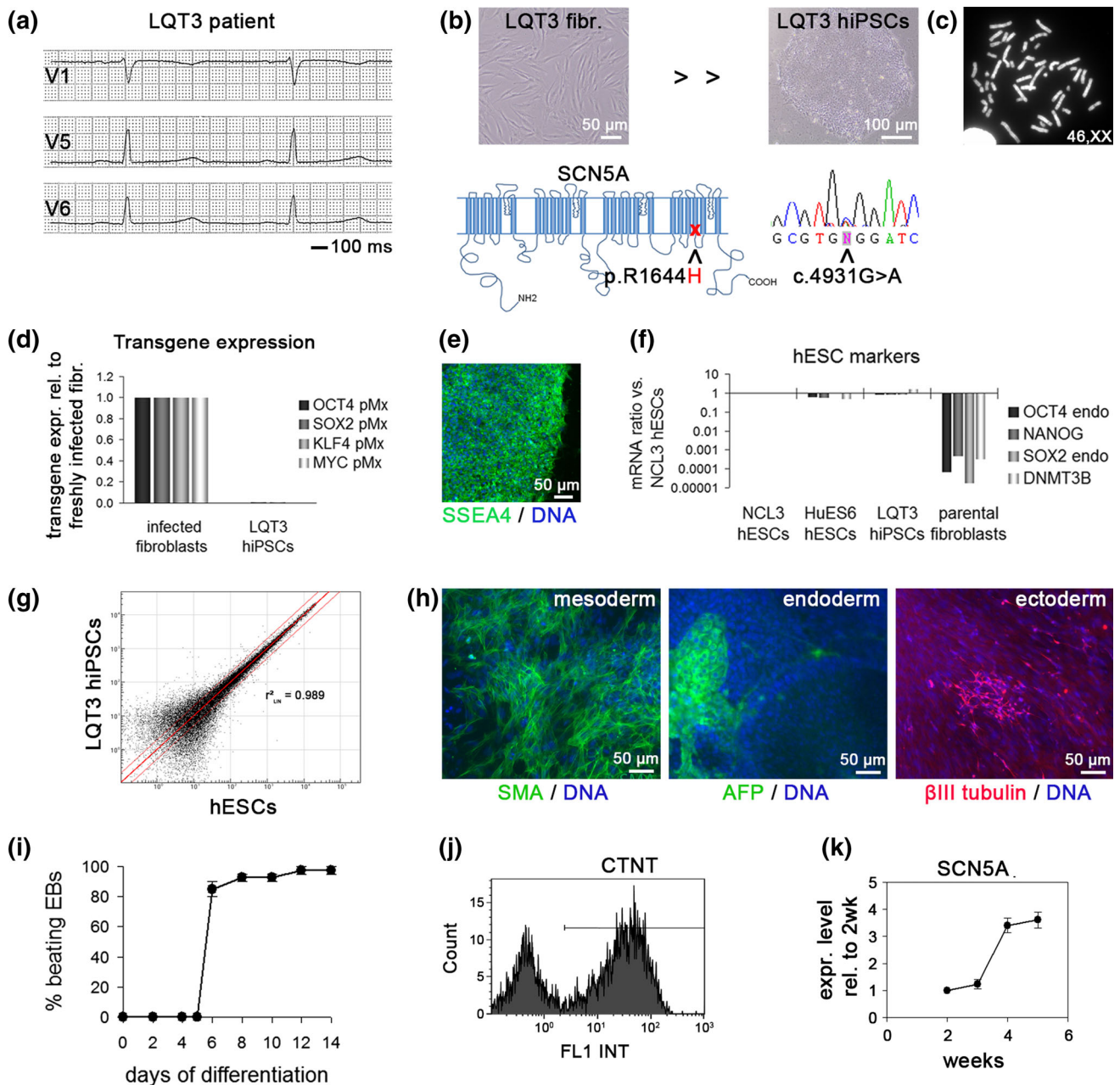


Fig. 1 Generation and characterization of R1644H hiPSCs. **a** Electrocardiogram of the donor LQT3 patient displaying QT prolongation (QTc: \sim 507 ms). **b** Phase contrast morphology of LQT3 skin fibroblasts and reprogrammed hiPSCs (top). Bottom Illustration of amino acid substitution in SCN5A (bottom left) and sequencing confirmation of underlying heterozygous c.4931G>A nucleotide exchange at the DNA level (bottom right, reverse complement strand). **c** R1644H hiPSCs have a normal karyotype ($n = 10$). **d** RT-qPCR analysis of retroviral transgene expression in freshly infected LQT3 fibroblasts and LQT3 hiPSCs. **e** Immunofluorescence analysis of the pluripotency marker SSEA4 in LQT3 hiPSCs. **f** RT-qPCR expression analysis of endogenous pluripotency genes in LQT3 hiPSCs, in comparison to two hESC lines and the parental fibroblasts. **g** Scatter plot analysis of microarray gene expression data from LQT3

hiPSCs and NCL3 hESCs. Note the high global similarity indicated by linear regression analysis. Red lines denote intervals of twofold changes in gene expression. **h** Immunofluorescence analysis of spontaneous differentiation into derivatives of the three germ layers. SMA smooth muscle actin, AFP alpha-fetoprotein. **i** Percentage of beating EBs over time generated from LQT3 hiPSCs through directed differentiation ($n = 2$). **j** Representative FACS analysis of differentiated LQT3 EBs indicating the cardiomyocyte fraction based on cardiac Troponin T (CTNT) staining. **k** RT-qPCR time-course analysis of SCN5A expression during cardiac differentiation of LQT3 hiPSCs. Cells were differentiated on END-2 feeders. Data are normalized against pan-cardiac markers to account for differences in CM yield between samples ($n = 3$)

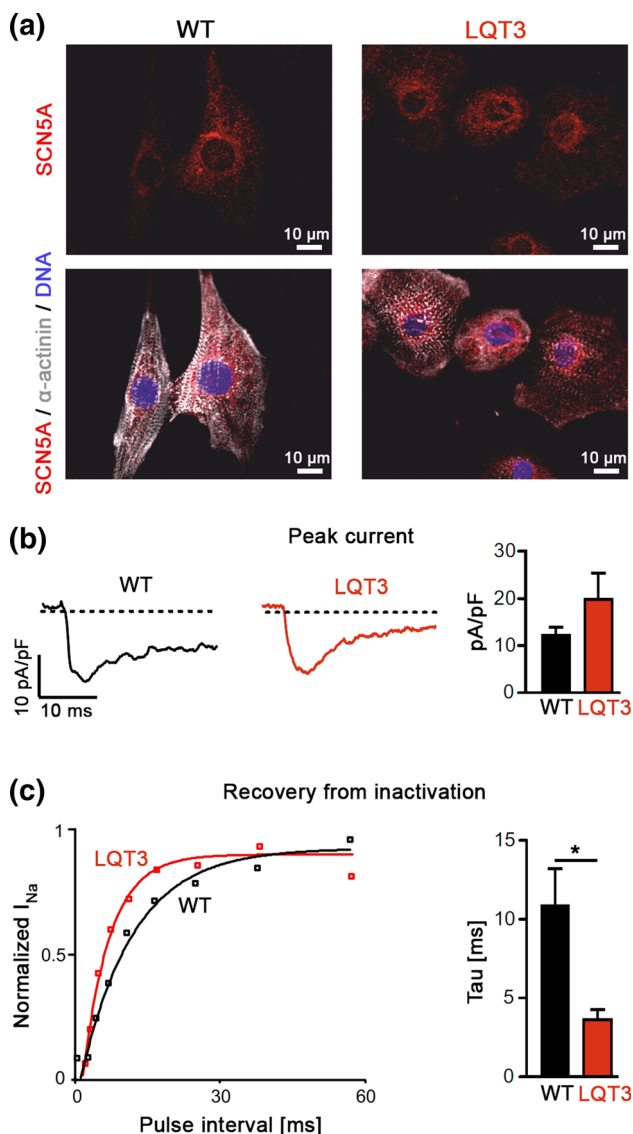


Fig. 2 Sodium channel function in LQT3 and control hiPSC-CMs. **a** Immunofluorescence stainings of SCN5A (red) in CMs derived from LQT3 and WT hiPSCs show perinuclear and partial outer membrane localization. **b** Representative peak sodium current traces (left) and average peak current densities (right, $n = 11$ WT, $n = 6$ LQT3, n.s.). **c** Analysis of recovery from inactivation using a 2-pulse protocol. Left: Examples of normalized sodium currents plotted against pulse intervals. Note the accelerated recovery in the LQT3 hiPSC-CM. Right: Averaged time constant of recovery from inactivation ($n = 13$ WT and $n = 5$ LQT3, $p < 0.05$)

frequency of 1 Hz were increased in LQT3 hiPSC-CMs (Fig. 3a). This was true for averaging data from all types of cells (Fig. 3b, left: APD₉₀ WT: 95.1 ± 12.3 ms, $n = 14$; LQT3: 155.7 ± 25.7 ms, $n = 27$, $p < 0.05$), whereas the phenotype became somewhat more pronounced when confining the analysis to ventricular-like cells (Fig. 3b, right: APD₉₀ WT: 122.9 ± 15.2 ms, $n = 7$; LQT3: 225.5 ± 36.6 ms, $n = 15$, $p < 0.05$). Moreover, as a hallmark of LQT3, APD is highly frequency dependent and expected to

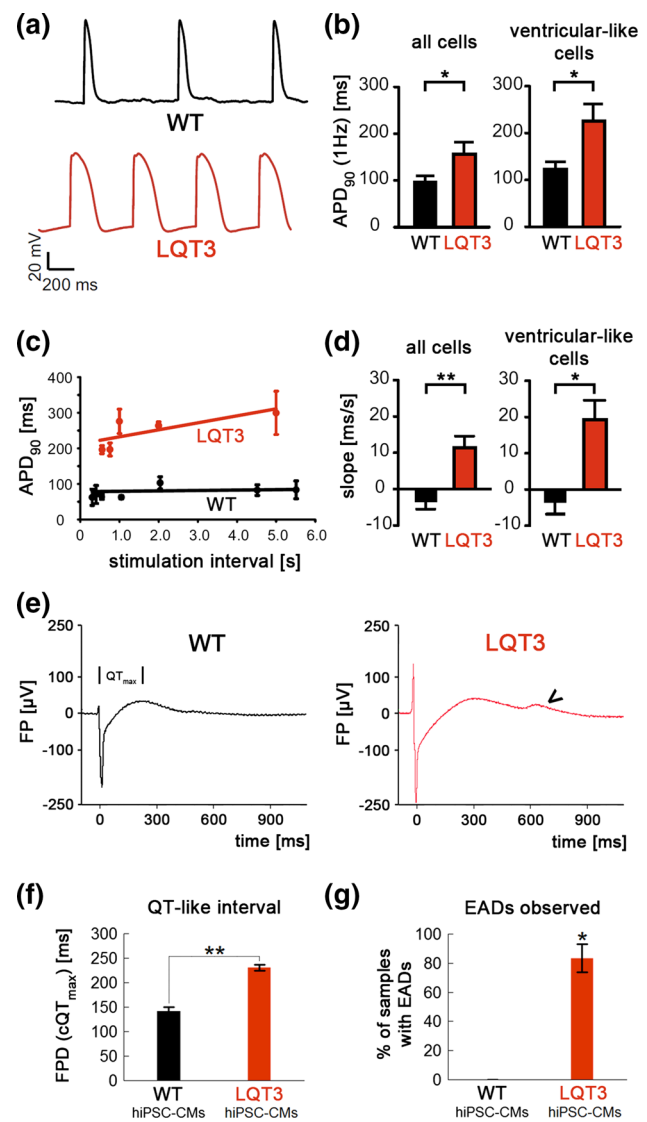


Fig. 3 APD and FPD phenotypes of LQT3 hiPSC-CMs. **a** Representative APs from WT and LQT3 hiPSC-CMs. **b** APD₉₀ quantification at a stimulation frequency of 1 Hz. LQT3 hiPSC-CMs showed a significant prolongation (all cells: $n = 14$ WT, $n = 27$ LQT3, $p < 0.05$; ventricular-like cells: $n = 7$ WT, $n = 15$ LQT3, $p < 0.05$). **c** Action potential restitution (APD₉₀/pacing period relationship) in a representative WT (black) and LQT3 (red) hiPSC-CM. Note the positive slope in the LQT3 cell. **d** Statistical quantification of the slope of APD restitution in WT and LQT3 hiPSC-CMs (all cells: $n = 8$ WT, $n = 17$ LQT3, $p < 0.01$; ventricular-like cells: $n = 5$ WT, $n = 8$ LQT3, $p < 0.05$). **e** Representative field potential recordings of WT and LQT3 hiPSC-CM clusters using MEAs. FPD (QT_{max}) was quantified on the basis of Q and maximum T wave-like signals (see indicated interval). The arrowhead marks a typical EAD-like signal observed in LQT3 CMs. **f** FPD quantification from independent WT and LQT3 hiPSC-CM preparations ($n = 3$ WT, $n = 5$ LQT3, $p < 0.01$). **g** Field potentials with EADs were observed in a high percentage of LQT3 samples ($n = 7$ WT, $n = 17$ LQT3, $p < 0.05$)

increase at low beating rates, as shown previously [8, 16]. Hence, APD was determined in individual hiPSC-CMs at various stimulation frequencies (see examples given in

Fig. 3c). The APD restitution slope (dependency of APD on the pacing period) was determined through linear regression analysis. Analysis across all cardiac subtypes yielded a steep APD restitution slope for LQT3 hiPSC-CMs ($+11.4 \pm 3.2$ ms/s, $n = 17$; Fig. 3d, left) indicating prolonged APD especially at low stimulation rates, whereas this dependency was absent in WT hiPSC-CMs (-3.2 ± 2.2 ms/s, $n = 8$). The difference became even more accentuated when including only cells with ventricular-like AP shapes into the analysis (Fig. 3d, right, WT: -3.2 ± 3.5 ms/s, $n = 5$; LQT3: $+19.3 \pm 5.3$ ms/s, $n = 8$).

Further, we used bulk cultures of hiPSC-CMs on microelectrode arrays (MEAs) in order to explore, whether these pathognomonic features of LQT3 could also be detected using an independent assay based on extracellular field potential recordings. Clear T wave-like signals were readily detectable with both WT and LQT3 CMs, permitting field potential duration (FPD) measurements (Fig. 3e). Frequency-corrected FPDs determined under spontaneous beating conditions were significantly increased in LQT3 hiPSC-CMs compared to WT cells (Fig. 3f). Interestingly, most FP traces from LQT3 hiPSC-CMs displayed notched T wave-like signals, which we attribute to EADs evoked by reactivating Na^+ currents in the mutant cells (arrow head in Fig. 3e). Quantification from independent cell preparations revealed that these EAD signals were highly reproducible in LQT3 hiPSC-CMs but never seen in WT cells (Fig. 3g). Collectively, these data reveal typical LQT3 features in R1644H hiPSC-CMs by electrophysiological analysis, including EADs at high probability.

Pharmacological rescue of LQT3 phenotypes

Likely, the above phenotypes are a direct consequence of the reactivating sodium current in R1644H CMs. To demonstrate this, and to assess the predictability of our model for drug screening, we employed mexiletine, a Na^+ channel inhibitor commonly used in LQT3 therapy [20]. Using patch clamp analysis, we found that mexiletine (100 μM) significantly reduced APD in LQT3 hiPSC-CMs (-25.8 ± 6.7 %, $n = 5$, $p < 0.05$), thereby correcting the APD prolongation phenotype at the single cell level (Fig. 4a, b). Importantly, this effect was not seen in WT cells (APD: $+3.2 \pm 4.7$ %, $n = 8$) suggesting that this drug preferentially acts on the reactivated sodium current (Fig. 4a, b). Similarly, mexiletine reduced the FPD in bulk cultures of LQT3 hiPSC-CMs, in a dose-dependent manner, and showed virtually no effect in WT cells (Fig. 4c). 10–20 μM of mexiletine were sufficient to reduce FPDs of LQT3 CMs to WT-like values (Fig. 4d). Interestingly, we noticed that the EADs were also affected by mexiletine treatment of LQT3 hiPSC-CMs. In a highly reproducible and dose-dependent manner, mexiletine administration

progressively shifted the EAD signal towards later time points, outside the T wave-like repolarization window, and doses above 20 μM fully suppressed EADs (Fig. 4e, f). To substantiate the idea that late sodium current blockage was the basis for these patient-specific effects, we additionally evaluated alternative drugs, ranolazine and phenytoin, acting via the same principle [3, 25]. Indeed, both compounds specifically reduced APDs in LQT3 hiPSC-CMs (phenytoin: -29.7 ± 9.2 %, $n = 6$; ranolazine: -26.3 ± 9.2 %, $n = 7$) but not in WT cells (Fig. S2 a–d). Similarly, ranolazine administration (20 μM) abolished spontaneous EADs in patient hiPSC-CMs and caused significant LQT3-specific FPD shortening (Fig. S2e, f).

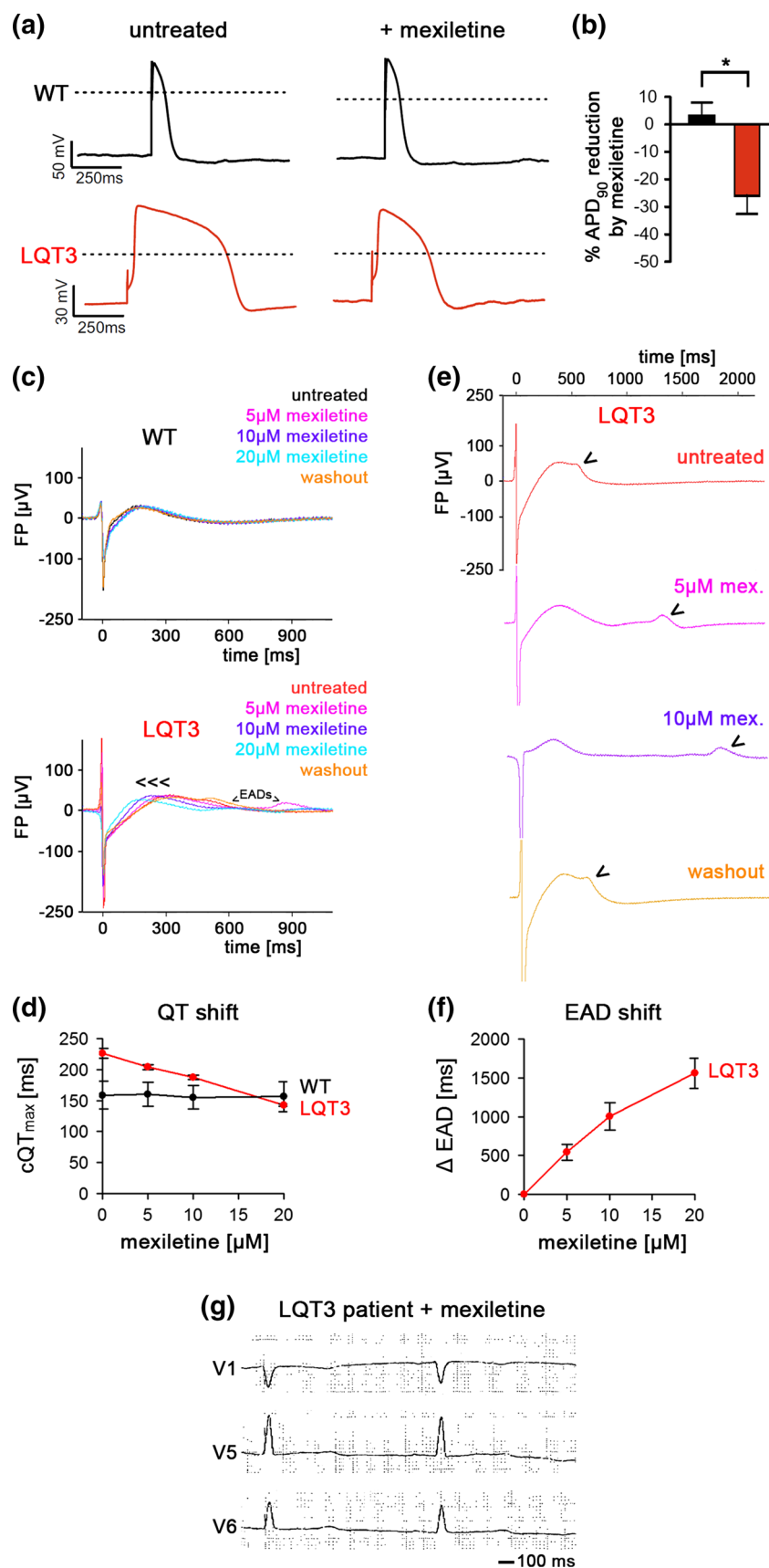
Interestingly, these data provide support of the therapeutic strategy applied to the affected LQT3 family members, including the individual who donated cells for hiPSC derivation (Table S1). Interpretation of these data is, however, complicated by the fact that several patients of this family were treated both with antiarrhythmics and beta blockers. As a tendency, though, beta blocker monotherapy was applied to family members with a baseline QTc below 500 ms and this caused a rather moderate decline (17 ± 4 ms, $n = 3$). In comparison, patients with a baseline QTc > 500 ms were treated with antiarrhythmics (mexiletine or phenytoin) \pm additional beta blocker, which caused a more pronounced QTc reduction (62 ± 18 ms, $n = 5$, $p < 0.01$ vs. beta blocker monotherapy). In support of this notion, the patient underlying our study showed a QTc reduction from ~ 507 to ~ 440 ms following mexiletine monotherapy (2×100 mg/day, Fig. 4g), whereas additional treatment with bisoprolol only had a slight additive effect (~ 435 ms, Table S1). Using this strategy, adverse cardiac events were prevented in a sustained manner in all patients who had experienced syncope prior to therapy (Table S1).

Discussion

Mutations in *SCN5A* can give rise to distinct disease phenotypes, namely LQT3, Brugada syndrome, progressive cardiac conduction disease, and sinus node diseases [18]. Moreover, LQT3 may be caused by diverse gain-of-function mutations in *SCN5A* and, as a result of this fact, not all patients respond to a given pharmacological treatment at similar efficacy [19]. Patient-specific hiPSC-CMs can be utilized for evaluating putative disease-correcting effects of drugs, as exemplified with models of LQT2 and JLNS [14, 32]. However, because electrophysiological analysis at the single-cell level is technically challenging and because hiPSC-CMs present a heterogeneous mixture of cardiac subtypes, more integrated and disease-associated readouts are desirable. EADs are considered triggers of life-

Fig. 4 Rescue of disease-specific phenotypes in LQT3 hiPSC-CMs by mexiletine.

a Representative action potential traces before (*left*) and after (*right*) mexiletine treatment (100 μ M). Note the AP shortening following drug administration in the LQT3 cells. **b** Quantification of mexiletine-induced APD₉₀ reduction ($n = 8$ WT, $n = 5$ LQT3, $p < 0.05$). **c** Representative field potential recordings showing that mexiletine reduces FPD specifically in LQT3 hiPSC-CMs but not in WT cells. **d** Quantification of mexiletine effect at different dosages on FPD in WT and LQT3 hiPSC-CMs ($n = 3$). **e** Mexiletine shifts EADs in LQT3 hiPSC-CMs towards later time-points in a dose-dependent and reversible manner (representative MEA traces). *Arrowheads* mark EADs. **f** Average quantification of induced EAD shift in FPs of LQT3 hiPSC-CMs as dependent on mexiletine dosage ($n = 3$). EADs were fully suppressed using >20 μ M of mexiletine. **g** Electrocardiogram of the donor LQT3 patient under mexiletine monotherapy (2×100 mg/day; QTc: ~ 440 ms).



threatening Torsade de Pointes (TdP) tachycardia in LQTS, as they may contribute to increased dispersion of ventricular repolarization [1]. Interestingly, on microelectrode arrays, prominent EADs were consistently observed in our LQT3 model but were never seen in WT controls, neither in the cell line used here nor in other independent hiPSC lines [32]. MEAs may be particularly reliable in detecting EADs as they tend to overcome cell-to-cell variation by averaging field potentials from many cells in a given preparation. Furthermore, intracellular ion concentrations in cardiomyocytes (Na^+ , K^+ , Ca^{2+}) are not disturbed in MEA recordings, in contrast to the patch-clamp technique that dialyzes Na^+ , K^+ against the electrode solution and usually buffers Ca^{2+} . Perhaps for these reasons, we and others did not observe EADs in LQT3 hiPSC-CMs using patch-clamp analysis of single cells [15, 29]. It will be interesting, therefore, to see whether EADs are a universal feature also of CMs from other LQT3 hiPSC models, as revealed here using field potential recordings.

Mexiletine is a commonly used drug for treating LQT3 patients because it is more effective in inhibiting late Na^+ currents than peak current density and therefore acts preferentially on the pathogenic feature of mutant channels [7, 26, 29]. This drug thereby appeared well-suited for balancing consequences of the R1644H mutation which causes a sustained, non-inactivating sodium current as a result of disperse reopenings following initial fast channel inactivation [7, 30]. Indeed, mexiletine specifically and dose-dependently reduced APDs and FPDs in R1644H hiPSC-CMs but had no effect on WT cells. Moreover, EAD-like signals arising specifically in field potential recordings from LQT3 hiPSC-CMs were shifted towards later time-points by mexiletine administration in a dose-dependent manner or were fully suppressed at higher concentrations. Thus, at least in the cellular model, even low dosages of mexiletine exerted beneficial effects by shifting EADs outside the critical repolarization time-window. Notably, the phenotype-correcting effects in LQT3 hiPSC-CMs were in accordance with the beneficial response to mexiletine administration in the LQT3 patient underlying our study. Moreover, alternative drugs counteracting the late sodium current, phenytoin and ranolazine, also reduced APDs/FPDs in our model. Indeed, phenytoin was successfully used to treat several affected members of our LQT3 family, as an alternative to mexiletine (Table S1). Hence, our data show that drug testing results from LQT3 hiPSC-CMs may be predictive for medical treatment.

This concordance between hiPSC and patient-based data is noteworthy because mexiletine treatment is not effective in all LQT3 patients and models [19]. For instance, Ma et al. analysed an independent hiPSC model of LQT3 and obtained only a partial rescue of the APD prolongation phenotype following high-dosage (50 μM) mexiletine

treatment [15]. Moreover, Terrenoire et al. observed inhibitory side-effects on the hERG channel using mexiletine administration in yet a different LQT3 hiPSC model, which complicated medical interpretation [29]. We did not observe any effects on APD or FPD when monitoring mexiletine treatment of WT hiPSC-CMs, suggesting no side-effects at the moderate drug concentrations used in our study ($\leq 20 \mu\text{M}$). In summary, monitoring effects on FPD and EADs provides integrated readouts that might be most robust and predictive for investigating candidate drug responses in hiPSC models of LQT3.

Acknowledgments Open access funding provided by Max Planck Society (or associated institution if applicable). DM, BKF and PS were supported by the StemCellFactory I and II projects which are co-funded by the European Union (European Regional Development Fund—Investing in your future) and the German federal state North Rhine-Westphalia (NRW). MZ and BG were supported by the Chemical Genomics Centre of the Max Planck Society, and the Bundesinstitut für Risikobewertung, grants FK-3-1329-471 and 1328-539.

Compliance with ethical standards

Conflict of interest The authors declare no conflicts of interest.

Open Access This article is distributed under the terms of the Creative Commons Attribution 4.0 International License (<http://creativecommons.org/licenses/by/4.0/>), which permits unrestricted use, distribution, and reproduction in any medium, provided you give appropriate credit to the original author(s) and the source, provide a link to the Creative Commons license, and indicate if changes were made.

References

1. Antzelevitch C, Shimizu W (2002) Cellular mechanisms underlying the long QT syndrome. *Curr Opin Cardiol* 17:43–51
2. Balser JR (2001) The cardiac sodium channel: gating function and molecular pharmacology. *J Mol Cell Cardiol* 33:599–613. doi:10.1006/jmcc.2000.1346
3. Belardinelli L, Shryock JC, Fraser H (2006) Inhibition of the late sodium current as a potential cardioprotective principle: effects of the late sodium current inhibitor ranolazine. *Heart* 92(Suppl 4):iv6–iv14. doi:10.1136/hrt.2005.078790
4. Bennett PB, Yazawa K, Makita N, George AL Jr (1995) Molecular mechanism for an inherited cardiac arrhythmia. *Nature* 376:683–685. doi:10.1038/376683a0
5. Crotti L, Celano G, Dagradi F, Schwartz PJ (2008) Congenital long QT syndrome. *Orphanet J Rare Dis* 3:18. doi:10.1186/1750-1172-3-18
6. Davis RP, Casini S, van den Berg CW, Hoekstra M, Remme CA, Dambrot C, Salvatori D, Oostwaard DW, Wilde AA, Bezzina CR, Verkerk AO, Freund C, Mummery CL (2012) Cardiomyocytes derived from pluripotent stem cells recapitulate electrophysiological characteristics of an overlap syndrome of cardiac sodium channel disease. *Circulation* 125:3079–3091. doi:10.1161/CIRCULATIONAHA.111.066092
7. Dumaine R, Wang Q, Keating MT, Hartmann HA, Schwartz PJ, Brown AM, Kirsch GE (1996) Multiple mechanisms of Na^+ channel-linked long-QT syndrome. *Circ Res* 78:916–924

8. Fabritz L, Kirchhof P, Franz MR, Nuyens D, Rossenbacker T, Ottenhof A, Haverkamp W, Breithardt G, Carmeliet E, Carmeliet P (2003) Effect of pacing and mexiletine on dispersion of repolarisation and arrhythmias in DeltaKPQ SCN5A (long QT3) mice. *Cardiovasc Res* 57:1085–1093
9. Fatima A, Kaifeng S, Dittmann S, Xu G, Gupta MK, Linke M, Zechner U, Nguemo F, Milting H, Farr M, Hescheler J, Saric T (2013) The disease-specific phenotype in cardiomyocytes derived from induced pluripotent stem cells of two long QT syndrome type 3 patients. *PLoS One* 8:e83005. doi:[10.1371/journal.pone.0083005](https://doi.org/10.1371/journal.pone.0083005)
10. Frank S, Zhang M, Scholer HR, Greber B (2012) Small molecule-assisted, line-independent maintenance of human pluripotent stem cells in defined conditions. *PLoS One* 7:e41958. doi:[10.1371/journal.pone.0041958](https://doi.org/10.1371/journal.pone.0041958)
11. Greber B, Coulon P, Zhang M, Moritz S, Frank S, Muller-Molina AJ, Arauzo-Bravo MJ, Han DW, Pape HC, Scholer HR (2011) FGF signalling inhibits neural induction in human embryonic stem cells. *EMBO J* 30:4874–4884. doi:[10.1038/emboj.2011.407](https://doi.org/10.1038/emboj.2011.407)
12. Hedley PL, Jorgensen P, Schlamowitz S, Wangari R, Moolman-Smook J, Brink PA, Kanters JK, Corfield VA, Christiansen M (2009) The genetic basis of long QT and short QT syndromes: a mutation update. *Hum Mutat* 30:1486–1511. doi:[10.1002/humu.21106](https://doi.org/10.1002/humu.21106)
13. Huangfu D, Maehr R, Guo W, Eijkelenboom A, Snitow M, Chen AE, Melton DA (2008) Induction of pluripotent stem cells by defined factors is greatly improved by small-molecule compounds. *Nat Biotechnol* 26:795–797. doi:[10.1038/nbt1418](https://doi.org/10.1038/nbt1418)
14. Itzhaki I, Maizels L, Huber I, Zwi-Dantsis L, Caspi O, Winterstern A, Feldman O, Gepstein A, Arbel G, Hammerman H, Boulos M, Gepstein L (2011) Modelling the long QT syndrome with induced pluripotent stem cells. *Nature* 471:225–229. doi:[10.1038/nature09747](https://doi.org/10.1038/nature09747)
15. Ma D, Wei H, Zhao Y, Lu J, Li G, Sahib NB, Tan TH, Wong KY, Shim W, Wong P, Cook SA, Liew R (2013) Modeling type 3 long QT syndrome with cardiomyocytes derived from patient-specific induced pluripotent stem cells. *Int J Cardiol* 168:5277–5286. doi:[10.1016/j.ijcard.2013.08.015](https://doi.org/10.1016/j.ijcard.2013.08.015)
16. Malan D, Friedrichs S, Fleischmann BK, Sasse P (2011) Cardiomyocytes obtained from induced pluripotent stem cells with long-QT syndrome 3 recapitulate typical disease-specific features in vitro. *Circ Res* 109:841–847. doi:[10.1161/CIRCRESAHA.111.243139](https://doi.org/10.1161/CIRCRESAHA.111.243139)
17. Mummery C, Ward-van Oostwaard D, Doevendans P, Spijker R, van den Brink S, Hassink R, van der Heyden M, Ophof T, Pera M, de la Riviere AB, Passier R, Tertoolen L (2003) Differentiation of human embryonic stem cells to cardiomyocytes: role of coculture with visceral endoderm-like cells. *Circulation* 107:2733–2740. doi:[10.1161/01.CIR.0000068356.38592.6801](https://doi.org/10.1161/01.CIR.0000068356.38592.6801)
18. Napolitano C, Rivolta I, Priori SG (2003) Cardiac sodium channel diseases. *Clin Chem Lab Med* 41:439–444. doi:[10.1515/CCLM.2003.066](https://doi.org/10.1515/CCLM.2003.066)
19. Ruan Y, Liu N, Bloise R, Napolitano C, Priori SG (2007) Gating properties of SCN5A mutations and the response to mexiletine in long-QT syndrome type 3 patients. *Circulation* 116:1137–1144. doi:[10.1161/CIRCULATIONAHA.107.707877](https://doi.org/10.1161/CIRCULATIONAHA.107.707877)
20. Schwartz PJ, Ackerman MJ (2013) The long QT syndrome: a transatlantic clinical approach to diagnosis and therapy. *Eur Heart J* 34:3109–3116. doi:[10.1093/eurheartj/ehd089](https://doi.org/10.1093/eurheartj/ehd089)
21. Schwartz PJ, Crotti L, Insolia R (2012) Long-QT syndrome: from genetics to management. *Circ Arrhythm Electrophysiol* 5:868–877. doi:[10.1161/CIRCEP.111.962019](https://doi.org/10.1161/CIRCEP.111.962019)
22. Schwartz PJ, Priori SG, Locati EH, Napolitano C, Cantu F, Towbin JA, Keating MT, Hammoude H, Brown AM, Chen LS (1995) Long QT syndrome patients with mutations of the SCN5A and HERG genes have differential responses to Na⁺ channel blockade and to increases in heart rate. Implications for gene-specific therapy. *Circulation* 92:3381–3386
23. Schwartz PJ, Priori SG, Spazzolini C, Moss AJ, Vincent GM, Napolitano C, Denjoy I, Guicheney P, Breithardt G, Keating MT, Towbin JA, Beggs AH, Brink P, Wilde AA, Toivonen L, Zareba W, Robinson JL, Timothy KW, Corfield V, Wattanasirichaigoon D, Corbett C, Haverkamp W, Schulze-Bahr E, Lehmann MH, Schwartz K, Coumel P, Bloise R (2001) Genotype-phenotype correlation in the long-QT syndrome: gene-specific triggers for life-threatening arrhythmias. *Circulation* 103:89–95
24. Schwartz PJ, Spazzolini C, Crotti L, Bathen J, Amlie JP, Timothy K, Shkolnikova M, Berul CI, Bitner-Grindzicz M, Toivonen L, Horie M, Schulze-Bahr E, Denjoy I (2006) The Jervell and Lange-Nielsen syndrome: natural history, molecular basis, and clinical outcome. *Circulation* 113:783–790. doi:[10.1161/CIRCULATIONAHA.105.592899](https://doi.org/10.1161/CIRCULATIONAHA.105.592899)
25. Segal MM, Douglas AF (1997) Late sodium channel openings underlying epileptiform activity are preferentially diminished by the anticonvulsant phenytoin. *J Neurophysiol* 77:3021–3034
26. Shimizu W, Antzelevitch C (1997) Sodium channel block with mexiletine is effective in reducing dispersion of repolarization and preventing torsade des pointes in LQT2 and LQT3 models of the long-QT syndrome. *Circulation* 96:2038–2047
27. Splawski I, Shen J, Timothy KW, Lehmann MH, Priori S, Robinson JL, Moss AJ, Schwartz PJ, Towbin JA, Vincent GM, Keating MT (2000) Spectrum of mutations in long-QT syndrome genes. KVLQT1, HERG, SCN5A, KCNE1, and KCNE2. *Circulation* 102:1178–1185
28. Takahashi K, Tanabe K, Ohnuki M, Narita M, Ichisaka T, Tomoda K, Yamanaka S (2007) Induction of pluripotent stem cells from adult human fibroblasts by defined factors. *Cell* 131:861–872. doi:[10.1016/j.cell.2007.11.019](https://doi.org/10.1016/j.cell.2007.11.019)
29. Terrenoire C, Wang K, Tung KW, Chung WK, Pass RH, Lu JT, Jean JC, Omari A, Sampson KJ, Kotton DN, Keller G, Kass RS (2013) Induced pluripotent stem cells used to reveal drug actions in a long QT syndrome family with complex genetics. *J Gen Physiol* 141:61–72. doi:[10.1085/jgp.201210899](https://doi.org/10.1085/jgp.201210899)
30. Wang DW, Yazawa K, George AL Jr, Bennett PB (1996) Characterization of human cardiac Na⁺ channel mutations in the congenital long QT syndrome. *Proc Natl Acad Sci USA* 93:13200–13205
31. Wang Q, Shen J, Li Z, Timothy K, Vincent GM, Priori SG, Schwartz PJ, Keating MT (1995) Cardiac sodium channel mutations in patients with long QT syndrome, an inherited cardiac arrhythmia. *Hum Mol Genet* 4:1603–1607
32. Zhang M, D'Aniello C, Verkerk AO, Wrobel E, Frank S, Ward-van Oostwaard D, Piccini I, Freund C, Rao J, Seeböhm G, Atsma DE, Schulze-Bahr E, Mummery CL, Greber B, Bellin M (2014) Recessive cardiac phenotypes in induced pluripotent stem cell models of Jervell and Lange-Nielsen syndrome: disease mechanisms and pharmacological rescue. *Proc Natl Acad Sci USA*. doi:[10.1073/pnas.1419553111](https://doi.org/10.1073/pnas.1419553111)
33. Zhang M, Schulte JS, Heinick A, Piccini I, Rao J, Quaranta R, Zeuschner D, Malan D, Kim KP, Ropke A, Sasse P, Arauzo-Bravo M, Seeböhm G, Scholer H, Fabritz L, Kirchhof P, Müller FU, Greber B (2015) Universal cardiac induction of human pluripotent stem cells in two and three-dimensional formats: implications for in vitro maturation. *Stem Cells* 33:1456–1469. doi:[10.1002/stem.1964](https://doi.org/10.1002/stem.1964)
34. Zumhagen S, Grace AA, O'Connor S, Loher A, Kobe J, Eckardt L, Schulze-Bahr E (2012) Totally subcutaneous implantable cardioverter defibrillator with an alternative, right parasternal, electrode placement. *Pacing Clin Electrophysiol* 35:e254–e257. doi:[10.1111/j.1540-8159.2011.03043.x](https://doi.org/10.1111/j.1540-8159.2011.03043.x)

3.3 Future perspective using optogenetic tools within stem cell derived cardiomyocytes:

3.3.1 Optogenetic Stimulation of Gi Signaling Enables Instantaneous Modulation of Cardiomyocyte Pacemaking. Frontiers in Physiology DOI: 10.3389/fphys.2021.768495 Nov. 2021 (IF:4.5)

Aim of the study

G protein-coupled receptors (GPCR) are the principal activators of critical intracellular signaling pathways that regulate many cardiac functions. Gs- and Gi-activated intracellular signaling pathways play a fundamental role in neurohormonal control of the circulatory system, heart rate regulation and contractility. The sympathetic nervous system through β -adrenergic receptors (β -ARs) signals via Gs, whereas the parasympathetic system through muscarinic receptors via Gi. A precise understanding of these signaling pathways is essential to understand disease mechanisms. For instance, both axes of the autonomous nerve system are affecting AF initiation and progression (Hanna et al., 2021) through sympathetic stimulation and Gs signaling that trigger atrial extra beats (Makowka et al., 2019) and by parasympathetic stimulation of muscarinic acetylcholine receptor 2 / G protein-coupled inwardly-rectifying potassium channels (GIRK) which shortens APs. GIRK channels are a type of potassium channel that are activated by beta-gamma subunits of Gi proteins. GIRK activation is a suggested trigger mechanism, and patients with sustained AF have constitutive GIRK activity in the atria, even in the absence of the receptor ligand (Dobrev et al., 2001). Investigations in a canine model of AF have shown that selective inhibition of Gai/o-mediated parasympathetic signaling nearly eliminated AF inducibility (Aistrup et al., 2011). Furthermore, the highly selective GIRK channel blocker, NTC-801, dose-dependently decreased AF inducibility and converted AF to normal sinus rhythm in a canine model of LA tachypacing (Yamamoto et al., 2014). However, drugs that affect the molecular mechanisms of AF cannot discern the areas of the atrium most sensitive to Gi signaling. Thus, from this data we could assume that local and selective inhibition of Gi signaling and GIRK channel function may be a novel therapeutic target for some patients with AF. To better analyze the local behavior of Gi signaling and the

influence on AF, we have established optogenetic stimulation of Gi signaling in cardiomyocytes using the Gi-coupled, long-wavelength-sensitive cone-opsin (LWO).

Optogenetics is a technique for controlling the behavior of cells with light after expressing light-sensitive proteins. The great advantage of optogenetic stimulation is the temporal and spatial accuracy: it is possible to locate the signal of a particular cell type or in specific subcellular regions within a complex cellular system with high specificity. Therefore, optogenetics has been used to investigate G-protein signaling pathways and also as a new tool for compound screening to enhance efficiency. Our group showed that opsin proteins like Jellyfish opsin can selectively activate Gs-protein signaling in cardiomyocytes and in the heart by specific blue light application, allowing localized and precisely timed Gs stimulation (Makowka et al., 2019). To extend the optogenetic toolbox for Gi signaling in cardiomyocytes in this study we used LWO, which was previously shown to activate Gi signaling by light in HeLa cells, neurons and mouse brains. Most importantly, this opsin has been shown in neurons to activate Gi/t over Go opsin with a specific 650nm wavelength, which is in the red spectrum and is thus not absorbed by myoglobin and hemoglobin. The red-light activation property could offer advantages in better tissue penetration and less phototoxic effects. Thus, this study aimed to characterize the effectiveness of the red light-stimulated Gi signaling pathways in cardiomyocytes from murine ES cells by LWO.

Methods and results:

To study the LWO-activated signaling pathways in cardiomyocytes, we generated mouse ES cell lines by electroporation with a plasmid consisting of the human long-wave opsin fused with eYFP under the control of a ubiquitous CAG promoter. Employing cardiomyocytes derived from ES cells offers a distinct advantage due to their expression of genes, which encompass genes specific to pacemaker functionality. Notably, prior studies have demonstrated that G protein signaling pathways under receptor regulation are already established in these cells. Consequently, this existing signaling landscape provides a conducive platform for exploring the expression of GIRK channels. The differentiation protocol was also modified to obtain more

atrial-like cells by adding Noggin and Dickkopf-related protein 1 to inhibit BMP signaling after mesoderm formation so to facilitate cardiac development and retinoic acid to improve atrial specification (Zhang et al., 2011).

LWO should specifically activate a Gi-mediated signaling pathway by red light illumination. To analyze the beating frequency, video microscopy with infrared light was used to avoid accidental LWO activation. Beating cardiomyocytes in embryoid bodies (EBs) illuminated with 625nm light showed an almost complete block in the basal frequency with high temporal precision. Moreover, repetitive light stimulations showed a long-lasting inhibitory effect (Fig 1, page 4, (Cokić et al., 2021)). Because Gi coupled receptors can be promiscuous as observed by the activation of Opn4 in heterologous expression system, or ES cell-derived cardiomyocytes where both Gi/o and Gq/11 signaling pathways can be activated, ES-derived cardiomyocyte model is ideal for discriminating between Gq and Gi signaling, as Gq will increase the beating rate through PLC/iP3/Ca²⁺ pathways, enhancing the Ca²⁺ clock pacemaker machinery. In contrast, the Gi will reduce the beating rate through either α subunits and PKA-dependent phosphorylation, or the $\beta\gamma$ subunits and GIRK channel activation. To prove that LWO could selectively activate the Gi signaling pathway, we incubated EBs with PTX (a known Gi/o blocker), which inhibits the light effect on frequency reduction. Importantly, we did not observe even the slightest increase in frequency by light in PTX-treated LWO EBs, excluding Gq activation (see Fig 2 a-b, page 5). Tertiapin-Q, a GIRK channel blocker, prevented LWO from instantaneously decreasing frequency by 75%. In the presence of tertiapin-Q we still observed a frequency reduction by light which was ~25% of controls. This remaining component is likely due to Gi-dependent inhibition of PKA activity, which has been shown to reduce If pacemaker currents and I_{Ca-L} currents (see Fig 2 c-d, page 5).

One of the advantages of LWO in comparison to pharmacological approaches is that no ligand must be applied and the repetitive application of light activates the receptor without desensitization. Comparing the light response with the response upon Carbachol (CCh) application, we observed that the mean time to maximal effect after LWO activation was around

30 times faster than CCh, and the mean recovery time to 50% of baseline after stimulation was about 100 times faster (see Fig 4, page 7). To further characterize the light properties of the opsin tool, we tested various calibrated light intensities to determine a high light sensitivity with half-maximal effective light intensity (ELi50) of 2.4 $\mu\text{W}/\text{mm}^2$ and a maximum effect at 100 $\mu\text{W}/\text{mm}^2$. Curve fitting of frequency decreased due to illumination with gradually extending exposure time but with fixed light intensity showed a half-maximal effective exposure time of 1.2 s and a maximal effect at 10s (see Fig 3, page 6). Thus, due to its light physical properties, LWO allows the application of brief continuous light pulses with fine modulation of stimulation intensities and periods, which would be almost impossible with a drug agonist perfusion and washout.

Conclusion

LWO is a suitable optogenetic tool to specifically activate Gi signaling in cardiomyocytes with red light. This red light activated opsin has higher temporal effectiveness in activating and deactivating the Gi intracellular signaling pathways than the classic pharmacological approach. This optogenetic tool, combined with other types of light-sensitive G-protein-coupled receptors, will allow for the future study of the interaction between sympathetic and parasympathetic stimulation, which is of fundamental importance for cardiac function.

Contribution: Designed the experiments, discussed data analysis and results, manuscript writing.



Optogenetic Stimulation of G_i Signaling Enables Instantaneous Modulation of Cardiomyocyte Pacemaking

Milan Cokić¹, Tobias Bruegmann^{1,2†}, Philipp Sasse^{1*} and Daniela Malan^{1*}

¹ Medical Faculty, Institute of Physiology I, University of Bonn, Bonn, Germany, ² Research Training Group 1873, University of Bonn, Bonn, Germany

OPEN ACCESS

Edited by:

T. Alexander Quinn,
Dalhousie University, Canada

Reviewed by:

Matthew W. Kay,
George Washington University,
United States
Matteo Elia Mangoni,
Centre National de la Recherche
Scientifique (CNRS), France

*Correspondence:

Daniela Malan
dmalan@uni-bonn.de
Philipp Sasse
philipp.sasse@uni-bonn.de
orcid.org/0000-0002-8502-9472

†Present address:

Tobias Bruegmann,
Institute for Cardiovascular Physiology,
University Medical Center Goettingen,
Goettingen, Germany

Specialty section:

This article was submitted to
Cardiac Electrophysiology,
a section of the journal
Frontiers in Physiology

Received: 31 August 2021

Accepted: 18 November 2021

Published: 20 December 2021

Citation:

Cokić M, Bruegmann T, Sasse P and
Malan D (2021) Optogenetic
Stimulation of G_i Signaling Enables
Instantaneous Modulation of
Cardiomyocyte Pacemaking.
Front. Physiol. 12:768495.
doi: 10.3389/fphys.2021.768495

G-protein signaling pathways are central in the regulation of cardiac function in physiological and pathophysiological conditions. Their functional analysis through optogenetic techniques with selective expression of opsin proteins and activation by specific wavelengths allows high spatial and temporal precision. Here, we present the application of long wavelength-sensitive cone opsin (LWO) in cardiomyocytes for activation of the G_i signaling pathway by red light. Murine embryonic stem (ES) cells expressing LWO were generated and differentiated into beating cardiomyocytes in embryoid bodies (EBs). Illumination with red light (625 nm) led to an instantaneous decrease up to complete inhibition (84–99% effectivity) of spontaneous beating, but had no effect on control EBs. By using increasing light intensities with 10 s pulses, we determined a half maximal effective light intensity of $2.4 \mu\text{W}/\text{mm}^2$ and a maximum effect at $100 \mu\text{W}/\text{mm}^2$. Pre-incubation of LWO EBs with pertussis toxin completely inhibited the light effect proving the specificity for G_i signaling. Frequency reduction was mainly due to the activation of GIRK channels because the specific channel blocker tertiapin reduced the light effect by ~80%. Compared with pharmacological stimulation of M_2 receptors with carbachol with slow kinetics (>30 s), illumination of LWO had an identical efficacy, but much faster kinetics (<1 s) in the activation and deactivation demonstrating the temporal advantage of optogenetic stimulation. Thus, LWO is an effective optogenetic tool for selective stimulation of the G_i signaling cascade in cardiomyocytes with red light, providing high temporal precision.

Keywords: optogenetics, cardiomyocyte, GPCR (G protein coupled receptor), G_i signaling pathway, GIRK channel, pacemaking

INTRODUCTION

G-Protein-coupled receptors (GPCR) play a pivotal role in regulating cardiac function. The counteracting effects of G_s and G_i proteins are fundamental for the heart rate regulation, contractility, neurohormonal control of circulatory system, and in pathophysiological conditions (Capote et al., 2015). As an antagonist of G_s -pathway, the G_i -pathway inhibits the adenylate cyclase, decreasing intracellular cAMP level, diminishing protein kinase A (PKA) activity, and thus, reducing L-type Ca^{2+} currents. In atrial myocytes and cells of the sinus node and AV node, acetylcholine opens a type of inwardly rectifying potassium channel ($I_{K, \text{ACh}}$ /GIRK) through direct

effects of the G_i $\beta\gamma$ subunit (Krapivinsky et al., 1995; Ivanova-Nikolova et al., 1998). This results in hyperpolarization, slowing of heart rate, prolongation of AV-node conduction, and shortening of the action potential duration in atrial cardiomyocytes (Belardinelli and Isenberg, 1983). Some G_i coupled receptors, such as adenosine-A1, are cardioprotective (Hutchinson and Scammells, 2004) and reduce the risk of cardiac arrhythmia, moreover G_i -coupled α_2 receptors exert an important sympatho-inhibitory function (Xiang and Kobilka, 2003).

Optogenetics is a photostimulation technique which selectively activates opsin proteins by specific wavelengths and the use of light has a much higher spatial and temporal precision than application and diffusion of receptor agonists (Beiert et al., 2014; Guru et al., 2015; Makowka et al., 2019). For instance, the blue light-sensitive receptor Jellyfish Opsin has been used for selective activation of G_s signaling cascade in cardiomyocytes and the heart with high spatial and temporal precision (Makowka et al., 2019), but direct control of the $G_{i/o}$ signaling cascade in cardiomyocytes with light has not been shown yet.

Short- and long-wavelength-sensitive opsins (LWO) have been used before for control of neuronal $G_{i/o}$ signaling pathways (Masseck et al., 2014) and LWO has been shown to activate rather $G_{i/t}$ than G_o signaling (Ballister et al., 2018). Thus, the aim of this study was to use the red light-activated LWO to stimulate G_i signaling pathways in cardiomyocytes.

METHODS

Vector Construction and Transfection of Embryonic Stem (ES) Cells

An LWO-enhanced yellow fluorescent protein (eYFP) plasmid was generated for the expression of LWO (human long-wavelength-sensitive opsin 1, NP_064445.1) c-terminally fused with eYFP using codon optimized synthesized DNA (GeneArt, Life Technologies, Germany) excised with SpeI and MluI and subcloned into a backbone vector with the chicken β -actin promoter (CAG) described before (Beiert et al., 2014). In this study, 40 μ g of DNA was linearized with Bgl II and electroporated into 4×10^6 mouse embryonic stem (ES) cells (D3 line) with a single electrical pulse (250 V, 750 μ F, 0.4 cm electrode gap, BioRad Gene Pulser, CA, USA). The electroporated cells were plated and 400 μ g/ml neomycin was added for selection 24 h after transfection. The eYFP positive clones were picked and cultured separately. Two positive clones were chosen, because of their specific eYFP expression in cardiomyocytes and stable light reaction. As a control group, we used the D3 ES cells with stable expression of the enhanced green fluorescent protein (eGFP) under the control of the CAG promoter as reported before (Beiert et al., 2014).

ES Cell Culture and Differentiation

Embryonic stem cells were cultured and differentiated within embryoid bodies (EBs) using the hanging drop method as previously described (Bruegmann et al., 2010; Beiert et al., 2014). For differentiation, we used Iscove's Modified Eagle's Medium (Invitrogen, MA, USA) supplemented with 20% fetal calf serum

(FCS) (Pan-Biotech, Germany), 0.1 mM non-essential amino acids (Invitrogen), 100 U/ml penicillin (Invitrogen), 100 mg/ml streptomycin (Invitrogen), and 0.1 mmol/L β -mercaptoethanol (Sigma Aldrich, MO, USA). At day 5 of differentiation, EBs were either plated on 0.1% gelatin-coated glass cover slips for the analysis of beating frequency conducted at day 9–14 or fixated for immunohistochemical analysis. In some differentiations, the method was modified by adding Noggin (R&D System, MN, USA, 250 ng/ml) from day 4 to 6 and retinoic acid (Sigma Aldrich, 1 μ M) from day 6 to 8 and Dickkopf-related protein 1 (R&D system, 200 ng/ml) from day 6 to 11.

Immunofluorescence

Embryoid bodies were fixed with 4% paraformaldehyde (Sigma Aldrich) and permeabilized with 0.2% of Triton X-100 (Sigma Aldrich) for 20 min, blocked with 5% of donkey serum (Jackson ImmunoResearch, UK) for 20 min and stained for 2 h at room temperature with primary antibody against α -actinin (1:400, Sigma Aldrich). Alexa Fluor 647 conjugated secondary antibody (1:400, Invitrogen) diluted in 1 μ g/ml Hoechst 33342 (Sigma Aldrich) was applied for 1 h at room temperature. The pictures were taken with an Eclipse Ti2 microscope with NIS-Elements and deconvolution software (Nikon, Japan).

Frequency Analysis and Light Stimulation of EBs

Beating EBs that showed eYFP expression in beating areas were used at day 9–14 of differentiation. Then, 1–2 h before experiment, the medium was replaced with Tyrode external solution (in mM: 142 NaCl, 5.4 KCl, 1.8 CaCl_2 , 2 MgCl_2 , 10 glucose, and 10 HEPES; pH 7.4) containing 11-cis retinal (1 μ M, Santa Cruz Biotechnology, TX, USA) or 9-cis retinal (1 μ M, Sigma Aldrich). Video microscopy of beating EBs was performed while perfusing EBs with Tyrode solution without retinal at $\sim 35^\circ\text{C}$ on an Axiovert 200 microscope with a $5\times$ objective (Fluar, NA 0.25, Zeiss, Germany) using infrared light (760 nm, 1.8 $\mu\text{W}/\text{mm}^2$ at the focal plane) to avoid accidental LWO activation. Spontaneous contraction was recorded with a charge-coupled device (CCD) camera (piA640-210gm, Basler, Germany) at 51 fps and analyzed online using custom designed software (LabView, National Instruments, TX, USA) as described before (Bruegmann et al., 2010; Makowka et al., 2019). Optogenetic stimulation was performed with a 625 nm LED within the LedHUB (Omicron Laserage, Germany) equipped with a 10% neutral density filter and coupled to the objective with an optical fiber and a 660 nm dichroic filter (AHF Analysentechnik, Germany). Illumination was controlled by a recording system (PowerLab 4/35 and Labchart software, AD Instruments, Sydney, Australia), which was also used to record time points of individual beats to calculate the frequency. Light intensity was calibrated at the objective with a power meter (PM100 power meter, S130A sensor, Thorlabs, NJ, USA) before each experiment.

Analysis of LWO Effect and Light Sensitivity

For statistical analysis, only stable beating EBs without arrhythmical episodes over 5 min before illumination were included. The average frequency during 10 s continuous

illumination was analyzed and normalized to baseline 10 s before. To describe the effectivity of LWO, we calculated the blocking effect with 100% as complete block and 0% as no effect on beating frequency. To determine light sensitivity, the light intensity of individual light pulses was gradually increased (in $\mu\text{W}/\text{mm}^2$: 0.3; 1; 3; 10; 30; 100; and 300). In addition, 100 $\mu\text{W}/\text{mm}^2$ individual light pulses of increasing durations (0.1; 0.3; 0.5; 1; 3; 5; 10; and 30 s) were applied and the frequency was averaged 5 s after onset of illumination compared with 5 s before. Half maximal effects were analyzed by fitting the normalized frequency with a Hill function with upper level set to 100% (GraphPad Prism, CA, USA).

Pharmacology

To compare LWO effect with pharmacological activation, we used supramaximal illumination (100 $\mu\text{W}/\text{mm}^2$, 10 s) and stimulation of the muscarinic acetylcholine receptor with carbachol (60 s, 100 μM , Sigma Aldrich). Effectiveness of the inhibition was calculated 5 s after the lowest frequency (to account for variations in perfusion kinetics) compared with 5 s before illumination/perfusion. The delay to maximum block was calculated between onset of illumination/perfusion and maximal effect and the delay to 50% recovery as end of stimulation/perfusion until frequency reached 50% of initial baseline. To block G_i proteins, pertussis-toxin (PTX, Invitrogen) was applied for 24 h in IMDM medium without FCS at a final concentration of 0.5 $\mu\text{g}/\text{ml}$. The blocker of G protein-coupled inwardly-rectifying potassium channels (GIRK) tertiapin-q (100 nM, Tocris, Bristol, UK) was incubated for 30 min after one initial measurement and kept in the solution for the second measurement (Figure 2C).

Statistics

Data are shown as mean \pm SEM and GraphPad Prism 7.0 was used to perform the statistical analysis. For frequency experiments in Figures 1D,E one-way ANOVA with Tukey's multiple comparison test was used. Pertussis toxin (PTX) effect (Figure 2B) was analyzed with an unpaired Student's *t*-test. For the other experiments (Figures 1G, 2D, 4B–D), two-sided paired Student's *t*-tests were used. A *p*-value < 0.05 was considered statistically significant. The *n* values indicate the number of independent experiments (EBs).

RESULTS

Red Light Activation of LWO Decreases Beating Frequency of Cardiomyocytes

The human LWO in fusion with eYFP was stably expressed under the control of the CAG promoter in ES-cells (D3 line) (Figure 1A). For differentiation of ES cells into spontaneously beating cardiomyocytes, EBs were generated with the hanging drop method (Wobus et al., 1991; Maltsev et al., 1993; Beiert et al., 2014). Spontaneously beating areas in the EBs showed differentiation into α -actinin and eYFP positive cardiomyocytes indicating LWO expression (Figure 1B). An analysis of beating frequency was performed by infra-red video microscopy to avoid LWO activation. Illumination of beating areas with red

light pulses ($\lambda = 625 \text{ nm}$, 10 s, 100 $\mu\text{W}/\text{mm}^2$) led to an almost complete block of spontaneous beating in EBs from two separately differentiated ES cell clones (Figures 1C,D; clones C1 and C2). In contrast, illumination of EBs expressing only eGFP but not LWO did not reduce beating frequency (Figures 1C,D; Ctr). Importantly, the baseline beating frequency was similar between EBs from the two LWO clones and the control eGFP clone, suggesting that LWO expression does not negatively affect pacemaking and shows no dark activity (Figure 1E). Application of two identical light pulses with 90 s delay showed similar effectivity of beating block (Figures 1E,G) indicating that LWO can be activated repetitively without desensitization.

LWO Activates G_i -Proteins and GIRK Channels in Cardiomyocytes

To confirm the LWO specificity for G_i activation, EBs were pre-treated with PTX (0.5 $\mu\text{g}/\text{ml}$) for 24 h to block all $G_{i/o}$ proteins. Subsequent frequency measurements showed that PTX almost completely inhibited the light effect (Figures 2A,B) and the blocking effectivity was only 4% in contrast to an effectivity of 88% in non-treated EBs recorded in parallel. Because activation of GIRK channels by G_i -protein $\beta\gamma$ subunits is the main mechanism for slowing the heart rate (Huang et al., 1995; Nobles et al., 2018), we compared light effects before and after application of the GIRK channel blocker tertiapin (100 nM, 30 min, Figure 2C, blue color) and found that tertiapin reduced the light effect significantly from 91 to 21% blocking effectivity (Figure 2D).

Dose-Response Relationship Shows High Light Sensitivity of LWO

To determine LWO light sensitivity, we repetitively applied light with increasing light energy by using ascending light intensities or durations (Figure 3). Application of 10 s long pulses with stepwise increasing light intensities from 0.3 to 300 $\mu\text{W}/\text{mm}^2$ led to a gradual decrease of beating frequency after each light pulse (Figure 3A) with a sigmoidal dependency of the blocking effect on the logarithm of intensity (averaged data in Figure 3C). The data points of each individual experiment were fitted with the Hill equation resulting in an average half maximal effective light intensity (ELi50) of $2.4 \pm 0.7 \mu\text{W}/\text{mm}^2$ ($n = 9$) and a maximum blocking effect at $\sim 100 \mu\text{W}/\text{mm}^2$. Similarly, application of light pulses of 100 $\mu\text{W}/\text{mm}^2$ with increasing durations from 0.1 to 30 s led to gradual block of beating after each pulse (Figure 3B). The statistical analysis and Hill-fitting of individual experiments showed a sigmoidal dependence of blocking effect on logarithm of pulse duration with a half maximal effect at $1.2 \pm 0.4 \text{ s}$ ($n = 6$) and maximal effect at $\sim 10 \text{ s}$ (averaged data in Figure 3D). To compare both gradual stimulation protocols, we calculated and overlaid the total light energy in each light pulse as $\text{s} \cdot \mu\text{W}/\text{mm}^2$ (Figure 3E). Surprisingly, we found that the light intensity protocol seemed to be more effective than the pulse duration protocol (as shown in discussion).

To determine if light sensitivity and blocking efficiency is constant, we applied two brief (0.5 s) subthreshold pulses at 100 $\mu\text{W}/\text{mm}^2$ with only 20 s in-between. Because the blocking effect

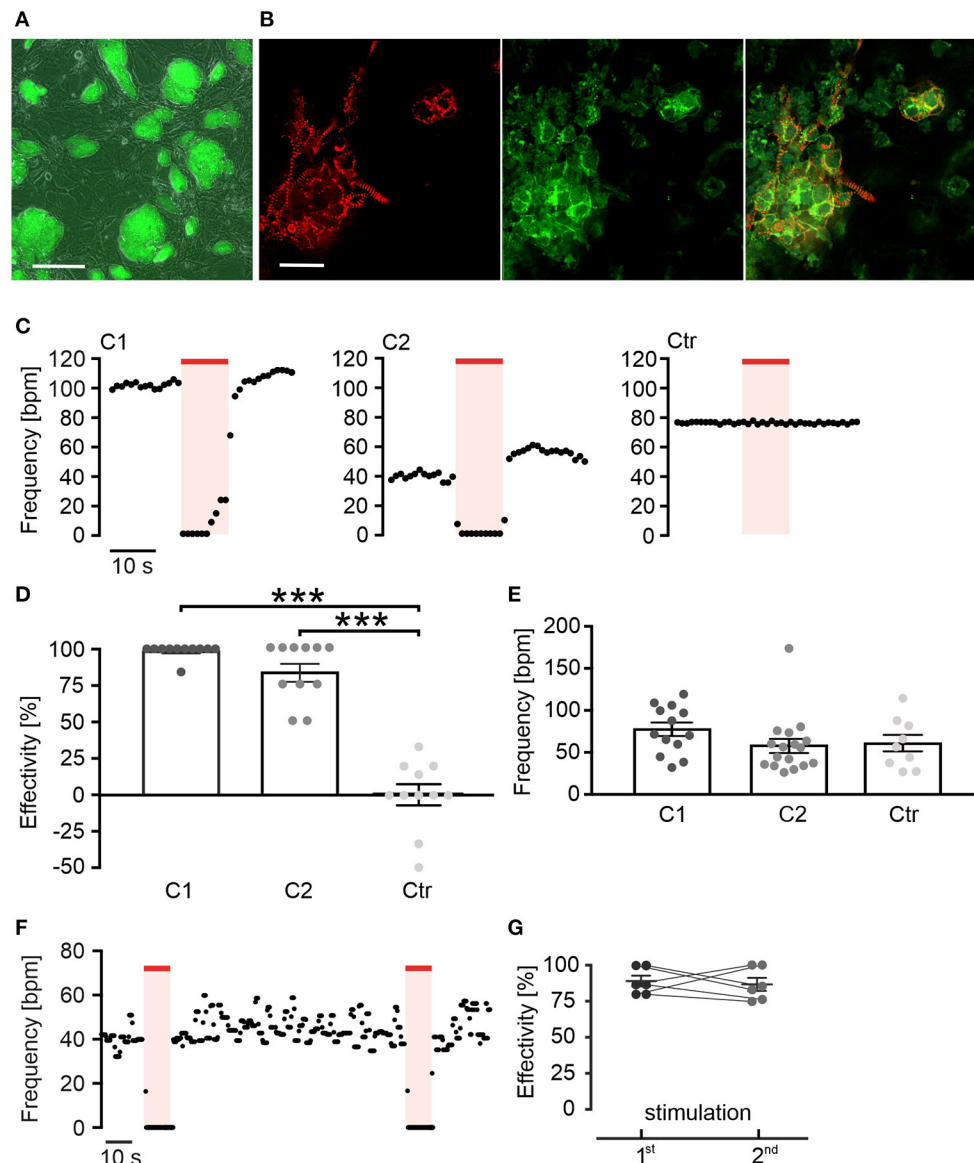


FIGURE 1 | Red light activation of long wavelength-sensitive cone opsin (LWO) decreases beating frequency of cardiomyocytes. **(A)** Embryonic stem (ES) cell colonies with LWO expression indicated by eYFP fluorescence (green, bar = 200 μm). **(B)** EYFP fluorescence (green) in α -actinin (red) positive cardiomyocytes differentiated within an embryoid body (EB), generated from LWO ES cells (bar = 25 μm). **(C)** Representative frequency traces of spontaneous beating within two EBs differentiated from ES cell LWO clones (C1 and C2) and one EB from eGFP control ES cells (Ctr) stimulated with light (625 nm, 100 μ W/mm², red line). **(D)** Effectivity of inhibition (100% = complete block of spontaneous beating) by illumination [ANOVA Tukey's multiple comparison test: *** p < 0.001 (C1, C2, n = 11) vs. control (n = 11)]. **(E)** Statistical comparison of spontaneous beating frequency of EBs from two LWO clones and the wild-type ES cells [ANOVA Tukey's multiple comparison test, p = 0.98 (C2, n = 17) p = 0.46 (C1, n = 13) vs. control (n = 9)]. **(F)** Representative frequency trace of two supramaximal (10 s, 100 μ W/mm²) repetitive light stimuli. **(G)** Comparison of frequency reduction effectivity of the first and the second light pulse (two side paired t -test: p = 0.73, n = 6).

of the second light pulse was not different (Figures 3F,G, n = 5, p = 0.46), we conclude that light sensitivity was similar and the submaximal blocking effect was not compromised by LWO refractoriness at this pulse interval.

LWO Illumination Has Much Higher Temporal Precision Than Agonist Perfusion

To illustrate the temporal precision of LWO and the advantage over agonist perfusion, we compared the

LWO effect with pharmacological stimulation of the G_i pathway (Figure 4A) by illumination (LWO, 625 nm) and perfusion of EBs with the acetylcholine-receptor agonist carbachol (CCh, 100 μ M). Both stimulations led to similar blocking effectivity (Figure 4B, LWO $78.6 \pm 8.5\%$, n = 7, CCh $72.6 \pm 13.2\%$, n = 7), however, activation kinetics (delay to maximum block, Figure 4C: LWO 0.8 ± 0.1 s, n = 7; CCh 33.4 ± 7.8 s, n = 7) and deactivation kinetics (time from end of stimulation to 50% recovery, Figure 4D, LWO 0.8 ± 0.3 s, n = 7; CCh 99.6

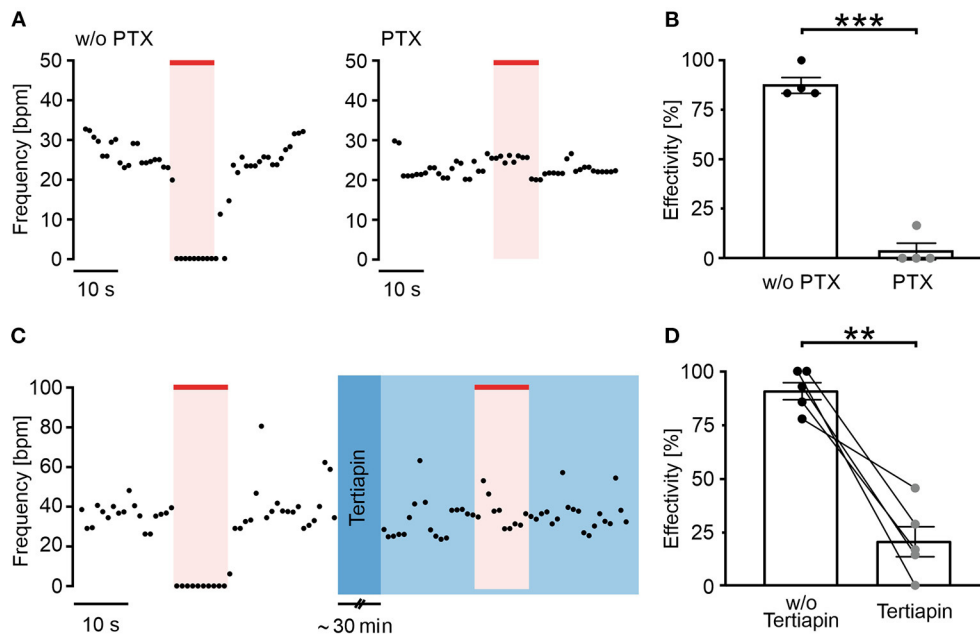


FIGURE 2 | Long wavelength-sensitive cone opsin acts through G_i proteins and GIRK channels. **(A)** Representative frequency traces of LWO-EBs without (w/o, left) and with pertussis toxin (PTX) (0.5 μ g/ml, 24 h, right) treatment with illumination (625 nm, 100 μ W/mm², red line). **(B)** Aggregated data of frequency reduction effectivity with and without PTX (unpaired t -test: *** $p < 0.001$, $n = 4$). **(C)** Representative frequency trace of an LWO-EB before (left) and after treatment with tertiapin (30 min incubation, right, blue) with illumination (625 nm, 100 μ W/mm², red line). **(D)** Statistical analysis of frequency reduction effectivity with or without tertiapin treatment (two side paired t -test: ** $p = 0.003$, $n = 5$).

± 21.9 s, $n = 7$) was significant and up to two orders of magnitude faster using LWO illumination compared with CCh perfusion.

DISCUSSION

Optogenetic methods have many advantages over pharmacological stimulation, because they allow modulation of G-protein signaling of specific cell types with high temporal and spatial precision using light instead of receptor ligands. The aim of this study was to explore the use of LWO for optogenetic activation of G_i -signaling in cardiomyocytes. For this purpose, we used stem-cell derived cardiomyocytes which resemble an early embryonic phenotype and show spontaneous beating in cell culture. Importantly, in these cells, the pacemaking mechanism is already well-controlled by G-protein signaling (Boheler et al., 2002; Touhara et al., 2016), such as G_q , G_s , and G_i proteins (Layden et al., 2010; Beiert et al., 2014; Makowka et al., 2019).

Rationale for Using LWO to Control G_i Signaling

To modulate G_i signaling in cardiomyocytes by light, we have chosen the LWO, which has been shown to activate $G_{i/o}$ proteins in HeLa cells (Karunaratne et al., 2013) as well as cultured neurons and the brain of mice (Masseck et al., 2014). Importantly, LWO is well-suited for the repetitive and long-lasting activation of G_i -dependent GIRK currents by light in HEK293 cells and neurons without desensitization (Masseck

et al., 2014). This is of great advantage over vertebrate Rhodopsin, which also activates G_i signaling but the responses decline during repetitive stimulation (Masseck et al., 2014). We have chosen LWO over short-wavelength opsin (activated by 350–450 nm) because LWO can be activated by red light >600 nm, which is not absorbed by myoglobin and hemoglobin, penetrates deeper into cardiac tissue (Bruegmann et al., 2016), and has less phototoxic effects. Furthermore, red light >600 nm is spectrally compatible with blue light-activated optogenetic tools, such as Channelrhodopsin-2 for optical depolarization of cardiomyocytes (Bruegmann et al., 2010) or Jellyfish Opsin for light-induced stimulation of the G_s signaling cascade (Makowka et al., 2019) which are both not activated by red light and therefore can be combined with LWO co-expression.

LWO Is G_i Specific in Cardiomyocytes and Activates GIRK Channels

It is known that GPCR can show a promiscuous behavior and thereby activate multiple, even counteracting signaling pathways. For instance, Melanopsin, a photoreceptor of intrinsically photosensitive retinal ganglion cells, has been initially described as a G_q coupled optogenetic GPCR (Qiu et al., 2005) but it was shown later that it can signal both to G_q and G_i proteins (Bailes and Lucas, 2013) and can thus activate GIRK channels by $G_i \beta\gamma$ subunits (Spoida et al., 2016). Our model of spontaneous beating ES-cell derived cardiomyocytes is ideal to discriminate between G_q and G_i signaling as the former will increase beating rate through PLC/IP₃/Ca²⁺

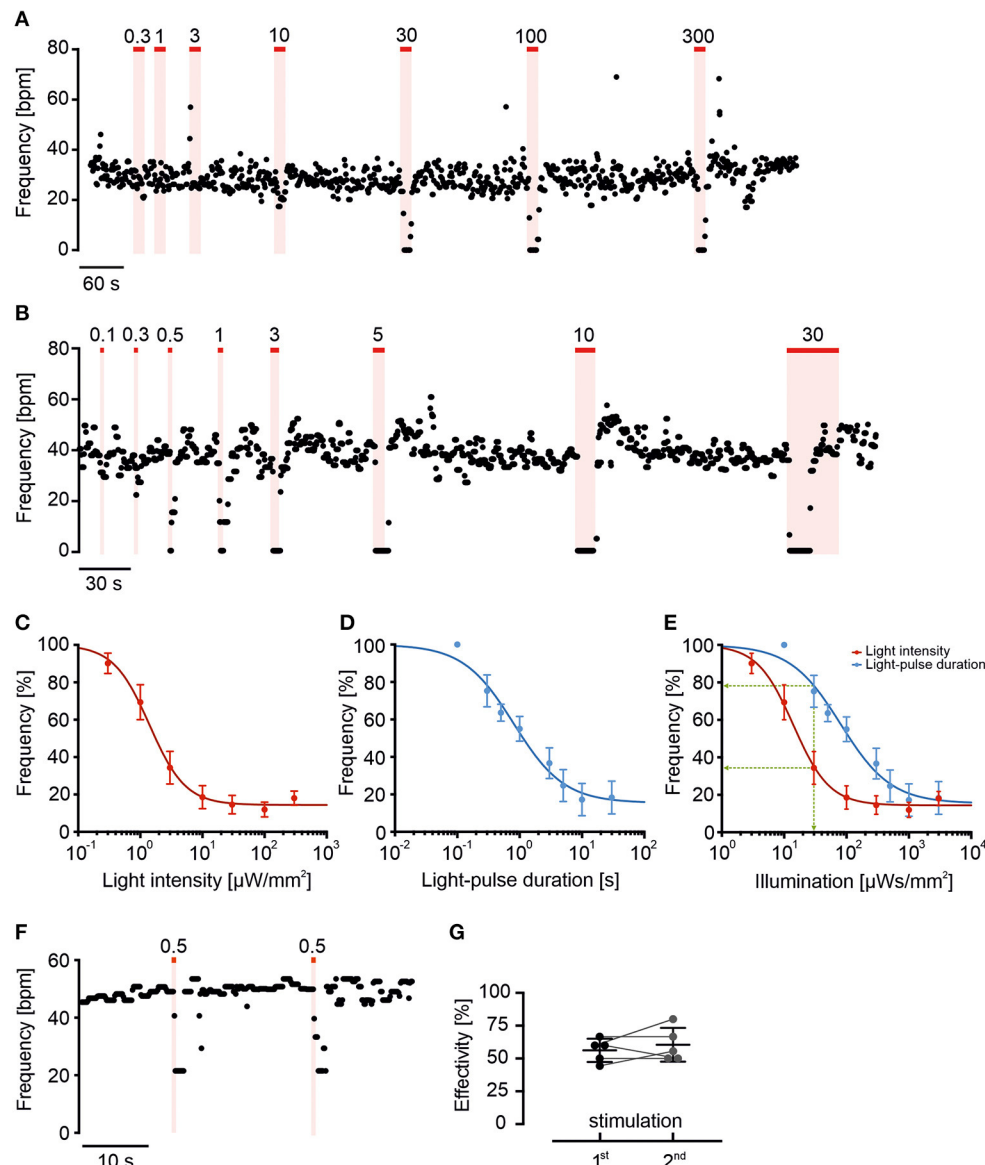


FIGURE 3 | Long wavelength-sensitive cone opsin response can be fine-tuned by light intensity and duration. **(A,B)** Representative frequency traces of LWO-EBs with light stimulation (625 nm, red line) with increasing light intensities **(A)**, 10 s light, indicated values in $\mu\text{W}/\text{mm}^2$ or different pulse durations **(B)**, 100 $\mu\text{W}/\text{mm}^2$, indicated pulse duration in s. **(C,D)** Relationship between change in normalized beating frequency and light intensity **[(C), $n = 9$]** or light pulse duration **[(D), $n = 6$]** on a logarithmic scale fitted with Hill equation. **(E)** Relationship between change in beating frequency and total light energy calculated as $\text{s} \cdot \mu\text{W}/\text{mm}^2$ from data in **(C)** (red) and **(D)** (blue). Note that the effect of 30 $\text{s} \cdot \mu\text{W}/\text{mm}^2$ light energy (green line) is stronger using 10 s at 3 $\mu\text{W}/\text{mm}^2$ (red) compared with 0.3 s at 100 $\mu\text{W}/\text{mm}^2$ (blue). **(F)** Representative frequency trace and **(G)** statistical analysis of two submaximal (0.5 s, 100 $\mu\text{W}/\text{mm}^2$) repetitive light stimuli (two side paired t -test: $p = 0.46$, $n = 5$).

release mechanisms enhancing the Ca^{2+} clock pacemaking machinery (Lakatta and DiFrancesco, 2009; Beiert et al., 2014), whereas the latter will reduce beating through G_i proteins (Lyashkov et al., 2009). As we have exclusively observed frequency reduction or even complete block of beating by LWO activation (**Figure 1D**), LWO signals through G_i proteins in cardiomyocytes. To confirm this, we blocked G_i proteins with PTX that completely abolished all light effects. Notably, we never observed a slightest frequency increase by light in PTX

treated LWO EBs (**Figure 2B**), therefore, excluding G_q activation by LWO.

Activated G_i proteins can reduce beating rate by two mechanisms: block of adenylate cyclases by $G_i \alpha$ subunits with subsequent lowering of PKA-dependent phosphorylation or activation of GIRK potassium channels by $G_i \beta\gamma$ subunits (Lyashkov et al., 2009). In our experiments, application of the specific GIRK channel inhibitor tertiapin did not affect basal beating rate but reduced the effect of LWO illumination by

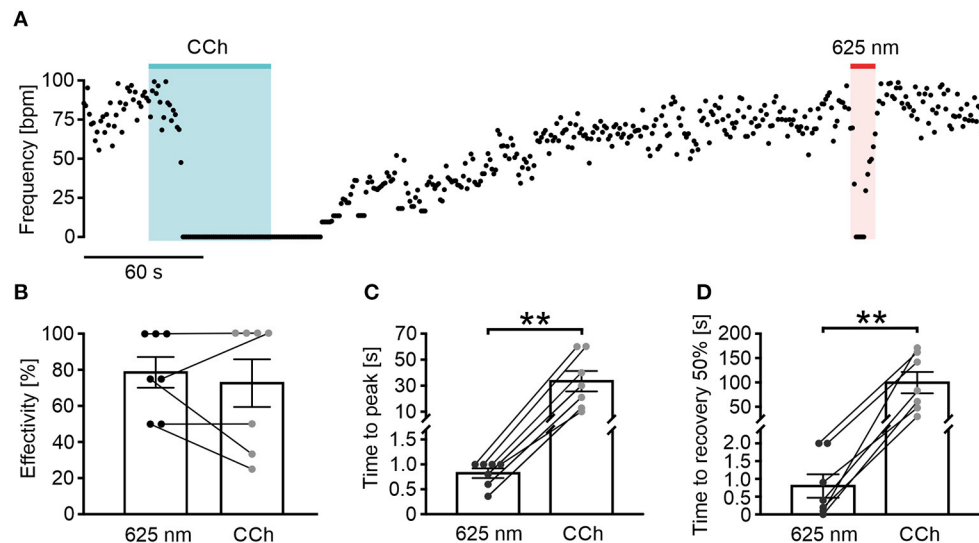


FIGURE 4 | Long wavelength-sensitive cone opsin has higher temporal precision than pharmacological G_i stimulation. **(A)** Representative frequency trace of an LWO-EB upon perfusion with carbachol (CCh, 100 μ M, 60 s, blue bar) and light stimulation (625 nm, 10 s, 100 μ W/mm², red line). **(B–D)** Statistical comparison between CCh and light application for frequency reduction effectivity **(B)**, paired t -test: $p = 0.49$, $n = 7$], time to maximal frequency reduction **(C)**, paired t -test: $p = 0.006$, $n = 7$], and time to 50% of beating frequency recovery **(D)**, paired t -test: $p = 0.0039$, $n = 7$].

~75% suggesting that the major G_i effect in ES-cell derived cardiomyocytes obtained by our differentiation protocol is through G_i $\beta\gamma$ GIRK channel activation. In contrast, GIRK-based reduction of heart rate in mouse sinus nodal cells is only responsible for ~50% of heart rate regulation (Mesirca et al., 2013) presumably reflecting the more robust pacemaking machinery in these cells or differences in GIRK expression. The remaining ~25% of regulation we observed is most likely due to G_i α -dependent reduction of basal adenylate cyclase and PKA activity, which has been shown to reduce HCN/ I_f currents (Abi-Gerges et al., 2000) and L-type- Ca^{2+} currents (Ji et al., 1999) in ES-cell derived cardiomyocytes.

LWO Overexpression Has No Negative Side-Effects

Overexpression of artificial light sensitive proteins might have negative side effects on the intracellular signaling machinery because of dark activity, G-protein binding, alteration of microdomain signaling, or other overexpression artifacts. In our experience, the spontaneous beating rate is a very sensitive parameter for such side effects. Similar to the expression of Melanopsin for optogenetic G_q stimulation (Beiert et al., 2014) and Jellyfish Opsin for optogenetic G_s stimulation (Makowka et al., 2019), we did not observe effects on basal beating rate by LWO expression. Since we did not analyze protein expression levels or performed RNA sequencing analysis in this work, we cannot fully exclude minor side effects. However, it must be admitted that the ES-cell system itself cannot exclude side effects for future *in vivo* applications and thus generation of *in vivo* models of LWO overexpression in the heart will be an important next step.

Fast Kinetics and Light Sensitivity of LWO

Parasympathetic stimulation of the intact heart can be very fast which has been shown for both electrical stimulation of the vagal nerve with ~1.5 s delay (Ng et al., 2001) and optogenetic stimulation of parasympathetic neurons (Moreno et al., 2019) with an immediate reduction of heart rate. In contrast, diffusion-limited pharmacological activation of M2-cholinergic receptors with CCh in the three-dimensional cardiac body *in vitro* resulted in slow activation (~30 s) and deactivation (~100 s). In this *in vitro* setting stimulation of LWO led to 30–100 times faster effects with delays of only 0.8 s from the start of illumination to maximal effect or from end of illumination to 50% of recovery, which is similar to the *in vivo* kinetics. Thereby LWO allows the application of brief continuous light pulses with gradually increasing stimulation intensities; such a stimulation protocol would be almost impossible with slow agonist perfusion and wash out, especially in multicellular preparation, such as EB or in intact organs.

We found that gradual stimulation allows fine tuning the response of G_i -stimulation on pacemaking activity by either changing pulse duration or light intensity with a sigmoidal dependence on the logarithm of light energy (duration * intensity in $s^*\mu$ W/mm²). Interestingly, the half-maximal light energy was slightly higher using variations of intensity (24 $s^*\mu$ W/mm²) than pulse duration (120 $s^*\mu$ W/mm²). Specifically, for a fixed total light energy at mid-sensitivity (e.g., 30 $s^*\mu$ W/mm² green line in Figure 3E), longer light pulses (10 s at 3 μ W/mm², light intensity protocol) are more effective than shorter light pulses (0.3 s at 100 μ W/mm², pulse duration protocol) indicating that temporal integration of G_i signaling is affecting the threshold blocking effect.

Compared with previous reported LWO sensitivity for GIRK activation in HEK293 cells ($4 \text{ s}^* \mu\text{W}/\text{mm}^2$, Eli50 at 590 nm: 0.2 s, $20 \mu\text{W}/\text{mm}^2$, Masseck et al., 2014), we observed lower LWO sensitivity ($14\text{--}80 \text{ s}^* \mu\text{W}/\text{mm}^2$ at 625 nm), which could be due to difference in the wavelength used.

The calculation of total light energy allows comparison with other optogenetic GPCR, we have employed to modulate pacemaking of ES-cell derived cardiomyocytes. Using Melanopsin to accelerate pacemaking by G_q/PLC/IP₃ signaling, we determined a half maximal energy of $2.4 \text{ s}^* \mu\text{W}/\text{mm}^2$ (Eli50 of $40 \text{ nW}/\text{mm}^2$ at 60 s pulses, Beiert et al., 2014) and using Jellyfish Opsin to stimulate G_s/cAMP/PKA signaling, we determined a half maximal energy of only $0.16 \text{ s}^* \mu\text{W}/\text{mm}^2$ (Eli50 of $8 \text{ nW}/\text{mm}^2$ at 20 s pulses Makowka et al., 2019). Thus, LWO is less light sensitive than Melanopsin and Jellyfish Opsin, which is also advantageous in experimental handling at normal lab room light. In addition, LWO kinetics on frequency reduction (time to peak and 50% deactivation $\sim 0.8 \text{ s}$) was much faster than kinetics of frequency increase by Melanopsin or Jellyfish Opsin in EBs (activation $\sim 10\text{--}50 \text{ s}$) which underscores the involvement of fast GIRK channels in G_i signaling.

Outlook

In the future, the combination of LWO with the spectrally compatible JellyOP in transgenic mice (Makowka et al., 2019) will allow spatially confined simultaneous or alternating activation of G_i and G_s signaling in cardiomyocytes in the heart *in vivo*. This will be a valid approach to study the impact of balanced, dysbalanced, and wrong timing of parasympathetic and sympathetic input which seems to be important for the development of pathologies, such as atrial fibrillation (Ang et al., 2012). The high temporal precision of light enables to study short-term (seconds) and mid-term (minutes and hours) effects and, using implantable light emitting devices, also long-term (days and weeks) chronic G_i and G_s signaling. Furthermore, selective illumination of left and right ventricle, or of epicardial and endocardial cardiomyocytes will allow to determine regional differences of vegetative nerve input on cardiac function, arrhythmia generation or development of cardiac hypertrophy. Finally, optogenetics has the advantage of cell type-specific expression using specific promoters. Thus, using the Cre-LoxP

system, expression of LWO or JellyOpsin in the different cells of the heart (cardiomyocytes, fibroblast, endothelial cells, and smooth muscle cells) will enable investigation of their G_i- and G_s-signaling *in vivo* which cannot be performed by agonists applied to the circulation or by electrical stimulation of vegetative nerves.

CONCLUSION

Long wavelength-sensitive cone opsin enables optogenetic stimulation of G_i-signaling cascade in ES-cell derived cardiomyocytes with red light, resulting in a high effective and very fast inhibition of spontaneous pacemaking, mainly through the activation of GIRK channels. Thus, LWO itself or in combination with the G_s coupled spectrally compatible optogenetic GPCR JellyOP will allow to investigate the physiological and pathological effects of balanced and dysbalanced vegetative nerve input on the heart.

DATA AVAILABILITY STATEMENT

The raw data supporting the conclusions of this article will be made available by the authors, without undue reservation.

AUTHOR CONTRIBUTIONS

MC, DM, TB, and PS designed the research. MC performed the research. MC, DM, and PS wrote the manuscript. All authors contributed to the article and approved the submitted version.

FUNDING

This work was supported by the Deutsche Forschungsgemeinschaft (DFG, German Research Foundation)—313904155/SA 1785/7-1, 380524518/SA1785/9-1, and 214362475/GRK1873/2.

ACKNOWLEDGMENTS

We thank Frank Holst for technical assistance.

REFERENCES

- Abi-Gerges, N., Ji, G. J., Lu, Z. J., Fischmeister, R., Hescheler, J., and Fleischmann, B. K. (2000). Functional expression and regulation of the hyperpolarization activated non-selective cation current in embryonic stem cell-derived cardiomyocytes. *J. Physiol.* 523, 377–389. doi: 10.1111/j.1469-7793.2000.t01-2-00377.x
- Ang, R., Opel, A., and Tinker, A. (2012). The role of inhibitory g proteins and regulators of G protein signaling in the *in vivo* control of heart rate and predisposition to cardiac arrhythmias. *Front. Physiol.* 3:96. doi: 10.3389/fphys.2012.00096
- Bailes, H. J., and Lucas, R. J. (2013). Human melanopsin forms a pigment maximally sensitive to blue light ($\lambda_{\text{max}} \approx 479 \text{ nm}$) supporting activation of Gq/11 and Gi/o signalling cascades. *Proc. R. Soc. B Biol. Sci.* 280:20122987. doi: 10.1098/rspb.2012.2987
- Ballister, E. R., Rodgers, J., Martial, F., and Lucas, R. J. (2018). A live cell assay of GPCR coupling allows identification of optogenetic tools for controlling Go and Gi signaling. *BMC Biol.* 16:10. doi: 10.1186/s12915-017-0475-2
- Beiert, T., Brueggemann, T., and Sasse, P. (2014). Optogenetic activation of Gq signalling modulates pacemaker activity of cardiomyocytes. *Cardiovasc. Res.* 102, 507–516. doi: 10.1093/cvr/cvu046
- Belardinelli, L., and Isenberg, G. (1983). Isolated atrial myocytes: adenosine and acetylcholine increase potassium conductance. *Am. J. Physiol.* 244, H734–H737. doi: 10.1152/ajpheart.1983.244.5.H734
- Boheler, K. R., Czyz, J., Tweedie, D., Yang, H. T., Anisimov, S. V., and Wobus, A. M. (2002). Differentiation of pluripotent embryonic stem cells into cardiomyocytes. *Circ. Res.* 91, 189–201. doi: 10.1161/01.RES.0000027865.61704.32
- Brueggemann, T., Boyle, P. M., Vogt, C. C., Karathanos, T. V., Arevalo, H. J., Fleischmann, B. K., et al. (2016). Optogenetic defibrillation terminates

- ventricular arrhythmia in mouse hearts and human simulations. *J. Clin. Invest.* 126, 3894–3904. doi: 10.1172/JCI88950
- Bruegmann, T., Malan, D., Hesse, M., Beiert, T., Fuegmann, C. J., Fleischmann, B. K., et al. (2010). Optogenetic control of heart muscle *in vitro* and *in vivo*. *Nat. Methods* 7, 897–900. doi: 10.1038/nmeth.1512
- Capote, L. A., Mendez Perez, R., and Lymporopoulos, A. (2015). GPCR signaling and cardiac function. *Eur. J. Pharmacol.* 763, 143–148. doi: 10.1016/j.ejphar.2015.05.019
- Guru, A., Post, R. J., Ho, Y.-Y., and Warden, M. R. (2015). Making sense of optogenetics. *Int. J. Neuropsychopharmacol.* 18:pyv079. doi: 10.1093/ijnp/pyv079
- Huang, C. L., Slesinger, P. A., Casey, P. J., Jan, Y. N., and Jan, L. Y. (1995). Evidence that direct binding of G beta gamma to the GIRK1 G protein-gated inwardly rectifying K⁺ channel is important for channel activation. *Neuron* 15, 1133–1143. doi: 10.1016/0896-6273(95)90101-9
- Hutchinson, S. A., and Scammells, P. J. (2004). A(1) adenosine receptor agonists: medicinal chemistry and therapeutic potential. *Curr. Pharm. Des.* 10, 2021–2039. doi: 10.2174/1381612043384204
- Ivanova-Nikolova, T. T., Nikolov, E. N., Hansen, C., and Robishaw, J. D. (1998). Muscarinic K⁺ channel in the heart. Modal regulation by G protein beta gamma subunits. *J. Gen. Physiol.* 112, 199–210. doi: 10.1085/jgp.112.2.199
- Ji, G., Fleischmann, B. K., Bloch, W., Feelisch, M., Andressen, C., Addicks, K., et al. (1999). Regulation of the L-type Ca²⁺ channel during cardiomyogenesis: switch from NO to adenylyl cyclase-mediated inhibition. *FASEB J.* 13, 313–324. doi: 10.1096/fasebj.13.2.313
- Karunarathne, W. K. A., Giri, L., Kalyanaraman, V., and Gautam, N. (2013). Optically triggering spatiotemporally confined GPCR activity in a cell and programming neurite initiation and extension. *Proc. Natl. Acad. Sci. U. S. A.* 110, E1565–E1574. doi: 10.1073/pnas.1220697110
- Krapivinsky, G., Krapivinsky, L., Wickman, K., and Clapham, D. E. (1995). G beta gamma binds directly to the G protein-gated K⁺ channel, IKACH. *J. Biol. Chem.* 270, 29059–29062. doi: 10.1074/jbc.270.49.29059
- Lakatta, E. G., and DiFrancesco, D. (2009). What keeps us ticking: a funny current, a calcium clock, or both? *J. Mol. Cell Cardiol.* 47, 157–170. doi: 10.1016/j.yjmcc.2009.03.022
- Layden, B. T., Newman, M., Chen, F., Fisher, A., and Lowe, W. L. (2010). G protein coupled receptors in embryonic stem cells: a role for Gs-alpha signaling. *PLoS ONE* 5:e9105. doi: 10.1371/journal.pone.0009105
- Lyashkov, A. E., Vinogradova, T. M., Zahanich, I., Li, Y., Younes, A., Nuss, H. B., et al. (2009). Cholinergic receptor signaling modulates spontaneous firing of sinoatrial nodal cells via integrated effects on PKA-dependent Ca(2+) cycling and I(KACH). *Am. J. Physiol. Heart Circ. Physiol.* 297, H949–H959. doi: 10.1152/ajpheart.01340.2008
- Makowka, P., Bruegmann, T., Dusend, V., Malan, D., Beiert, T., Hesse, M., et al. (2019). Optogenetic stimulation of Gs-signaling in the heart with high spatio-temporal precision. *Nat. Commun.* 10:1281. doi: 10.1038/s41467-019-09322-7
- Maltsev, V. A., Rohwedel, J., Hescheler, J., and Wobus, A. M. (1993). Embryonic stem cells differentiate *in vitro* into cardiomyocytes representing sinusnodal, atrial and ventricular cell types. *Mech. Dev.* 44, 41–50. doi: 10.1016/0925-4773(93)90015-P
- Masseck, O. A., Spoida, K., Dalkara, D., Maejima, T., Rubelowski, J. M., Wallhorn, L., et al. (2014). Vertebrate cone opsins enable sustained and highly sensitive rapid control of Gi/o signaling in anxiety circuitry. *Neuron* 81, 1263–1273. doi: 10.1016/j.neuron.2014.01.041
- Mesirca, P., Marger, L., Toyoda, F., Rizzetto, R., Audoubert, M., Dubel, S., et al. (2013). The G-protein-gated K⁺ channel, IKACH, is required for regulation of pacemaker activity and recovery of resting heart rate after sympathetic stimulation. *J. Gen. Physiol.* 142, 113–126. doi: 10.1085/jgp.201310996
- Moreno, A., Endicott, K., Skancke, M., Dwyer, M. K., Brennan, J., Efimov, I. R., et al. (2019). Sudden heart rate reduction upon optogenetic release of acetylcholine from cardiac parasympathetic neurons in perfused hearts. *Front. Physiol.* 10:16. doi: 10.3389/fphys.2019.00016
- Ng, G. A., Brack, K. E., and Coote, J. H. (2001). Effects of direct sympathetic and vagus nerve stimulation on the physiology of the whole heart – a novel model of isolated langendorff perfused rabbit heart with intact dual autonomic innervation. *Exp. Physiol.* 86, 319–329. doi: 10.1113/eph8602146
- Nobles, M., Montaigne, D., Sebastian, S., Birnbaumer, L., and Tinker, A. (2018). Differential effects of inhibitory G protein isoforms on G protein-gated inwardly rectifying K⁺ currents in adult murine atria. *Am. J. Physiol. Cell. Physiol.* 314, C616–C626. doi: 10.1152/ajpcell.00271.2016
- Qiu, X., Kumbalasiri, T., Carlson, S. M., Wong, K. Y., Krishna, V., Provencio, I., et al. (2005). Induction of photosensitivity by heterologous expression of melanopsin. *Nature* 433, 745–749. doi: 10.1038/nature03345
- Spoida, K., Eickelbeck, D., Karapinar, R., Eckhardt, T., Mark, M. D., Jancke, D., et al. (2016). Melanopsin variants as intrinsic optogenetic on and off switches for transient versus sustained activation of G protein pathways. *Curr. Biol.* 26, 1206–1212. doi: 10.1016/j.cub.2016.03.007
- Touhara, K. K., Wang, W., and MacKinnon, R. (2016). The GIRK1 subunit potentiates G protein activation of cardiac GIRK1/4 hetero-tetramers. *ELife* 5:e15750. doi: 10.7554/eLife.15750.010
- Wobus, A. M., Wallukat, G., and Hescheler, J. (1991). Pluripotent mouse embryonic stem cells are able to differentiate into cardiomyocytes expressing chronotropic responses to adrenergic and cholinergic agents and Ca²⁺ channel blockers. *Differentiation* 48, 173–182. doi: 10.1111/j.1432-0436.1991.tb00255.x
- Xiang, Y., and Kobilka, B. K. (2003). Myocyte adrenoceptor signaling pathways. *Science* 300, 1530–1532. doi: 10.1126/science.1079206

Conflict of Interest: The authors declare that the research was conducted in the absence of any commercial or financial relationships that could be construed as a potential conflict of interest.

Publisher's Note: All claims expressed in this article are solely those of the authors and do not necessarily represent those of their affiliated organizations, or those of the publisher, the editors and the reviewers. Any product that may be evaluated in this article, or claim that may be made by its manufacturer, is not guaranteed or endorsed by the publisher.

Copyright © 2021 Cokić, Bruegmann, Sasse and Malan. This is an open-access article distributed under the terms of the Creative Commons Attribution License (CC BY). The use, distribution or reproduction in other forums is permitted, provided the original author(s) and the copyright owner(s) are credited and that the original publication in this journal is cited, in accordance with accepted academic practice. No use, distribution or reproduction is permitted which does not comply with these terms.

4 Discussion

In my studies, I took advantage of pluripotent stem cells, which allowed me to gain insights into the involvement of specific ECM proteins in physiological development and in pathophysiological processes.

4.1 Role of ECM in development and in the functional integrity of cardiovascular cells

Our work has contributed to a better understanding of the role of extracellular matrix components in the development of cells of the cardiovascular system. In addition, alterations of the composition and/or structure of the ECM are also known to underlie cardiac and vascular diseases. For instance, ECM remodeling correlated with increased deposition of ECM proteins is a hallmark of dilated cardiomyopathy, hypertrophy, and heart failure in humans (Berk et al., 2007, Bayomy et al., 2012) and it is accompanied by fibrosis or arrhythmias.

Although genetically modified mouse models exist for several ECM proteins, these models are not optimal because most knock-out mice for laminin, integrins or ILK are lethal at the embryonic level (Friedrich et al., 2004; Smyth et al., 1999). When I became interested in laminin and integrins, the use of CRISPR-Cas9 for fast genetic manipulation was not yet available. Additionally, generating conditional Cre-loxP knock-out mice by crossing a mouse carrying the Cre recombinase under a tissue-specific promoter with a mouse containing loxP-flanked (floxed) target genes (such as ILK, laminins, collagen) was not a common technique in every laboratory, likewise, inducible models involving tamoxifen-inducible Cre recombinase or the Tet-On/Tet-Off system were not widely used. The Tet-On/Off models involves crossing mice carrying tetracycline-controlled transactivators (tTA/rtTA) with mice containing target genes under the control of tetracycline response elements (TRE), enabling researchers to manipulate gene expression in a doxycycline-dependent manner. However, nowadays, conditional or inducible mouse models are frequently employed to target gene deletion in specific tissues or cell types. This approach allows for a more focused analysis of gene function within the context of a living organism, facilitating the investigation of complex interactions

among various cellular components, signaling pathways, and other ECM molecules in vivo. It is important to note that ECM-related gene knock-outs can result in embryonic lethality, like for the laminin $\gamma 1$ (Smyth et al., 1999) or if the phenotype significantly affects the animals' viability. Even with new models of induction or conditional control, there is a limit in the ability to study gene function during development. In my studies, I opted to use pluripotent cells, as the differentiation of these cells into specific cell types in culture allows me to study early embryonic stages that are challenging to access in vivo, also in mice. The global knock-out for ECM proteins in ES cells has the distinct advantage of letting me explore, similar to an in vivo model, the possible interactions of laminin or ILK in different cell type and their influence overall during development. Moreover, with ES cells, it is possible to differentiate different types of cells to perform single-cell analysis with a nearly unlimited supply of cells through selection methods such as FACS or MAC sorting. In fact, I demonstrate that I could dissect the tyrosine kinase signaling defects by Ca^{2+} imaging in ILK knock-out or the electrophysiological properties of cardiomyocytes with the laminin $\gamma 1$ knock-out. At the same time the differentiation into 3D cluster, EBs permitted to analyze the role of ECM components during the early stage of development and to dissect their role for different cell types. Furthermore, considering the principles of the 3Rs (replacement, reduction, and refinement) pluripotent cells serve as an optimal alternative model to in vivo studies.

A clear example of how genetically modified ES cells permit the analysis of the development of a defined cell type under the influence of a specific ECM molecule is the study conducted on ILK. ILK deficiency resulted in a striking phenotype, as ECs fail to mature and form vessel tube-like structures resulting in impaired vasculogenesis. The experiments revealed that this phenotypic change was not due to this matrix component's altered mechanical property but to impaired signaling. It was found that the defect in signaling primarily affected VEGF receptor 2 (VEGFR2), which is crucial for mediating VEGF-induced cellular responses in ECs. VEGF signaling plays a vital role in various EC functions, including proliferation, apoptosis, and migration. Our experiments detected a Ca^{2+} release defect, indicating a disruption in the

downstream signaling pathways associated with VEGFR2 activation. This defect was not restricted to the VEGF receptor but a more general defect of tyrosine kinase receptors because EGF could not activate this signaling pathway either. In contrast, bradykinin, a G_i protein agonist, exerted intact Ca^{2+} release.

It has been known for some time that microdomains are specialized regions within the cell membrane that provide a spatial organization and concentration of signaling molecules enhancing the efficiency and specificity of signal transduction. Caveolae are microdomains that possess a typical flask shape invagination of the plasma membrane. They are made of caveolins which bind to cholesterol and stabilize their structure. Caveolae function as signaling hubs, therefore are particularly important in regulating receptor internalization, trafficking, and downstream signaling events, and they are highly enriched in EC (Chidlow and Sessa, 2010; Leo et al., 2020). As platforms for the assembly and compartmentalization of signaling molecules, they influence the strength and duration of signaling responses. During my studies on ECM it was known that the global knock-out mouse of caveolin 1 and 3 reduced the number of caveolae and it was demonstrated that caveolae are involved in muscular development (Hagiwara et al., 2006; Zhao et al., 2002). Specifically, in constitutive caveolin 3 knockout mice, it was possible to observe the exclusion of the dystrophin-glycoprotein complex from microdomains in muscle and abnormalities in the organization of the T-tubule system which causes limb girdle muscular dystrophy (Galbiati et al., 2001; Hagiwara et al., 2006). In addition, a general caveolin 1 knock-out mouse displayed dilated cardiomyopathy, pulmonary hypertension correlated with enhanced systemic levels of NO (Zhao et al., 2002). Furthermore, in caveolin-1-disrupted mice the lungs of knock-out animals displayed thickening of alveolar septa caused by uncontrolled EC proliferation and fibrosis (Drab et al., 2001). Recent literature showed how caveolin 1 interacts with receptors like EGF-R, platelet-derived growth factor receptor, and TGF β , thus affecting signaling and being implicated in pulmonary hypertension or in enhancing tumorigenic potential (Codrici et al., 2018; Oliveira et al., 2019). These findings are in line with our studies highlighting the fundamental role of intact signaling microdomains

in controlling cardiovascular cells' function and development. An indication that ILK was involved in the organization of caveolae was known from studies conducted on keratinocytes (Wickström et al., 2010). Therefore, using a caveolin 1-egfp fusion protein transfection strategy, we could explore not only in fixed cells but also with live imaging the dynamics of caveolae formation, positioning and turnover. Trafficking of caveolin 1 was disrupted, and the positioning to the plasma membrane was impaired in the absence of ILK. The VEGF receptor 2-PLC γ axis appeared to be phosphorylated by VEGF, indicating preserved functionality. However, defective crosstalk between PLC γ and downstream signaling molecules clustered in caveolae was proposed as a mechanism for the observed caveolin 1 trafficking abnormalities. These findings align with other studies demonstrating that disruption of plasma membrane microdomains may not affect PLC γ activation but can impact the function of molecules such as PIP2, which depends on cytoskeletal integrity (Jang et al., 2001). Surprisingly, the absence of ILK did not influence acetylcholine and bradykinin signaling pathways in ECs. It has been shown that G-protein-associated receptors clustering is not always essential for the correct signaling, as lipid rafts disruption did not affect β 2 receptor response in adult cardiomyocytes (Calaghan et al., 2008). This observation sheds light on the signaling mechanism in EC lacking Integrin-Linked Kinase (ILK). Further, the time lapse imaging experiments highlighted an altered transport of caveolin 1 due to abnormal microtubule and cortical actin interaction. This data confirmed the dual role of the ECM: ILK acts as a structural element that directly modulates cytoskeletal integrity through actin and microtubule crosstalk. Additionally, structural preservation is crucial for the transport, positioning, and turnover of caveolin 1 to the plasma membrane. In ECs, ILK's modulation of caveolin 1 movement and positioning interferes with tyrosine kinase receptor-mediated signaling, which requires precise subcellular positioning for proper functioning. With these findings, I highlighted how a close relationship between structure and function governs the regulation of intracellular signaling pathways. ILK deficiency affected cytoskeleton and RTK receptors microdomains thus impairing vessel development and angiogenesis. These findings were entirely in line with the tissue specific deletion in EC with the Cre-lox system and Tie2 promoter which have shown the critical role

of ILK in vascular development and integrin-matrix interactions (Friedrich et al., 2004). It has been demonstrated that patients with familial exudative vitreoretinopathy who show retinal vascularization defects possess three distinct mutations in the human ILK gene that compromise the gene product's function in vitro. Taken together, the data from this study suggest that defective cell-matrix interactions involving ILK and its interacting partner α -parvin, are linked to Wnt signaling and contribute to the pathogenesis of this hereditary disorder characterized by abnormal retinal vascular development. These findings further highlight the critical role of ILK in angiogenesis and its potential implications for understanding and treating retinal vascular disease (Park et al., 2019). Recently was shown that ILK plays a crucial role in VEGFR3 signaling by controlling its interaction with β 1 integrin, thereby ensuring proper lymphatic vessel development. ILK emerges as a key mediator in the intricate signaling pathways that govern lymphatic vascular growth, making it a potential target for understanding and modulating lymphatic-related disorders (Urner et al., 2019). Our studies on the deletion of β 1 integrin also showed that a reorganization of the cytoskeleton with consequent alteration of Gi- protein-coupled receptor distribution and muscarinic receptor coupling malfunction occurred (Bloch et al., 2001). Dysregulation of G-protein coupled receptors has been associated with arrhythmias, including atrial fibrillation, as well as detrimental effects such as myocyte death and maladaptive cardiac remodeling (Nattel and Dobrev, 2012). By highlighting the significance of fine regulation in intracellular signaling pathways and the interplay between structure and function, my findings align with the growing body of evidence that underscores the importance of the extracellular matrix in cellular physiology and disease processes. Further studies and discussions on these topics are essential to deepen our understanding of cellular signaling mechanisms and their implications in various physiological and pathological conditions.

Thus, considering the relevant role of β 1 integrins in Gi-signaling, we thought that its extracellular binding partner, laminin, could also play a central role in regulating cardiomyocyte signaling. Studies on embryos of transgenic mice, in which both alleles of the γ 1 chain gene

were inactivated, showed early embryonic lethality. The Laminin $\gamma 1$ chain is necessary for laminin heterotrimer assembly, and laminin turnover, on the one hand, induces the organization of the cellular basement membranes; on the other hand, it forms a structured network of components of the cortical cytoskeleton, such as $\beta 1$ integrin, vinculin, and talin. The creation of this intracellular signaling network could regulate, as observed for ILK in ECs, the receptor function (Fässler et al., 1996). In line with the findings on the role of $\beta 1$ integrins in muscarinic signaling and knowing that $\beta 1$ integrins are the primary cell surface receptors that mediate the interaction between cells and laminin, we decided to use the laminin $\gamma 1$ ES knock-out model to study its role in cardiac development and function. In this study, we opted also for a constitutive knock-out in ES cells. Cardiomyocytes were differentiated in embryoid bodies 3D clusters, thus allowing to investigate the effect of global laminin $\gamma 1$ absence and cellular interactions on cardiomyocyte development. Even though the lack of laminin determines a reduced $\beta 1$ integrin expression, the hormonal regulation of the contractility of cardiac cells was preserved, as observed with electrophysiological measurements on Ca^{2+} currents and frequency modulation by adrenergic and muscarinergic agonists. Thus, the presence of $\beta 1$ integrin was enough to preserve the receptors' clustering and function. Although the sarcomeric arrangement was not affected, laminin deletion caused ECM deposits that hinder normal electrical conductions, and because of cellular isolation, more ectopic centers developed. The study's novelty lay in highlighting a role for laminins other than structural and morphological action. The specific consequence of laminin $\gamma 1$ deficiency is the disruption of the electrical properties of cardiomyocytes, and the study highlighted the significance of laminin $\gamma 1$ in promoting homogeneous electrical spreading, which is essential for coordinated and efficient cardiac function. It was known that there could be abnormal ECM deposition and remodeling in various cardiac conditions, such as myocardial fibrosis, hypertrophic cardiomyopathy, and heart failure. Excessive ECM deposition, particularly of collagen fibers, can lead to the formation of fibrotic tissue within the heart. This fibrosis alters the normal electrical properties of the heart, affecting electrical conduction and leading to arrhythmias

(Boldt et al., 2004). Interestingly the laminin $\gamma 1$ absence could not alter the matrix protein-myocyte interactions which regulate Cx43 expression via $\beta 1$ integrin signaling, in fact Cx43 expression was preserved at the protein level, as shown in western blots (Shanker et al., 2005). That suggests that the electrical coupling is also depending on correct assembly of the matrix, indicating the deleterious effect of that fibrotic deposition. More recently, a case study reported that partial laminin $\alpha 2$ deficiency in patients developed dilated cardiomyopathy with conduction defects and ventricular arrhythmia, thus proving the arrhythmogenic potential of laminin defects (Carboni et al., 2011; Marques et al., 2014).

4.2 Modeling cardiovascular disease with iPS cells

Cardiac model of LQTS3

Cardiovascular diseases, including arrhythmias, pose significant challenges in diagnosis and treatment. To gain deeper insights into the underlying mechanisms of these diseases and develop effective therapies, we thought that iPS cells could be a promising tool for disease modeling. After iPS cells discovery, we had the motivation to see if we could use them to model monogenetic diseases like channelopathies. Channelopathies were chosen because mutations in ion channel genes cause them. This genetic simplicity allows researchers to establish a causal link between the specific mutation and the observed disease phenotype and enhances the fidelity of disease modeling. In several studies summarized above, I explored how iPS cell-derived cardiomyocytes can be used as LQTS3 model, a monogenetic cardiac disorder with distinct phenotypic alterations. The primary motivation of the study on disease-specific cardiomyocytes from iPS cells derived from the fibroblasts of the LQTS3 mouse, was to see if, after reprogramming and in vitro differentiation, the typical phenotype of the mouse carrying the human mutation was detectable. LQTS3 is known to be associated with severe and malignant arrhythmias, making it also of particular clinical interest. I explored the delta KPQ mutation, which consists of the deletion of the amino acids lysine-proline-glutamine, in the intracellular loop between domain III and IV of the cardiac Na^+ (Nav1.5, Scn5a) channel (Nuyens et al., 2001). This mutation in humans is one of the most commonly associated with

LQTS3, and it generates an abnormal late Na⁺ current during the prolonged repolarization phase of the cardiac action potential. Usually, the late sodium current is small, but due to the mutation, the gating, trafficking, and anchoring with cytoskeletal proteins are altered, and the current increases. This late current reduces repolarization reserve in cardiomyocytes, leads to delayed repolarization, prolonged APD, prolonged QT intervals on electrocardiograms, and induction of EADs which increases the risk of life-threatening ventricular arrhythmias, including Torsades de Pointes (Schwartz et al., 2001; Wilde and Amin, 2018). At the time of our studies, LQTS3 was particularly interesting to model because there was no therapeutic approach. LQTS patients were all treated with β -blockers which makes sense in LQTS1 and 2, where the increased frequency can lead to arrhythmic events, but in LQTS3, the depression of the frequency is the trigger for the life-threatening arrhythmias. In LQTS3, more pronounced QT interval prolongation and arrhythmic events occur more frequently at rest (Schwartz et al., 2001; Wilde and Amin, 2018). We decided to reprogram fibroblasts from the mouse model for LQTS3 because mouse iPS cells culture was well established in the scientific literature, and the laboratory had expertise in mouse ES cells. The LQTS3 mouse showed a 2-fold larger initial fast Na⁺ current density and a faster recovery from inactivation, which might favor reentry arrhythmias. It was possible to detect the mutation-induced phenotype, namely a prolongation of the AP and a propensity for arrhythmias, as well as a specific dependence of QT prolongation at lower beating frequencies. It was intriguing to see that LQTS3-derived cardiomyocytes displayed in the electrophysiological analysis the hallmarks of LQTS3 even if they did not resemble a completely mature cardiomyocyte. Moreover, the essential role of the late Na⁺ current in inducing arrhythmic events was shown confirming to use this current as target for the implementation of a specific therapeutic approach. LQTS3 model could help to detect new drugs which act on the biophysical properties of the mutation. We have then successfully established a patient-derived iPS cell model with a heterozygous SCN5A mutation (p.R1644H). This is a missense mutation in the sodium channel protein, with an arginine-to-histidine exchange at the cytoplasmic face of the D4S4 transmembrane segment. R1644H was one of the first LQTS3-causing mutations identified and has been shown to impair fast

Na⁺ channel inactivation, thereby giving rise again to a persistent late sodium inward current (INa) (Hedley et al., 2009). The pathogenesis of this typical LQTS3 mutation also involves the dispersion of sodium channel re-openings after fast initial inactivation. Although the late Na⁺ current has a small amplitude (~5%) compared to the initial inward current, the premature recovery from inactivation of the Na⁺ current will counteract cardiomyocyte repolarization, leading to a prolongation of AP duration, QT interval and EAD propensity (Balser, 2001). The motivation for using patient-derived- cardiomyocytes was to prove the possibility of using them for evaluating putative disease-correcting effects of drugs, as shown before with the model of LQTS2 (Itzhaki et al., 2011). Until 2010 the LQTS3 patients at high risk for sudden death were treated with implantable converter defibrillator (ICD) combined with β -blockers. However, ICD firing can be associated with complications. Alternative drugs that inhibit late INa have been proposed, such as mexiletine, ranolazine, and flecainide (Wilde and Amin, 2018). We also showed in our patient derived-cardiomyocytes specific effects on electrophysiological properties such as reduction of APD and FPD prolongation with mexiletine. This drug did not show any side effect linked to hERG channel alteration in the specific mutation that we investigated, thus proving to be a good therapeutic candidate. This study demonstrated that patient-derived iPS cell-derived cardiomyocytes provided readouts that might be most robust and predictive for investigating candidate drugs for LQTS3. Recently, reports showed that a more selective and potent late INa inhibitor, GS-458967, did not affect other ion currents and was proved on iPS-derived cardiomyocytes from a SCN5a 1795 ins D+/- mutation (Portero et al., 2017). This mutation is associated with both loss (reduced peak INa) and gain (increased late INa) of sodium channel function.

Nevertheless, several challenges must be addressed when iPS cell-derived cardiomyocytes are used to model cardiovascular diseases. One significant challenge is achieving robust and consistent differentiation of iPS cells into mature and functional cardiomyocytes that faithfully recapitulate the phenotypic features observed in the diseased heart. Capturing the disease phenotype at the appropriate developmental stage is crucial, as certain disease-related

alterations may be more pronounced during specific stages of cardiomyocyte development. This will be further discussed in the next paragraphs.

Challenges in personalized medicine: non-clonal iPS and automated iPS cell generation

Indeed, human iPS cells could be generated in a patient-matched manner, implicating that each patient could have their pluripotent cell lines. iPS cell line generation opened the possibility that human iPS cells could be used to decipher the impact of a mutation in a specific genetic context because the genetic background can compensate for or exacerbate the intensity of the phenotype. In fact, in one study of LQTS2 family members with mother and daughter carrying the same mutation, KCNH2 G1681A, the genetic background is implicated in the severity of the phenotype. The mother was asymptomatic, whereas the daughter showed signs of prolonged QT interval and arrhythmic events. The analysis of the phenotype of patient derived-cardiomyocytes which show, for instance the LQTS3 characteristics, could predict whether a certain drug is indicated for that disease, even if the biophysical characterization or even which mutation the patient has, is not known. Drugs for LQTS3 should shorten the APD or FPD and prevent EADs, thus, this simple readout can predict their benefit or not for the patient. This idea underlies the motivation for studying the generation of non-clonal iPS lines. Using lentivirus expressing the Rex-1 stem cell-specific promoter under neomycin antibiotic selection effectively generated non-clonal mixed clones of wild-type and LQTS3 mutated iPS cells (Friedrichs et al., 2015). Usually, after gene transfer, several clones are picked, expanded and individually analyzed. The selection work requires a great deal of time and can be very expensive. Instead, we decided to combine all the cells selected by neomycin and create a non-clonal line. Our motivation was to identify a relatively fast method to generate iPS lines to test whether iPS cells derived from non-clonal selection could express the phenotypic characteristics of LQTS3. The idea was that for patient-tailored medicine, non-clonal cell lines could be generated in a shorter time frame, and used for testing drugs to find the best therapy. However, non-clonal lines have a mixed genetic background, which can be challenging when establishing standardized experimental conditions and may hinder the reproducibility of

experiments. Of course, this procedure could also generate ablated clones with lentivirus-induced mutations and an altered chromosome number. Despite this possibility, we observed that stem cell morphology and expression of stem cell markers were intact. Furthermore, we showed a specific LQTS3 phenotypic fingerprint in differentiated cardiac cells with prolonged APD at slow pacing rates. This data confirms previous studies on the generation of iPS cell lines in a bulk culture that showed intact pluripotency and maintained gene expression profiles and differentiation potential (Willmann et al., 2013). Therefore, this non-clonal technique allows to create lines quickly and cost effectively for eventually high-throughput drug screening. Nevertheless, we cannot exclude the generation of clones with variations in copy numbers and integration sites, which could cause insertional mutagenesis. In addition, it might be possible that clones with certain SNVs could have a selective benefit in comparison to others and create an unwanted monoclonal population which not always represent the “standard” patient cell lines.

However, the gold standard procedure is creating iPS cells from single clones, which is preferable because the presence of the mutation can be unambiguously validated. Compared to the mixed clone, it is prevented from having cells that do not express the mutation and could affect the size of the mutation-dependent phenotype. To minimize genetic variation, more clones must be created, and if the mutation in all clones shows the same phenotype and the drugs show the same effect, the validity of the screening is more meaningful. The StemCellFactory project in which we participated aimed to implement automated solutions for iPS cell line generation. One of the key features of the StemCellFactory is its use of robotics and automated modular platforms across the process, from the expansion of adult human fibroblasts to Sendai virus-based reprogramming, automated isolation, and parallel expansion of iPS cell clones. A high-speed microscope achieves quality control by acquiring whole well large images and their evaluation through confluence, colony morphology, and topology by a trained deep learning algorithm, also used for automatic dilution ratio calculation. The system can perform repetitive tasks with high precision, consistency, and speed, and, due to the

robotics, can reduce human error and variability, making it a powerful tool for generating large quantities of iPS cells in defined conditions and cost-effective for disease modeling and drug screening at an industrial scale (Elanzew et al., 2020). Since the patient-specific approach is often considered unfeasible due to its high cost, some companies and national research units have adopted an alternative strategy by creating iPS cell lines from HLA-homozygous donors from CD34⁺ cord blood cells (Álvarez-Palomo et al., 2022; Yoshida et al., 2023). HLA genes are crucial for the immune system's recognition of tissues. The advantage of using HLA haplotype homozygote donors implies that with a limited number of HLA-homozygous iPS cell lines representing the most frequent HLA haplotypes in a population, it is possible to establish immune compatibility for a large fraction of that population. Unlike autologous cell therapies, where patient-derived cell lines are used for the same patient, these off-the-shelf HLA-homozygous iPS cell lines can potentially treat millions of patients with compatible conditions. Standardizing the iPS cell generation and differentiation process reduces the time and resources needed for patient-specific iPS cell production, accelerating the development and translation of iPS cell-based therapies to clinical applications. To use iPS cells for therapeutic purposes and give standard in research results, companies must establish a robust, reproducible, well-characterized, and GMP-compliant manufacturing process covering generation and expansion of starting materials, followed by directed differentiation into specialized cells. As far as I know the current industrial supply chain costs are still a limiting factor in medical applications (Suresh Babu et al., 2023).

Challenges in disease modeling: Genetic variability and choice of controls

A limitation in the praxis of the use of iPS cells as a disease model is the high phenotypic variability among the different lines from the same donor, which requires large cohorts of iPS cell lines to decipher the impact of individual genetic variants. Many genetic disease variants might have a negligible effect size and thus require many control or disease samples to obtain a statistically relevant effect.

The gold standard control nowadays when studying patient specific iPS cells as a disease model, is to create isogenic lines that have corrected the point mutation, instead of iPS cells from siblings or other healthy subjects, as was some years ago. Recently, the CRISPR/Cas9 genome editing technique has been used to generate isogenic controls or mutations to obtain an ideal disease model, for instance, for multiple endocrine neoplasia 1, thereby helping the understanding of the genotype and phenotype relationship of the disease (Guo et al., 2017). The perfect disease model should compare the patient's diseased cells with a genetically modified version, and a functional rescue related explicitly to the function of the mutated gene should be included. If the mutation is obtained by gene editing, it is possible to use as control mock clones. In this case, cells are transfected without Cas nuclease and guide RNA. The cells are still going through the stressful transfection conditions induced by electroporation or lipofection, but nothing is being delivered to the inside of the cells. Therefore, a mock control will provide insight whether the phenotype observed from the CRISPR editing experiment is a true phenotype or just due to cellular responses that the cells creates upon being exposed to transfection conditions.

Alternatively, a diseased human iPS cell line can be generated from a sick individual, and gene editing can be used to correct the mutation to develop therapeutic applications. In this field, the CRISPR/Cas9-based genome editing technique has become relevant to correcting the cells' disease-causing mutations before differentiation and transplantation. These edited human iPS cell lines are clonally selected and are a renewable source for diseased and healthy cells controlled for genetic variability. They can be used for various downstream applications to study and treat the disease. For instance, it has been shown in inherited retinal degeneration that restored iPS cell lines can be generated with a comprehensive CRISPR-based genome editing strategy regardless of genomic location and mode of inheritance, and used for autologous retinal cell replacement (Burnight et al., 2017).

However, achieving this level of quality control in every cell model is not always possible. Another point that raises concern is the permanence of the epigenetic memory of the somatic cells of origin which can impact the differentiation of the cell of interest. In some case the

epigenetic memory could be used to help to generate specific cell types, like in the study of β -like cells. Human pancreatic islet β cells derived from multiple human donors manifested enhanced and reproducible spontaneous and induced differentiation towards insulin-producing cells, compared with iPS cells derived from isogenic non- β -cell types and fibroblast-derived iPS cells (Efrat, 2021). Of course, epigenetic memory could also hinder the differentiation or the expression of a specific phenotype in differentiated cells; thus, using several diseased lines and more controls would also be an attempt to minimize this problem.

Challenges in disease modeling: Maturation and purification of differentiated cells

Using pluripotent cells to recapitulate mature cell defects of late-onset disorders has proven more challenging as differentiation protocols better reflect immature rather than adult cell types (Hrvatin et al., 2014, Anderson and Francis, 2018). It should be noted that there is no single marker for maturation to the adult stage. Maturity is due to changes in morphology, structural, metabolic and in excitable cells in electrophysiological properties. We know that human cardiomyocytes require years to complete their growth in a human heart. Studies with human iPS-derived cardiomyocytes differentiated in EBs kept for one year in culture showed that cardiac cells displayed larger cell size and sarcomere development with Z-, A-, H-, I bands and even M band-specific alignment, and expressed maturation-related genes such as MYH7 (Kamakura et al., 2013, Lewandowski et al., 2018, Lundy et al., 2013).

In the research using iPS cells, cardiomyocyte differentiation was necessary because of their use as a disease model or screening tool. It is known that iPS-derived cardiomyocytes have a different morphology to adult ones; the highly organized sarcomeres are missing and the sarcoplasmic reticulum and t-tubules are not well developed (Denning et al., 2016, Yang et al., 2014). iPS cell-derived cardiomyocytes lack the clustering of stable t-tubules with Ca^{2+} channels (Cav1.2) near to sarcoplasmic reticulum building the dyads, the Ca^{2+} release unit. The maturation of cardiomyocytes with adult-like t-tubules and Ca^{2+} release units could provide a useful human model for pathological excitation-contraction coupling-related conditions. It has been recently shown that the overexpression of BIN1, a member of the Bin1-Amphiphysin-Rvs

domain superfamily, can promote the progressive formation of t-tubules and has a direct effect on clustering of Ca^{2+} channels with stable dyads, thus improving the synchronization of Ca^{2+} release during excitation contraction coupling (De La mata et al., 2019, Guo et al., 2022).

Other solutions to the maturation problem come from special cultivation techniques such as 3D force-generating engineered heart tissue (EHT) (Eschenhagen et al., 2012, Mannhardt et al., 2016). EHT consists of dissociated cardiomyocytes plated in casting molds anchored between two flexible silicone posts which generate a defined preload. The EHT technique has been used for pre-clinical drug development and safety toxicology. EHTs perform auxotonic contractile work against elastic posts, and this favors the creation of muscle bundles with cardiomyocytes alignment showing good sarcomeres organization and cross-striation approaching the classical rod shape of adult cells. EHT with human iPS-derived cardiomyocytes allows the monitoring of the effects of drugs on the force, pacemaking activity, contraction, and relaxation kinetics. Nowadays, the state of the art to create a miniaturized cardiac tissue model in vitro is the generation of organotypic organoids, which showed signs of maturation of cardiomyocytes. The group of Forte in Finland developed scaffold-free multicellular beating human cardiac microtissues from human iPS cells that show a degree of proto-self-organization upon codifferentiation and can be cultured for long term (Ergir et al., 2022). The 3D organoids observed up to 85 days with TEM microscopy demonstrated sarcomere assembly with z disk with a length of $1.5\mu\text{m}$ and a sarcolemma around the contractile apparatus to maximize the efficiency of calcium exchange. The transcriptional landscape showed differences with the 2D monolayer culture, showing regulation of genes for heart contraction, sarcomere organization, Ca^{2+} machinery, and ATP synthesis. Moreover, compared to standard 2D monolayer cardiac differentiation, metabolic maturation was enhanced when comparing the data set of adult atrial and ventricular tissue genes. Oxidative phosphorylation, fatty acid lipids and glycogen metabolisms were closer to adult tissues than the 2D monolayer differentiation. Furthermore, organotypic microtissues could respond to cardioactive and cardiotoxic drugs in a dose dependent manner. Thus, organoids are used in

drug testing for cardiovascular diseases because they provide much more throughput than EHT or animal models. After all, the starting cells are relatively low (~ 5000 cells) and the culture is relatively simple (Kim et al., 2022; Paik et al., 2020). However, there are till now no standardized protocols or commercially available cardiac organotypic organoids. There is still a lack of real vascularization perfusion, and the maturity remains at fetal stages. Therefore, further studies will be needed to find effective methods for the maturation of cardiac organoids and implement throughput efficiency due to the size limitation of organoids, thus suffering of internal necrosis. Another point to act on concerning maturation is that most iPS cell-derived cardiomyocytes have an immature ion channel expression profile. For instance, cardiac currents like I_{Na^+} , I_{Ca-L} , I_{to} , I_{Kr} , and I_{Ks} are present, but many clones lack I_{K1} or, as in our investigated clones, I_{Na^+} has low expression at early differentiation stages (Dhamoon and Jalife, 2005, Malan et al., 2011, Hoekstra et al., 2012, Knollmann, 2013). Another point to consider in analyzing diseases involving ion channel defects is that current density can also differ between stem cell lines and differentiation stages. Moreover, these immature features that influence regular electrical activity, such as depolarized membrane potential, lack of a complete dyads system and spontaneous beating due to a Ca^{2+} regulation which is different to adults, could be critical to predicting arrhythmias in patients (Chong et al., 2014, Shiba et al., 2016). In the case of LQTS3, we waited for at least four weeks of differentiation to have enough *Scn5a* channel expression to analyze the phenotype. We could prove that this was sufficient to see the characteristic features of the disease on I_{Na^+} and APs. However, a more mature phenotype would be essential for pathologies that show a phenotype exclusively in adult differentiated cells. For example, deficiency in I_{K1} could impact the phenotype of different types of LQTS, influencing the membrane potential to more depolarized values than in the in vivo situation. This could also affect the pharmacological and toxicological screenings of drugs. I_{K1} expression enhancement was thought to play a role in maturation of cardiomyocytes. I_{K1} stabilizes the resting membrane potential and shapes the action potential's initial depolarization and final repolarization. It has been shown that iPS cell-derived cardiomyocytes expressed low I_{K1} density, showing spontaneous beating, a longer APD and a more

depolarized membrane potential than adults (Vaidyanathan et al., 2016). Therefore, an overexpression of IK_1 should hyperpolarize the cell membrane potential, thus stabilizing and reducing spontaneous beating. In this study, upregulation of IK_1 in human iPS-derived cardiomyocytes infected with an adenoviral construct determined a mature AP. Indeed, IK_1 -expressing cardiomyocytes lacked spontaneous beating, have a stable membrane potential at around -80 mV, and could be electrically paced. Also, Ca^{2+} transient amplitudes as well as late sodium current were larger (Vaidyanathan et al., 2016, Quach et al., 2018). However, no sarcomeres and contractile apparatus morphology or related genes were investigated in this study.

Together with the idea of IK_1 overexpression, the dynamic clamp technique was used to implement the immature electrophysiology of iPS cell-derived cardiomyocytes. The dynamic clamp injects current representing the insufficient potassium current, IK_1 . However, dynamic clamp requires patch clamp and is therefore low throughput for large-scale drug screening. The group of Christini (Quach et al., 2018) used optogenetics, modulation of light-sensitive proteins, to generate by optical dynamic clamp outward currents using an opsin, ArchT, delivered by adenovirus. The light sensitive ArchT was controlled optically and used to mimic IK_1 -like current. Compared to genetic overexpression optical dynamic clamp offers more precise dosing and control of applied current. The idea behind this study was to establish a first step towards a high throughput all-optical approach that is of non-contact nature, can be scalable and allows parallel examination of multiple cells, and implement maturity of cardiomyocytes. However, the measurement of membrane potential was still achieved through an electrode. In the future, a complete optical readout with genetically encoded voltage indicators would be a further advantage, enabling all-optical high-throughput screening (Quach et al., 2018).

All the differentiation protocols considered and cited in the introduction of this work, are forced to contribute to a specific cell type through directed differentiation. However, they also induce different cell types from mesodermal origin as well as different subtype of cardiomyocytes. The

heterogeneous differentiated population is a significant limitation for screening, disease modeling, and also for regenerative therapy, as it increases the risks of tumors, rejection by the immune system of the host, or other adverse effects due to unwanted cells. To overcome this limitation, methods exist to select a high purity population of cardiomyocytes either by antibiotic or by metabolic selection. In my work, I also used a double antibiotic selection with a lentivirus strategy that allowed stable integration in the genome (Ma et al., 2003) of a stem cell-specific promoter, Rex-1, which controls a neomycin resistance gene, used to maintain undifferentiated cells. The short α MHC cardiac promoter controls puromycin resistance and the green fluorescent protein (GFP). Differentiated cardiomyocytes that expressed the short α MHC promoter survived puromycin application, and puromycin selection eliminated non-cardiac cells, allowing for the purification of cardiomyocytes. Importantly, purified cardiomyocytes maintained an intact electrophysiological phenotypic fingerprint comparable to those of non-antibiotic selected cardiomyocytes therefore, were well suited to investigate LQTS (Kolossova et al., 2006, Friedrichs et al., 2015). A potential drawback is that the α MHC promoter might not be optimal for adult cardiomyocytes. Furthermore, we could not exclude that lentiviral silencing upon differentiation could affect puromycin expression in some clones. Although less frequent, there is a risk of insertional mutagenesis due to random integration. Currently, the prevailing approach for obtaining human iPS cell-derived cardiomyocytes involves metabolic purification and is described in the introduction section. This method obviates the necessity for genetically modified cells or selection based on specific promoters. Despite its success in yielding purified cardiomyocyte populations using lactate and glucose-free medium (Tohyama et al., 2013), the metabolic purification methods' efficacy can vary among human iPS cell clones and may lack consistency in murine iPS cells (Ordoño et al., 2020). This method, however, is most efficient in human iPS cell-derived cardiomyocytes, and it has proven to be higher throughput; in fact it was used for bioreactor culture expansion, obtaining ~ 7 million cells/mL with a purity of 90% (Laco et al., 2020).

Comparison of readout systems for disease modeling and screening

The analysis of mouse and human iPS-derived LQTS3 disease cardiomyocytes in our studies proved that cardiomyocytes could be used for drug screening. One area of interest that opened up with human iPS cells is the unveiling of novel drug targets. iPS cell lines, derived from individuals afflicted by genetically-driven disorders, offer an invaluable resource for generating patient-specific cardiomyocytes. By conducting in vitro studies using these patient-specific cardiomyocytes, researchers can identify molecules or pathways that play a role in the disease's pathophysiology. These molecules may represent potential novel drug targets.

The acquisition of the patient phenotype in cell culture and its straightforward analysis is essential if we want to use these cells to test the efficacy of the potential pharmacological treatment. However, LQTS affected patients receiving therapy, 10% of LQTS1, 23% of LQTS2, and 32% of LQTS3 patients treated with β -blockers still experience cardiac arrhythmias (priori et al., 2004, Han et al., 2020). In iPS-derived cardiomyocytes, applying Na⁺ channel blocker drugs such as mexiletine or phenytoin showed encouraging results, eliminating typical pathology features, for example, EADs or prolonged AP duration at low pacing frequency, and showed no effects on wild-type cells. However, more integrated and automated readout assays are desirable because the single-cell analysis in the patch clamp is technically challenging. Microelectrode arrays proved exceptionally reliable in detecting EADs because cell-to-cell variation was overcome by averaging the field potential from many cells. With the mexiletine or phenytoin application, the multielectrode assay showed a reduction of field potential duration and could be used as a treatment against EADs. Indeed, phenytoin was successfully used to treat several family members affected by the R1644H mutation as an alternative to mexiletine in the LQTS3 study. This concordance between human iPS cells and patient-based data is noteworthy because mexiletine treatment is not efficient across all LQTS3 patients. It has been shown that in some cases, mexiletine can interact with the hERG channel or only partially rescue the phenotype. In contrast, we did not observe any effects on APD or field potential

duration when monitoring mexiletine treatment in wild-type iPS-derived cardiomyocytes, which suggests no side effects to the moderate drug concentration used in the study.

In the field of safety pharmacology, it is imperative to rigorously evaluate candidate drugs for their potential to induce adverse cardiac effects, notably concerning QT interval prolongation and the induction of torsades de pointes arrhythmias. This enables early detection of potential cardiotoxic effect during the drug development process, helping to prioritize safer compounds for further development. A staggering 28% of drug candidates are withdrawn in the United States due to an elevated risk of cardiac arrhythmias, underscoring the criticality of this preclinical scrutiny. While heterologous systems such as HEK cells engineered to express hERG channels present an expedient platform for high-throughput assays, they exhibit notable disparities from cardiomyocytes. Though these systems are easy to maintain and permit high throughput, they would need ideally the comprehensive repertoire of cardiac ion channels of cardiomyocytes. They can consequently yield potentially misleading assessments of drug effects. Here, the value of human iPS cell-derived cardiomyocytes becomes apparent. These cells express hERG at levels akin to those found in adults. For instance, testing verapamil on these cells revealed its neutral, non-toxic profile concerning QT prolongation. In contrast in heterologous systems verapamil acts on both hERG and Ca^{2+} channels, leading to false positive toxic signals. The drug alfuzosin further underscores the disparities between hERG-expressing lines and human iPS cell-derived cardiomyocytes. While alfuzosin exhibited no toxicity in hERG-expressing lines, it demonstrated clear toxicity in the latter due to its impact on Na^+ channels, thereby triggering QT prolongation (Blinova et al., 2017; Burnett et al., 2021; Kirby et al., 2018; Navarrete et al., 2013). The US Food and Drug Administration (FDA) endorsement further validates the utility of iPS cell-derived cardiomyocytes in predicting the proarrhythmic risks of drugs (Blinova et al., 2017; Musunuru et al., 2018). However, it remains a complementary model in the preclinical screening landscape. Drug screening with human iPS cell-derived cardiomyocytes can act as a pivotal filter, disqualifying drugs with toxicity in some lines and picking drugs for further investigation when there is evidence of efficacy.

Nowadays, it is recognized from institutions and companies that incorporate human iPS cell-derived cardiomyocytes into drug development could empower precision medicine and safer pharmaceutical innovation (Musunuru et al., 2018).

Moreover, their application in high-throughput phenotypic assays could enable the systematic screening of compound libraries, specifically identifying compounds that confer beneficial cardiovascular effects (Sinnecker et al., 2014). Several high throughput screening readout systems for pluripotent cell-derived cardiomyocytes or ECs exist. The research studies presented here used high throughput electrophysiological methods such as MEA or automated patch clamp. These readout systems permit the parallelization of the measurements. One limitation of the automated patch clamp system tested in our studies is the use of the cell in suspension, as in this process, the contractility properties of cardiomyocytes can be affected. Furthermore, some channels clustered in membrane microdomains may show altered functions, such as modified biophysical properties, as they depend strictly on the clustering environment.

Cellular disease models can also be analyzed by high-content imaging. This technique involves a combination of automated microscopy and image analysis software. The goal is to acquire and analyze high-resolution images of thousands of cells simultaneously to obtain quantitative data on parameters such as cell morphology, protein expression, beating frequency, contractility, calcium handling, and cell viability. This readout system provides a powerful tool for researchers to investigate cellular pathologies and the effects of drugs or other treatments on these cells and are less time-consuming or invasive than electrophysiological methods such as patch clamp or dynamic clamp (Cao et al., 2020, Chesnais et al., 2022). Additionally, the cells are in a more physiological environment than with electrophysiological measurements; and with these techniques would be easier to obtain information from 3D organoids or intact tissues.

As acquisition techniques become increasingly automated, so has the interest jumped for automated open-source software used in data analysis, in screening systems. One recent

example is the muscle motion system that has been validated in analyzing contraction, not only in cellular models but also in complex 3D organoid models. The muscle motion software allows rapid and reliable identification of disease phenotypes. It can detect potential cardiotoxic effects in drug-screening pipelines and used for the translational comparison of contractile behavior (Sala et al., 2018). Moreover, organ-on-a-chip technologies have been developed to address the limitations of 2D systems. The co-culture of different cells, such as EC fibroblasts and cardiomyocytes, can form tissue in 3D biomimetic hydrogel in microfluidic devices. The devices are typically made of silicone and contain tiny chambers that can be used to manipulate fluids or cells. It has been shown that it is possible to use the microfluidic device to model the behavior in heart tissue and therefore analyze contractility by Ca^{2+} transients' behavior in baseline or after drug application. In one study with iPS cells, gene editing with the CRISPR-Cas9 technique introduced a point mutation in the *KCNH2* gene, causing LQTS2. The generated iPS cells were used to build a 3D heart-on-a-chip to be used for personalized medicine (Veldhuizen et al., 2022). With lab-on-a-chip readouts, it is also possible to test the permeability and assess the integrity of the endothelial barrier and its ability to prevent the passage of harmful substances in physiological conditions since complex organoid systems could be built.

4.3 Future perspectives: organoids

A single-cell model can recapitulate monogenetic diseases, as the monogenetic mutation is reflected in a phenotypical effect confined to one cell type. The cellular disease model is adequate, as shown in the LQTS studies. However, a higher degree of complexity in other pathologies, such as cardiac hypertrophy, for example, metabolic or psychiatric disorders, involves several levels of interaction between organs. Furthermore, some pathologies takes years until the full development of the disease phenotype, and this cannot be modeled by pluripotent cells. As already mentioned, iPS cell-derived cells may have different maturation levels, gene expression profiles, and electrophysiological properties, affecting their ability to model complex diseases consistently. Mimicking the physiological characteristics of organs or

tissues would be particularly important for complex biological processes unique to humans. In fact, despite many biological processes being conserved in mice, there are striking differences as human development is protracted. In recent decades, numerous efforts have been made to generate in vitro functional organs with human pluripotent stem cells. Pioneering work on organoid models was conducted for the developing brain (Eiraku et al., 2008), and the actual rise of the organoids field started when it was demonstrated that cerebral organoids recapitulate features of human cortex development. Cerebral organoids were used to model microcephaly, a disorder that could not be studied in mice. Patient-derived-cerebral organoids showed premature neuronal differentiation. This defect was correlated to the disease and could help to get insights into the disease's development even in complex human tissue (Lancaster et al., 2013).

Recent studies on skin and vascular organoids evidence the need for multi-step protocols that mimic embryonic development into endoderm ectoderm and mesoderm, then cellular specification applying growth factors and subsequently cultures in architectural structures like spheroid to produce cystic organoids. In the end, a complex inside-out model is formed, with specific cellular organization resembling that of tissue (Corsini and Knoblich, 2022; Hofbauer et al., 2021; Wimmer et al., 2019). A critical point for organoids as in vitro systems is that they can recapitulate the microarchitecture of the tissue; still, they fail to rebuild the entire structure of a human organ. During organoid formation, the architecture can be quite variable, and subsets of cell types are often missing or not adequately arranged; therefore, the tissue's maturation is also lacking. The incompleteness of the architecture is clearly visible in mimicking the heart tissue; the most elaborate model so far is the so-called cardioid (Hofbauer et al., 2021). Cardioids display a coelom-like cavity surrounded by cardiomyocytes, endocardial and epicardial cells lined with ECs. Despite not containing end-differentiated cells and lacking typical chamber division, cardioids have been used to model hypoplastic left syndrome and gestational diabetes (Hofbauer et al., 2021, Lewis-Israeli et al., 2021).

Blood vessel organoids have recently been created from human iPS cells and have been shown to recapitulate the structure and function of human blood vessels and mimic the microvascular changes found in patients with diabetes potentially helping to study metabolic diseases. The organoid disease model system helped identify key signals like DLL4 and NOTCH3 of vascular remodeling in diabetes, thus indicating that human vessel organoids are suitable systems to model and detect regulators of diabetic vasculopathy (Wimmer et al., 2019). A drawback of organoids in metabolic research is the lack of oxygen and nutrients, especially in their inner part, which can cause metabolic changes per se. Oxygen imbalances can perturb proliferation and differentiation, affecting the subset of cell types developed. Nevertheless, it will be exciting to see if organoids can also model adult cardiovascular diseases or provide a source of cells for cell-based therapies. For example, skin organoids have already been used to improve disease modeling and drug discovery for genetic skin disorders. Their degree of complexity has reached levels that suggest they are a promising alternative to skin grafting approaches (Lee et al., 2020).

4.4 Future perspectives: Drug screening for GPCRs using optogenetics

Recently, we showed that combining pluripotent stem cells and optogenetics allows us to analyze Gi signaling with high spatiotemporal resolution (Cokić et al., 2021). GPCR are relevant in the cardiovascular system because they control several signaling pathways involved in the modulation of chronotropy and dromotropy, contractility, vascular tone regulation and blood pressure. To study Gi signaling stimulation which is fundamental to regulating heart rate and controlling arrhythmic events, we used a LWO, which was reported to activate Gi/o signaling in neurons (Masseck et al., 2014). A significant advantage of this opsin is the possibility of repetitive and long-lasting activation compared to vertebrate rhodopsin because, in rhodopsin, the response to light fades during close repetitions. Another advantage of LWO over short wavelength opsins is that it is activated by light with a wavelength toward red which has better tissue penetrability and less phototoxic effects. LWO was characterized in our study using mouse stem cell-derived 3D beating clusters. The EB model

can effectively and quickly evaluate the effect of light-activated signaling pathways on cardiomyocytes using a screening method that exploits their beating rate. By frequency analysis of beating clusters in EBs expressing LWO, we could discriminate between the activation of a G_i signaling pathway which would decrease their beating frequency, or the activation of a G_q signaling pathway which would increase the beating rate. Moreover, we fine modulated the receptor with gradual light stimulation, changing either the intensity or duration of light application.

In patients the precise control of the parasympathetic and sympathetic activity seems vital to prevent developing pathologies such as atrial fibrillation (AF) (Ang et al., 2012). AF is the most common cardiac arrhythmia, leading to atrial volume overload, stretch, and fibrosis (Nattel, 2017). Parasympathetic modulation of muscarinic acetylcholine receptor 2 (M2R)/ G protein-coupled inwardly-rectifying potassium channel (GIRK) (Dobrev et al., 2001, Makowka et al., 2019, Hanna et al., 2021) is fundamental for the stabilization of the fibrillating activity, and it has been seen that patients with sustained AF have constitutive GIRK activity without M2R agonist stimulation. Investigations in a canine model have shown that selective inhibition of $G_{ai/o}$ -mediated parasympathetic signaling nearly eliminated AF inducibility (Aistrup et al., 2011, Yamamoto et al., 2014). Furthermore, the highly selective GIRK channel blocker NTC-801 dose-dependently decreased AF inducibility and converted AF to normal sinus rhythm in a canine model (Yamamoto et al., 2014). However, drugs that affect the molecular mechanisms of AF cannot discern the cardiac areas in atria which are the most sensitive to G_i signaling. These findings prove that local and selective inhibition of G_i signaling and the GIRK channel may be a novel therapeutic. High-throughput screening systems would be required to discover selective and potent GIRK channel blockers. Currently, screening methods use membrane potential sensitive dyes or thallium-flux assays to determine GIRK channel activity. These assays are mainly utilized in non-excitabile HEK293 cells with M2R overexpression, require high-end instruments, and allow only an indirect measurement of GIRK channel activity. In addition, such screening assays always require two consecutive pipetting steps:

first, the compound being screened, and then an M2R agonist to activate GIRK channels. Thus, every substance blocking M2R or downstream Gi signaling will appear as a false-positive hit, reducing the specificity of the screening assays. Moreover, diffusion limitation when applying pharmacological substances and every instrument, such as the patch pipette for single cell electrophysiology, would reduce the throughput capability of the assays. Therefore, the research on applying all-optical system for drug screening has increased in recent years. A new study conducted with neuronal tissue opsin OPN5, which activates light-induced Gq signaling pathways, showed the advantage of optogenetics compared to pharmacological screening. In this study, in collaboration with the pharma industry Bayer, more than 200,000 substances were tested to determine whether they block an intermediate step in the Gq signaling cascade. A classical approach using pharmacological activation resulted in over 3,000 false-positive hits. In contrast, the light method did not produce a single false-positive hit. Thus, the tested compound does not affect the optogenetic activation and decisively increases the specificity and, thereby, the drug screening efficiency (Wagdi et al., 2022). In the next decade, it remains to be seen whether the optogenetic approach transferred to iPS cells will become a standard screening method, and pharma companies become increasingly interested in optogenetics as a screening tool. Optogenetic-engineered stem cell-derived cardiovascular cells or even 3D systems could be used as a tool for drug screening. Specifically, actuators like LWO have a better penetrability because red light is not absorbed by myoglobin; therefore, also 3D organotypic systems could be implemented in preclinical drug screening, if red light stimulation compared to blue would be preferred. In theory, optogenetic stimulation in a 3D system could allow for precise and spatially controlled activation of cells, enabling detailed studies of signaling pathways and cellular behavior. Nevertheless, we cannot exclude that false positive hits would be generated when considering the Gi screening also with optogenetics. In fact, LWO cannot discriminate between Gi α and $\beta\gamma$ subunits, and we also do not know whether it could modulate the intrinsic GIRK activity that some patients may have.

Ultimately the real disadvantage for screening is that 3D systems present variability between different labs, and the need for standardization in the organotypic organoids may lead to challenges in validation of important factors for consistent and reproducible research.

Standardized organoids that mimic cardiovascular or heart tissue or lab-on-a-chip hearts expressing optogenetic proteins in specific cell types could further help tackle the effect of balanced and dysbalanced vegetative nerve systems. Combining the LWO Gi activation by red light with possibly red shifted Gs actuators cardiomyocytes and organotypic cardioids would allow to investigate the effect of synergic or alternating stimulation of the muscarinergic and adrenergic pathways on cardiac pathophysiology, just by changing the pacing frequency and wavelength of stimulation.

5 Summary

Embryonic stem (ES) cells and induced pluripotent stem (iPS) cells, known for their pluripotency, provide versatile tools for studying tissue development and disease mechanisms. Their ability to differentiate into various cell types, self-renew, and undergo clonal expansion makes them valuable for addressing challenges in cardiovascular research. Cardiovascular diseases claimed a staggering 17.9 million lives globally in 2019, as reported by the World Health Organization (WHO), making up 32% of total worldwide mortality, particularly in aging populations, thus underscoring the need for innovative approaches.

My working hypothesis presented in this text, was to use ES and iPS cells to explore the early steps of cardiovascular development. These are challenging to investigate directly in vivo due to limited accessibility. First, using murine ES cells, I provided insights into the role of ECM in cardiovascular development. It was known that ILK, a pseudokinase that interacts with cytoskeleton and signaling pathways, in a Tie2-Cre-loxP system to remove ILK from ECs selectively, resulted in vascular disruption (Friedrich et al., 2004). Due to early embryonic death in these mice, the molecular mechanisms causing delayed vascular development remained unexplored. To overcome this limitation, ILK-deficient (-/-) ES cells were employed, and a notable reduction in the formation of vessel-like structures within ILK-deficient (-/-) EBs were observed. Building upon ILK's established role in keratinocytes, where it regulates the stabilization of caveolae within the plasma membrane, I considered its significant involvement in EC signaling pathways for vital processes like proliferation, migration, and apoptosis. Our findings elucidated that ILK affects the signaling pathways, by impairing intracellular Ca^{2+} elevation upon VEGFR2 activation. In essence, ILK emerges as a key orchestrator of tyrosine kinase receptor-dependent signaling, significantly shaping EC development and function by modulating caveolae positioning and upholding the structural integrity of actin and tubulin subcellular networks. One key ECM component, laminin $\gamma 1$, known for its role for embryonic development and in severe skeletal muscle pathologies and cardiac disorders, such as dystrophy, cardiac hypertrophy, and vessel malformation was also studied. Disruption of

laminin $\gamma 1$ resulted in altered basement membrane formation, changes in $\beta 1$ integrin distribution, and collagen VI deposits in 3D cardiomyocyte models. These ECM deposits create isolated pacemaker regions, offering insights into disrupted electrical signal propagation and arrhythmicity.

The discovery of iPS cells enables the generation of cell lines with gene defects from patients with cardiovascular diseases or through gene editing like CRISPR-Cas9. Channelopathy-related diseases, resulting from mutations in ion channel genes, could be used to recreate disease traits in patient-specific iPS cell-derived monotypic cell cultures. The gene mutation in a specific ion channel establishes a clear link between the genetic change and the consequent disease phenotype. Therefore, I focus on exploring LQTS, a monogenetic disorder leading to prolonged cardiac APD due to delayed repolarization, extended QT interval and ventricular arrhythmia, using a mouse model with the prevalent delta KPQ mutation in the cardiac sodium channel. The main objective of the study was to see if disease-specific cardiomyocytes derived from iPS cells obtained from LQTS3 mouse fibroblasts, after undergoing reprogramming and subsequent in vitro differentiation, could accurately replicate the distinct phenotype observed in LQTS3 mice carrying the human mutation. Patient-specific cardiomyocytes accurately replicate the distinct phenotype, mirroring prolonged action potentials and early afterdepolarizations. This finding underscores the potential utility of iPS-derived cardiomyocytes for investigating monogenetic disease mechanisms, even prior to reaching full terminal maturation.

I then focus on developing a scalable method for purifying iPS cell-derived cardiomyocytes for electrophysiological investigations. I optimized a lentiviral-non-clonal gene transfer method with antibiotic selection which offers the potential for expediting cardiomyocyte production. Genetically modified iPS cell-derived cardiomyocytes retain disease characteristics, suitable for automated drug screening using planar patch clamp analysis and scalable microelectrode array technologies.

Next, I used human iPS cell-derived cardiomyocytes from patients harboring a heterozygous p.R1644H mutation. The study demonstrated the cells' potential for evaluating drug responses relevant to LQTS3 treatment in humans. Drugs like mexiletine and ranolazine effectively mitigated LQTS3 features, aligning with clinical effectiveness. This correspondence between iPS-derived cells and clinical data offers a promising screening platform for predicting and validating therapeutic agents.

Finally, the application of optogenetics in ES cell-derived cardiomyocytes introducing LWO expression allowed me to achieve instantaneous-time control over pacemaking activity via Gi signaling pathway activation. LWO is a red light-sensitive opsin, with better tissue penetration compared to blue lights actuators like ChR. The data showed that its red-light responsiveness surpasses traditional pharmacological methods in terms of temporal efficacy in activating and deactivating the Gi intracellular signaling pathways. The specificity and efficacy of optogenetic techniques make them promising for high-throughput all optical drug screening, minimizing false positive or negative hits, due to its specificity in activating the target proteins without interfering with other signaling components and limiting diffusion problems.

In conclusion, pluripotent stem cells, particularly ES and iPS cells, emerge as valuable tools for studying cardiovascular development and serving as reliable models for drug screening, offering insights and applications that contribute to the advancement of cardiovascular research and therapeutics.

6 Overlapping uses of current research activities declaration

This thesis is based on six published original papers. I am the first author of five of the papers, two as a single first author (Malan D, et al. 2013 and Malan D, et al. 2009) and three papers as first coauthor together with Mrs. Zhang M. (Zhang M*, Malan D* et al. 2016) and Mrs. Friedrichs S. (Friedrichs S*, Malan D* et al. 2015; Malan D*, Friedrichs S* et al. 2011), one paper as a co-shared last authorship (Cokić M, Brüggmann T, Sasse P * and Malan D*. 2021)

Together with Mrs. Miao Zhang and Mrs. Stephanie Friedrichs, I designed the experimental settings, acquired analyzed and interpreted the data. I wrote part of the manuscript. The work was initiated and conceived by the authors. The authorship was shared in accordance with their commitment.

In the publication Cokić M, Brüggmann T, Sasse P * and Malan D*, Nov. 2021 I am sharing the last coauthorship with Prof Sasse. I have contributed intellectually, planning the experiments, supervising the collection and the analysis of the data, planning, writing and correcting the text.

There is no overlap with other habilitation theses.

7 Bibliography

Aistrup, G.L., Cokic, I., Ng, J., Gordon, D., Koduri, H., Browne, S., Arapi, D., Segon, Y., Goldstein, J., Angulo, A., et al. (2011). Targeted nonviral gene-based inhibition of Gα(i/o)-mediated vagal signaling in the posterior left atrium decreases vagal-induced atrial fibrillation. *Heart Rhythm* 8, 1722–1729. <https://doi.org/10.1016/j.hrthm.2011.06.018>.

Alday-Parejo, B., Stupp, R., and Rüegg, C. (2019). Are Integrins Still Practicable Targets for Anti-Cancer Therapy? *Cancers (Basel)* 11, E978. <https://doi.org/10.3390/cancers11070978>.

Álvarez-Palomo, B., Veiga, A., Raya, A., Codinach, M., Torrents, S., Ponce Verdugo, L., Rodriguez-Aierbe, C., Cuellar, L., Alenda, R., Arbona, C., et al. (2022). Public Cord Blood Banks as a source of starting material for clinical grade HLA-homozygous induced pluripotent stem cells. *Stem Cell Res Ther* 13, 408. <https://doi.org/10.1186/s13287-022-02961-6>.

Antoninus, A.A., Widowati, W., Wijaya, L., Agustina, D., Puradisastra, S., Sumitro, S.B., Widodo, M.A., and Bachtiar, I. (2015). Human platelet lysate enhances the proliferation of Wharton's jelly-derived mesenchymal stem cells. *Biomarkers and Genomic Medicine* 7, 87–97. <https://doi.org/10.1016/j.bgm.2015.06.001>.

Asahara, T., Murohara, T., Sullivan, A., Silver, M., van der Zee, R., Li, T., Witzenbichler, B., Schatteman, G., and Isner, J.M. (1997). Isolation of Putative Progenitor Endothelial Cells for Angiogenesis. *Science* 275, 964–966. <https://doi.org/10.1126/science.275.5302.964>.

Balser, J.R. (2001). The cardiac sodium channel: gating function and molecular pharmacology. *J Mol Cell Cardiol* 33, 599–613. <https://doi.org/10.1006/jmcc.2000.1346>.

Bar-Nur, O., Russ, H.A., Efrat, S., and Benvenisty, N. (2011). Epigenetic memory and preferential lineage-specific differentiation in induced pluripotent stem cells derived from human pancreatic islet beta cells. *Cell Stem Cell* 9, 17–23. <https://doi.org/10.1016/j.stem.2011.06.007>.

Bayomy, A.F., Bauer, M., Qiu, Y., and Liao, R. (2012). Regeneration in heart disease-Is ECM the key? *Life Sci* 91, 823–827. <https://doi.org/10.1016/j.lfs.2012.08.034>.

Berk, B.C., Fujiwara, K., and Lehoux, S. (2007). ECM remodeling in hypertensive heart disease. *J Clin Invest* 117, 568–575. <https://doi.org/10.1172/JCI31044>.

Blinova, K., Stohman, J., Vicente, J., Chan, D., Johannesen, L., Hortigon-Vinagre, M.P., Zamora, V., Smith, G., Crumb, W.J., Pang, L., et al. (2017). Comprehensive Translational Assessment of Human-Induced Pluripotent Stem Cell Derived Cardiomyocytes for Evaluating Drug-Induced Arrhythmias. *Toxicol Sci* 155, 234–247. <https://doi.org/10.1093/toxsci/kfw200>.

Bloch, W., Fan, Y., Han, J., Xue, S., Schöneberg, T., Ji, G., Lu, Z.J., Walther, M., Fässler, R., Hescheler, J., et al. (2001). Disruption of cytoskeletal integrity impairs Gi-mediated signaling due to displacement of Gi proteins. *J Cell Biol* 154, 753–761. <https://doi.org/10.1083/jcb.200103011>.

Boldt, A., Wetzel, U., Lauschke, J., Weigl, J., Gummert, J., Hindricks, G., Kottkamp, H., and Dhein, S. (2004). Fibrosis in left atrial tissue of patients with atrial fibrillation with and without underlying mitral valve disease. *Heart* 90, 400–405. <https://doi.org/10.1136/hrt.2003.015347>.

Brodehl, A., Rezazadeh, S., Williams, T., Munsie, N.M., Liedtke, D., Oh, T., Ferrier, R., Shen, Y., Jones, S.J.M., Stiegler, A.L., et al. (2019). Mutations in ILK, encoding integrin-linked kinase, are associated with arrhythmogenic cardiomyopathy. *Translational Research* 208, 15–29. <https://doi.org/10.1016/j.trsl.2019.02.004>.

Buikema, J.W., Lee, S., Goodyer, W.R., Maas, R.G., Chirikian, O., Li, G., Miao, Y., Paige, S.L., Lee, D., Wu, H., et al. (2020). Wnt Activation and Reduced Cell-Cell Contact Synergistically Induce Massive Expansion of Functional Human iPSC-Derived Cardiomyocytes. *Cell Stem Cell* 27, 50-63.e5. <https://doi.org/10.1016/j.stem.2020.06.001>.

Burnett, S.D., Blanchette, A.D., Chiu, W.A., and Rusyn, I. (2021). Cardiotoxicity Hazard and Risk Characterization of ToxCast Chemicals Using Human Induced Pluripotent Stem Cell-Derived Cardiomyocytes from Multiple Donors. *Chem Res Toxicol* 34, 2110–2124. <https://doi.org/10.1021/acs.chemrestox.1c00203>.

Burnight, E.R., Gupta, M., Wiley, L.A., Anfinson, K.R., Tran, A., Triboulet, R., Hoffmann, J.M., Klaahsen, D.L., Andorf, J.L., Jiao, C., et al. (2017). Using CRISPR-Cas9 to Generate Gene-Corrected Autologous iPSCs for the Treatment of Inherited Retinal Degeneration. *Molecular Therapy* 25, 1999–2013. <https://doi.org/10.1016/j.ymthe.2017.05.015>.

- Calaghan, S., Kozera, L., and White, E. (2008). Compartmentalisation of cAMP-dependent signalling by caveolae in the adult cardiac myocyte. *J Mol Cell Cardiol* 45, 88–92. <https://doi.org/10.1016/j.yjmcc.2008.04.004>.
- Cao, L., Meer, A. van der, Passier, R., and Verbeek, F.J. (2020). High Throughput Image Analysis for Cardiotoxicity Study using Human Pluripotent Stem Cell-Derived Cardiomyocytes. *J Cell Immunol Volume 2*, 326–332. <https://doi.org/10.33696/immunology.2.062>.
- Capecchi, M.R. (2005). Gene targeting in mice: functional analysis of the mammalian genome for the twenty-first century. *Nat Rev Genet* 6, 507–512. <https://doi.org/10.1038/nrg1619>.
- Carboni, N., Marrosu, G., Porcu, M., Mateddu, A., Solla, E., Cocco, E., Maioli, M.A., Oppo, V., Piras, R., and Marrosu, M.G. (2011). Dilated cardiomyopathy with conduction defects in a patient with partial merosin deficiency due to mutations in the laminin- α 2-chain gene: A chance association or a novel phenotype? *Muscle & Nerve* 44, 826–828. <https://doi.org/10.1002/mus.22228>.
- Carter, J.L., Halmai, J.A.N.M., and Fink, K.D. (2020). The iNs and Outs of Direct Reprogramming to Induced Neurons. *Front. Genome Ed.* 2, 7. <https://doi.org/10.3389/fgeed.2020.00007>.
- Chesnais, F., Hue, J., Roy, E., Branco, M., Stokes, R., Pellon, A., Le Caillec, J., Elbahtety, E., Battilocchi, M., Danovi, D., et al. (2022). High-content image analysis to study phenotypic heterogeneity in endothelial cell monolayers. *Journal of Cell Science* 135, jcs259104. <https://doi.org/10.1242/jcs.259104>.
- Chidlow, J.H., and Sessa, W.C. (2010). Caveolae, caveolins, and cavins: complex control of cellular signalling and inflammation. *Cardiovasc Res* 86, 219–225. <https://doi.org/10.1093/cvr/cvq075>.
- Chong, J.J.H., Yang, X., Don, C.W., Minami, E., Liu, Y.-W., Weyers, J.J., Mahoney, W.M., Van Biber, B., Cook, S.M., Palpant, N.J., et al. (2014). Human embryonic-stem-cell-derived cardiomyocytes regenerate non-human primate hearts. *Nature* 510, 273–277. <https://doi.org/10.1038/nature13233>.
- Codrici, E., Albuлесcu, L., Popescu, I.D., Mihai, S., Enciu, A.-M., Albuлесcu, R., Tanase, C., and Hinescu, M.E. (2018). Caveolin-1-Knockout Mouse as a Model of Inflammatory Diseases. *J Immunol Res* 2018, 2498576. <https://doi.org/10.1155/2018/2498576>.

Cokić, M., Bruegmann, T., Sasse, P., and Malan, D. (2021). Optogenetic Stimulation of Gi Signaling Enables Instantaneous Modulation of Cardiomyocyte Pacemaking. *Front Physiol* 12, 768495. <https://doi.org/10.3389/fphys.2021.768495>.

Corsini, N.S., and Knoblich, J.A. (2022). Human organoids: New strategies and methods for analyzing human development and disease. *Cell* 185, 2756–2769. <https://doi.org/10.1016/j.cell.2022.06.051>.

De La Mata, A., Tajada, S., O'Dwyer, S., Matsumoto, C., Dixon, R.E., Hariharan, N., Moreno, C.M., and Santana, L.F. (2019). BIN1 Induces the Formation of T-Tubules and Adult-Like Ca²⁺ Release Units in Developing Cardiomyocytes. *Stem Cells* 37, 54–64. <https://doi.org/10.1002/stem.2927>.

Denning, C., Borgdorff, V., Crutchley, J., Firth, K.S.A., George, V., Kalra, S., Kondrashov, A., Hoang, M.D., Mosqueira, D., Patel, A., et al. (2016). Cardiomyocytes from human pluripotent stem cells: From laboratory curiosity to industrial biomedical platform. *Biochim Biophys Acta* 1863, 1728–1748. <https://doi.org/10.1016/j.bbamcr.2015.10.014>.

Dhamoon, A.S., and Jalife, J. (2005). The inward rectifier current (IK1) controls cardiac excitability and is involved in arrhythmogenesis. *Heart Rhythm* 2, 316–324. <https://doi.org/10.1016/j.hrthm.2004.11.012>.

Dobrev, D., Graf, E., Wettwer, E., Himmel, H.M., Hála, O., Doerfel, C., Christ, T., Schüler, S., and Ravens, U. (2001). Molecular basis of downregulation of G-protein-coupled inward rectifying K(+) current (I(K,ACh) in chronic human atrial fibrillation: decrease in GIRK4 mRNA correlates with reduced I(K,ACh) and muscarinic receptor-mediated shortening of action potentials. *Circulation* 104, 2551–2557. <https://doi.org/10.1161/hc4601.099466>.

Drab, M., Verkade, P., Elger, M., Kasper, M., Lohn, M., Lauterbach, B., Menne, J., Lindschau, C., Mende, F., Luft, F.C., et al. (2001). Loss of caveolae, vascular dysfunction, and pulmonary defects in caveolin-1 gene-disrupted mice. *Science* 293, 2449–2452. <https://doi.org/10.1126/science.1062688>.

Efrat, S. (2021). Epigenetic Memory: Lessons From iPS Cells Derived From Human β Cells. *Frontiers in Endocrinology* 11. .

Eiraku, M., Watanabe, K., Matsuo-Takasaki, M., Kawada, M., Yonemura, S., Matsumura, M., Wataya, T., Nishiyama, A., Muguruma, K., and Sasai, Y. (2008). Self-organized formation of polarized cortical

tissues from ESCs and its active manipulation by extrinsic signals. *Cell Stem Cell* 3, 519–532. <https://doi.org/10.1016/j.stem.2008.09.002>.

Elanzew, A., Nießing, B., Langendoerfer, D., Rippel, O., Piotrowski, T., Schenk, F., Kulik, M., Peitz, M., Breitzkreuz, Y., Jung, S., et al. (2020). The StemCellFactory: A Modular System Integration for Automated Generation and Expansion of Human Induced Pluripotent Stem Cells. *Front. Bioeng. Biotechnol.* 8, 580352. <https://doi.org/10.3389/fbioe.2020.580352>.

Ergir, E., Oliver-De La Cruz, J., Fernandes, S., Cassani, M., Niro, F., Pereira-Sousa, D., Vrbský, J., Vinarský, V., Perestrelo, A.R., Debellis, D., et al. (2022). Generation and maturation of human iPSC-derived 3D organotypic cardiac microtissues in long-term culture. *Sci Rep* 12, 17409. <https://doi.org/10.1038/s41598-022-22225-w>.

Erharter, A., Rizzi, S., Mertens, J., and Edenhofer, F. (2019). Take the shortcut - direct conversion of somatic cells into induced neural stem cells and their biomedical applications. *FEBS Lett* 593, 3353–3369. <https://doi.org/10.1002/1873-3468.13656>.

Eschenhagen, T., Eder, A., Vollert, I., and Hansen, A. (2012). Physiological aspects of cardiac tissue engineering. *Am J Physiol Heart Circ Physiol* 303, H133-143. <https://doi.org/10.1152/ajpheart.00007.2012>.

Evans, M.J., and Kaufman, M.H. (1981). Establishment in culture of pluripotential cells from mouse embryos. *Nature* 292, 154–156. <https://doi.org/10.1038/292154a0>.

Fässler, R., Georges-Labouesse, E., and Hirsch, E. (1996). Genetic analyses of integrin function in mice. *Current Opinion in Cell Biology* 8, 641–646. [https://doi.org/10.1016/S0955-0674\(96\)80105-0](https://doi.org/10.1016/S0955-0674(96)80105-0).

Festag, M., Sehner, C., Steinberg, P., and Viertel, B. (2007). An in vitro embryotoxicity assay based on the disturbance of the differentiation of murine embryonic stem cells into endothelial cells. I: Establishment of the differentiation protocol. *Toxicology in Vitro* 21, 1619–1630. <https://doi.org/10.1016/j.tiv.2007.06.018>.

Friedrich, E.B., Liu, E., Sinha, S., Cook, S., Milstone, D.S., MacRae, C.A., Mariotti, M., Kuhlencordt, P.J., Force, T., Rosenzweig, A., et al. (2004). Integrin-Linked Kinase Regulates Endothelial Cell Survival and Vascular Development. *Mol Cell Biol* 24, 8134–8144. <https://doi.org/10.1128/MCB.24.18.8134-8144.2004>.

- Friedrichs, S., Malan, D., Voss, Y., and Sasse, P. (2015). Scalable Electrophysiological Investigation of iPS Cell-Derived Cardiomyocytes Obtained by a Lentiviral Purification Strategy. *J Clin Med* 4, 102–123. <https://doi.org/10.3390/jcm4010102>.
- Galbiati, F., Razani, B., and Lisanti, M.P. (2001). Caveolae and caveolin-3 in muscular dystrophy. *Trends in Molecular Medicine* 7, 435–441. [https://doi.org/10.1016/S1471-4914\(01\)02105-0](https://doi.org/10.1016/S1471-4914(01)02105-0).
- Ghaedi, M., and Niklason, L.E. (2019). Human Pluripotent Stem Cells (iPSC) Generation, Culture, and Differentiation to Lung Progenitor Cells. *Methods Mol Biol* 1576, 55–92. https://doi.org/10.1007/7651_2016_11.
- Glentis, A., Gurchenkov, V., and Vignjevic, D.M. (2014). Assembly, heterogeneity, and breaching of the basement membranes. *Cell Adhesion & Migration* 8, 236–245. <https://doi.org/10.4161/cam.28733>.
- Gouas, L., Bellocq, C., Berthet, M., Potet, F., Demolombe, S., Forhan, A., Lescasse, R., Simon, F., Balkau, B., Denjoy, I., et al. (2004). New KCNQ1 mutations leading to haploinsufficiency in a general population; Defective trafficking of a KvLQT1 mutant. *Cardiovasc Res* 63, 60–68. <https://doi.org/10.1016/j.cardiores.2004.02.011>.
- Guo, D., Liu, H., Gao, G., Liu, Y., Zhuang, Y., Yang, F., Wang, K., Zhou, T., Qin, D., Hong, L., et al. (2017). Creating a patient carried Men1 gene point mutation on wild type iPSCs locus mediated by CRISPR/Cas9 and ssODN. *Stem Cell Research* 18, 67–69. <https://doi.org/10.1016/j.scr.2016.12.007>.
- Guo, J., Tian, Q., Barth, M., Xian, W., Ruppenthal, S., Schaefers, H.-J., Chen, Z., Moretti, A., Laugwitz, K.-L., and Lipp, P. (2022). Human BIN1 isoforms grow, maintain, and regenerate excitation–contraction couplings in adult rat and human stem cell-derived cardiomyocytes. *Cardiovascular Research* 118, 1479–1491. <https://doi.org/10.1093/cvr/cvab195>.
- Gurdon, J.B. (1962). The developmental capacity of nuclei taken from intestinal epithelium cells of feeding tadpoles. *J Embryol Exp Morphol* 10, 622–640. .
- Gyöngyösi, M., Wojakowski, W., Navarese, E.P., Moye, L.À., and ACCRUE Investigators (2016). Meta-Analyses of Human Cell-Based Cardiac Regeneration Therapies: Controversies in Meta-Analyses Results on Cardiac Cell-Based Regenerative Studies. *Circ Res* 118, 1254–1263. <https://doi.org/10.1161/CIRCRESAHA.115.307347>.

Hagiwara, Y., Fujita, M., Imamura, M., Noguchi, S., and Sasaoka, T. (2006). Caveolin-3 deficiency decreases the gene expression level of osteopontin in mdx mouse skeletal muscle. *Acta Myol* 25, 53–61. .

Han, L., Liu, F., Li, Q., Qing, T., Zhai, Z., Xia, Z., and Li, J. (2020). The Efficacy of Beta-Blockers in Patients With Long QT Syndrome 1-3 According to Individuals' Gender, Age, and QTc Intervals: A Network Meta-analysis. *Front Pharmacol* 11, 579525. <https://doi.org/10.3389/fphar.2020.579525>.

Hanna, P., Buch, E., Stavrakis, S., Meyer, C., Tompkins, J.D., Ardell, J.L., and Shivkumar, K. (2021). Neuroscientific therapies for atrial fibrillation. *Cardiovasc Res* 117, 1732–1745. <https://doi.org/10.1093/cvr/cvab172>.

Hedley, P.L., Jørgensen, P., Schlamowitz, S., Wangari, R., Moolman-Smook, J., Brink, P.A., Kanter, J.K., Corfield, V.A., and Christiansen, M. (2009). The genetic basis of long QT and short QT syndromes: a mutation update. *Hum Mutat* 30, 1486–1511. <https://doi.org/10.1002/humu.21106>.

Helbling-Leclerc, A., Zhang, X., Topaloglu, H., Cruaud, C., Tesson, F., Weissenbach, J., Tomé, F.M.S., Schwartz, K., Fardeau, M., Tryggvason, K., et al. (1995). Mutations in the laminin $\alpha 2$ -chain gene (LAMA2) cause merosin-deficient congenital muscular dystrophy. *Nat Genet* 11, 216–218. <https://doi.org/10.1038/ng1095-216>.

Hoekstra, M., Mummery, C.L., Wilde, A.A.M., Bezzina, C.R., and Verkerk, A.O. (2012). Induced pluripotent stem cell derived cardiomyocytes as models for cardiac arrhythmias. *Front Physiol* 3, 346. <https://doi.org/10.3389/fphys.2012.00346>.

Hofbauer, P., Jahnel, S.M., Papai, N., Giesshammer, M., Deyett, A., Schmidt, C., Penc, M., Tavernini, K., Grdseloff, N., Meledeth, C., et al. (2021). Cardioids reveal self-organizing principles of human cardiogenesis. *Cell* 184, 3299-3317.e22. <https://doi.org/10.1016/j.cell.2021.04.034>.

Hohenester, E., and Yurchenco, P.D. (2013). Laminins in basement membrane assembly. *Cell Adhesion & Migration* 7, 56–63. <https://doi.org/10.4161/cam.21831>.

Hou, P., Li, Y., Zhang, X., Liu, C., Guan, J., Li, H., Zhao, T., Ye, J., Yang, W., Liu, K., et al. (2013). Pluripotent stem cells induced from mouse somatic cells by small-molecule compounds. *Science* 341, 651–654. <https://doi.org/10.1126/science.1239278>.

Hrvatin, S., O'Donnell, C.W., Deng, F., Millman, J.R., Pagliuca, F.W., Dilorio, P., Rezania, A., Gifford, D.K., and Melton, D.A. (2014). Differentiated human stem cells resemble fetal, not adult, β cells. *Proc Natl Acad Sci U S A* *111*, 3038–3043. <https://doi.org/10.1073/pnas.1400709111>.

Iozzo, R.V., and Gubbiotti, M.A. (2018). Extracellular matrix: The driving force of mammalian diseases. *Matrix Biology* *71–72*, 1–9. <https://doi.org/10.1016/j.matbio.2018.03.023>.

Itzhaki, I., Maizels, L., Huber, I., Zwi-Dantsis, L., Caspi, O., Winterstern, A., Feldman, O., Gepstein, A., Arbel, G., Hammerman, H., et al. (2011). Modelling the long QT syndrome with induced pluripotent stem cells. *Nature* *471*, 225–229. <https://doi.org/10.1038/nature09747>.

Jang, I.H., Kim, J.H., Lee, B.D., Bae, S.S., Park, M.H., Suh, P.G., and Ryu, S.H. (2001). Localization of phospholipase C-gamma1 signaling in caveolae: importance in EGF-induced phosphoinositide hydrolysis but not in tyrosine phosphorylation. *FEBS Lett* *491*, 4–8. [https://doi.org/10.1016/s0014-5793\(01\)02165-2](https://doi.org/10.1016/s0014-5793(01)02165-2).

Kadari, A., Mekala, S., Wagner, N., Malan, D., Köth, J., Doll, K., Stappert, L., Eckert, D., Peitz, M., Matthes, J., et al. (2015). Robust Generation of Cardiomyocytes from Human iPS Cells Requires Precise Modulation of BMP and WNT Signaling. *Stem Cell Rev and Rep* *11*, 560–569. <https://doi.org/10.1007/s12015-014-9564-6>.

Kamakura, T., Makiyama, T., Sasaki, K., Yoshida, Y., Wuriyanghai, Y., Chen, J., Hattori, T., Ohno, S., Kita, T., Horie, M., et al. (2013). Ultrastructural maturation of human-induced pluripotent stem cell-derived cardiomyocytes in a long-term culture. *Circ J* *77*, 1307–1314. <https://doi.org/10.1253/circj.cj-12-0987>.

Kehat, I., Kenyagin-Karsenti, D., Snir, M., Segev, H., Amit, M., Gepstein, A., Livne, E., Binah, O., Itskovitz-Eldor, J., and Gepstein, L. (2001). Human embryonic stem cells can differentiate into myocytes with structural and functional properties of cardiomyocytes. *J Clin Invest* *108*, 407–414. .

Kim, H., Kamm, R.D., Vunjak-Novakovic, G., and Wu, J.C. (2022). Progress in multicellular human cardiac organoids for clinical applications. *Cell Stem Cell* *29*, 503–514. <https://doi.org/10.1016/j.stem.2022.03.012>.

- Kim, J., Efe, J.A., Zhu, S., Talantova, M., Yuan, X., Wang, S., Lipton, S.A., Zhang, K., and Ding, S. (2011a). Direct reprogramming of mouse fibroblasts to neural progenitors. *Proc Natl Acad Sci U S A* *108*, 7838–7843. <https://doi.org/10.1073/pnas.1103113108>.
- Kim, S.-H., Turnbull, J., and Guimond, S. (2011b). Extracellular matrix and cell signalling: the dynamic cooperation of integrin, proteoglycan and growth factor receptor. *J Endocrinol* *209*, 139–151. <https://doi.org/10.1530/JOE-10-0377>.
- Kim, T.M., Lee, R.H., Kim, M.S., Lewis, C.A., and Park, C. (2023). ETV2/ER71, the key factor leading the paths to vascular regeneration and angiogenic reprogramming. *Stem Cell Research & Therapy* *14*, 41. <https://doi.org/10.1186/s13287-023-03267-x>.
- Kirby, R.J., Divlianska, D.B., Whig, K., Bryan, N., Morfa, C.J., Koo, A., Nguyen, K.H., Maloney, P., Peddibhotla, S., Sessions, E.H., et al. (2018). Discovery of Novel Small-Molecule Inducers of Heme Oxygenase-1 That Protect Human iPSC-Derived Cardiomyocytes from Oxidative Stress. *J Pharmacol Exp Ther* *364*, 87–96. <https://doi.org/10.1124/jpet.117.243717>.
- Klug, M.G., Soonpaa, M.H., Koh, G.Y., and Field, L.J. (1996). Genetically selected cardiomyocytes from differentiating embryonic stem cells form stable intracardiac grafts. *J. Clin. Invest.* *98*, 216–224. <https://doi.org/10.1172/JCI118769>.
- Knöll, R., Postel, R., Wang, J., Krätzner, R., Hennecke, G., Vacaru, A.M., Vakeel, P., Schubert, C., Murthy, K., Rana, B.K., et al. (2007). Laminin- α 4 and Integrin-Linked Kinase Mutations Cause Human Cardiomyopathy Via Simultaneous Defects in Cardiomyocytes and Endothelial Cells. *Circulation* *116*, 515–525. <https://doi.org/10.1161/CIRCULATIONAHA.107.689984>.
- Knollmann, B.C. (2013). Induced pluripotent stem cell-derived cardiomyocytes: boutique science or valuable arrhythmia model? *Circ Res* *112*, 969–976; discussion 976. <https://doi.org/10.1161/CIRCRESAHA.112.300567>.
- Kolossov, E., Bostani, T., Roell, W., Breitbach, M., Pillekamp, F., Nygren, J.M., Sasse, P., Rubenchik, O., Fries, J.W.U., Wenzel, D., et al. (2006). Engraftment of engineered ES cell-derived cardiomyocytes but not BM cells restores contractile function to the infarcted myocardium. *J Exp Med* *203*, 2315–2327. <https://doi.org/10.1084/jem.20061469>.

- Kubikova, I., Konecna, H., Sedo, O., Zdrahal, Z., Rehulka, P., Hribkova, H., Rehulkova, H., Hampl, A., Chmelik, J., and Dvorak, P. (2009). Proteomic profiling of human embryonic stem cell-derived microvesicles reveals a risk of transfer of proteins of bovine and mouse origin. *Cytotherapy* 11, 330–340. <https://doi.org/10.1080/14653240802595531>.
- Laco, F., Lam, A.T.-L., Woo, T.-L., Tong, G., Ho, V., Soong, P.-L., Grishina, E., Lin, K.-H., Reuveny, S., and Oh, S.K.-W. (2020). Selection of human induced pluripotent stem cells lines optimization of cardiomyocytes differentiation in an integrated suspension microcarrier bioreactor. *Stem Cell Res Ther* 11, 118. <https://doi.org/10.1186/s13287-020-01618-6>.
- Lancaster, M.A., Renner, M., Martin, C.-A., Wenzel, D., Bicknell, L.S., Hurles, M.E., Homfray, T., Penninger, J.M., Jackson, A.P., and Knoblich, J.A. (2013). Cerebral organoids model human brain development and microcephaly. *Nature* 501, 373–379. <https://doi.org/10.1038/nature12517>.
- Lee, J., Rabbani, C.C., Gao, H., Steinhart, M.R., Woodruff, B.M., Pflum, Z.E., Kim, A., Heller, S., Liu, Y., Shipchandler, T.Z., et al. (2020). Hair-bearing human skin generated entirely from pluripotent stem cells. *Nature* 582, 399–404. <https://doi.org/10.1038/s41586-020-2352-3>.
- Leo, F., Hutzler, B., Ruddiman, C.A., Isakson, B.E., and Cortese-Krott, M.M. (2020). Cellular microdomains for nitric oxide signaling in endothelium and red blood cells. *Nitric Oxide* 96, 44–53. <https://doi.org/10.1016/j.niox.2020.01.002>.
- Lewandowski, J., Rozwadowska, N., Kolanowski, T.J., Malcher, A., Zimna, A., Rugowska, A., Fiedorowicz, K., Łabędź, W., Kubaszewski, Ł., Chojnacka, K., et al. (2018). The impact of in vitro cell culture duration on the maturation of human cardiomyocytes derived from induced pluripotent stem cells of myogenic origin. *Cell Transplant* 27, 1047–1067. <https://doi.org/10.1177/0963689718779346>.
- Lewis-Israeli, Y.R., Wasserman, A.H., Gabalski, M.A., Volmert, B.D., Ming, Y., Ball, K.A., Yang, W., Zou, J., Ni, G., Pajares, N., et al. (2021). Self-assembling human heart organoids for the modeling of cardiac development and congenital heart disease. *Nat Commun* 12, 5142. <https://doi.org/10.1038/s41467-021-25329-5>.
- Lian, X., Hsiao, C., Wilson, G., Zhu, K., Hazeltine, L.B., Azarin, S.M., Raval, K.K., Zhang, J., Kamp, T.J., and Palecek, S.P. (2012). Robust cardiomyocyte differentiation from human pluripotent stem cells via

temporal modulation of canonical Wnt signaling. *Proceedings of the National Academy of Sciences* 109, E1848–E1857. <https://doi.org/10.1073/pnas.1200250109>.

Lian, X., Zhang, J., Azarin, S.M., Zhu, K., Hazeltine, L.B., Bao, X., Hsiao, C., Kamp, T.J., and Palecek, S.P. (2013). Directed cardiomyocyte differentiation from human pluripotent stem cells by modulating Wnt/ β -catenin signaling under fully defined conditions. *Nat Protoc* 8, 162–175. <https://doi.org/10.1038/nprot.2012.150>.

Lian, X., Bao, X., Al-Ahmad, A., Liu, J., Wu, Y., Dong, W., Dunn, K.K., Shusta, E.V., and Palecek, S.P. (2014). Efficient Differentiation of Human Pluripotent Stem Cells to Endothelial Progenitors via Small-Molecule Activation of WNT Signaling. *Stem Cell Reports* 3, 804–816. <https://doi.org/10.1016/j.stemcr.2014.09.005>.

Lian, X., Bao, X., Zilberter, M., Westman, M., Fisahn, A., Hsiao, C., Hazeltine, L.B., Dunn, K.K., Kamp, T.J., and Palecek, S.P. (2015). Chemically defined, albumin-free human cardiomyocyte generation. *Nat Methods* 12, 595–596. <https://doi.org/10.1038/nmeth.3448>.

Lin, Y., and Zou, J. (2020). Differentiation of Cardiomyocytes from Human Pluripotent Stem Cells in Fully Chemically Defined Conditions. *STAR Protocols* 1, 100015. <https://doi.org/10.1016/j.xpro.2020.100015>.

Lundy, S.D., Zhu, W.-Z., Regnier, M., and Laflamme, M.A. (2013). Structural and functional maturation of cardiomyocytes derived from human pluripotent stem cells. *Stem Cells Dev* 22, 1991–2002. <https://doi.org/10.1089/scd.2012.0490>.

Ma, Y., Ramezani, A., Lewis, R., Hawley, R.G., and Thomson, J.A. (2003). High-level sustained transgene expression in human embryonic stem cells using lentiviral vectors. *Stem Cells* 21, 111–117. <https://doi.org/10.1634/stemcells.21-1-111>.

Makielski, J.C. (2016). Late sodium current: A mechanism for angina, heart failure, and arrhythmia. *Trends in Cardiovascular Medicine* 26, 115–122. <https://doi.org/10.1016/j.tcm.2015.05.006>.

Makowka, P., Bruegmann, T., Dusend, V., Malan, D., Beiert, T., Hesse, M., Fleischmann, B.K., and Sasse, P. (2019). Optogenetic stimulation of Gs-signaling in the heart with high spatio-temporal precision. *Nature Communications* 10, 1281. <https://doi.org/10.1038/s41467-019-09322-7>.

- Malan, D., Reppel, M., Dobrowolski, R., Roell, W., Smyth, N., Hescheler, J., Paulsson, M., Bloch, W., and Fleischmann, B.K. (2009). Lack of laminin gamma1 in embryonic stem cell-derived cardiomyocytes causes inhomogeneous electrical spreading despite intact differentiation and function. *Stem Cells* 27, 88–99. <https://doi.org/10.1634/stemcells.2008-0335>.
- Malan, D., Wenzel, D., Schmidt, A., Geisen, C., Raible, A., Böck, B., Fleischmann, B.K., and Bloch, W. (2010). Endothelial beta1 integrins regulate sprouting and network formation during vascular development. *Development* 137, 993–1002. <https://doi.org/10.1242/dev.045377>.
- Malan, D., Friedrichs, S., Fleischmann, B.K., and Sasse, P. (2011). Cardiomyocytes obtained from induced pluripotent stem cells with long-QT syndrome 3 recapitulate typical disease-specific features in vitro. *Circ Res* 109, 841–847. <https://doi.org/10.1161/CIRCRESAHA.111.243139>.
- Malan, D., Elischer, A., Hesse, M., Wickström, S.A., Fleischmann, B.K., and Bloch, W. (2013). Deletion of integrin linked kinase in endothelial cells results in defective RTK signaling caused by caveolin 1 mislocalization. *Development* 140, 987–995. <https://doi.org/10.1242/dev.091298>.
- Malan, D., Zhang, M., Stallmeyer, B., Müller, J., Fleischmann, B.K., Schulze-Bahr, E., Sasse, P., and Greber, B. (2016). Human iPS cell model of type 3 long QT syndrome recapitulates drug-based phenotype correction. *Basic Res Cardiol* 111, 14. <https://doi.org/10.1007/s00395-016-0530-0>.
- Mannhardt, I., Breckwoldt, K., Letuffe-Brenière, D., Schaaf, S., Schulz, H., Neuber, C., Benzin, A., Werner, T., Eder, A., Schulze, T., et al. (2016). Human Engineered Heart Tissue: Analysis of Contractile Force. *Stem Cell Reports* 7, 29–42. <https://doi.org/10.1016/j.stemcr.2016.04.011>.
- Marques, J., Duarte, S.T., Costa, S., Jacinto, S., Oliveira, J., Oliveira, M.E., Santos, R., Bronze-da-Rocha, E., Silvestre, A.R., Calado, E., et al. (2014). Atypical phenotype in two patients with LAMA2 mutations. *Neuromuscul Disord* 24, 419–424. <https://doi.org/10.1016/j.nmd.2014.01.004>.
- Masseck, O.A., Spoida, K., Dalkara, D., Maejima, T., Rubelowski, J.M., Wallhorn, L., Deneris, E.S., and Herlitze, S. (2014). Vertebrate cone opsins enable sustained and highly sensitive rapid control of Gi/o signaling in anxiety circuitry. *Neuron* 81, 1263–1273. <https://doi.org/10.1016/j.neuron.2014.01.041>.
- Matsa, E., Rajamohan, D., Dick, E., Young, L., Mellor, I., Staniforth, A., and Denning, C. (2011). Drug evaluation in cardiomyocytes derived from human induced pluripotent stem cells carrying a long QT syndrome type 2 mutation. *Eur Heart J* 32, 952–962. <https://doi.org/10.1093/eurheartj/ehr073>.

- Miner, J.H., Li, C., Mudd, J.L., Go, G., and Sutherland, A.E. (2004). Compositional and structural requirements for laminin and basement membranes during mouse embryo implantation and gastrulation. *Development* *131*, 2247–2256. <https://doi.org/10.1242/dev.01112>.
- Moik, D., Böttcher, A., Makhina, T., Grashoff, C., Bulus, N., Zent, R., and Fässler, R. (2013). Mutations in the paxillin-binding site of integrin-linked kinase (ILK) destabilize the pseudokinase domain and cause embryonic lethality in mice. *J Biol Chem* *288*, 18863–18871. <https://doi.org/10.1074/jbc.M113.470476>.
- Morello, F., Perino, A., and Hirsch, E. (2009). Phosphoinositide 3-kinase signalling in the vascular system. *Cardiovascular Research* *82*, 261–271. <https://doi.org/10.1093/cvr/cvn325>.
- Morrison, S.J., Wandycz, A.M., Hemmati, H.D., Wright, D.E., and Weissman, I.L. (1997). Identification of a lineage of multipotent hematopoietic progenitors. *Development* *124*, 1929–1939. <https://doi.org/10.1242/dev.124.10.1929>.
- Mummery, C., Ward-van Oostwaard, D., Doevendans, P., Spijker, R., van den Brink, S., Hassink, R., van der Heyden, M., Opthof, T., Pera, M., de la Riviere, A.B., et al. (2003). Differentiation of Human Embryonic Stem Cells to Cardiomyocytes. *Circulation* *107*, 2733–2740. <https://doi.org/10.1161/01.CIR.0000068356.38592.68>.
- Musunuru, K., Sheikh, F., Gupta, R.M., Houser, S.R., Maher, K.O., Milan, D.J., Terzic, A., and Wu, J.C. (2018). Induced Pluripotent Stem Cells for Cardiovascular Disease Modeling and Precision Medicine: A Scientific Statement From the American Heart Association. *Circulation: Genomic and Precision Medicine* *11*, e000043. <https://doi.org/10.1161/HCG.0000000000000043>.
- Naba, A., Clauser, K.R., Ding, H., Whittaker, C.A., Carr, S.A., and Hynes, R.O. (2016). The extracellular matrix: Tools and insights for the “omics” era. *Matrix Biology* *49*, 10–24. <https://doi.org/10.1016/j.matbio.2015.06.003>.
- Nakagawa, M., Koyanagi, M., Tanabe, K., Takahashi, K., Ichisaka, T., Aoi, T., Okita, K., Mochiduki, Y., Takizawa, N., and Yamanaka, S. (2008). Generation of induced pluripotent stem cells without Myc from mouse and human fibroblasts. *Nat Biotechnol* *26*, 101–106. <https://doi.org/10.1038/nbt1374>.
- Nam, Y.-J., Song, K., Luo, X., Daniel, E., Lambeth, K., West, K., Hill, J.A., DiMaio, J.M., Baker, L.A., Bassel-Duby, R., et al. (2013). Reprogramming of human fibroblasts toward a cardiac fate. *Proc. Natl. Acad. Sci. U.S.A.* *110*, 5588–5593. <https://doi.org/10.1073/pnas.1301019110>.

- Nattel, S. (2017). Molecular and Cellular Mechanisms of Atrial Fibrosis in Atrial Fibrillation. *JACC: Clinical Electrophysiology* 3, 425–435. <https://doi.org/10.1016/j.jacep.2017.03.002>.
- Nattel, S., and Dobrev, D. (2012). The multidimensional role of calcium in atrial fibrillation pathophysiology: mechanistic insights and therapeutic opportunities. *Eur Heart J* 33, 1870–1877. <https://doi.org/10.1093/eurheartj/ehs079>.
- Navarrete, E.G., Liang, P., Lan, F., Sanchez-Freire, V., Simmons, C., Gong, T., Sharma, A., BurrIDGE, P.W., Patlolla, B., Lee, A.S., et al. (2013). Screening Drug-Induced Arrhythmia Using Human Induced Pluripotent Stem Cell–Derived Cardiomyocytes and Low-Impedance Microelectrode Arrays. *Circulation* 128, S3–S13. <https://doi.org/10.1161/CIRCULATIONAHA.112.000570>.
- Noguchi, S., Yasui, Y., Iwasaki, J., Kumazaki, M., Yamada, N., Naito, S., and Akao, Y. (2013). Replacement treatment with microRNA-143 and -145 induces synergistic inhibition of the growth of human bladder cancer cells by regulating PI3K/Akt and MAPK signaling pathways. *Cancer Letters* 328, 353–361. <https://doi.org/10.1016/j.canlet.2012.10.017>.
- Nuyens, D., Stengl, M., Dugarmaa, S., Rossenbacker, T., Compennolle, V., Rudy, Y., Smits, J.F., Flameng, W., Clancy, C.E., Moons, L., et al. (2001). Abrupt rate accelerations or premature beats cause life-threatening arrhythmias in mice with long-QT3 syndrome. *Nat Med* 7, 1021–1027. <https://doi.org/10.1038/nm0901-1021>.
- Okita, K., Ichisaka, T., and Yamanaka, S. (2007). Generation of germline-competent induced pluripotent stem cells. *Nature* 448, 313–317. <https://doi.org/10.1038/nature05934>.
- Oliveira, S.D.S., Chen, J., Castellon, M., Mao, M., Raj, J.U., Comhair, S., Erzurum, S., Silva, C.L.M., Machado, R.F., Bonini, M.G., et al. (2019). Injury-Induced Shedding of Extracellular Vesicles Depletes Endothelial Cells of Cav-1 (Caveolin-1) and Enables TGF- β (Transforming Growth Factor- β)-Dependent Pulmonary Arterial Hypertension. *Arterioscler Thromb Vasc Biol* 39, 1191–1202. <https://doi.org/10.1161/ATVBAHA.118.312038>.
- Ordoño, J., Pérez-Amodio, S., Ball, K., Aguirre, A., and Engel, E. (2020). Lactate promotes cardiomyocyte dedifferentiation through metabolic reprogramming (Bioengineering).

- Orlova, V.V., van den Hil, F.E., Petrus-Reurer, S., Drabsch, Y., ten Dijke, P., and Mummery, C.L. (2014). Generation, expansion and functional analysis of endothelial cells and pericytes derived from human pluripotent stem cells. *Nat Protoc* 9, 1514–1531. <https://doi.org/10.1038/nprot.2014.102>.
- Paik, D.T., Chandy, M., and Wu, J.C. (2020). Patient and Disease–Specific Induced Pluripotent Stem Cells for Discovery of Personalized Cardiovascular Drugs and Therapeutics. *Pharmacol Rev* 72, 320–342. <https://doi.org/10.1124/pr.116.013003>.
- Papp, B., and Plath, K. (2011). Reprogramming to pluripotency: stepwise resetting of the epigenetic landscape. *Cell Res* 21, 486–501. <https://doi.org/10.1038/cr.2011.28>.
- Park, H., Yamamoto, H., Mohn, L., Ambühl, L., Kanai, K., Schmidt, I., Kim, K.-P., Fraccaroli, A., Feil, S., Junge, H.J., et al. (2019). Integrin-linked kinase controls retinal angiogenesis and is linked to Wnt signaling and exudative vitreoretinopathy. *Nat Commun* 10, 5243. <https://doi.org/10.1038/s41467-019-13220-3>.
- Park, I.-H., Lerou, P.H., Zhao, R., Huo, H., and Daley, G.Q. (2008). Generation of human-induced pluripotent stem cells. *Nat Protoc* 3, 1180–1186. <https://doi.org/10.1038/nprot.2008.92>.
- Park, K.-H., Piron, J., Dahimene, S., Mérot, J., Baró, I., Escande, D., and Loussouarn, G. (2005). Impaired KCNQ1-KCNE1 and phosphatidylinositol-4,5-bisphosphate interaction underlies the long QT syndrome. *Circ Res* 96, 730–739. <https://doi.org/10.1161/01.RES.0000161451.04649.a8>.
- Peichev, M., Naiyer, A.J., Pereira, D., Zhu, Z., Lane, W.J., Williams, M., Oz, M.C., Hicklin, D.J., Witte, L., Moore, M.A., et al. (2000). Expression of VEGFR-2 and AC133 by circulating human CD34(+) cells identifies a population of functional endothelial precursors. *Blood* 95, 952–958. .
- Peters, K., Helmert, T., Gebhard, S., Mailänder, V., Unger, R.E., Nezi-Cahn, S., Hasenburg, A., Heller, M., Schwab, R., and Brenner, W. (2022). Standardized Human Platelet Lysates as Adequate Substitute to Fetal Calf Serum in Endothelial Cell Culture for Tissue Engineering. *Biomed Res Int* 2022, 3807314. <https://doi.org/10.1155/2022/3807314>.
- Portero, V., Casini, S., Hoekstra, M., Verkerk, A.O., Mengarelli, I., Belardinelli, L., Rajamani, S., Wilde, A.A.M., Bezzina, C.R., Veldkamp, M.W., et al. (2017). Anti-arrhythmic potential of the late sodium current inhibitor GS-458967 in murine *Scn5a*-1798insD^{+/-} and human *SCN5A*-1795insD^{+/-} iPSC-derived cardiomyocytes. *Cardiovasc Res* 113, 829–838. <https://doi.org/10.1093/cvr/cvx077>.

- Prasad, A., Manivannan, J., Loong, D.T., Chua, S.M., Gharibani, P.M., and Ali, A.H. (2016). A review of induced pluripotent stem cell, direct conversion by trans-differentiation, direct reprogramming and oligodendrocyte differentiation. *Regenerative Medicine* 11, 181–191. <https://doi.org/10.2217/rme.16.5>.
- Priori, S.G., Napolitano, C., Schwartz, P.J., Grillo, M., Bloise, R., Ronchetti, E., Moncalvo, C., Tulipani, C., Veia, A., Bottelli, G., et al. (2004). Association of long QT syndrome loci and cardiac events among patients treated with beta-blockers. *JAMA* 292, 1341–1344. <https://doi.org/10.1001/jama.292.11.1341>.
- Quach, B., Krogh-Madsen, T., Entcheva, E., and Christini, D.J. (2018). Light-Activated Dynamic Clamp Using iPSC-Derived Cardiomyocytes. *Biophys J* 115, 2206–2217. <https://doi.org/10.1016/j.bpj.2018.10.018>.
- Quirici, N., Soligo, D., Caneva, L., Servida, F., Bossolasco, P., and Delilieri, G.L. (2001). Differentiation and expansion of endothelial cells from human bone marrow CD133(+) cells. *Br J Haematol* 115, 186–194. <https://doi.org/10.1046/j.1365-2141.2001.03077.x>.
- Richards, M., Tan, S.-P., Tan, J.-H., Chan, W.-K., and Bongso, A. (2004). The transcriptome profile of human embryonic stem cells as defined by SAGE. *Stem Cells* 22, 51–64. <https://doi.org/10.1634/stemcells.22-1-51>.
- Sakai, T., Li, S., Docheva, D., Grashoff, C., Sakai, K., Kostka, G., Braun, A., Pfeifer, A., Yurchenco, P.D., and Fässler, R. (2003). Integrin-linked kinase (ILK) is required for polarizing the epiblast, cell adhesion, and controlling actin accumulation. *Genes Dev.* 17, 926–940. <https://doi.org/10.1101/gad.255603>.
- Sala, L., van Meer, B.J., Tertoolen, L.G.J., Bakkers, J., Bellin, M., Davis, R.P., Denning, C., Dieben, M.A.E., Eschenhagen, T., Giacomelli, E., et al. (2018). Musclemotion. *Circulation Research* 122, e5–e16. <https://doi.org/10.1161/CIRCRESAHA.117.312067>.
- Santoro, F., Chien, K.R., and Sahara, M. (2021). Isolation of human ESC-derived cardiac derivatives and embryonic heart cells for population and single-cell RNA-seq analysis. *STAR Protoc* 2, 100339. <https://doi.org/10.1016/j.xpro.2021.100339>.
- Sasaki, T., Fässler, R., and Hohenester, E. (2004). Laminin : the crux of basement membrane assembly. *Journal of Cell Biology* 164, 959–963. <https://doi.org/10.1083/jcb.200401058>.

- Schlaeger, T.M., Daheron, L., Brickler, T.R., Entwisle, S., Chan, K., Cianci, A., DeVine, A., Ettenger, A., Fitzgerald, K., Godfrey, M., et al. (2015). A comparison of non-integrating reprogramming methods. *Nat Biotechnol* 33, 58–63. <https://doi.org/10.1038/nbt.3070>.
- Schwartz, P.J., Priori, S.G., Spazzolini, C., Moss, A.J., Vincent, G.M., Napolitano, C., Denjoy, I., Guicheney, P., Breithardt, G., Keating, M.T., et al. (2001). Genotype-phenotype correlation in the long-QT syndrome: gene-specific triggers for life-threatening arrhythmias. *Circulation* 103, 89–95. <https://doi.org/10.1161/01.cir.103.1.89>.
- Serrano, I., De Frutos, S., Grier, M., Medrano, D., Rodríguez-Puyol, M., Dedhar, S., Ruiz-Torres, M.P., and Rodríguez-Puyol, D. (2013). Ilk conditional deletion in adult animals increases cyclic GMP-dependent vasorelaxation. *Cardiovasc Res* 99, 535–544. <https://doi.org/10.1093/cvr/cvt131>.
- Shalaby, F.Y., Levesque, P.C., Yang, W.P., Little, W.A., Conder, M.L., Jenkins-West, T., and Blam, M.A. (1997). Dominant-negative KvLQT1 mutations underlie the LQT1 form of long QT syndrome. *Circulation* 96, 1733–1736. <https://doi.org/10.1161/01.cir.96.6.1733>.
- Shanker, A.J., Yamada, K., Green, K.G., Yamada, K.A., and Saffitz, J.E. (2005). Matrix Protein-Specific Regulation of Cx43 Expression in Cardiac Myocytes Subjected to Mechanical Load. *Circulation Research* 96, 558–566. <https://doi.org/10.1161/01.RES.0000158964.42008.a2>.
- Shiba, Y., Gomibuchi, T., Seto, T., Wada, Y., Ichimura, H., Tanaka, Y., Ogasawara, T., Okada, K., Shiba, N., Sakamoto, K., et al. (2016). Allogeneic transplantation of iPS cell-derived cardiomyocytes regenerates primate hearts. *Nature* 538, 388–391. <https://doi.org/10.1038/nature19815>.
- Silva, J., Barrandon, O., Nichols, J., Kawaguchi, J., Theunissen, T.W., and Smith, A. (2008). Promotion of reprogramming to ground state pluripotency by signal inhibition. *PLoS Biol* 6, e253. <https://doi.org/10.1371/journal.pbio.0060253>.
- Sinnecker, D., Laugwitz, K.-L., and Moretti, A. (2014). Induced pluripotent stem cell-derived cardiomyocytes for drug development and toxicity testing. *Pharmacology & Therapeutics* 143, 246–252. <https://doi.org/10.1016/j.pharmthera.2014.03.004>.
- Smyth, N., Vatansever, H.S., Murray, P., Meyer, M., Frie, C., Paulsson, M., and Edgar, D. (1999). Absence of Basement Membranes after Targeting the LAMC1 Gene Results in Embryonic Lethality Due

to Failure of Endoderm Differentiation. *Journal of Cell Biology* 144, 151–160. <https://doi.org/10.1083/jcb.144.1.151>.

Stadtfield, M., and Hochedlinger, K. (2010). Induced pluripotency: history, mechanisms, and applications. *Genes Dev* 24, 2239–2263. <https://doi.org/10.1101/gad.1963910>.

Stoddard-Bennett, T., and Reijo Pera, R. (2019). Treatment of Parkinson's Disease through Personalized Medicine and Induced Pluripotent Stem Cells. *Cells* 8, 26. <https://doi.org/10.3390/cells8010026>.

Suresh Babu, S., Duvvuru, H., Baker, J., Switalski, S., Shafa, M., Panchalingam, K.M., Dadgar, S., Beller, J., and Ahmadian Baghbaderani, B. (2023). Characterization of human induced pluripotent stems cells: Current approaches, challenges, and future solutions. *Biotechnology Reports* 37, e00784. <https://doi.org/10.1016/j.btre.2023.e00784>.

Tada, M., Takahama, Y., Abe, K., Nakatsuji, N., and Tada, T. (2001). Nuclear reprogramming of somatic cells by in vitro hybridization with ES cells. *Curr Biol* 11, 1553–1558. [https://doi.org/10.1016/s0960-9822\(01\)00459-6](https://doi.org/10.1016/s0960-9822(01)00459-6).

Takahashi, K., and Yamanaka, S. (2006). Induction of pluripotent stem cells from mouse embryonic and adult fibroblast cultures by defined factors. *Cell* 126, 663–676. <https://doi.org/10.1016/j.cell.2006.07.024>.

Takahashi, K., Tanabe, K., Ohnuki, M., Narita, M., Ichisaka, T., Tomoda, K., and Yamanaka, S. (2007). Induction of pluripotent stem cells from adult human fibroblasts by defined factors. *Cell* 131, 861–872. <https://doi.org/10.1016/j.cell.2007.11.019>.

Thomson, J.A., Itskovitz-Eldor, J., Shapiro, S.S., Waknitz, M.A., Swiergiel, J.J., Marshall, V.S., and Jones, J.M. (1998). Embryonic stem cell lines derived from human blastocysts. *Science* 282, 1145–1147. <https://doi.org/10.1126/science.282.5391.1145>.

Tohyama, S., Hattori, F., Sano, M., Hishiki, T., Nagahata, Y., Matsuura, T., Hashimoto, H., Suzuki, T., Yamashita, H., Satoh, Y., et al. (2013). Distinct Metabolic Flow Enables Large-Scale Purification of Mouse and Human Pluripotent Stem Cell-Derived Cardiomyocytes. *Cell Stem Cell* 12, 127–137. <https://doi.org/10.1016/j.stem.2012.09.013>.

- Ueno, S., Weidinger, G., Osugi, T., Kohn, A.D., Golob, J.L., Pabon, L., Reinecke, H., Moon, R.T., and Murry, C.E. (2007). Biphasic role for Wnt/ β -catenin signaling in cardiac specification in zebrafish and embryonic stem cells. *Proc. Natl. Acad. Sci. U.S.A.* *104*, 9685–9690. <https://doi.org/10.1073/pnas.0702859104>.
- Urner, S., Planas-Paz, L., Hilger, L.S., Henning, C., Branopolski, A., Kelly-Goss, M., Stanczuk, L., Pitter, B., Montanez, E., Peirce, S.M., et al. (2019). Identification of ILK as a critical regulator of VEGFR3 signalling and lymphatic vascular growth. *EMBO J* *38*, e99322. <https://doi.org/10.15252/embj.201899322>.
- Vaidyanathan, R., Markandeya, Y.S., Kamp, T.J., Makielski, J.C., January, C.T., and Eckhardt, L.L. (2016). IK1-enhanced human-induced pluripotent stem cell-derived cardiomyocytes: an improved cardiomyocyte model to investigate inherited arrhythmia syndromes. *Am J Physiol Heart Circ Physiol* *310*, H1611–H1621. <https://doi.org/10.1152/ajpheart.00481.2015>.
- Veldhuizen, J., Mann, H.F., Karamanova, N., Van Horn, W.D., Migrino, R.Q., Brafman, D., and Nikkhah, M. (2022). Modeling long QT syndrome type 2 on-a-chip via in-depth assessment of isogenic gene-edited 3D cardiac tissues. *Sci. Adv.* *8*, eabq6720. <https://doi.org/10.1126/sciadv.abq6720>.
- Ventura, C., Zinellu, E., Maninchedda, E., and Maioli, M. (2003). Dynorphin B Is an Agonist of Nuclear Opioid Receptors Coupling Nuclear Protein Kinase C Activation to the Transcription of Cardiogenic Genes in GTR1 Embryonic Stem Cells. *Circulation Research* *92*, 623–629. <https://doi.org/10.1161/01.RES.0000065169.23780.0E>.
- Volz, K.S., Miljan, E., Khoo, A., and Cooke, J.P. (2012). Development of pluripotent stem cells for vascular therapy. *Vascul Pharmacol* *56*, 288–296. <https://doi.org/10.1016/j.vph.2012.02.010>.
- Wagdi, A., Malan, D., Sathyanarayanan, U., Beauchamp, J.S., Vogt, M., Zipf, D., Beiert, T., Mansuroglu, B., Dusend, V., Meininghaus, M., et al. (2022). Selective optogenetic control of Gq signaling using human Neuropsin. *Nat Commun* *13*, 1765. <https://doi.org/10.1038/s41467-022-29265-w>.
- Wahl, P., Bloch, W., and Schmidt, A. (2007). Exercise has a Positive Effect on Endothelial Progenitor Cells, which Could be Necessary for Vascular Adaptation Processes. *Int J Sports Med* *28*, 374–380. <https://doi.org/10.1055/s-2006-924364>.

- Wallace, E., Howard, L., Liu, M., O'Brien, T., Ward, D., Shen, S., and Prendiville, T. (2019). Long QT Syndrome: Genetics and Future Perspective. *Pediatr Cardiol* 40, 1419–1430. <https://doi.org/10.1007/s00246-019-02151-x>.
- Wang, D., Sang, H., Zhang, K., Nie, Y., Zhao, S., Zhang, Y., He, N., Wang, Y., Xu, Y., Xie, X., et al. (2017). Stat3 phosphorylation is required for embryonic stem cells ground state maintenance in 2i culture media. *Oncotarget* 8, 31227–31237. <https://doi.org/10.18632/oncotarget.16112>.
- Wang, D.W., Yazawa, K., Alfred L. George, J., and Bennett, P.B. (1996). Characterization of human cardiac Na⁺ channel mutations in the congenital long QT syndrome. *Proceedings of the National Academy of Sciences of the United States of America* 93, 13200. <https://doi.org/10.1073/pnas.93.23.13200>.
- Wang, H., Yang, Y., Liu, J., and Qian, L. (2021). Direct cell reprogramming: approaches, mechanisms and progress. *Nat Rev Mol Cell Biol* 22, 410–424. <https://doi.org/10.1038/s41580-021-00335-z>.
- Wang, J., Hoshijima, M., Lam, J., Zhou, Z., Jokiel, A., Dalton, N.D., Hultenby, K., Ruiz-Lozano, P., Ross, J., Tryggvason, K., et al. (2006). Cardiomyopathy associated with microcirculation dysfunction in laminin alpha4 chain-deficient mice. *J Biol Chem* 281, 213–220. <https://doi.org/10.1074/jbc.M505061200>.
- Wang, L., Wang, L., Huang, W., Su, H., Xue, Y., Su, Z., Liao, B., Wang, H., Bao, X., Qin, D., et al. (2013). Generation of integration-free neural progenitor cells from cells in human urine. *Nat Methods* 10, 84–89. <https://doi.org/10.1038/nmeth.2283>.
- Wernig, M., Meissner, A., Cassady, J.P., and Jaenisch, R. (2008). c-Myc is dispensable for direct reprogramming of mouse fibroblasts. *Cell Stem Cell* 2, 10–12. <https://doi.org/10.1016/j.stem.2007.12.001>.
- White, D.E., Coutu, P., Shi, Y.-F., Tardif, J.-C., Nattel, S., St Arnaud, R., Dedhar, S., and Muller, W.J. (2006). Targeted ablation of ILK from the murine heart results in dilated cardiomyopathy and spontaneous heart failure. *Genes Dev* 20, 2355–2360. <https://doi.org/10.1101/gad.1458906>.
- Wickström, S.A., Lange, A., Hess, M.W., Polleux, J., Spatz, J.P., Krüger, M., Pfaller, K., Lambacher, A., Bloch, W., Mann, M., et al. (2010). Integrin-Linked Kinase Controls Microtubule Dynamics Required for Plasma Membrane Targeting of Caveolae. *Dev Cell* 19, 574–588. <https://doi.org/10.1016/j.devcel.2010.09.007>.

- Wilde, A.A.M., and Amin, A.S. (2018). Clinical Spectrum of SCN5A Mutations: Long QT Syndrome, Brugada Syndrome, and Cardiomyopathy. *JACC: Clinical Electrophysiology* 4, 569–579. <https://doi.org/10.1016/j.jacep.2018.03.006>.
- Willmann, C.A., Hemeda, H., Pieper, L.A., Lenz, M., Qin, J., Jousen, S., Sontag, S., Wanek, P., Denecke, B., Schüler, H.M., et al. (2013). To clone or not to clone? Induced pluripotent stem cells can be generated in bulk culture. *PLoS One* 8, e65324. <https://doi.org/10.1371/journal.pone.0065324>.
- Wimmer, R.A., Leopoldi, A., Aichinger, M., Wick, N., Hantusch, B., Novatchkova, M., Taubenschmid, J., Hämmerle, M., Esk, C., Bagley, J.A., et al. (2019). Human blood vessel organoids as a model of diabetic vasculopathy. *Nature* 565, 505–510. <https://doi.org/10.1038/s41586-018-0858-8>.
- Wobus, A.M. (2005). Embryonic Stem Cells: Prospects for Developmental Biology and Cell Therapy.
- Wobus, A.M., and Boheler, K.R. (2005). Embryonic Stem Cells: Prospects for Developmental Biology and Cell Therapy. *Physiological Reviews* 85, 635–678. <https://doi.org/10.1152/physrev.00054.2003>.
- Wobus, A.M., Kaomei, G., Shan, J., Wellner, M.C., Rohwedel, J., Ji Guanju, null, Fleischmann, B., Katus, H.A., Hescheler, J., and Franz, W.M. (1997). Retinoic acid accelerates embryonic stem cell-derived cardiac differentiation and enhances development of ventricular cardiomyocytes. *J Mol Cell Cardiol* 29, 1525–1539. <https://doi.org/10.1006/jmcc.1997.0433>.
- Wray, J., Kalkan, T., and Smith, A.G. (2010). The ground state of pluripotency. *Biochem Soc Trans* 38, 1027–1032. <https://doi.org/10.1042/BST0381027>.
- Yamamoto, W., Hashimoto, N., Matsuura, J., Machida, T., Ogino, Y., Kobayashi, T., Yamanaka, Y., Ishiwata, N., Yamashita, T., Tanimoto, K., et al. (2014). Effects of the selective K_{ACh} channel blocker NTC-801 on atrial fibrillation in a canine model of atrial tachypacing: comparison with class Ic and III drugs. *J Cardiovasc Pharmacol* 63, 421–427. <https://doi.org/10.1097/FJC.000000000000065>.
- Yamanaka, S. (2020). Pluripotent Stem Cell-Based Cell Therapy—Promise and Challenges. *Cell Stem Cell* 27, 523–531. <https://doi.org/10.1016/j.stem.2020.09.014>.
- Yang, X., Pabon, L., and Murry, C.E. (2014). Engineering adolescence: maturation of human pluripotent stem cell-derived cardiomyocytes. *Circ Res* 114, 511–523. <https://doi.org/10.1161/CIRCRESAHA.114.300558>.

Ying, Q.-L., Wray, J., Nichols, J., Battle-Morera, L., Doble, B., Woodgett, J., Cohen, P., and Smith, A. (2008). The ground state of embryonic stem cell self-renewal. *Nature* 453, 519–523. <https://doi.org/10.1038/nature06968>.

Yoshida, S., Kato, T.M., Sato, Y., Umekage, M., Ichisaka, T., Tsukahara, M., Takasu, N., and Yamanaka, S. (2023). A clinical-grade HLA haplobank of human induced pluripotent stem cells matching approximately 40% of the Japanese population. *Med* 4, 51-66.e10. <https://doi.org/10.1016/j.medj.2022.10.003>.

Yu, J., Vodyanik, M.A., Smuga-Otto, K., Antosiewicz-Bourget, J., Frane, J.L., Tian, S., Nie, J., Jonsdottir, G.A., Ruotti, V., Stewart, R., et al. (2007). Induced Pluripotent Stem Cell Lines Derived from Human Somatic Cells. *Science* 318, 1917–1920. <https://doi.org/10.1126/science.1151526>.

Zhang, M., Schulte, J.S., Heinick, A., Piccini, I., Rao, J., Quaranta, R., Zeuschner, D., Malan, D., Kim, K.-P., Röpke, A., et al. (2015). Universal Cardiac Induction of Human Pluripotent Stem Cells in Two and Three-Dimensional Formats: Implications for In Vitro Maturation. *Stem Cells* 33, 1456–1469. <https://doi.org/10.1002/stem.1964>.

Zhang, Q., Jiang, J., Han, P., Yuan, Q., Zhang, J., Zhang, X., Xu, Y., Cao, H., Meng, Q., Chen, L., et al. (2011). Direct differentiation of atrial and ventricular myocytes from human embryonic stem cells by alternating retinoid signals. *Cell Res* 21, 579–587. <https://doi.org/10.1038/cr.2010.163>.

Zhao, M., Tang, Y., Zhou, Y., and Zhang, J. (2019). Deciphering Role of Wnt Signalling in Cardiac Mesoderm and Cardiomyocyte Differentiation from Human iPSCs: Four-dimensional control of Wnt pathway for hiPSC-CMs differentiation. *Sci Rep* 9, 19389. <https://doi.org/10.1038/s41598-019-55620-x>.

Zhao, Y.-Y., Liu, Y., Stan, R.-V., Fan, L., Gu, Y., Dalton, N., Chu, P.-H., Peterson, K., Ross, J., and Chien, K.R. (2002). Defects in caveolin-1 cause dilated cardiomyopathy and pulmonary hypertension in knockout mice. *Proc Natl Acad Sci U S A* 99, 11375–11380. <https://doi.org/10.1073/pnas.172360799>.

Zhou, Z., Gong, Q., Epstein, M.L., and January, C.T. (1998). HERG channel dysfunction in human long QT syndrome. Intracellular transport and functional defects. *J Biol Chem* 273, 21061–21066. <https://doi.org/10.1074/jbc.273.33.21061>.

8 Acknowledgments

I would like to thank Prof. Dr. med. Fleischmann, Director of the Institute of Physiology I at the University of Bonn, for his support, generous helpfulness and commitment and for his constructive help in planning the experimental projects. He supported me in the best possible way from the very beginning, both ideally in the development of the projects and financially in the realization of the projects. Only thanks to his immense commitment, his contacts at national and international level, projects could be realized in the form presented. Thanks to him I learnt how there are no linear paths in science.

I would like to thank also Prof. Dr. Philipp Sasse, University of Bonn, who made my involvement in basic research possible, provided me with the best possible support, and genial ideas even remotely, his support is always present.

I would also like to thank all the staff at the Institute of Physiology I, who contributed to the realization of the projects in the form presented, a special thanks to Dr. Caroline Geisen, Frank Holst and the staff of the affiliated laboratories.

Special thanks go to Prof. Dr. W. Bloch, Director of the Department of Molecular and Cellular Sports Medicine, German University of Sport Cologne, for his warm welcome and generous support.

I would also like to thank Prof. Dr. Wilhelm Röhl, and Prof. Dr. M. Reppel for showing me at the beginning how to have fun in science.

9 Curriculum Vitae

<u>Persönlichen Daten</u>	
Name	Malan
Vorname	Daniela
Adresse	
Telefon	
E-Mail	
Geburtsdatum	
Geburtsort	
Nationalität	Italienisch/Deutsch
Familienstand	
<u>Beruflicher Werdegang</u>	
Aktuell	<p>Wissenschaftliche Mitarbeiterin am Institut für Physiologie I der Universität Bonn (Prof. Dr. B. Fleischmann und Prof. Dr. P. Sasse). Thema: Kardiovaskuläre Optogenetik:</p> <ol style="list-style-type: none"> 1. Optogenetische Stimulierung der Gi-Signalübertragung für das Screening von Arzneimitteln und die Untersuchung lokaler Mechanismen des Vorhofflimmerns. 2. Biologische Validierung von Photonenumwandlungsstrategien unter Verwendung von Lanthanid-haltigen upconverting Nanopartikeln (UCNP) in Streptavidin-getagten ChR2-Zellen. 3. Strategien für Optogenetik in Richtung Rotverschiebung unter Verwendung der Vitamin A2-erzeugenden Dehydrogenase Cyp27c1 in rotverschobenen ChR2-Varianten.
2012 - 2016	Wissenschaftliche Koordination des von Bio NRW und der Europäischen Union geförderten Drittmittelprojektes: "Stammzellenfabrik".
2007 - 2012	<p>Post Doc- Stelle gefördert durch die Deutsche Forschungsgemeinschaft (DFG) am Institut für Physiologie I der Universität Bonn (Prof. Dr. B. Fleischmann und Jun.-Prof. Dr. P. Sasse). Projekte:</p> <ol style="list-style-type: none"> 1. Untersuchung der electrophysiologischen Merkmale von LQTS3 bei ΔKPQ Mutation unter Verwendung von iPS Zell-abgeleiteten Maus-Kardiomyozyten. 2. Generierung von genetisch manipulierten iPS Zell abgeleiteten-LQTS3-Kardiomyozyten, zur <i>in-vitro</i>-Untersuchung von Krankheitsmechanismen und zur Durchführung patientenspezifischer Arzneimittelscreenings.
2002 - 2006	<p>Post Doc- Stelle gefördert durch die Deutsche Forschungsgemeinschaft (DFG) am Institut für Physiologie I, Universität Bonn (Prof. Dr. B. Fleischmann) und an der Deutschen Sporthochschule Köln (Prof. Dr. W. Bloch), Abteilung Molekulare und Zelluläre Sportmedizin. Projekte:</p> <ol style="list-style-type: none"> 1. Analyse des selektiven muskarinischen Signals in embryonalen Herzzellen und in aus β1- Integrin (-/-) embryonalen Stammzellen abgeleiteten Kardiomyozyten.

	2. Analyse verschiedener Basalmembranmoleküle (Laminin, Perlecan und Integrin-linked-kinase) während der Entwicklung und Differenzierung von ES-abgeleiteten Kardiomyozyten und Endothelzellen.
1998 - 2002	Doktorarbeit im Labor für allgemeine Physiologie, Universität Turin, unter Leitung von Prof. G. Alloatti, Prof. R.C. Levi und Prof. G. Losano. Ein Teil der Doktorarbeit wurde im Labor von Prof. Dr. B. Fleischmann, Institut für Neurophysiologie, Universität zu Köln durchgeführt (2001). Thema: Regulation des kardialen Calciumstroms durch NO und seine radikalen Derivate.
1999 - 2000	Praktikum für die Staatsexamensprüfung an der A.R.P.A. (Regionales Institut für Umweltschutz, Piemont).
<u>Ausbildung und Zusatzqualifikationen</u>	
2023	Fortbildung nach § 23 Abs. 3 Gentechnik-Sicherheitsverordnung (GenTSV) in der Fassung von 01.03.2021. Aufbaukurs „Tierschutz/Versuchstierkunde“ (online, synchron/asynchron) Sachkunde-Kurs für Antragsteller, Planer und Leiter tierexperimenteller Studien (ehemals FELASA C-Level; Funktion B gemäß RL 2010/63/EU).
2022	Landesakademie für Medizinische Ausbildung NRW (LAMA) Zertifikat, Workshop mit praktischen Übungen „Planung von Lehrveranstaltungen“ vom 20.-21.01.2022 Bonn. Landesakademie für Medizinische Ausbildung NRW (LAMA) Zertifikat, Workshop „Richtig prüfen?!“ vom 5.-6.05.2022 Bonn.
2016-2017	Intensivseminar „Klinisches Monitoring“, berufsbegleitende Weiterbildung des mibeg - Instituts Medizin zum Clinical Research Associate.
2013	Fortbildung für Projektleiter und Beauftragte für die Biologische Sicherheit (BBS) gem. § 15 (2) und (4) Gentechnik-Sicherheitsverordnung (GenTSV), Universität Bonn.
2012	Goethe-Zertifikat C1 (85/100), Goethe Institut Bonn.
2011	Teilnahme am Kurs Versuchstierkunde und tierexperimentelle Methoden, Universität Bonn.
2002	Preis der italienischen Gesellschaft für kardiovaskuläre Forschung. Italienischer Nationalkongress für kardiovaskuläre Forschung. Bologna 29-30.11.2002: Role of PI3Kgamma in beta-adrenergic stimulation of cardiac contractility and L-type calcium current. Malan D., Marcantoni A., Gallo M.P., Bedendi I., Penna C., Alloatti G., Levi R.C., Hirsch E., Alloatti G.
2000	Teilnahme am Kurs: "Espressione eterologa di proteine di membrana: metodi di transfezione e di rilevazione" - "Heterologe Expression von Membranproteinen: Methoden der Transfektion und Detektion", Physiologische und Biophysiologische Schule der Insubria Universität, Varese (I).
2000	Biologisches Staatsexamen (I), Universität Turin.
1999	Gen-Therapie Kurs, Genetische Schule von Cortona.

1998-2002	<p>“XIV Dottorato di Ricerca in Fisiologia” (PhD-Kurs) der medizinischen Fakultät der Universität Turin, Labor für allgemeine Physiologie, Leitung Prof. G. Alloatti und Prof. G. Losano.</p>
1993-1998	<p>Biologie Studium, Universität Turin. Biologie Abschluss mit Thema: Regolazione della corrente di calcio cardiaca da parte del monossido d’azoto e del GMP ciclico“- „Regulation von kardialen Kalziumstrom durch NO und zyklisches GMP“</p>
1993	<p>Musikhochschule: Erstes Theorie Diplom Conservatorio G. Verdi Turin, Endnote:</p>
1992	<p>Liceo Linguistico Valdese (Gymnasium), Torre Pellice (TO), Abitur Endnote:</p>
Sprachen	<p>Englisch: fließend in Wort und Schrift Deutsch: fließend in Wort und Schrift (Goethe Institut Prüfung C1) Französisch: fließend in Wort und Schrift Italienisch: Muttersprache</p>
Wissenschaftliches Profil	<p>Zellkultur mit primären Zellen und Zell-Linien: Maus embryonale Kardiomyozyten, Maus embryonale Stammzellen, Maus und Humane induzierte pluripotente Stammzellen, Differenzierung von Stammzellen in kardiovaskuläre Zellen.</p> <p>Elektrophysiologische Untersuchungen an einzelnen Kardiomyozyten aus adulten Maus Herzen oder von embryonalen Stammzellen (ES) der Maus und induzierten pluripotenten Stammzellen (iPS) von Maus und Mensch abgeleiteten Kardiomyozyten (knock-outs für ECM-Proteine oder von Patienten mit LQT-Syndrom) mittels manueller und automatisierter Patch-clamp Technik in „whole cell“ und „current clamp modus“.</p> <p>Optogenetische Untersuchungen von Kardiomyozyten, aus adulten Maus Herzen und aus induzierten pluripotenten Stammzellen (iPS) abgeleiteten Kardiomyozyten.</p> <p>Elektrophysiologische Untersuchung von Stammzellaggregaten und Zellen mittels Multi-Electrode-Array (MEA) und CardioExcyte 96.</p> <p>Analyse der morphologischen und funktionellen Eigenschaften mittels Apotome und Konfokalmikroskopie und Kalzium-dyes (FURA2, Fluo 4, Cal630).</p> <p>Grundlegende Klonierungstechniken für die Erzeugung von Plasmiden zur Analyse von lichtaktivierten Proteinen wie ChR, RearChR, LWopsins, die an der Aktivierung von Signalwegen in Kardiomyozyten beteiligt sind.</p>
<p><u>Internationale Kollaborationen und Forschungsreisen</u></p>	
2014	<p>Besuch des ersten deutsch-brasilianischen Workshops an der Bundesuniversität Rio de Janeiro. Instituto de Biofísica Carlos Chagas Filho, Brasilien, Prof. Emiliano Medei und Prof. Antonio Campos de Carvalho.</p> <p>Kollaboration mit dem Lund Biomedical Center, Schweden, Dr. Stefan Jovinge Kollaboration mit dem Max-Planck- Institut für Herz- und Lungenforschung Bad Nauheim, Prof. Dr. Thomas Braun Kollaboration mit dem Universitätsklinikum Ulm, Zentrum für Innere Medizin I, PD Alex Kleger</p>

Gutachtertätigkeit für

Kollaboration mit der University of Turin, Dept. of Life Sciences and System Biology, Prof Maria Pia Gallo and Dr. Giulia Querio
Kollaboration mit Dr. Jonas Wietek, Weizmann Institute of Science, Rehovot, Israel.

Journal of Cardiology Case Reports.
Frontiers in Pharmacology
Frontiers in Physiology
MDPI Pharmaceuticals special issue Editor, Cardiovascular Diseases: Where Do We Stand with Human-Derived Stem Cells?

Lehrtätigkeit

Grundvorlesung Physiologie für Studierende der Pharmazie.
Praktikum und Seminar Physiologie für Studierende der Human-, Bio- und Zahnmedizin.
Forschungspraktikum für Medizinstudenten "Scimed".
Praktikum "Biologie für Medizinstudenten".
Seminar für "Development and Physiology" im Masterstudiengang Molecular Cell Biology.

Drittmittelförderung

BONFOR 01.06.2023 - 31.05.2024 SciMed-Promotionsstipendium für Herrn Caspar Timpe, Ko-Antrag mit Prof. Philipp Sasse.

10 Statements

Hiermit bestätige ich, dass ich die Richtlinien zur guten wissenschaftlichen Praxis der Universität Bonn, laut Habilitations-Ordnung, zur Kenntnis genommen habe und ich versichere an Eides statt, dass ich diese Habilitationsschrift selbst abgefasst habe und die hier behandelten wissenschaftlichen Untersuchungen von mir ausgeführt wurden. Insbesondere versichere ich, dass ich alle in der Habilitationsschrift benutzten Quellen und Hilfsmittel angegeben habe.

Bonn, den 06.03.2024

PhD/ Daniela Malan